Adsorptive Reactor Technology for VOC Abatement

by

Mary Abiola Kolade

October 2007

A thesis submitted for the degree of Doctor of Philosophy of the University of London and for the Diploma of Membership of Imperial College

Department of Chemical Engineering and Chemical Technolgy

Imperial College London

SW7 2BY

UK

For Wol & Kerry

The use of the monolith as an adsorptive reactor (M-AR) is proposed as a viable and novel alternative for VOC disposal. The M-AR combines adsorptive separation and catalytic combustion of the VOC in a single reactor unit and is thought to make effective utilisation of energy due to efficient heat integration. This work involves theoretical studies on the feasibility and application of the adsorptive reactor concept for VOC oxidation. Thus unlike previous work, studies focus on an exothermic reaction system and the ability of the M-AR to control thermal runaway.

The process is operated cyclically in two steps – adsorption and desorption / reaction. The VOC is fed into the reactor in the adsorption step and captured to produce a pure carrier gas effluent. Concentration and thermal swing is induced in the second step by means of an air feed.

The most outstanding feature of the M-AR is its ability to prevent thermal runaway whilst maintaining a high VOC conversion. Simulation results indicate that the careful selection of step times for adsorption and desorption, feed temperatures and inlet velocities lead to stability and energy requirements which outperform equivalent conventional designs such as packed beds and monolith reactors. The M-AR is thermally more stable due to the controlled release of the reactant from the adsorbed phase into the reaction zone, and also the heat integration of an endothermic desorption and exothermic reaction.

Further M-AR design guidance is achieved through a combination of numerical optimisation strategies and the analytical derivation of scaling rules. Optimisation results indicate that inlet velocity and step times play an important part in reactor performance. Scaling rules enable the transformation of a given process to one which meets new and / or additional system specifications (and / or constraints) without the necessity for performing further simulation. Examples in the use of scaling rules are presented and include increasing the VOC processing rate whilst maintaining a desired conversion.

ACKNOWLEDGEMENTS

I would like to thank God, my heavenly Father for granting me the strength and perseverance to complete this research degree.

Special thanks to my supervisor, Dr. Esat Alpay, who provided the original ideas for this thesis. His guidance, patience, understanding and continuous support is deeply appreciated. Gratitude is also expressed to Dr. Andreas Kogelbauer who took me under his wing in the latter stages of this project.

I wish to extend my sincere gratitude and appreciation to my parents and my brothers especially Wol, for their financial and moral support, their love, and encouragement over the years and most importantly, for their prayers.

I would like to thank my research colleagues, George, Pann, Ana, Manal and Vangelis for their support and encouragement.

Finally, I would like to express my deepest gratitude to my husband, Ben, for his love, financial support, patience and understanding. Most of all I would like to thank him for believing in me and encouraging me to persevere at times when I most certainly wanted to give up.

A	cross sectional area	m
C	concentration of gas	mol m^{-3}
C*	normalised C	-
C_{pg}	gas specific heat capacity	J mol^{-1} K^{-1}
C_{ps}	solid phase heat capacity	J kg^{-1} K^{-1}
C_{time}	cycle time	s
D_A	effective axial dispersion coefficient	m^2 s^{-1}
$D_{channel}$	diameter of monolith channel (also = R_1)	m
D_{ei}	effective diffusivity	m^2 s^{-1}
D_k	Knudsen diffusion coefficient	m^2 s^{-1}
D_m	molecular diffusion coefficient	m^2 s^{-1}
D_p	diffusion coefficient for a single cylindrical pore	m^2 s^{-1}
D_z	effective axial dispersion coefficient	m^2 s^{-1}
d_c	internal diameter of monolith channel	m
d_m	total diameter of monolith structure	m
d_p	particle diameter	m
d_{pore}	adsorbent pore diameter	m
E_{act}	activation energy	kJ mol^{-1}
E_{AR}	rate of energy input for adsorptive reactor	kJ m^{-2} s^{-1}
E_{RXTN}	rate of energy input for monolith reactor	kJ m^{-2} s^{-1}
f	ratio of monolith diameter to packed bed column diameter	-
F_{PR}	ethene feed processed per cycle	mol $cycle^{-1}$
F_{pr}	production rate scaling factor	-
f_{st}	step duration scaling factor	-
J	molecular flux	mol m^{-2} s^{-1}
k_1	reaction rate constant	mol kg^{-1} s^{-1} Pa^{-1}
k_2	reaction rate constant of oxygen	mol kg^{-1} s^{-1} Pa^{-1}
k_1'	= $\upsilon . k_{1r} / k_2 . P_{O2}$	Pa^{-1}
k_i	LDF mass transfer coefficient	s^{-1}
k_∞	pre-exponential factor	mol kg^{-1} s^{-1} Pa^{-1}
K_{H2O}	adsorption constant of water	Pa^{-1}

K	adsorption equilibrium constant		k Pa^{-1}
L	length of reactor		m
L_e	length monolith entrance zone		m
L_m	monolith reactor length		m
L_{pb}	packed bed reactor length		m
M (or MW)	molecular weight		g mol^{-1}
MVL	molar volume		cm^3 mol^{-1}
m_i	reference adsorption isotherm gradient		mol kg^{-1} Pa^{-1}
N_A	molar flux of A		mol m^{-2} s^{-1}
N_{ads}	number of moles of reactant fed in the adsorption step		mol
N_{RE}	particle Reynolds number		-
n_i	molar flow rate of component i		mol s^{-1}
n_d	cell density in number of cells per unit area		cells cm^{-2}
P (or p)	pressure		Pa
Pe	Peclect number		-
P_R	productivity		mol m^{-2} s^{-1}
			kg^{-1} (solid)
q_i	average adsorbed phase concentration of component i		mol kg^{-1}
q^*	equilibrium adsorbed-phase concentration		mol kg^{-1}
q_{ri}	adsorbed phase concentration of i in radial diffusion		mol kg^{-1}
q^{sat}	saturation amount adsorbed		mol kg^{-1}
Q^*	normalised q		-
R_{HC}	rate of reaction		mol kg^{-1}(solid) s^{-1}
$\tilde{r}$	normalised R_{HC}		-
r_{ads}	rate of adsorption		mol kg^{-1} s^{-1}
r	radial coordinate		m
r_p	mean particle radius		m
R*	normalised r		-
R	universal gas constant (= 8.314)	J $mol^{-1}K^{-1}$ or	$Pa.m^3$ mol^{-1} K^{-1}
R_e	Reynolds number		-
R_p	spherical particle radius		m

R_{PB}	packed bed reactor radius	m
R_1	monolith core channel radius	m
R_2	monolith total radius	m
S_R	step time ratio	-
Sc	Schmidt number	-
t	time	s
t	characteristic parameter in Tóth isotherm (see Section 3.2)	-
t_a	time step adsorption	s
t_d	time step desorption	s
T	temperature	K
T^*	normalised T	-
T_b	boiling point temperature at 101.325 kPa	K
T_c	critical temperature	K
u / u_m	average velocity in the monolith channel	$m\ s^{-1}$
v / v_m	average velocity in the monolith channel	$m\ s^{-1}$
v_{pb}	superficial velocity in packed bed reactor	$m\ s^{-1}$
V^*	normalised v	-
V	volume of reactor	m^3
V_p	pore volume	$cm^3\ g^{-1}$
W_R	reaction front propagation velocity	$m\ s^{-1}$
W_{therm}	thermal front propagation velocity	$m\ s^{-1}$
X	conversion	-
y	gas phase mole fraction	-
z	axial coordinate	m
Z^*	normalised z	-

Greek Letters

α	molecular polarizability	$Å^3$
δ	thickness of adsorbent solid zone (R_2-R_1)	m
γ	mean free path	m

γ	combined fitting parameter defined by Eq. (3.14)	-
β	combined fitting parameter defined by Eq. (3.15)	-
λ	thermal conductivity	$W\ m^{-1}\ K^{-1}$
$\Delta\ E$	energy input	$kJ\ m^{-2}\ s^{-1}$
ΔH_{ads}	heat of adsorption	$kJ\ mol^{-1}$
ΔH_r	heat of reaction	$kJ\ mol^{-1}$
ΔH_v	molar enthalpy of vaporization at component boiling point	$kJ\ mol^{-1}$
ΔT_{max}	maximum temperature rise	K
ε / ε_b	bed void fraction	-
ε_m	fraction of monolith cross section area available for flow	-
ε_p	intraparticle void fraction	-
ε_t	total voidage of reactor	-
ζ	operator ratio	-
$\prod$	dimensional groups in normalised M-AR model equations for scaling rule derivation(see Section 5.3)	-
τ	space time	s
τ_p	tortuosity factor	-
ρ_b	bulk density	$kg\ m^{-3}$
ρ_g	gas density	$mol\ m^{-3}$
μ	viscosity	Pa. s
ν	volumetric flow rate	$m^3\ s^{-1}$
σ	collision diameter, Lennard-Jones constant	Á
σ_k	kinetic diameter	nm
Ω_{AB}	collision integral	-
Ω^{min} / Ω^{max}	optimisation decision variables (see Section 5.2)	-
Ω	normalised t	-
Ω_f	normalised temporal domain of feeding step	-
Ω_r	normalised temporal domain of regeneration step	-

Sub / Superscripts

0	reference / base

a	adsorption
b	base value
d	desorption
i	reaction component
f / o	inlet or feed
g	gas
m, n	parameters utilised in Model IV (see Table (3.3))
max / min	maximum / minimum
r	reaction
s	solid
1 / 2	adsorption / desorption
A / B	component A / component B
HC	hydrocarbon (e.g. VOC)

Abbreviations

1D	one dimensional
2D	two dimensional
Vol. %	percentage volume
gPROMS	general PROcess Modelling System
ACF	activated carbon fiber
ACFM	activated carbon fiber monoliths
AE	algebraic equation
AR	adsorptive reactor
BDDT	Brunauer, Deming, Deming and Teller
BFDM	backward finite difference method
CPU	central processing unit
CSS	cyclic steady state
DAE	differential algebraic equation
ILE	instantaneous local equilibrium
LDF	linear driving force

LEL	lower explosive limit
M-AR	monolith adsorptive reactor
M-ADS	monolith adsorber
M-RXTN	monolith reactor
MILP	mixed-integer linear programming
MINLP	mixed-integer non-linear programming
MMSCFD	million standard cubic feet per day of gas ≈ (28317 m^3 day^{-1})
NLP	non-linear programming
ODE	ordinary differential equation
PAP	periodic adsorption processes
PB-AR	packed bed adsorptive reactor
PB-ADS	packed bed adsorber
PB-RXTN	packed bed reactor
Pd	palladium
PDAE	partial differential and algebraic equation
PSA	pressure swing adsorptiom
PSR	pressure swing reactor
ppm	parts per million
RPSA	rapid pressure swing adsorption
RPSAR	rapid pressure swing adsorption with reaction
RPSR	rapid pressure swing reaction
SERP	sorption-enhanced reaction process
SMR	steam methane reforming
SR	steam reforming
TSA	temperature swing adsorption
TSR	temperature swing reactor
UEL	upper explosive limit
URPSA	ultra rapid pressure swing adsorption
VOC	volatile organic compound
ZLC	zero length column

Chapter 1 Introduction

Volatile organic compounds (VOCs) such as ethylene and propane are environmentally damaging chemicals emitted into air from chemical, petro-chemical and allied industries. The effect of VOCs causes ozone degradation and the formation of smog leading to various environmental hazards. Growing environmental awareness has led to stringent regulations to control VOC emissions and as a result a disposal process with high efficiency, reliability and cost effectiveness is necessary to capture and convert these harmful compounds.

In recent years, many processes such as thermal and catalytic oxidation have been used to control VOC emission but the use of the adsorptive reactor has never been considered. This work proposes the adsorptive reactor as a viable and efficient alternative for VOC disposal. Adsorptive reactors couple the operations of adsorption and chemical reaction into a single process. Reactive separation provides a means for removing product or reaction species from the reaction zone. The benefits of combined separation and reaction include process intensification, higher catalyst productivity and reduced requirements for external energy supply or cooling capacity.

The operation of an adsorptive reactor is transient in nature due to the need for adsorbent regeneration on a periodic basis. Forced-periodic variations in feed concentration, pressure and temperature can be

imposed for this purpose (Yongsunthon, 1999). The main objective of this work is to perform theoretical studies on the feasibility of cyclic adsorptive reactor applications to exothermic reaction systems with VOC abatement initially employed as a case study. Within this, attention is given to the catalytic combustion of ethene ($C_2H_4 + 3O_2 \rightarrow 2CO_2 + 2H_2O$) and propane ($C_3H_8 + 5O_2 \rightarrow 3CO_2 + 4H_2O$) over an activated carbon adsorbent and Pd/γ-Al_2O_3 catalyst. With this novel technology, the separative properties of the process can be utilised to give a smaller and more concentrated CO_2 product stream available for treatment. There are two steps in the operation of this reactor system; see Fig. (1.1) – adsorption and regeneration. Regeneration is followed by the complete combustion of the VOC. During the feeding step of the cycle, the feed stream containing the VOC is fed to the reactor bed at temperature T_f and the VOC is adsorbed. During the regeneration step, the inert regeneration gas stream of temperature T_r flows through the bed and the adsorbent is regenerated and reacts with the O_2 gas to give the reaction products, CO_2 and H_2O.

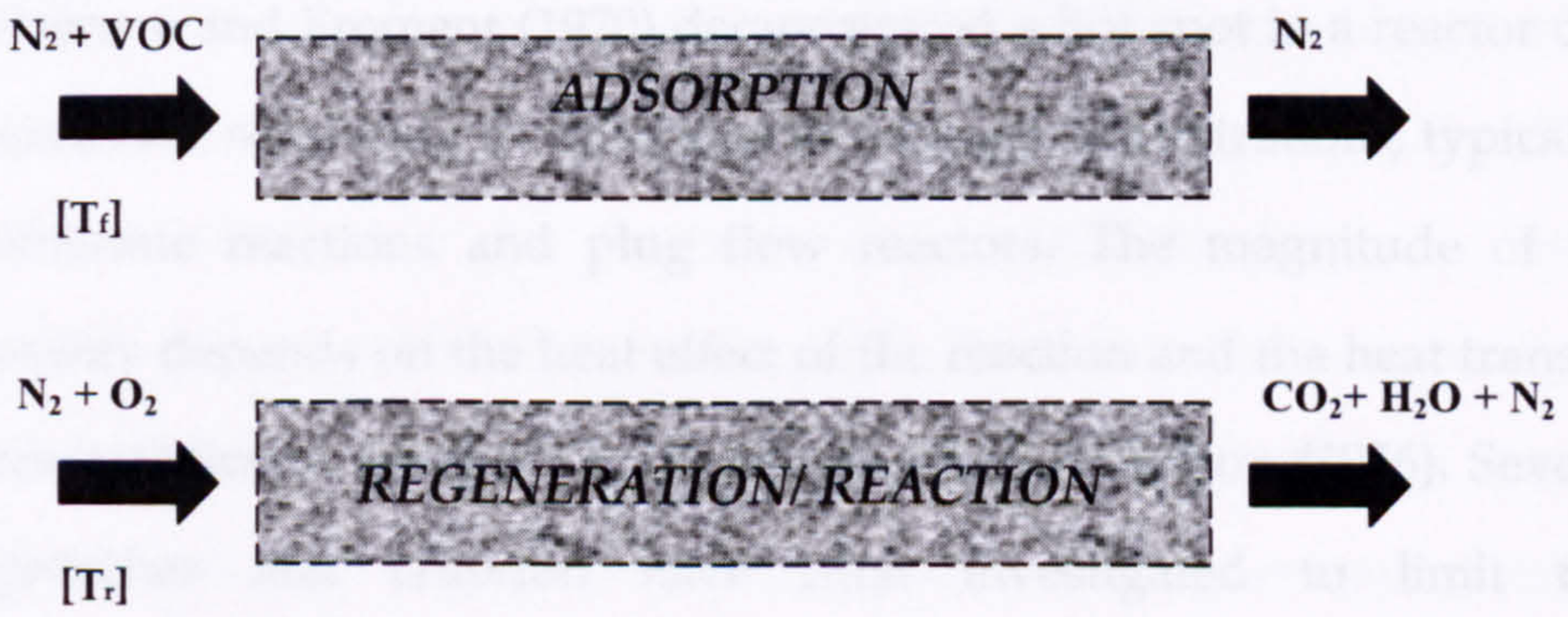

Fig.1.1: Feeding and regeneration step operations

Past studies on the adsorptive reactor have exclusively focused mainly on reversible and endothermic reaction systems (see Alpay *et al.*, 1994; Chatsiriwech *et al.*, 1994; Carvill *et al.*, 1996; Cheng *et al.*, 1998; Sheikh *et al.*,1998; Hufton *et al.*, 1999; Yongsunthon and Alpay, 1999; Waldron *et al.*, 2001). However, the use of adsorptive reactors for irreversible exothermic reactions has received much less attention (Kodde, 2001). In dealing with such an exothermic system, issues such as thermal runaway and effective heat and energy integration and utilization are addressed and the adsorptive reactor is evaluated on its performance and ability to effectively and efficiently combat and control these issues.

Adsorption is in itself an exothermic process and desorption or regeneration is endothermic. For the system under consideration, the adsorptive reactor can be used to control thermal runaway due to the relatively controlled release of the reactant from the adsorbed phase into the reaction zone and the efficient integration of heat from an endothermic desorption and exothermic reaction. Runaway is the origin of a high number of serious accidents in the chemical industry. Van Welsenare and Froment (1970) demonstrated a hot spot in a reactor due to excessive sensitivity to variations in reactant concentrations, typical of exothermic reactions and plug flow reactors. The magnitude of the runaway depends on the heat effect of the reaction and the heat transfer characteristics of the reactor; see Bilous and Amundson (1956). Several approaches and criterion have been investigated to limit this phenomenon. Different reactor configurations and operational modes have also been suggested. Reverse flow operation, and auto thermal

operation are concepts that have been applied to take advantage of the dynamic temperature profile within the reactor. Extensive research has been carried out in these areas. It must be noted however that these applications are for conventional fixed bed catalytic reactors.

Extensive research and experiments have also been performed on adsorptive reactors, their configurations, process optimisation and modelling, which date back to the early 1980's and 1990's. A review of this area is presented in Chapter 2. Most adsorptive reactors are based on the principles of the fixed bed catalytic reactor. The novelty of this work is in the use of the structured reactor e.g. monolith reactor, as an adsorptive reactor (M-AR) and studying the dynamics and feasibility of operation specific to exothermic systems.

Structured reactors are an alternative to fixed bed catalytic reactors and are reactors that have a regular structure or fixed spatial arrangement. Basic structure reactor types include monolith reactors, membrane reactors and arranged catalyst reactors. Conventional fixed bed catalytic reactors and therefore adsorptive reactors modelled on this principle exhibit drawbacks which include high pressure drop, solids handling and mal-distribution of gas flow which originates from the looser packing of the particles near reactor walls. This results in a non uniform access of reactants to the catalytic surface which worsens overall performance and gives rise to unexpected hot spots and thermal runaways as mentioned above. Structured reactors are promising as they eliminate the drawbacks of the fixed bed catalytic reactor and

significantly contribute to the search for better catalytic processes which improve activity, selectivity and also decrease operational costs through the decrease in pressure drop (Cybulski and Moulijn, 1998).

In the literature (see Chapter 2), structured bed configurations especially monoliths have been used extensively as either reactors or adsorbers, but little or no attention has been given to their combined use as multi-functional reactors. Monolithic reactors are used in catalytic combustion and a major application is in the catalytic converter system for automobiles. Conventionally in an adsorptive reactor, the adsorbent and catalyst particles are randomly packed in a fixed bed. In structured reactors, the catalysts may be supported on channel walls or on a catalytic support and the adsorber may consist of the reactor material itself.

This hybrid configuration employs aspects of thermal and concentration swing adsorption and the effective utilisation and integration of heat/energy.The design methodology involves the development of 2D mathematical models and the use of model-based optimisation techniques. The model equations are solved within the *gPROMS* simulation environment. The overall performance of the reactor is dependent on the complete function of the design parameters, operating conditions and properties of the adsorbent, catalyst and reaction mixture. The performance of the M-AR is compared to that of a conventional monolith reactor (M-RXTN) in terms of conversion, thermal stability and energy utilisation.

Finally, analytical scaling rules are derived in order to enable process transformation to meet new and/or additional system specifications for a given desired reactor performance (e.g. conversion, energy input) without recourse to further simulation.

The remainder of this thesis is divided into 5 main chapters namely:

- Chapter 2: Background and Literature Review

  This chapter outlines the basic concepts of adsorption and adsorptive – reactor processes. A brief overview of monolith reactors and their applications in the field of adsorption and catalytic reaction for VOC oxidation is also presented. Reviews of past and present developments within this field are also presented with the aim of supporting the research questions raised in this work.

- Chapter 3: Modelling Adsorptive Reactors

  This chapter presents mathematical models for the integrated adsorber-reactor proposed in this work. The equations are described in partial differential and algebraic equations to depict the transport phenomena as well as adsorption and reaction processes occuring in the system.

- Chapter 4: Results and Discussion - Monolith and Packed Bed Configurations

  The model equations described in Chapter 3 are applied to the VOC oxidation case study. Results and discussions focus mainly on comparisons of the performance of the conventional monolith reactor, M-RXTN and the M-AR.

- Chapter 5: Process Optimisation and Scaling Rules

  In this chapter an optimisation strategy is formulated together with the model equations described in Chapter 3 and applied to the VOC oxidaton case study. Scaling rules are also derived and applied to the M-AR process.

- Chapter 6: Conclusions and Recommendations for Future Work

  The final chapter presents an overall conclusion of the research work undertaken with recommendations for further future work.

CHAPTER 2: BACKGROUND AND LITERATURE REVIEW

2.1 Introduction

Volatile organic compounds (VOCs) are organic substances characterised by their high vapour pressure at ambient temperature and their low boiling point (Hunter and Oyama, 2000). They are environmentally damaging chemicals emitted into the air from chemical, petro-chemical and allied industries. In the atmosphere, they can react with nitrogen oxides (NO*x*) to produce ozone (O_3) which is highly toxic for the environment and human health (Valdes-Solis *et al.*, 2004). Growing environmental awareness has led to stringent regulations to control VOC emissions and as a result a disposal process with high efficiency, reliability and cost effectiveness is necessary to destroy these harmful compounds.

There are many different techniques available to control VOC emission. An effective and efficient method, though limited in applicability is the modification in itself of process equipment, raw materials and/or change of process. Khan and Ghoshal (2000) have reviewed other techniques which include destruction-based methods (*e.g.* thermal oxidation, catalytic oxidation, biological treatment) and recovery based methods (*e.g.* condensation, absorption, adsorption coupled with desorption, membrane based recovery), which convert the VOCs into harmless

products – carbon dioxide and water vapour. The major problem however with the above VOC technologies is the increase of energy consumption for gas purification with a decrease of VOC concentration in the waste gases (Zagoruiko *et al.*, 1996).

This work proposes the adsorptive reactor as a viable alternative for VOC disposal. The adsorptive reactor combines adsorptive separation and oxidation of the VOC in a single reactor unit and is thought to make effective utilization of energy due to efficient heat integration. It is interesting to note that the concept of the adsorptive reactor makes use of both the destructive based method of catalytic VOC oxidation and the recovery based method of adsorption mentioned above and discussed in greater detail by Khan and Ghoshal (2000).

The literature review and background of the thesis are presented in this chapter. Section 2.2 outlines the fundamental principles of adsorption within a solid particle including adsorption isotherms, and mass and heat transport of the adsorbate within the solid particle. The description of periodic adsorption processes and periodic adsorptive reactors are presented in Section 2.3 and 2.4 respectively. Section 2.5 focuses on the adsorbent, describing in general the primary requirements of an effective adsorbent and describing in detail the two common adsorbent types – activated carbon and zeolites. Finally, Section 2.6 gives a comprehensive description and review of the Monolith reactor with emphasis on the utilisation of the monolith for adsorption purposes and for catalytic combustion.

2.2 Adsorption Principles

2.2.1 Adsorption

The term adsorption is believed to have been first introduced by Kayser in 1881 to describe his observations of the condensation of gases on free surfaces, a phenomenon discovered independently by both Scheele and Fontana some years earlier (Fontana 1777, McBain 1932). Adsorption is a surface phenomenon and is defined as a process in which fluid molecules e.g. gas/liquid (adsorbate) come into contact with forces acting on a solid surface forming an adsorbed phase. Depending on the type of forces between the fluid molecules and solid molecules adsorption may be classified as chemisorption or physisorption. Most applications of adsorption in separation and purification processes depend on physical adsorption (Ruthven, 1997) where surface attraction is due to weak van der Waals forces. Chemisorption shows many characteristics of chemical reactions – it generally takes place at temperatures greater than 200°C and may be slow and irreversible (Seader and Henley, 1998). The initial amounts adsorbed increases with temperature. The rate of chemical adsorption is relatively fast at first and then slows. Physisorption occurs at the location of the adsorption site and is readily reversible with respect to temperature and pressure whereas with chemisorption, removal even by heating and evacuation is difficult. Physical adsorption is therefore more useful for developing practical periodic adsorption processes as it is easier to reverse the adsorption (*i.e.* regenerate the original solid phase) by manipulating the external operating conditions (Ruthven, 1994).

The mechanism via which surface adsorption occurs is very complex. The molecules/atoms/ions in a gas or liquid diffuse to the surface of a solid where they bond with the solid surface or are held by weak intermolecular forces (Seader and Hendley, 1998). Many theories have been formulated to explain adsorption, details of which can be found in the literature.

In general, adsorptive processes are exothermic. The heat of adsorption due to surface attraction is much greater than the heat of condensation of gases being adsorbed. The amount of gas adsorbed by physical adsorption at a given pressure increases as the saturation temperature is approached. At a given temperature and pressure the amount of gas adsorbed increases with the normal boiling point of the gas or with the critical temperature and decreases as the temperature is increased.

2.2.2 Adsorption within a Solid Particle

In order to adsorb the maximum amount of adsorbate, a large surface area per unit volume is required by the solid adsorbent and as such commercial adsorbents are usually produced from micro-porous materials through which the gas molecules diffuse. The gas molecules are adsorbed onto the solid surface until their concentration in the gaseous phase is equal to the equilibrium value corresponding to the adsorbed phase concentration. The rate at which the adsorbate is adsorbed onto the solid surface is directly related to the concentration in the micro-pores and the presence of free active sites.

A typical porous particle consists of both macro-pores and micro-pores. The macro-pore is the empty space between the micro-particles. The micro-pores are the pores within the micro-particles which contain active site deposits for adsorption. Concentration gradients exist across the film boundary surrounding the particle, and within the particle itself, in non-equilibrium operations.

The process of adsorption and desorption can be viewed as involving a number of sequential steps at the microscopic level:

1. The adsorbate diffuses from the bulk fluid to the external surface of the pellet.
2. The adsorbate diffuses from the external surface of the pellet into and through the macro-pores.
3. The adsorbate diffuses through micro-pores.
4. The adsorbate is adsorbed onto the surface of the micro-pores.
5. The adsorbate is desorbed off the surface of the micro-pores.
6. The adsorbate diffuses from the micro-pores into macro-pores.
7. The adsorbate diffuses from the macro-pores to the surface of the pellet.
8. The adsorbate is transported back into the bulk fluid.

The gas phase diffusion occurring in the pores of a particle depends on the relative magnitude of the pore diameter and the mean free path of the adsorbate under the operating conditions in the pores (Coulson *et al.*, 1975). Pores are classified as micro-pores ($d_{pore} < 3 \times 10^{-10}$m), macro-pores

(d_{pore}> 200 x 10^{-10} m) and meso-pores (3 x 10^{-10} m < d_{pore}< 200 x 10^{-10} m) (Treybal, 1980). Mass transport within each type of pores (*intra-particle*) can be classified as detailed below:

1. *Molecular and Knudsen diffusion:* The ratio of the pore diameter to mean free path of the fluid, γ, is established to determine whether the pore wall affects the diffusion behaviour or not. When $d_{pore} >> \gamma$, collisions among the adsorbate molecules are far more than between the adsorbate molecules and the pore wall, *i.e.* molecular diffusion, D_m dominates. When $d_{pore} << \gamma$, fluid-fluid collisions are no longer frequent and Knudsen diffusion dominates.

2. *Surface diffusion:* The adsorbate molecule diffuses along the micro-pore wall surface which results in adsorbate concentration gradients on the wall surface. Many researchers consider surface diffusion, also termed micro-pore diffusion (Ruthven, 1984; Yang, 1987; van den Broeke, 1994; Ruthven *et al.*, 1994) to be the dominant transport mechanism for diffusion in micro-pores and this is especially important for activated carbon based processes (Doong and Yang, 1987; Kapoor and Yang, 1991). For zeolite particles, surface diffusion is insignificant, since adsorption onto the macro-porous mix (binder phase) is negligible.

3. *Hydrodynamic flow:* Pressure gradient within the pore may lead to a hydrodynamic flow of gas. This effect can usually be neglected for operation in an adsorber bed since pressure gradient across an

individual particle is small in comparison with pressure drop across the bed.

In addition to the types of intra-particle diffusion described above, there is also mass transfer through a stagnant gas layer (or film) around the exterior surface of a particle *i.e.* extra-particle diffusion, commonly known as film diffusion. The importance of film diffusion on the overall gas-solid mass transport can be approximated by the characteristic time constant based on Stefan's law of diffusion (Yongsunthon, 1999). Detailed calculations of intraparticle and extraparticle diffusions for VOC adsorption on activated carbon adsorbent are given in Appendix A.

2.2.3 Adsorption Isotherms

The quantity of a species adsorbed is generally characterized by an isotherm, which is a plot of the fraction of the surface covered with a specific adsorbed atom or molecule (θ) versus the gas phase partial pressure at a fixed temperature. The relationship between the equilibrium amount of component *i*, adsorbed onto the adsorbent, q_i^* (mol kg^{-1}), and the gas phase partial pressure, P_i (Pa), at a given temperature, T, is referred to as the adsorption isotherm and expressed in the general mathematical form as follows:

$$[q_i^*]_T = q_i^*(P_i) \qquad (2.1)$$

For a host of adsorbents *e.g.* zeolites, activated carbon; adsorption isotherms are of Type I in terms of the Brunauer, Deming, Deming and Teller classification (BDDT) and can be adequately represented by Tóth or Langmurian models. This work focuses on the use of activated carbon as an adsorbent and the Tóth isotherm is used. For more details on the Tóth isotherm, see Section 3.2.

2.2.4 Adsorbate - Particle Mass Transport

Gas-solid mass transfer resistances determine the rate of adsorption of a molecule onto the adsorbent particle. These may either be due to the internal particle structure i.e. intra-particle resistance, or due to an external fluid film surrounding a particle, i.e. extra-particle resistance or a combination of both (see Section 2.2.2).

For mathematical modelling, in describing the transportation of the adsorbate to the adsorbent it is useful to identify the rate controlling step, i.e. that offering the highest resistance to mass transfer. All other steps can then be omitted from the model. In the case of intra-particle mass transfer limitations, they mainly arise from the micro-porous structure of adsorbents and are dependent on the pore diameter distribution.

The three most widely used ones are listed below:

- *Instantaneous local equilibrium model (ILE)*

  The instantaneous local equilibrium model is applicable when the mass transfer resistance between the gas and solid phases is

negligible. Under these circumstances, equilibrium between the gas and solid phases is reached instantaneously at all points in the adsorption bed. *ILE* is expressed by:

$$\frac{\partial q_i}{\partial t} = \frac{\partial q_i^*}{\partial t} \tag{2.2}$$

where q_i (mol kg^{-1}) is the amount of component *i* adsorbed on the pellet, and q^*_i (mol kg^{-1}) denotes the adsorbed amount on the pellet at equilibrium as determined by the adsorption isotherm (see Section 3.2).

- *Pore diffusion model*

  The pore diffusion model assumes that the rate of mass transfer is approximated as the fluxes at the pore mouths of the micro-particles by solving the diffusion equations for the micro-particle (Yang and Doong, 1985).

- *Linear driving force model (LDF)*

  In cases where mass transfer or diffusional resistances to adsorption are important, the linear driving force approximation of Glueckauf and Coates (1947) is often used. This model is given as:

$$\frac{\partial q}{\partial t} = k(q^* - q) \tag{2.3}$$

Where q, is the average adsorbed phase concentration, (mol kg^{-1}), q^*, (mol kg^{-1}) denotes the equilibrium adsorbed phase concentration (mol kg^{-1}), and k, the external film mass transfer coefficient (s^{-1}).

This is in contrast to the diffusion equation where the adsorbed concentration is dependent on the particle radius or plate thickness (see Alpay (1992)) expressed by:

$$\frac{\partial q_{ri}}{\partial t} = \frac{\overline{D}_{ei}}{r^2}\frac{\partial}{\partial r}\left(r^2 \frac{\partial q_{ri}}{\partial r}\right),\ \forall \in (0, R_p), t \geq 0 \qquad (2.4)$$

where q_{ri} denotes the solid phase adsorbed concentration of component *i*, r, the radial position within a spherical particle of radius R_p (m), and $\overline{D_{ei}}$ the modified effective diffusivity of component *i*, ($m^2\ s^{-1}$).

For the solution of an actual separation process, Eq. (2.4) must be solved simultaneously with the inter-pellet material balances, which can be quite computationally demanding. For computational convenience, therefore, the adsorbed phase concentration is often expressed as the adsorbed phase concentration averaged over the entire volume of a particle radius R_p, i.e.

$$q = \frac{3}{R_p^3}\int_0^{R_P} q_{ri} r^2 dr \qquad (2.5)$$

With this simplification, Eq. (2.4) can be approximated by the adsorption rate, $\frac{dq_i}{dt}$, in a simpler form, such as the linear driving force (LDF) model as was first suggested by Glueckauf and Coates(1947) or other non-linear driving force models (Vermuelen, 1984; Do and Rice, 1986).

In depth research into the LDF models have been performed by Alpay and Scott (1992), Carta (1995), Sheng and Costa (1997), Choong and Scott (1998) and more recently, Rouse (2004).

2.2.5 Adsorbate – Particle Heat Transfer

Heat release and consumption by reaction and adsorption /desorption results in a deviation from the isothermal bed situation. The heat transport processes at any given location in the bed are never at steady state. The temperature profiles inside and outside of a given particle is continually changing until the particle is totally saturated. The relative magnitudes of the differentials inside and outside the particle reflect the relative importance of resistances. These heat transfer resistances arise from the external gas film and/or within the particle itself. For typical periodic adsorption processes, the rate controlling step is that in the external film (Ruthven, 1984; Alpay, 1992). When the heat transfer resistance between the solid particle and the gas phase is negligible, instantaneous thermal equilibrium is established between the two phases. When the heat transfer resistances are important the two phases are of different temperatures requiring a separate energy balance for

each phase. In this work, instantaneous thermal equilibrium is assumed due to the physical properties and the operating nature of combined adsorption and reaction. Therefore a homogeneous energy balance is also assumed; see also Eqs. ((3.25) and (3.26)) in Chapter 3 and Appendix B for further discussion and justifications.

2.2.6 Desorption

A given adsorbent has a finite capacity for a given adsorbate, and adsorption is terminated when the solid is saturated with the adsorbate. Desorption or regeneration as it more commonly known restores the adsorption capacity of the spent adsorbent and thus recovery of the pure adsorbate is possible. Desorption occurs in one of the following ways (see Ruthven, 1984):

- Thermal swing whereby the solid bed is heated by a hot gas purge.
- Pressure swing whereby the system pressure is reduced to desorb the adsorbate and the bed is purged at low pressure.
- Purge gas stripping whereby the bed is purged with a non-adsorbing and inert fluid.
- Displacement desorption whereby the adsorbate is displaced by purging the bed with a stream containing a competitively adsorbing species.

For a practical adsorptive reactor process, the regeneration itself is of more importance than adsorption. Rodrigues *et al.* (2002), suggest that

the choice of the regeneration process is mainly determined by the choice of the adsorption isotherm and that one single process is not sufficient enough to efficiently accomplish adsorbent regeneration. Thus, hybrid regeneration processes are necessary e.g. pressure swing coupled with intermediate purge. The authors found that combining a low pressure purge step (as in the case of hydrogen production, see Hufton *et al.*, (2001)), with thermal swing could be a better method to regenerate the adsorbent. This is called reaction-enhanced desorption process and is termed reactive regeneration. Adsorbent regeneration is accomplished in this work based on these principles via concentration swing (altering the fluid phase composition so as to control the direction of the adsorption) and thermal swing.

2.3 Periodic Adsorption Processes

Periodic adsorption processes (PAPs) involve adsorption and desorption steps operating in sequence over a fixed time cycle in one or more packed beds. Cyclic (semi-batch) adsorption processes are grouped according to the regeneration methods employed. The two main mechanisms are pressure swing and temperature swing discussed briefly in Sections 2.3.1 and 2.3.2.

PAPs are intrinsically dynamic, never being allowed to reach steady state as no useful separation can be achieved at the latter. After a sufficiently large number of cycles, each bed in the process normally

reaches a *cyclic steady state* (CSS) in which the conditions in the bed at the end of each cycle are exactly the same as those at the beginning of the cycle. Although the number of cycles required to reach CSS can be large, typically it is relatively small in comparison to the total number of cycles between successive process start-ups and shut-downs. Thus, most PAPs are practically at CSS for most of their useful operation. As a result, it is this CSS that determines their technical and economic performance.

2.3.1 Pressure Swing Adsorption

Pressure swing adsorption can be divided into three groups:

- Pressure swing adsorption (PSA)
- Rapid pressure swing adsorption (RPSA)
- Single and dual piston-driven PSA

Extensive research has been carried out on PSA processes. These include operational configurations for PSA and RPSA e.g. multi-step and multi-bed processes, piston driven ultra rapid PSA and radial flow bed geometry (see Liow and Kenney, 1990; Kumar, 1994; Singh and Jones, 1997; Ritter and Liu, 1998). Process optimisation techniques include mixed-integer linear programming (MILP) and mixed-integer non-linear programming (MINLP) which involve discrete decisions such as the number of beds and step scheduling (see Smith & Westerberg, 1990 ; Nilchan & Pantelides, 1998). Analyses of LDF and pore diffusion models have also been investigated (Lu *et al.*, 1993, Alpay *et al.*, 1994; Crittenden *et al.*, 1994). Cyclic steady state determination and the existence of

multiple steady states have also been researched into by Ritter and Yang (1991) and Levan and Croft (1995).

PSA

Early reports of pressure swing adsorption (PSA) processes refer to Finlayson and Sharp (1932) and Kahle (1941), however Skarstrom (1960) and de Montgareuil and Domine (1964) are generally considered the inventors of pressure swing adsorption. Major applications include air separation, separation of normal and iso alkanes, natural gas dew-pointing, hydrogen recovery and purification (Yang, 1987; Ruthven et al., 1994). PSA technology has also been evaluated for the separation of alkenes and alkanes (Yang and Kikkinides, 1995; Rege *et al.*, 1998; Zhu *et al.*, 2000).

In PSA, adsorption takes place under high pressure where the gas flows through a packed bed of adsorbent and the strongly adsorbing components are retained on the adsorbent. The bed pressure is then reduced to desorb the adsorbate and thus the already adsorbed components are recovered at the exhaust stream (Sheik, 1999).

The basic steps of a PSA process consists of the following steps

- Pressurisation (I): the product end of the bed is closed and the bed is pressurised with the feed gas mixture. The step duration is normally short. The strongly adsorbed components accumulate on

the adsorbent while the weakly adsorbed (and/or non-adsorbed) components are enriched at the product end.

- Product release (II): the gas mixture flows through the bed. The concentration of the strongly adsorbed component increases on the adsorbent while the weakly adsorbed components are withdrawn at the product end.
- Depressurisation (III): the product end in this step is closed. Gas flows in the reverse direction to that of the previous steps. As the bed pressure drops, the adsorbed components desorb from the adsorbent and elute from the feed end of the bed.

Advantages of the PSA process include low maintenance, readily automated operation and system flexibility. However, the overall process is quite complex and requires a large number of beds. A commercial multi-bed PSA process would involve two to ten bed configurations, operated according to complicated cycle sequences (Doong and Yang, 1988) in order to facilitate regeneration. Additional steps such as purge and backfill are therefore included to improve the performance of the separation.

Comprehensive reviews on the PSA process can be found in Ruthven (1984), Ruthven *et al.*, (1994) and Suzuki (1990).

Rapid Pressure Swing Adsorption

Turnock and Kadlec (1971) developed the RPSA cycle as a simple alternative to the two-bed four cycle process using smaller particles and

a shorter cycle time for nitrogen and methane separation. RPSA is based on the same principle as PSA but the major difference lies in the use of smaller particles (typically 250 to 420 μm) which leads to steep and dynamic pressure gradients within the bed as opposed to the PSA process where the flow is minimised to reduce pressure drop across the bed by the use of larger particles. This leads to an internal purge that enhances the regeneration of the adsorbent. Short step times (seconds or sub seconds) are characteristic of rapid pressure swing operation.

The process consists of a single bed operated in two steps:

- Pressurisation: Feed at high pressure is fed to the bed and the strongly adsorbed components are retained in the bed whilst the weakly adsorbed or non-adsorbed components elute from the bed.
- Depressurisation: Accumulated gas is allowed to exit the bed from both ends and with a decrease in bed pressure, the adsorbed gases desorb.

For both PSA and RPSA there are numerous possibilities in the way the processes can be operated and configured (Yongsunthon, 1999). Some of the more important operating decisions include the feed conditions (temperature, pressure, composition); cycle operations (steps involved, step duration, feed delivery rates) and the number of beds and bed interactions.

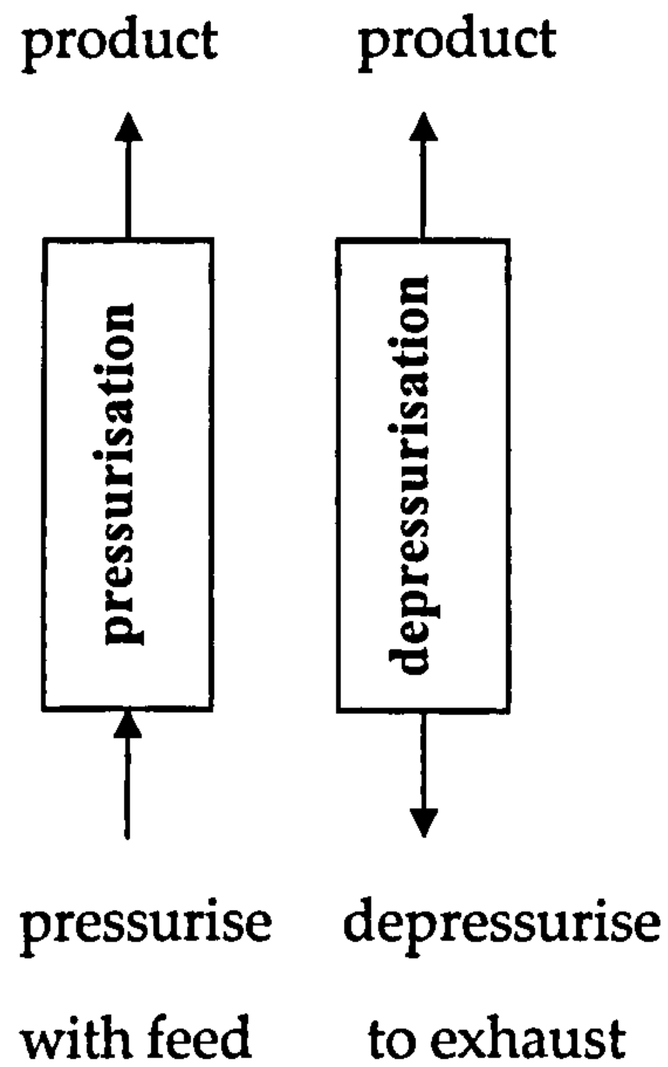

Fig 2.1: A general configuration of the rapid swing adsorption process

Modifications to the RPSA process were made through the work of Keller and Jones (1981) for air separation. The authors made changes employing an additional delay step to yield higher product recovery. During the delay step, the feed is closed but the product is still continuously withdrawn. It was shown that the modified RPSA may give higher product yields than the basic RPSA process but at the expense of higher feed gas pressure.

RPSA is suitable for separation of small to medium size gas streams. Its applications include oxygen production from air, hydrogen recovery, or recovery of valuable components in waste and vent streams (Jones and Keller, 1981). One major advantage of the RPSA process is its simplicity resulting in lower operating, capital and maintenance costs. It also often offers higher adsorbent productivity than multi-bed PSA processes since it requires lower adsorbent volume (Nilchan, 1997).

Work done by Alpay (1992) and Sheikh (1999) include other modifications to the RPSA also to obtain higher productivity. The major disadvantage of the RPSA is the large pressure drop across the bed (Kodde, 2001). Such a problem may be alleviated by implementing radial flow resistance distribution and considerably reduced adsorbent particle sizes in a radial flow RPSA configuration. This concept has been investigated experimentally by Chiang and Hong (1995). They conducted the experiment using a 75mm high annular basket of fine guaged stainless steel screen packed with three sizes of adsorbent particle, and fitted into a disk-shape container (as a replacement for the adsorption column) in order to force radial distribution of flow across the bed. When compared to an RPSA with axial flow, a lower pressure drop was obtained. The radial flow arrangement provides for a larger cross-sectional area for the same volume of bed packing and thus enables the use of smaller particle sizes for faster adsorption kinetics. This was further theoretically investigated by Huang and Chou (2003).

Single and dual piston-driven PSA

In his patent, Eriksson (1979) proposed a single piston system for nitrogen and air separation stating that the dynamics of such a system is achieved using a reciprocating moveable piston at each end of an adsorption column as the means of imposing cyclic gas flow and pressure variations on the gas mixture. Nitrogen is adsorbed at high pressure, whereby at this point a non-adsorbing gaseous mixture with a high content of oxygen passes through the bed. On expansion, the bed was flushed with non-adsorbed oxygen, and the nitrogen gas desorbs at

decreasing pressure. The patent claimed that the gas product, air, was far purer than that previously possible because part of the cycle was operated at partial vacuum (Rouse, 2004).

The dual piston-driven PSA was patented by Keller and Kuo (1982). Two driving pistons of unequal lengths were used to achieve high productivity separation of the components by gas volume displacement in the adsorption column at a reduced operating cost. Like the RPSA process, very rapid cycles were found to enhance the productivity of the process.

Suzuki *et.al*, (1997), demonstrated the use of a piston-driven ultra-rapid PSA (URPSA) process for CO_2 recovery and high capacity oxygen enrichment. The overall oxygen production capacity of the URPSA was found to be one order of magnitude higher than that of conventional PSA processes. The separation performance of this particular process was strongly dependent on the adsorbent particle size, which in turn affected the overall pressure drop and production rate of the adsorption bed.

Rouse (2004) carried out further experimental and theoretical studies on the exploitation of the dual piston-driven PSA system for CO_2 separation. The author tried to make the model more widely applicable for cyclic processes, through which a cycle time dependent parameter was introduced to modify the standard linear driving force (LDF)

equation. Implementation of phase lags and amplitude difference enabled the use of two parameters, which ensured that both bulk and adsorbed concentration profiles were accurately simulated. The selected activated carbon adsorbent extruded in monolith form was characterised using chromatography and zero length column (ZLC) techniques. The experiment was conducted in two columns for $CO_2 - N_2$ separation with column 1 configured in a honeycomb structure and in column 2, rectangular shaped carbon monoliths housed within an aluminium tubular casing. Parametric studies showed that employing a smaller monolith dimension led to better separation despite lower cycle times. However, there was significant pressure drop due to the small pipe work sections joining the composite sections of one of the columns. Under adsorbing total reflux conditions, good agreements were made of the pressure and cyclic steady state concentration profiles.

2.3.2 Temperature Swing Adsorption

Temperature swing adsorption (TSA) is a distinguished regeneration form of the PSA process based on thermal swing. After the onset of adsorption, by simply raising the temperature, the bed is regenerated co-currently or counter currently and purged with a pre-heated gas. Yongsunthon (1999) gives a comprehensive review of temperature swing adsorption. The regeneration step is the limiting factor in the design of the cyclic two bed process. The effectiveness of the regeneration is dependent upon the flow direction of the gas in which regeneration is performed and the initial adsorbate distribution on the solid phase. Regeneration carried out in the opposite axial direction to

the adsorption step is found to be more effective than the unidirectional operation of the two steps (Carter, 1975). The TSA operation is not very feasible for short cycle time and repeated thermal swing cycling. While short cycles reduce the duration necessary for bed heating and cooling. The increased frequency of thermal cycling tends to shorten the adsorbent life (Ruthven, 1984).

The effectiveness of the regeneration step depends on the intensity between the purge gas flow rate and the regeneration temperature. The combination of either a higher regeneration temperature coupled with a smaller purge gas flow rate or a relatively low temperature at high purge gas flow rate will be the cost-determining factor of a TSA process. Implementing reverse-flow regeneration instead of a forward-flow could prevent incomplete adsorbate removal (Ismail, 2006).

The efficiency of regeneration is dependent upon the amount of inert supplied during regeneration and the energy required to raise the purge gas or inert to the desired regeneration inlet temperature from a reference say, ambient temperature. For adiabatic operation, regeneration is complete when the effluent temperature reaches the regeneration inlet temperature. For non-adiabatic operation, complete regeneration is the duration for which the effluent gas concentration reduces to some small fraction, e.g. 1% of the feed concentration in the adsorption step.

Experimental and theoretical studies in this field are summarised below:

- Martin et al., (1997) show important energy saving implications for the thermal efficiency of adsorption processes. Adsorbents, degraded by coking must be periodically regenerated, which is an energy intensive process. Their work on coking and ageing has aided understanding of how these relate to adsorbent structure and hence allow for operation of these processes under conditions that require less frequent regeneration which in turn saves on energy.

- Purge gas consumption decreases with increasing temperature (Kumar and Dissinger, 1986; Schork and Fair, 1988). Energy requirement is an increasing function of both the regeneration temperature and the purge gas consumption; therefore it is at a minimum at an optimal purge gas temperature which in turn increases as the effluent gas concentration decreases. Incomplete regeneration may operationally be favourable (Huang *et al.*, 1993; Hwang *et al.*, 1997).

- Linear driving force mass transfer model provides an acceptable fit to the experimental adsorption and regeneration data (Kumar and Dissinger, 1986; Schork and Fair, 1988; Hwang *et al.*, 1997).

Research on complete cycle of thermal swing adsorption is relatively scant but a typical cycle consists of an adsorption step, desorption step and possibly a cooling step. Gas flow in both the desorption and cooling steps can be carried out either in the same or reverse axial direction as

the adsorption step. Desorption in the reverse step was found to be more energy efficient for a non uniform initial distribution of adsorbate on the solid phase. The duration of the desorption step has an effect on the speed of convergence towards cyclic steady state operation. Quicker steady state is achieved with a longer heating time and the reverse for shorter times. If regeneration is carried out to completion, cyclic steady state would be approached in one cycle, regardless of the initial bed conditions. A cool gas purge at the end of the desorption step can generally have an influence on the cycle efficiency, with the exception of when the thermal waves move faster than the concentration wave, such that breakthrough curves are independent of the initial bed temperature (Davis and LeVan, 1987). The norm is the thermal wave lagging behind the concentration wave and Davis and LeVan (1989) indicate from their theoretical and experimental results that a properly timed cooling step has a pronounced effect on the energy performance and purge gas use particularly for short regeneration times. They also suggested that an optimal cycle for adsorbate recovery using hot purge gas should involve a high-pressure heat-up step to create a high concentration plateau of adsorbate, followed by low-pressure purge.

2.4 Periodic Adsorptive Reactors

Adsorptive reactors are based on the principles of adsorption processes outlined above but couple reaction as well into a single unit operation. Insight into the interaction of local adsorption separation and the

kinetics and thermodynamics of the chemical reaction over an admixture of (solid) catalyst and adsorbent is therefore required. Adsorbate recovery depends on the strength of adsorbates for complete desorption and can be accomplished by imposing forced-periodic variations in gas concentration, pressure or temperature, which lead to a variety of reactor configurations. The objective in all cases is to achieve some degree of separation of the products and / or reactants by selective adsorption and also to increase catalyst productivity. Recent works have shown the enhancement of yield with simultaneous adsorption and reaction. One example proposed by Shiekh *et al.,* (1998) showed the performance of a well mixed reactor where he showed that conversion could be improved by selective adsorption of one or more product components. Industrial scale applications of adsorptive reactors are relatively few; moving bed applications exist and include the Molex, Parex and Sorbex processes of UOP to separate linear and branched alkanes, para-xylene and meta-xylene respectively (Ruthven and Ching, 1989). Major challenges involve materials development of catalysts and adsorbents and same temperature operation for both reaction and adsorption in order to increase the yield / selectivity (Stankiewicz, 2003).

2.4.1 General operating principles of the adsorptive reactor

There are several general operating principles which can be applied to the adsorptive reactor to aid realisation of the benefits of combined separation and reaction. These are described briefly below:

Removal of reaction products

This is of particular importance in reversible reactions where the removal of one or more of the reaction products from the reactive phase will favour the forward reaction and lead to increased conversion. This principle is by far the most widely applied and may allow for lower operating temperatures or smaller equipment (see Alpay *et al.*, 1994; Carvill *et al.*, 1996; Sheikh *et al.*, 1999).

Controlled addition of reactants

Reactants are normally pre-mixed in a single feed stream in traditional reactors, however reactants may also be fed in a staged and controlled manner, thereby keeping the average concentration of the staged specie low (Kodde, 2001). This may reduce undesirable side reactions and may circumvent the use of the stoichiometric excess of one reactant, which would lead to a recycle stream. More importantly, the controlled addition of a reactant may prevent entering regions of explosion limits, and thus control runaway which is an important issue in this work.

Reactant staging / accumulation

The accumulation of a reactant in the reactor vessel can be advantageous as one can increase the residence time of a reactant and thus increase its conversion (Kodde, 2001). This application is widely used in chromatographic reactors. A buffer of the reactant species can be formed, which makes the process less sensitive to fluctuations in the feed concentrations of another reactant. The selective reduction of NO with NH_3 uses this principle.

The adsorptive reactor is an inherent dynamic process, which is operated cyclically due to the need for periodic regeneration of the adsorbent as described earlier. Extensive research has been carried out for the different types of adsorptive reactors, as discussed below:

2.4.2 Chromatographic reactors

The chromatographic reactor is the earliest example of processes which integrate reaction and adsorption (see Roginskii *et al.*, 1961; Magee, 1963; Loureiro and Rodrigues, 1989). Extensions of this include the real and moving bed reactors and further extensions, in the form of periodic adsorption processes which are used to combat the major disadvantages of non-continuity and complex operations common to the chromatographic type reactor.

The chromatographic reactor involves a packed bed filled with both catalyst and adsorbent. (Kodde (2001) discusses several advantages and disadvantages of these reactors. Drawbacks include the large amount of eluent required for separation leading to highly diluted products and batch operation. Advantages over traditional reactions include increase of conversion in equilibrium limited reactions (Gore, 1967) and increase in breakthrough time of the reactant (Loureiro *et al.*, 1990).

2.4.3 Simulated moving bed reactors

An extension of the chromatographic reactor, the reactants are fed from the top of the reactor and flow downwards while the inert carrier gas flows upwards (Sheikh, 1999). The operation demonstrates counter-

current flow, though a major disadvantage is the fact that significant heating and cooling equipment is required to maintain the temperature conditions. An advantage, however as reviewed by Bjorkland and Carr (1995) is the fact that adsorption can be further split in two and intermediate product retrieval of very strongly adsorbed species is possible. Recent patent literature on simulated moving bed reactors can be read by Funk et al., (1995) and Dandekar et al., (1998).

2.4.4 Pressure Swing Reactors

The three steps of pressurisation, product release and counter current depressurisation as in PSA constitute the simple pressure swing reactor (PSR) cycle. One practical significance of conversion enhancement by PSA is a lower temperature operation which leads to energy saving and minimum degree of catalyst deactivation (Chatsiriwech *et al.*, 1994).

The PSR is a packed bed with a mixture of active catalyst and a selective adsorbent and during the pressurisation and product release steps, simultaneous reaction and adsorption occurs. In order to achieve continuous flow of exit gases, two beds are normally coupled. Other steps can be incorporated into the simple cycle to enhance product recovery or bed regeneration. For the latter one such employed is the counter current purge step.

The simplest configuration consists of two reactors individually packed with an admixture of catalyst and adsorbent, and involves three steps:

- Pressurisation: Simultaneous reaction and adsorption takes place at high pressure. The local removal of a strongly adsorbed component by adsorption at high pressure may favourably shift the reaction equilibrium towards further product formation
- Product release step: Enriched stream of weakly adsorbed components are withdrawn out of the product end
- Depressurisation: The reduction of total pressure resulting in desorption of the adsorbate which is subsequently eluded as exhaust from the bed.

Pressure swing operation of reversible reactions with regards to single or multiple products have been studied theoretically by (Chatsiriwech *et al.*,1994; Alpay *et al.*, 1994) and experimentally (Alpay *et al.*, 1994; Carvill *et al.*, 1996; Hufton *et al.*, 1999 and 2001; Ding and Alpay, 2000).

An important experimental achievement for PSR operation was carried out by Carvill et al., (1996) for the water gas shift reaction ($CO_2 + H_2 \Leftrightarrow H_20 + CO$) with the preferential adsorption of H_2O. The operation referred to as SERP (Sorption- enhanced reaction process) involved five steps in the sequence (1) product release, (2) depressurisation (3) purge (4) product CO purge and (5) product pressurisation. SERP was operated at a temperature of 523K to achieve 36% conversion (*c.f.* 9.8% in PFR at same operating temperature).

Waldron *et al.*, (2001) described the cyclic performance of the SERP concept for hydrogen production from a fixed bed reactor packed with

an admixture of a propriety SMR catalyst (noble metal on alumina) and a propriety CO_2 adsorbent, pelletized potassium carbonate promoted hydrotalcite as described by Hufton et al., (1999) for the selective removal of CO_2 using a pilot scale apparatus. Using the principles of PSA carried out over a moderate temperature range ~ 450 – 550°C (*c.f.* 800-900°C in conventional SMR packed with reforming catalyst only) and pressures between 180-450 kPa, the process was capable of producing directly 88-95% of H_2 with methane as the primary impurity. Since then, a number of studies relating to the SERP concept for the SMR process operated in the PSR have been carried out. Modifications are made to the adsorbent through the use of different precursors and a diverse range of operating conditions explored. Examples include work done by Ding and Alpay (2000), Xiu *et al.*, (2002) and the authors reviewed by them.

Kodde (2001), investigated the performance of a cooled packed bed admixed with a sorbent and catalyst and operated in a pressure swing mode. This unit was used to carry out the exothermic series reaction $\mathbf{A} \xrightarrow{+D} \mathbf{B} \xrightarrow{+D} \mathbf{C}$ where the feed stream consisted of a mixture of A and B and A removed by selective adsorption and D introduced to selectively react with A in the B depleted reactor. The author demonstrated that the heat generated by the exothermic reaction and adsorption does not render the PSR concept inviable as the heat of reaction may be utilized to accelerate sorbent regeneration, though the adsorbent capacity decreases. Overall this system, allowed for increased intermediate product selectivity.

2.4.5 Rapid Pressure Swing Reactors

Rapid pressure swing reactors (RPSR) employ the principle of pressurisation and counter current depressurisation although relatively short cycles and small adsorbent particles are utilized. The pressure damping effect of the bed results in an approximate constant pressure in the product end of the bed and thus a constant delivery of product without the need for sequencing a second bed and makes for an attractive alternative to the PSR as higher adsorbent / productivity is attainable (Sheik, 1999).

Early theoretical (Vaporciyan and Kadlec, 1987) and experimental work (Vaporciyan and Kadlec, 1989) evaluated a three step (pressurisation, delay and depressurisation) RPSR process. The product stream, consisting of reactants and products was continuously withdrawn from the reactor during all steps. The experimental study, was carried out for the oxidation of CO to CO_2 using a mixture of supported platinum catalyst and zeolite 5A as the selective adsorbent for CO_2. The reactants were diluted with N_2 to maintain isothermal operation. Enhanced conversion was demonstrated over a conventional reactor but a separation inversion i.e. high concentration of CO_2 eluting from the bed during the pressurisation step rather than the depressurisation step was observed when the O_2 feed concentration was low.

Alpay (1992) also reported on separation inversion behaviour from strong adsorption of a reactant component. For the reaction scheme $A \Leftrightarrow 2B$, with fast reaction kinetics, and an adsorbent capacity of A

greater than that of B, separation inversion was apparent due to the large conversion of A during the depressurisation step.

Cheng *et al.,* (1998) optimised a two step (pressurisation and depressurisation) RPSAR process. The system was applied to the reversible dissociation reaction $2A \Leftrightarrow B + C$ with C being the only adsorbed component. The authors addressed the issue of direct cyclic steady state determination and an optimisation formulated to determine the optimal operating policy (cycle times, feed pressures and product flow rates) which maximised the yield of C whilst maintaining minimum product stream purity. A 32% increase in conversion was achieved, while the stream purity of B was 95%.

The RPSR performance has also been theoretically and experimentally investigated for the in situ reaction-separation of 1-butene dehydrogenation as reported in the work of Sheikh *et al.,* (2001). The dehydrogenation reaction scheme in the form $A \Leftrightarrow B + C$ was theoretically analysed with particular emphasis on the relative effects of adsorption and reaction parameters on conversion enhancement. Simulation results were mostly in good agreement with the experimental results. For further information see Sheikh (1999) and Sheikh *et al.,* (2001).

2.4.6 Hybrid PSA/RPSA Reactor

Lu and Rodrigues (1994) studied reversible reaction schemes in a hybrid PSA/RPSA. Small adsorbents and catalysts were used and significant

pressure profiles developed in the axial axis of the reactor. The exhaust step in the RPSA cycle was replaced by the counter current purge of the PSA cycle. Conversion beyond the steady state limit was shown for this system. They also investigated an alternative purge step where the purge gas is introduced at both ends of the reactor and withdrawn in the middle. This yielded an even higher conversion.

2.4.7 Temperature Swing Reactor

In the temperature swing reactor (TSR), the pressure swing principle is replaced by a temperature swing. That is following the reaction / separation step in the cycle, the adsorbent is regenerated and one or more of the products is released by flushing the bed (co-currently or counter currently) with a hot inert gas to achieve desorption. The key point here is the fact that the energy used for desorption is not wasted but is used to preheat the bed for the subsequent step in the cycle and to also provide the heat to drive the endothermic reaction.

Yongsonthon and Alpay (1999) carried out theoretical work using the TSR process for the endothermic dehydrogenation of methylcyclohexane to toluene (represented by the reaction scheme $A \Leftrightarrow B + 3C$) over an admixture of platinum-alumina catalyst and zeolite 5A adsorbent. Two process configurations were considered – single and multi-stage. Preferential adsorption of component B increased as the temperature decreased, which increased the overall rate of reaction due to a favourable shift of reaction equilibrium. In the second step of the single step system, the adsorbent was regenerated by feeding hot inert gas

operated in either unidirectional or reverse flow. The hot purge gas also supplied the reaction heat by means of bed reheat. Multi-stage configurations were also employed using series and mixed series-parallel connections in either one of the above flow directions. Optimal results were observed using the multi-stage configuration involving mixed series-parallel connections of the stages and the disproportional splitting of feed streams to each stage. Substantial conversion enhancement as well as bulk gas separation was achieved at no additional energy input. This is an example of the possible reactor configurations that can increase the efficiency of a reactor system by taking advantage of the thermal effects associated with heat of reactions as studied extensively by Yongsunthon and Alpay (1998 & 1999).

2.5 The Adsorbent

The first and most important issue in any adsorption process is to find an appropriate sorbent for the proposed separation (Kikkinides *et al.*, 1993). In order to make the system efficient, the properties of the adsorbent must complement the design of the adsorptive separation process (Sircar, 1994). The accelerated growth in the field of adsorption is made possible by the commercial availability of a large spectrum of microporous adsorbents such as activated carbon, silica gel, aluminas, polymeric adsorbents and zeolites, and the various process designs under the generic category of pressure swing adsorption (PSA) and thermal swing adsorption (TSA) (Sircar *et al.*, 1995).

The primary requirements of an effective adsorbent are its selectivity, capacity and stability at a specified temperature and pressure. Commercial adsorbents may be thermodynamically selective or kinetically selective. In the former, the adsorbent selectively retains one or more of the adsorbates depending on their equilibrium affinity. In kinetic selectivity the relative adsorption depends on the differences of intra-particle diffusion rates amongst the different adsorbents. Adsorbent capacity is the maximum loading of an adsorbent with an adsorbate within the specified operating conditions while adsorption stability refers to the chemical and physical stability of the adsorbent under the operating conditions specified. In addition to the above criteria, depending on whether there is moisture in the process, the hydrophobicity of the material is important, as is, of course, the cost (Rouse, 2004). Of the adsorbents, zeolites and carbon molecular sieves are the most frequently used in commercial gas-solid physisorption processes.

2.5.1 Activated carbon adsorption

Activated carbon consists of thermally decomposed carbonaceous material, which is chemically treated to form an adsorbent of defined pore size distribution. Carbon adsorption systems are usually flexible and inexpensive to operate. Activated carbon makes a good adsorbent because of its large specific surface area, high micro-pore volumes and rapid adsorption capabilities. Activated carbon offers a large spectrum of pore structures and surface chemistry for adsorption of gases, which are being used to design practical pressure swing and thermal swing

adsorption processes for separation and purification of gas mixtures as well as in the characterisation of porous solids.

There are many different brands of activated carbon to choose from and their properties depend on the starting material and the manufacturing process (Zhu *et al.*, 2004). Different percursors, methods of carbonization and activation procedures have been used by many commercial manufacturers to produce a large variety of activated carbons for gas separation applications (Sircar *et al.*, 1996). In general, micro-porous activated carbon has a much higher surface area compared to that of zeolites, resulting in a higher adsorption capacity for non polar adsorptives (Zhu *et al.*, 2004) and is often preferred over zeolite adsorbents in a gas separation process because of their relatively moderate strengths of adsorption as they can easily be regenerated.

A number of commercially produced activated carbons, have different cumulative pore size distributions : mean pore size of these carbons can be of the order of the molecular diameter of the gaseous adsorbates (3-5 Å for molecular sieve carbons) and several times bigger than that (20-50) for others. These large differences in the physico-chemical properties of different activated carbons generate a large difference and therefore choice in the adsorptive characteristics of the components of the gas mixture to be separated.

Table (2.1) compares the performance of the steam reforming (SR) process for cleaning a 1 MMSCFD air stream containing 260 ppm vinyl

chloride monomer to a level of 1 ppm with that of a plug flow catalytic reactor using standard oxidation catalyst at 600K. The adsorbent catalyst used in this case was RB carbon impregnated with 1.5 wt% palladium chloride as the oxidation catalyst (Sircar *et al.*, 1996).

	SR Process	**Catalytic combustion**
Energy (MM BTU/h)	0.012	0.41
Adsorbent-catalyst (lbs)	5700	800

Table 2.1: Energy saving for Sorption-reaction process (Sircar *et al.*, 1996)

In the literature it is suggested that adsorption units based on activated carbon can reduce up to 99% of VOC present in the gas stream at concentrations below 5000ppm. Typical activated carbons are obtained in finely powdered form or in granular form. As mentioned in Section 2.1, the removal of VOCs is commonly performed by adsorption and is of great interest in air quality control. At a low-concentration level, adsorption on active carbon is the most employed method for the removal of VOCs (Centeno *et al.*, 2003; Fuertes *et al.*, 2003). Granular active carbon has been employed as an adsorbent for the removal and recovery of organic solvents due to its low costs (Valdes-Solis *et al.*, 2004) and its relative insensitivity to water vapour at a relative humidity of below 50% (Zerbonia *et al.*, 1995). However, despite the widespread utilization of granular beds there are drawbacks of high pressure drop associated with the flow of gas through the packed media, attrition of granular material, channelling, gas bypassing, etc. An alternate adsorbent material that overcomes these drawbacks is activated carbon

fibres, obtained from the carbonisation and activation of polymeric fibres diameters in the range of 10-20μm. This small diameter enables for homogeneous activation of fibres yielding a material with a narrow pore size distribution in the micro-pore range (Marban *et al.*, 2006).

More importantly, there is wide pore distribution which has negative effects for VOC adsorption. During the adsorption stage of low concentration VOCs micro-pores (in ambient air environments) rather than macro and meso-pores are preferentially filled at low pressures due to the overlapping of the attractive forces of opposite pore walls. This is fully described in the literature (Foster *et al.*, 1992; Derbyshire *et al.*, 2001).

Activated carbons offer a special advantage for VOC removal application because of their relative hydrophobicity. A significant adsorption capacity can be achieved when the feed gas is wet. Most polar substances like zeolites, silica and alumina gels adsorb very little hydrocarbon under moist conditions (Sircar *et al.*, 1996).

2.5.2 Zeolite based adsorption

Most literature indicates that activated carbon is the most suitable adsorbent for VOC removal. However, Blocki (1993) outlined the disadvantages of activated carbon. They are flammable, difficult to regenerate for high boiling point solvents, promote polymerisation or oxidation of some solvents to toxic or insoluble compounds and require humidity control. Hydrophobic zeolite is also now considered an

alternative adsorbent as it has good properties such as thermal stability and hydrophobicity (Takeuchi *et al.*, 1995, Tsai *et al.*, 1996) however, zeolite adsorbs water very strongly and is very difficult to desorb, and the process is very energy intensive.

Zeolites are crystalline aluminosilicates of alkali and alkali earth metals that have fixed pore sizes. The homogenous pore size prevents molecules larger than a certain size from entering the lattice so zeolites are sometimes called molecular sieves which allows them to adsorb selectively. The non-flammable, thermally stable and hydrophobic characteristics of zeolites play an important role in adsorption. Thermal stability and hydrophobicity of zeolites increase with Si/Al ratio in the zeolite framework.

The choice of adsorbent however depends on the application but activated carbon and styrene/divinylbenzene macroporous resins are the preferred adsorbents for VOC recovery (Khan and Ghoshal, 2000). In this work, activated carbon is the adsorbent used. The relative balance between capacity and selectivity of adsorption and the ease of desorption together with the justifications in the literature (see Section 2.5.1) dictates the use of activated carbon as the preferred adsorbent over zeolites in this work.

2.6 Monolith Reactors

Despite the huge advantages fixed bed reactors offer, there are still some drawbacks such as high pressure drop, solids handling and maldistribution of gas flow. Improvisations to the drawbacks mentioned above have led to the development of structured reactors as a promising alternative. The idea of structured reactors was originally developed in the 1960s and 1970s and applied to the catalytic converter system for automobiles using a monolithic catalyst (Cybulski and Moulijn, 1998). This system was efficient for the removal of gaseous air pollutant with a minimum pressure drop. The monolith reactor is an example of a structured reactor which has a regular structure or fixed spatial arrangement. The catalytic monolith reactor consists of a honeycomb structure with a large number of narrow channels or passages through which fluid flows. A comprehensive review of the monolith reactor is presented in Section 2.6.1. Conventionally, in an adsorptive reactor the adsorbent ad-mixed with the catalyst particles are randomly packed in a fixed bed reactor. In structured reactors, the catalyst may be supported on channel walls or on a catalytic support.

Other structured reactor types include membrane reactors and arranged catalyst reactors. In recent years, there has been a huge amount of research work done on membrane reactors. Sirkar *et al.*, (1999) describes how a membrane reactor can play various functions in the reactor system. Membrane reactors involve the selective permeation of a reaction specie through a porous mix i.e. the membrane, such as vycor

glass, ceramic or alumina based membranes (Aplay *et al.*, 1994). Until very recently, catalytic membranes incorporated in chemical reactor systems were mainly applied in biochemical reactions due to temperature limitations of the more widely used organic polymeric membranes (Belfort, 1989; Prezeres and Cabral, 1994). Scientific literature on catalytic membrane reactors include ideas of heat and mass integrated combination of hydrogenation and dehydrogenation processes in a single membrane unit. Their implementation on an industrial scale has also until recently been very limited due to the high price of membrane units, low permeability, sealing problems as well as mechanical and thermal fragileness of the membranes (Stankiewicz, 2003). Recent advances in material science engineering have resulted in newer materials which allow for higher temperature membrane processing. Inorganic membranes and metal membranes are more thermally stable when compared to other polymeric membranes. Hsieh (1996) gives a comprehensive overview on combined reaction and separation using these types of membranes with regards to hydrogen generating and consuming reactions. Potential application areas include methane steam reforming, water-gas shift reaction, selective oxidations, e.g. ethylene to ethylene oxide, butane to maleic anhydride, oxidative dehydrogenations of hydrocarbons and oxidative coupling of methane (Stankiewicz, 2003). Shell and tube and cross flow configurations are possible and the catalytically active material may be loaded on the inner surface of the passage or within the porous wall.

Monolithic catalysts for two-phase processes are characterised by poor heat transfer between the monolith and its surroundings therefore if intensive heat and mass transfer is needed within the catalyst bed, arranged catalysts provide an effective solution (Cybulski and Moulijn, 1998). There are two types of arranged catalyst reactors – (i) structural catalysts where the packings or surfaces are coated with catalyst such as the trickle bed reactor and open cross flow structures and (ii) particulate catalysts arranged in arrays or packed columns through the use of retention cages. Examples include parallel-passage and lateral-flow reactors, bead-string reactors.

2.6.1 Monoliths

Monolith structures were developed in the 1960s and 1970s to tackle automotive pollution because of their favourable properties to bring large volumes of gases in contact with a solid catalyst, such as low pressure drop, high geometric surface area, short diffusion lengths (small internal diffusion resistance) and the lack of attrition by vibration and thermal shock resistance. Monoliths can be located in a vertical or horizontal position or in mobile systems without losing their shape and are easier to handle than packed beds (Valdes-Solis *et al.*, 2004).

Monolithic catalysts are continuous unitary structures containing many narrow, parallel straight or zigzag passages through which gas flows (see Fig. (2.2)). Monolithic catalyst substrates may either be ceramic or metal. The walls of the channels may be washcoated with a high surface area catalyst support material such as γ-alumina and impregnated, or extruded directly into catalytic bodies using appropriate batch materials.

The transition from reactants to products involves transport of the reactants by convective flow in the channels and molecular diffusion towards the channel walls. Simultaneous diffusion and reaction occur inside the porous washcoat whereby the products diffuse back into the gas and are transported out from the reactor.

The monolith structure typically has a diameter of ~ 15cm and can be produced in a number of sizes and shapes. Typical shapes are round or oval cross-sectional areas for automotive exhaust applications and square shaped for stationery emission uses. In addition to the overall part dimension, the geometry of the monolith channel can be produced in many forms including square, round, hexagonal and triangular. The diameters of the channels range from 0.5 – 10 mm and the length of the monolith can be up to 1 m (Williams, 2001).

Apart from the increasing interest in multiphase catalytic applications (Kapteijn *et al.*, 1999, 2001), traditionally monoliths have been mainly used for single phase applications like combustion of various pollutants and deNO*x* in exhausts for many years (Valdes-Solis *et al.*, 2004). The successful use of the cordierite monolith (a type of ceramic monolith) in the treatment of automotive exhaust has given rise to their use in other applications. Monoliths are increasingly under development and evaluation for many new reactor applications e.g. chemical process and refining industries, catalytic combustion, ozone abatement, VOC abatement, automotive emission control and industrial heat recovery. For many of these applications, the use of other substrate materials and

designs can be utilized since the process requirements are not as demanding as that for automotive emissions control. In addition, due to the high manufacturing costs and malleability of monolithic catalysts only processes in which the catalysts are reasonably stable and/or easy to regenerate are feasible and these include liquid phase hydrogenations, oxidations of organics and biotechnology processes (Cybulski and Moulijn, 1998).

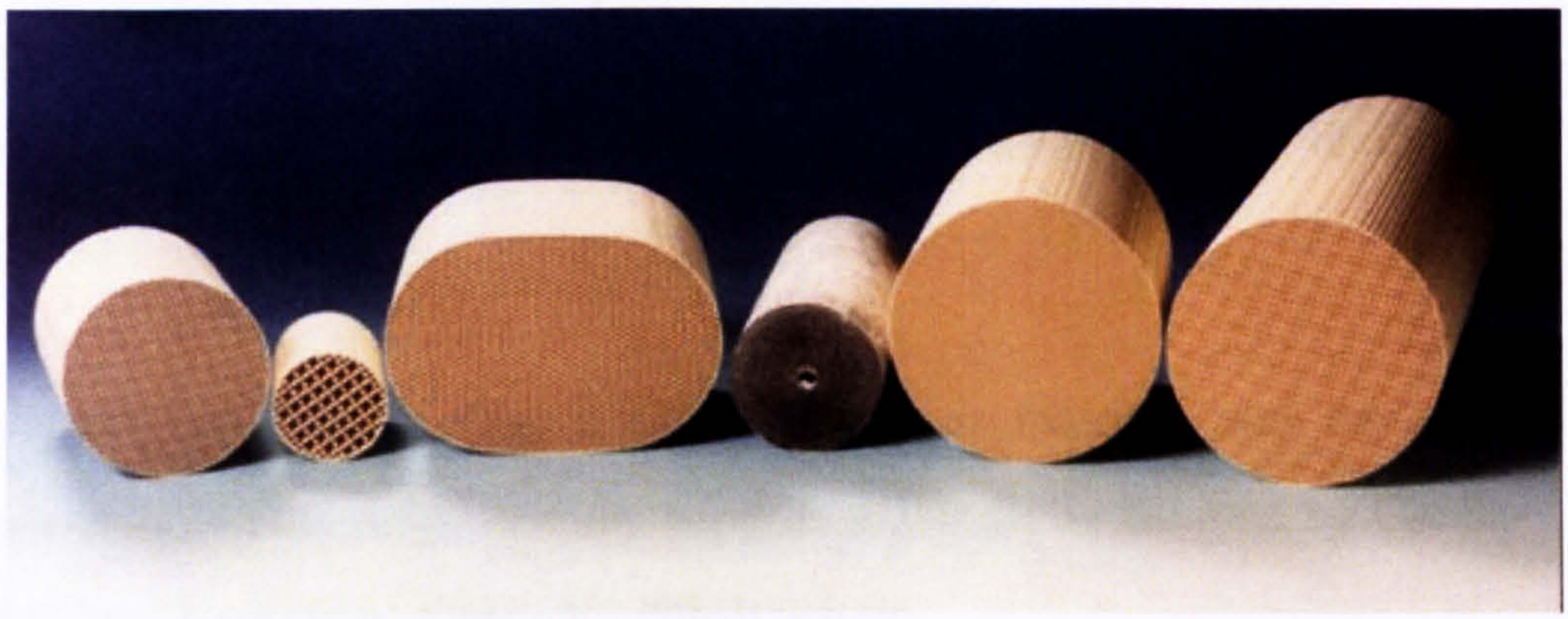

Fig. 2.2: Different shapes and sizes of monolithic material (Heiszwolf *et al.*, 2000)

2.6.2 Monolith Materials

Carbon monoliths (Yates *et al.*, 2000, 2003) and carbon-ceramic monoliths (Gadkaree, 1998), have been proposed as adsorbents of pollutants from gaseous streams. A great deal of work on carbon-ceramic monoliths has been carried out (Vergunst *et al.*, 2001) especially by researchers from Corning Inc. (Gadkaree and Mach, 1996; Gadkaree, 2001; DeLiso *et al.*, 1997). These researchers have developed several methods to prepare integral or coated carbon-ceramic monoliths. In many cases *n*-butane has

been employed as a reference molecule to compare the VOC adsorption capacity of various materials (Valdes-Solis *et al.*, 2004).

Monoliths are made by extrusion. A special mix of clay, binders and additives is pushed through a sophisticated dye to create the monolithic structure. The extruded material is then dried and cut to the required length and fired at high temperatures. The most widely used ceramic material for extruded monolithic substrate is cordierite. This is used for automotive systems where more durable wash coat formulations and high temperature stable catalysts are needed to achieve longer lifetime of the converter.

Carbon is often used as a catalyst support material and has clear advantages over other ceramic support materials as detailed by Garcia-Bordeje, Kapteijn and Moulijn (2002) below:

- Stability in acidic and alkaline media
- The physical and chemical surface properties of carbon can be tailored to fit the necessities of each reaction e.g. surface area, pore size distribution.
- Undesired side reactions catalysed by the support surface hardly occurs as the surface of the carbon is inert.
- Strong interactions with the active phase are limited. However, one clear disadvantage of carbon is that the mineral content of carbon from natural percursors may inardvently catalyse unwanted side reactions.

Carbon monoliths may be prepared either by full body extrusion as described above but the main difference is in the use of phenolic resins and fillers in the extrusion step followed by curing, carbonizing and activation steps (see Gadkaree, 1998) or they can be coated on cordierite substrates. Dipcoating of the monolith involves dipping the ceramic monolith in the carbon percursor, flushing with pressurised air to remove any excess, followed by curing, carbonisation and activation. Coated monolithic supports benefit from the high mechanical strength of the ceramic support while extruded monoliths have lower mechanical strength. (Garcia-Bordeje *et al.*, 2002).

Activated carbon coated monoliths are fabricated using high yield polymeric phenolic resins having low viscosity. A pore former polymer is added for mesopore formation. For more information on the manufacture of activated carbon monoliths see Gadkaree, (1998). Activated carbon monoliths have a wide range of applications which include water purification, VOC emission control, indoor air purification, industrial respirators amongst others.

2.6.3 Monoliths and Adsorption

The adsorption of VOCs on carbonaceous materials has received increasing attention in recent years, and several attempts to model the process have been published for granular active carbon in packed beds (Linders *et al.*, 2001, 2003), activated carbon fibres (ACF) (Cheng *et al.*, 2004; Das *et al.*, 2004) and carbon coated ceramic monoliths (Valdes-Solis *et al.*, 2004). However, very little is known about the dynamic

performance of monolithic structures in adsorption processes. Some of the models found in the literature made several simplifications; such as considering only gas diffusion in pores or assuming instantaneous adsorption kinetics (Cheng *et al.*, 2004; Linders *et al.*, 2001; Valdes-Solis *et al.*, 2004). Such model simplifications lead to huge savings in computation time. The use of monolithic configurations in catalytic applications has been well documented but its performance in physical adsorption processes has not attracted attention until now (Crittenden *et al.*, 1996).

Yates *et al.*, (2000), investigated the use of honeycomb monoliths of activated carbon for VOC removal. The activated carbon conformed as honeycomb monoliths take advantage of the low pressure drop characteristics not common to conventional reactors. Static adsorption capacities of various composite materials of activated carbon towards an aromatic probe molecule *o*-dichlorobenzene were studied in an attempt to study the viability of using monolithic adsorption units for the purification of effluent gas streams capable of regeneration. Results show that under experimental conditions, the maximum adsorption capacity of the materials was directly related to the pore volumes in pores of 0 to 15 nm. All the carbons studied were thermally stable in an air atmosphere up to 300°C allowing for the use of this temperature for regeneration purposes.

Of recent, there has been interest in the development of new microporous materials from activated carbon especially those based on

fibres or bindered particles (Vilaplana-Ortego, 2002). Section 2.5.1 discussed activated carbon adsorption and how activated carbon fibre overcomes the drawbacks associated with granular forms, (see Foster *et al.*, 1992; Derbyshire *et al.*, 2001). Jaroniec *et al.* (1991) suggest that thin fibres with diameters below 20μm ensured fast intraparticle adsorption kinetics compared to pelletised or granular activated carbon. This results in higher effective amounts of adsorption which decreases the sizes of the adsorption units. Particle entrainment is avoided and low pressure drop made possible.

Low-density activated carbon fiber monoliths (ACFM) have been developed recently (Burchell *et al.*, 2000; Marban *et al.*, 2001; Vilaplana-Ortego *et al.*, 2002) for several gas-solid applications due to their properties such as light-weight, high mechanical strength and fast adsorption kinetics. The monolithic structure makes them easier to handle than packed beds and produces low resistance to bulk gas flow (Marban *et al.*, 2006). One of the major drawbacks though, is its high price compared to that of conventional activated carbon. Among possible applications, ACFMs are of interest for the adsorption and recovery of organic vapours (Fuertes *et al.*, 2003; Marban and Fuertes, 2004), CO_2 adsorption (Burchel *et al.*, 1997), as catalysts or catalyst support for the removal of SO*x* and NO*x* from flue gas (Marban *et al.*, 2003) , water treatment (Suzuki, 1991) and CH_4 storage (Muto *et al.*, 2005).

Only a few works can be found on the use of activated carbon fibre monoliths for VOC removal, Andrews *et al.* (1998) prepared carbon fibre composites from petroleum pitched based fibres and analysed the adsorption of butane on carbon fibre composite beds. Fuertes *et al.* (2003) studied and analysed the adsorption of VOCs by means of activated carbon fibre-based monoliths prepared from inexpensive rejects of commercial polymeric fibres (Nomex) and also compared Nomex based activated carbon fibre monoliths to the different commercial activated carbon fibres. Adsorption experiments were conducted with *n*-butane at 30°C and show that at high adsorbate concentrations (p/p_o = 1), the amount adsorbed is a function of the pore volume, but at low concentrations (p/p_o = 0.004), this depends on the pore size distribution. The Nomex based samples exhibited higher adsorption capacities at low concentrations than commercial activated carbon fibres. More recently, Marban *et al.,* (2006) proposed a complete breakthrough model to describe the removal of volatile organic compounds from a diluted single-component gas stream passing through a micro-porous activated carbon fiber monolith (ACFM) under isothermal conditions. *n*-butane was employed as the test compound for obtaining the experimental breakthrough curves. The authors considered significant parameters which included adsorption isotherms, resistance to external gas diffusion, non-instantaneous adsorption kinetics at the external surface and the type of gas diffusion within the pore system. Good agreement between the experimental and simulated data was obtained for whole profiles at different values of *n*-butane concentration in the inlet gases.

2.6.4 Monoliths and Catalytic Combustion

The use of monoliths as catalytic reactors focuses mainly on applications where low pressure drop is an important item. When compared to fixed beds, which seem a natural first choice for catalytic reactors, monoliths consits of straight channels in parallel with a rather small diameter, because of the requirement of a comparably large surface area (Hoebink and Marin,1998). Monolithic catalysts provide an excellent opportunity to make catalytic combustion environmental friendly and energy saving compared to conventional systems. Catalytic combustion systems directly combust VOCs and have proved effective in cases of low VOC concentrations, when the adiabatic temperature rise is low. In addition, the operating temperatures of the conventional catalytic oxidation system are lower than that of other systems due to the use of catalysts. Catalytic combustion offers advantages of high efficiency at very low pollutant concentration, low energy consumption and very low production of secondary pollutants (NO*x*). The limiting factors of the catalytic process are catalyst poisoning and deactivation, thermal sensitivity and mass transfer limitations (Mazzarino and Barresi, 1993). A typical monolith for pollution control has a channel diameter of 1 mm and operates at inlet gas velocities of the order of 1-10 m s^{-1} (Thomas, 1986). These reactions frequently take place in honeycomb monolith reactors. The route from reactant to product molecule in a monolith reactor comprises reactant transport from the bulk gas flow in a channel toward the channel wall, simultaneous diffusion and reaction inside the porous wash coat on the channel wall and product transport from the wall back to the bulk flow of the gas phase.

The essence of monolith catalysts is their thin layers which account for negligible internal diffusion resistance. The laminar flow encountered in monoliths does not show the kinetic energy losses that occur in fixed beds due to inertia forces at comparable fluid velocities (Hoebink and Marin,1998), making the pressure drop smaller by two or three orders of magnitude than that of conventional fixed bed reactors. One good characteristic of the monolith is that the flow conditions are uniform across the monolith structure due to the surface characteristics of individual monolith passages. This reduces the occurrence of hot spots resulting from mal-distributions that occur in randomly packed catalyst beds (Cybulski and Moulijn, 1998).

The use of monoliths for catalytic oxidation is well documented in the literature where studies on various experiments and models have been carried out. Mazzarino and Barresi (1993) carried out the deep oxidation of VOC in air over a Pt/Al_2O_3 catalyst supported on a ceramic monolith. Experimental data was compared with computer simulations of the monolith reactor and a satisfactory agreement obtained.

Groppi and Tronconi (2001) investigated the replacement of conventional packed beds of pellets with "high conductivity" honeycomb catalysts in industrially externally-cooled multi-tubular fixed bed reactors. In their previous theoretical (1996, 2000) and experimental works (2000) they investigated the optimal design and thermal behavior of structured catalysts with high thermal conductivity in view of their use for strongly exothermic gas/solid reactions. Their parametric analysis for the case of a single reaction indicated that

metallic honeycombs are promising for limiting temperature gradients in externally-cooled multi-tubular fixed bed reactors as compared to conventional packed beds. They confirmed experimentally the feasibility of running strongly exothermic reactions in a fixed bed under nearly isothermal conditions. In their current work the epoxidation of ethylene to ethylene oxide was modelled and simulated. Results suggested that near isothermal operation of the fixed bed reactors can be achieved using monolithic catalyst supports based on relatively large volume fractions of highly conductive materials. Pressure drop reduced to <1% and selectivity was favoured by the excellent control of the intra-porous diffusional resistances resulting from the thin catalytic wash coats.

Hayes *et al.*,(2001) performed experiments and modelled the combustion of methane on a palladium catalyst in a wash coated honeycomb monolith reactor. The influence of water and carbon dioxide on the reaction was investigated together with the influence of γ-alumina diffusion barriers applied over a catalytic wash coat. Catalyst may be contained within the substrate material or more often dispersed within a wash coat that is coated onto the surface (Hayes and Kolac, 1997). Results showed that the dispersion of catalysts in the wash coat was an important factor for conversion. A monolith with the same amount of catalyst spread over a thicker wash coat gave a lower conversion when intra-phase diffusion was important. A patent application suggested the use of a diffusion barrier to limit the rate of a catalytic combustion reaction. The diffusion barrier is a layer of inactive porous material applied on to the top of the catalyst wash coat. Diffusion of methane had

an effect of slowing the reaction rate especially at high temperatures. By limiting the reaction rate, catalyst wall temperatures were thereby controlled with the aim of avoiding catalyst damage by over temperature. The diffusion barrier therefore, significantly reduces the observed reaction rate and only a thin barrier is needed to achieve significant reduction in conversion. They found water inhibition to be important even at low concentrations whilst carbon dioxide had a negligible effect.

2.6.5 Modelling Monolith Reactors

The modelling of monolith reactors has been extensively investigated and published. There are various mathematical models that describe the behaviour of the monolith reactor such as 1-D, 2-D and even 3-D models. These models are more or less realistic, depending on approximations used in their development, number of spatial dimensions, details of transport processes and chemical kinetics. Most of them simulate steady-state operation, but some deal with transient experiments and modelling as well (Hayes and Kolaczkowski, 1992; Zygourakis, 1989). A detailed description of the monolith reactor can be obtained by means of multidimensional models. These models are usually given in the form of several partial differential equations in at least two spatial co-ordinates and time. However, it might be quite difficult to validate them because of the large number of parameters, some of which can only be estimated with some uncertainty. Simplifications to approximate the performance of monolith reactors for modelling purposes include steady-state and isothermal conditions, plug flow and identical properties in all monolith

channels. A simple 1D heterogeneous model is based on the additional assumption of negligible pore diffusion resistance within a thin catalytic wash coat. This widely applied model does not retain qualitative features of a 2D model in describing simultaneous diffusion and chemical reaction within the catalytic wash coat (Tomašić and Gomzi, 2004). The main advantage of a 1D model over a 2D model is that less computer time is required for their solution. The 1D model requires an averaging of the radial concentration and temperature of the fluid. This creates discontinuity at the wall which is accounted for by introducing a heat or mass transfer coefficient into the model, requiring the 1D model to have good correlations for these values. In the 2D model, it is possible to impose correctly the flux boundary condition and the need for heat and mass transfer correlations does not exist (Hayes *et al.*, 1992). The mass and heat transfer coefficients, may be computed from the radial temperature and concentration gradients computed in a 2D model. In the literature, there is a good deal of controversy over the correct value of Nusselt and Sherwood number in a monolith channel under reacting conditions (Hayes and Kolaczkowski, 1994).

In automobile exhaust applications, laminar flow is the usual flow regime met in monolith reactors given that the typical Reynolds number has values below 500. The radial velocity profile in a single channel develops from the entrance of the monolith onward and up to the position where a complete Poiseuille profile has been established. The length of the entrance zone may be evaluated from the following relation:

$$\frac{L_e}{d_c} \leq 0.06Re \tag{2.6}$$

where d_c is the internal diameter of the monolith channel. It is usually neglected because it is typically less than 10% of the reactor length (Hoebink and Marin, 1998). Fully developed flow can be assumed in the main part of the monolith channel (Hayes *et al.*, 1992; Hayes and Kolaczkowski, 1994).

Research work has also focused on the issue of the velocity profile. In a laminar flow reactor, there is a radial velocity profile leading to the development of radial concentration and temperature gradients with the velocity at the centre-line being twice the average velocity. The magnitude of these gradients depends upon the relative rates of heat and mass transfer and chemical reaction (Hayes and Kolaczkowski, 1999). Groppi *et al.*, (1995a) assumed an invariant radial parabolic shape profile of axial velocity since the enhancement of gas solid heat transfer due to hydrodynamic development was minor compared to other phenomena studied. In other works, fully developed laminar velocity profiles varying with both radial and axial positions were considered in 2D models (Hayes and Kolaczkowski, 1994). For transient simulation a quasi static approximation is usually made based on the fact that the thermal capacities of solids are much larger than those of gases, thus the solid phase dominates the transient behaviour of the system (Young and Finlayson, 1976a; Heck *et al.*, 1976).

The radial heat effects occurring in the solid phase of the monolith are often not taken into account and a heat balance in the axial direction is simply used. As a result the radial heat conduction in the solid phase is a priori neglected and the wash coat is assumed to be isothermal at each point along the reactor (Hayes and Kolaczkowski, 1994; Wanker et al 2000; Tomašić and Gomzi, 2004). Some models consider axial heat dispersion (Sincule and Hlavacek, 1978; Hayes and Kolaczkowski, 1994). Lee and Aris (1977) studied the effect of wall conduction and showed that radiative heat transfer could be accounted for by properly increasing the wall heat conduction coefficient. 2D models have been developed considering axial conduction, radiation and catalytic reaction at the wall (Hayes *et al.*, 1992; Groppi 1995a; Leung *et al.*, 1996). Groppi *et al.*, (1995 a,b) concluded that the contributions of wall conduction and radiation could be reasonably neglected in the simulation of ceramic monoliths so computational time could be saved. Hayes *et al.*, (1992) demonstrated that the axial conduction in the solid has a bigger effect than radiation.

2.7 Conclusions

This chapter has reviewed some of the fundamentals of adsorption and adsorption processes which form the basis of this thesis. Furthermore, based on the reviews in the field of adsorption and adsorptive reactions the basis and novelty of this research occurs in the two areas discussed below:

1. Firstly, in the use of the adsorptive reactor for the decontamination of VOCs, a process that is exothermic. Past studies have focused mainly on reversible endothermic process schemes (Carvill et *al.*, 1996; Yongsunthon and Alpay, 1999; Sheik *et al.*, 1998; Kodde, 2001). Issues such as runaway and thermal stability of the reactor and efficient heat integration have been studied theoretically and experimentally for catalytic reactors where reverse flow reactors (see Matros, 1989; Matros and Bunimovich, 1996; Zagoruiko *et al.*, 1996) have been implemented to combat these issues.

2. Secondly, in the use of structured reactors in the form of monolith reactors which as reviewed in Section 2.6, provide an alternative to the fixed bed catalytic reactor and thus the conventional fixed bed adsorptive reactor. Drawbacks of high pressure drops and mal-distribution of gas flow and thus unexpected hotspots and run-a-ways are eliminated. As reviewed, the monolith reactor is currently used for catalytic combustion of VOCs and also for adsorption of low concentration VOCs but the combination of both oxidation and adsorption of the VOC within the monolith structure is yet to be seen. The novelty of this research is in exploring the possibilities of using the monolith reactor as an adsorptive reactor for simultaneous adsorption and reaction for exothermic reaction schemes with VOC abatement as an example in the first instance.

There is scope for the choice and configuration of the monolith structure. Activated carbon monoliths are considered for use in this work. Different methods or forms are available for the monolith structure in terms of using activated carbon monoliths that exhibit adsorptive properties, with a layer of catalytically active material coated on them or impregnating the monolith structure itself with catalysts. The monolith configuration and how the catalysts are arranged or integrated is in itself a challenge as the feasibility and performance of the process is dependent on this. Theoretical studies performed on the combined process of adsorption and reaction in a monolith reactor will therefore provide information on the feasibility of adsorptive-reactor technology. Mathematical models for the adsorptive reactor are presented in Chapter 3.

CHAPTER 3: Modelling Adsorptive Reactors

3.1 Introduction

In order to perform theoretical studies on the feasibility of non-isothermal adsorptive reactor operations, and in particular the use of the monolith reactor as an adsorptive reactor (M-AR), a mathematical model for the adsorptive reactor was developed. Models utilising the monolith reactor for the purposes of adsorption only (M-ADS) and reaction only (M-RXTN), were also developed. The models are based on the basic concepts of adsorption and catalytic combustion as reviewed in Chapter 2.

This chapter begins with an introduction to the M-AR concept in terms of the reactor geometry, general design parameters, adsorption parameters and reaction kinetic data employed for modelling purposes. In the monolith reactor, a clear distinction lies between the process behaviour in the gas and solid phases (Tomašić and Gomzi, 2004). Reactant gas is fed into an empty core gas channel and is dispersed radially along the axial direction by means of diffusion. In the solid phase, the monolith material itself acts as the solid adsorbent with layers of catalyst particles interspersed within the porous material. The process is operated dynamically, and both adsorption and reaction kinetic rate expressions are included in the modelling of the solid phase. These are presented in Section 3.2.

The set of model assumptions included non-isothermal operation, two-dimensional flow, a linear driving force model for adsorption and Tóth adsorption kinetics. These assumptions together with the governing equations, corresponding boundary equations and numerical methods for the adsorption / reaction models are detailed in Section 3.3.

The limitations of using the packed bed reactor in terms of high pressure drop per unit length and plugging of the feed stream have been well documented in the literature. Nonetheless, one-dimensional models of the packed bed reactor for adsorption only (PB-ADS) and reaction only (PB-RXTN) were developed to enable comparisons between the respective monolith reactors. The packed bed reactor model is presented in Section 3.5.

The adsorptive reactor for VOC oxidation – specifically the oxidation of ethene and propane using a $Pd/\gamma\text{-}Al_2O_3$ catalyst and activated carbon adsorbent was studied. The performance of the M-AR was compared to that of the M-ADS and M-RXTN. The effectiveness of this novel reactor to remove the VOC, the feed stream energy input and its ability to prevent reaction runaway were considered and used as key performance indices. These performance measures are described in Section 3.6.

Finally, Section 3.7 gives a brief overview of the numerical methods employed in this work. The adsorptive reactor model was developed within *gPROMS* (*general PROcess Modelling System*), a software package for the modelling and simulation of processes with both *discrete* and *continuous* as well as *lumped* and *distributed* characteristics. More

information on *gPROMS*, its concepts and language, can be found in Barton (1992), Barton and Pantelides (1994), Naf (1994) and Oh (1995).

3.2 The M-AR concept

3.2.1 Adsorptive reactor configuration

There are many different methods or forms available for the monolith structure in terms of using activated carbon monoliths that exhibit adsorptive properties. These forms include the monolith coated with a layer of catalytically active material or impregnating the monolith structure itself with catalysts (see Section 2.6). The M-AR modelled in this work is considered to be made up of parallel channels resembling a honeycomb structure that provides a high surface area to volume ratio with low pressure drop. Its open structure allows for little or no resistance to the transport of any particulate matter present in the feed. In Section 2.6 a comprehensive description and review of monoliths was presented. For modelling purposes a single channel is considered. This consists of an empty core gas channel and a solid zone which acts as the activated carbon adsorbent material itself. Within the porous structure of the solid zone, catalytically active material (palladium) is also deposited. It is also assumed that the catalyst is evenly distributed along the monolith material. Figs. (3.1) and (3.3) illustrate this.

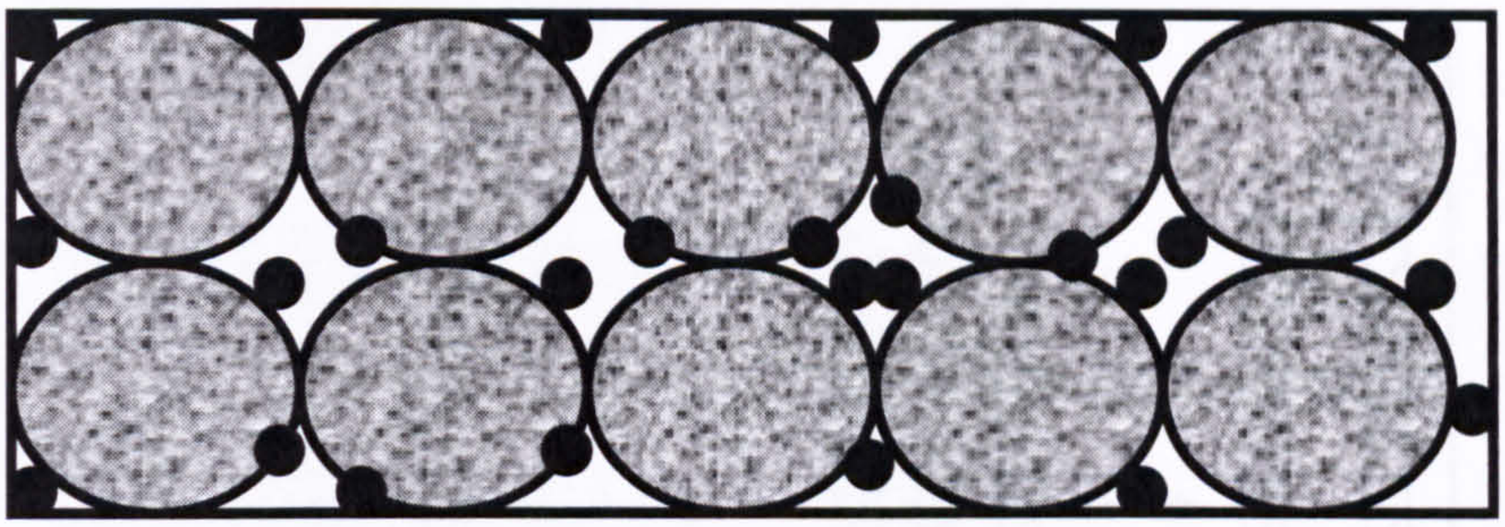

Fig. 3.1: Solid zone of the monolith reactor depicting porous adsorbent and catalytic material. ● represents catalytic material ; The larger particles represent the porous adsorbent.

In this work the concept for the M-AR is illustrated in Fig. (3.2). The conventional packed bed reactor of diameter d_c and length L consists of solid adsorbent particles randomly packed. The spherical beads i.e. the activated carbon adsorbent as shown in (A), essentially becomes the solid adsorbent block utilised in the monolith reactor. The packed bed is thus conceptually replaced by a single monolith with diameter d_m and length L_m as shown in (C). The monolith structure made out of activated carbon adsorbent has many channels of diameter $D_{channel}$ that run parallel to the length of the monolith as shown in (D). Fig. (3.3) further illustrates this concept whereby reactant gas is fed into the empty core gas channel and is dispersed radially along the axial direction by means of diffusion, with adsorption and reaction occurring in the solid zone comprising the adsorbent and catalyst.

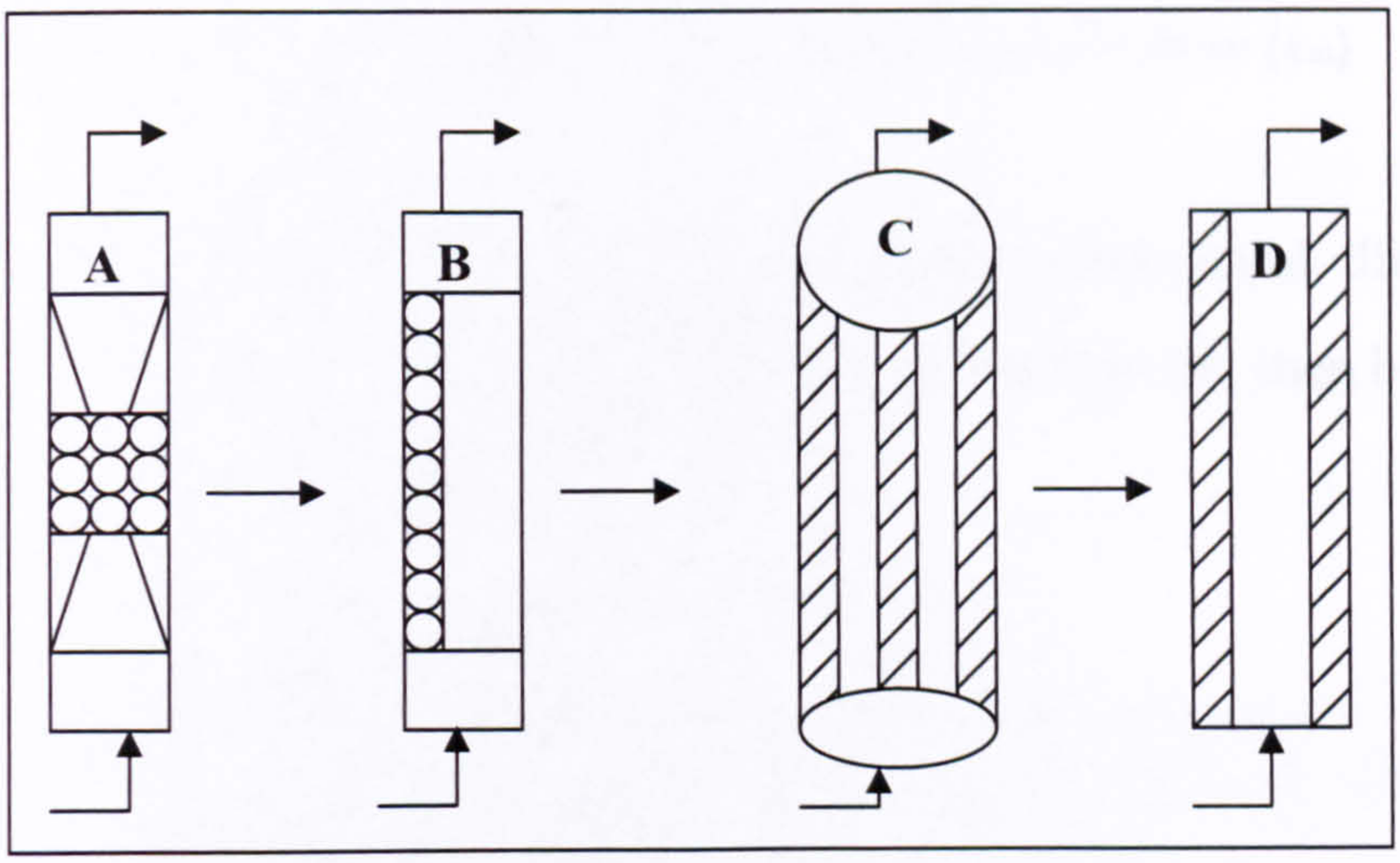

Fig 3.2: Packed bed and monolith reactor systems – (A) Packed bed, (B) Packed bed – Monolith transformation (C) Monolith, (D) Single monolith channel. (Adapted from Crittenden *et al.*, 1996)

Fig.3.3: The novel M-AR

The tortuous fluid flow path in the packed bed is replaced by flow through straight empty channels. The adsorbent and void spaces in the packed bed are now redistributed in the monolith configuration.

Crittenden *et al.*, (1996), performed theoretical studies into adsorption dynamics in a monolithic adsorbent. The authors identified three key independent variables for monolithic systems:

- Ratio of the monolith diameter to the column diameter (f)
- Cell density in the number of cells per unit area (n_d)

- Fraction of cross section area available for flow (ε_m)

Once these variables are defined, other geometrical dimensions e.g. channel diameter and the length of the monolith can then be calculated:

$$d_m = f d_c \tag{3.1}$$

$$D_{channel} = \left(\frac{4\varepsilon_m}{\pi n_d}\right)^{0.5} \tag{3.2}$$

$$L_m = \left[\left(\frac{L}{f^2}\right)(1-\varepsilon)/(1-\varepsilon_m)\right] \tag{3.3}$$

Eqs. (3.1) – (3.3) were obtained from Crittenden *et al.*, (1996). In this thesis, the cell density considered was 40 cells cm^{-2} with $\varepsilon_m = \varepsilon$ and f =1.5.

There are two steps in the operation of this reactor system – adsorption and regeneration. Regeneration is followed by the complete combustion of the VOC.

Step 1 – Adsorption

The VOC and inert carrier gas e.g. N_2, are fed into the reactor and the adsorbent becomes slowly saturated with the VOC. The solid phase is in the adsorption step and is operated without any VOC leakage (i.e. breakthrough). Nitrogen gas exits into the effluent stream and can therefore be reused.

Step 2 – Regeneration

In this step, the VOC is desorbed from the adsorbent by means of inert regeneration gas e.g. N_2 (concentration swing) and an increase in temperature. O_2 is fed into the reactor as a reactant for the oxidation reaction and also acts as a purge gas (concentration swing).

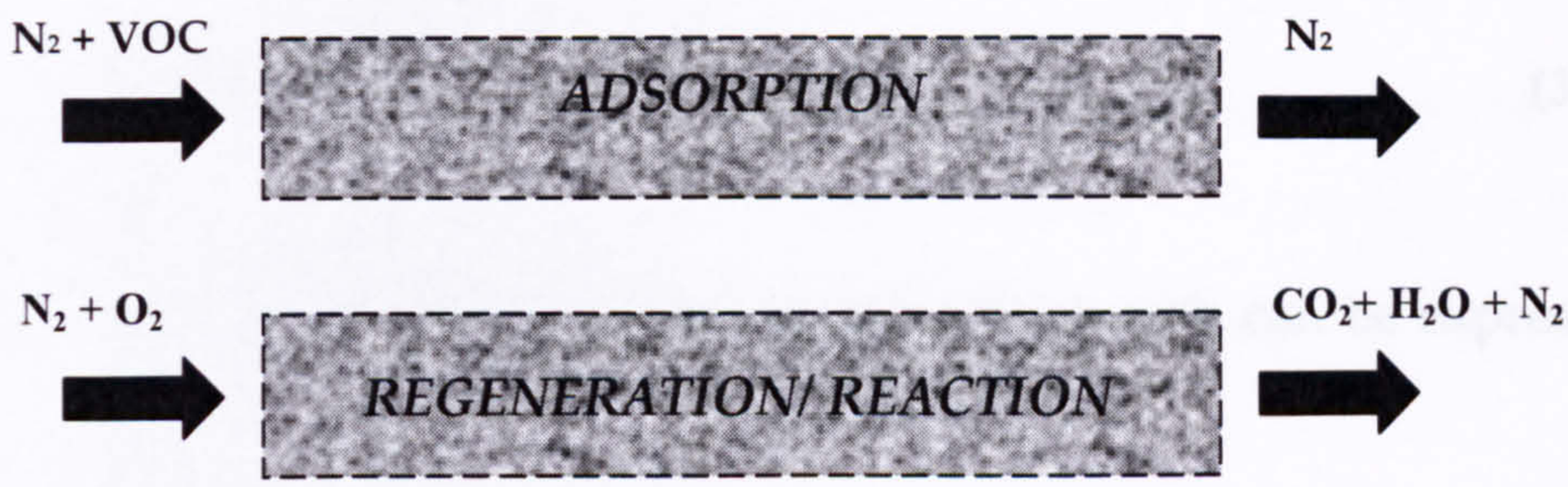

Fig.3.4: Schematic diagram of the two steps involved in M-AR operation

The reaction products, CO_2 and H_2O are sent to the atmosphere while nitrogen in the effluent stream may be recovered and used as a carrier gas. The key point in this step is the fact that the energy used for regeneration is not wasted but is used to preheat the bed for the subsequent step and furthermore provide the heat to drive desorption (an endothermic process). As reviewed in Section (2.4.3), Kodde (2001) demonstrated that the heat generated by an exothermic reaction i.e. the VOC oxidation reaction and adsorption (an exothermic process) does not render the PSR concept inviable as the heat of reaction may be utilized to accelerate sorbent regeneration.

3.2.2 Adsorption and reaction kinetics

Adsorption rate and kinetics

The linear driving force (LDF) model (Glueckauf and Coates (1947)) was adopted to describe the importance of intraparticle mass transfer. The rate of adsorption in a particle, r_{ads} (mol kg^{-1} s^{-1}) is expressed as:

$$r_{ads} = \frac{\partial q_i}{\partial t} = k_i(q_i^* - q_i) \tag{3.4}$$

The mass transfer coefficient for component *i*, k_i (s^{-1}), can be expressed as:

$$k_i = \frac{15\,\overline{Dei}}{r_p^2} \tag{3.5}$$

where r_p, is the mean particle radius (m) and $\overline{D_{ei}}$ the modified effective intraparticle diffusion coefficient (m^2s^{-1}) of component *i*, derived from Eqs. (2.4) and (3.6). $\overline{D_{ei}}$, is often dependent on contributions from more than one diffusional transport mechanism. This in turn determines the mass transfer coefficient, k_i which can be treated as a fitting parameter for mass transfer where a large value of k_i indicates instantaneous local equilibrium model. $\overline{D_{ei}}$ is given as:

$$\overline{D_{ei}} = \frac{\varepsilon_p(1-\varepsilon_b)D_{ei}}{\rho_b m_i RT} \tag{3.6}$$

The effective diffusion coefficient for component *i*, D_{ei} (m^2s^{-1}) accounts for the various mechanisms of transportation within the particle and its

complex pore structure. D_{ei} is related to the diffusion coefficient for a single cylindrical pore, D_p, by:

$$D_{ei} = \frac{\varepsilon_p D_p}{\tau_p} \tag{3.7}$$

ε_p, is the intraparticle porosity and τ, is the tortuosity factor. For a binary gas (A, B) in a porous solid, the D_p for component A is given by (see Evans *et al.*, (1961) and Scott and Dullien (1962)):

$$\frac{1}{D_p} = \frac{1}{D_k} + \frac{1}{D_m}\left[1 - \left(1 + \frac{J_B}{J_A}\right) y_A\right] \tag{3.8}$$

Where J is the molecular flux (mol m^{-2} s^{-1}), and y is the gas phase mole fraction.

For adsorption and desorption processes, the approximation of equimolar counter diffusion (J_A = - J_B) within the adsorbent particle is usually assumed (see Ruthven (1984)). Thus Eq. (3.8) reduces to:

$$\frac{1}{D_p} = \frac{1}{D_k} + \frac{1}{D_m} \tag{3.9}$$

Where D_k, denotes the Knudsen diffusion coefficient (m^2 s^{-1}) and D_m, the molecular diffusion coefficient (m^2 s^{-1}) respectively.

For molecular diffusion in a binary gas system, the Chapman-Enskog kinetic theory (see Bird *et al.*, (1960)) leads to

$$D_m = 1.8583 \times 10^{-7} \frac{\sqrt{T^3 (\frac{1}{M_A} + \frac{1}{M_B})}}{P \sigma_{AB}^2 \Omega_{AB}} \tag{3.10}$$

Where P is the total pressure (Pa), T is the temperature (K), M_A and M_B are the molecular weights of species A and B respectively (g mol^{-1}), σ_{AB} is the Lennard-Jones collision diameter for A and B (m), and Ω_{AB} is the corresponding dimensionless collision integral. For approximations of σ_{AB} and Ω_{AB} see Bird *et al.*, (1960).

The Knudsen diffusion coefficient of component A is given by:

$$D_k = 48.5 d_{pore} \sqrt{\frac{T}{M_A}} \tag{3.11}$$

Data and calculations for the diffusion coefficients can be found in Appendix A.

With reference to adsorption kinetics, the data used for modelling purposes is obtained from the works of Zhu *et al.*, (2005). The authors investigated the adsorption equilibria of light alkanes and alkenes e.g. ethene and propane on Kureha activated carbon (supplied by Kureha Chemical Industry) using a volumetric method. The physical and molecular properties of the adsorptives are listed in Table (3.1). Single

component adsorption isotherms were reported at pressures up to 120 kPa and at temperatures in the range 194 K to 338 K for ethene and from 273 K to 358 K for propane. Kureha activated carbon is a purely micro-porous material with a wide pore size distribution in the range 0.4 to 1.9 nm and is therefore considered as a heterogeneous adsorbent; See Zhu et al., (2004, 2005) for more information on Kureha activated carbon.

The Tóth model is often used to correlate isotherm data (Zhu *et al.*, 2005),

$$q = q^{sat}\frac{Kp}{\left[1+(Kp)^{t}\right]^{\frac{1}{t}}} \tag{3.12}$$

where q is the amount adsorbed (mol kg^{-1}), q^{sat} is the saturation amount adsorbed (mol kg^{-1}), K is the adsorption equilibrium constant (kPa^{-1}), p is the pressure (kPa) and t is the parameter that characterizes the system heterogeneity (Zhu *et al.*, 2005). In the Tóth isotherm, the parameters K and t are temperature dependent. The temperature dependence of K is described by the van't Hoff equation for the adsorption affinity given as follows (Rhee *et al.*,1972; James and Phillips, 1974):

$$K = K_0 \exp\left[-\frac{\Delta Hads}{R}\left(\frac{1}{T}-\frac{1}{T_0}\right)\right] \tag{3.13}$$

where T is the temperature (K), K_0 is the affinity at reference temperature T_0, R is the universal gas constant (= 8.314 J mol^{-1} K^{-1}), and

ΔH_{ads} is a measure of the enthalpy of adsorption. The parameter t and the maximum adsorption capacity q^{sat} can take the following functional forms of temperature dependence (Zhu *et al.*, 2005),

$$t = t_0 + \beta\left(1 - \frac{T_0}{T}\right) \tag{3.14}$$

$$q^{sat} = q_0^{sat} \exp\left[\gamma\left(1 - \frac{T}{T_0}\right)\right] \tag{3.15}$$

The temperature dependence of the parameter t does not have a theoretical basis; however, the authors suggest that one would expect this parameter to approach unity if the temperature increases thus reducing the Tóth isotherm to the Langmuir equation. The saturation capacity, decreases slightly with temperature due to a thermal expansion of the adsorbed phase (Zhu *et al.*, 2000). Within the temperature range investigated this value of q^{sat} should remain almost constant because the thermal expansion of the adsorbed phase is usually negligible. This means that γ in Eq. (3.15) should be close to zero. The lowest temperature investigated is used as T_0, since the measured isotherm at this temperature covers the widest range of loading.

The authors carried out nonlinear parameter estimation by combined fitting (see Zhu *et al.*, 2005). These values are listed in Table (3.2).

Adsorptive	MW, g mol^{-1}	α, Å^3	σ_k, nm	T_b, K	T_c, K	p_c, MPa	ΔH_v, kJmol^{-1}	MVL, cm^3 mol^{-1}
Ethene	28.05	4.25	0.39	169.5	282.3	5.041	13.53	49.40
Propane	44.11	6.37	0.43	231.1	369.8	4.248	19.04	75.50

Table 3.1: Summary of physical and molecular properties of ethene and propane
Source: ***Zhu et al. (2005)***

Adsorptive	Ethene	Propane
T_0, K	194	273
t_0	0.287 ± 0.004	0.326 ± 0.006
K_0, kPa^{-1}	26.9 ± 1.9	11.4 ± 0.9
q_0^{sat}, mol kg^{-1}	14.3 ± 0.1	8.37 ± 0.09
$-\Delta H_{ads}$, kJ mol^{-1}	29.5 ± 0.1	41.5 ± 0.3
B	(1.46 ± 0.04) x 10^{-1}	(1.45 ± 0.07) x 10^{-1}
γ	0	0
V_P, [a] cm^3 g^{-1}	0.706	0.632

Table 3.2: Estimated parameter values and 95% confidence limits for the combined fitting of the adsorption data by the Tóth model (see Eqs. (3.12) - (3.15)).

[a] Corresponding pore volume calculated from the estimated saturation capacity and the molar volume of the adsorptive (MVL in Table 3.1)

Source: ***Zhu et al. (2005)***

Oxidative reaction

The complete oxidation of ethene and propane on a Pd/γ-Al_2O_3 catalyst involves the following reactions:

$$C_2H_4 + 3O_2 \longrightarrow 2CO_2 + 2H_2O$$

$$\Delta H_{298K} = -1322 \text{ kJ mol}^{-1} \quad (3.16)$$

$$C_3H_8 + 5O_2 \longrightarrow 3CO_2 + 4H_2O$$

$$\Delta H_{298K} = -2043 \text{ kJ mol}^{-1} \quad (3.17)$$

Different mechanisms for catalytic oxidation reactions have been proposed and depend on the specific catalyst and hydrocarbon studied. Golodets (1983) proposed a kinetic model for the complete oxidation of VOCs:

$$R_{HC} = \frac{k_2 P_{O_2} k_1 P_{HC}}{k_2 P_{O_2} (1 + K_{H_2O} P_{H_2O}) + \upsilon k_1 P_{HC}} \quad (3.18)$$

Where R_{HC} is the rate of the reaction (mol kg^{-1} s^{-1}), k_1 and k_2 are the reaction rate constants (mol $kg^{-1}s^{-1}Pa^{-1}$), P_{02} and P_{HC}, the partial pressure of oxygen and VOC respectively (Pa), K_{H20} is the adsorption constant of water (Pa^{-1}) and υ is the stoichiometric coefficient of component i ($\nu_i < 0$ for reactants and $\nu_i > 0$ for products)

Many research groups have studied the catalytic oxidation of VOCs. The reaction kinetic model used for modeling purposes in this work is obtained from the work of van de Beld *et al.*, (1995) where first-order

kinetics is assumed to depict the reaction kinetics (the rate of reaction R_{HC}). van de Beld *et al.*(1995), studied the kinetics of the complete oxidation of ethene, propane and their mixtures on a palladium catalyst using an internal recycle reactor. The pressure was varied from 1.6 - 5 bar and the temperature from 453 K to 493 K for ethene oxidation and from 553 K to 603 K for propane oxidation. The maximum hydrocarbon concentration was ca. 3000 ppm or 0.3 vol. %. The catalyst properties as utilised in their work is given in Table (3.4). Under the conditions used in the work of the authors i.e. a large excess of oxygen with propane and ethene as low concentration contaminants and a palladium catalyst, it is assumed that chemisorption of oxygen followed by reaction with gaseous hydrocarbon is the mechanism involved. The reaction products, CO_2 and H_2O may also retard the oxidation reaction. The influence of CO_2 is neglected by almost all the authors quoted in the literature and water adsorbs onto the adsorbed oxygen (van de Beld et al., 1995).

Arrhenius temperature dependence is assumed for the reaction constant k_1:

$$k_1 = k_{1,\infty}\, e^{-E_{act}/RT} \qquad (3.19)$$

where $k_{1,\infty}$ is the pre-exponential factor (mol $kg^{-1}s^{-1}Pa^{-1}$), E_{act} is the activation energy (J mol^{-1}), R is the universal gas constant (= 8.314 J mol^{-1} K^{-1} or Pa m^3 mol^{-1} K^{-1}) and T is the temperature (K).

Table (3.3) lists four different rate expressions which have been used to describe the experiments performed by Van de Beld *et al.*(1995). Models

I, II and III can be derived from Eq.(3.18) with Model III being equivalent to Eq.(3.18) provided $k'_1 = vk_1/ k_2P_{O2}$. If the surface reaction is much slower than oxygen adsorption, then $vk_1P_{HC} \ll k_2P_{O2}$ and model II is obtained. A further simplification can be achieved by neglecting the influence of water on the process which is possible if $K_{H2O}P_{H2O} \ll 1$: this yields the rate expression given by model I. Model IV is a power law rate expression which cannot be deduced from Eq (3.18). Model IV does not provide any insight into the mechanism of the reaction but is convenient for engineering purposes and often yields good results provided it is not used for extrapolation outside the experimental range. The authors found the accuracy of these rate expressions to be within a 17% error for ethene oxidation and 13% for propane oxidation (van de Beld et *al.*1995).

Model	Reaction rate expression
I	$R_{HC} = k_{1,\infty} e^{-Eact/RT}. P_{HC}$
II	$R_{HC} = \frac{k_{1,\infty} e^{-Eact/RT}.P_{HC}}{1 + K_{H2O}.P_{H2O}}$
III	$R_{HC} = \frac{k_{1,\infty} e^{-Eact/RT}.P_{HC}}{1 + K_{H2O}.P_{H2O} + k'_1.P_{HC}}$
IV	$R_{HC} = k_{r,\infty} e^{-Eact/RT}. P^n_{HC} . P^m_{H2O}$

Table 3.3: Kinetic rate expressions for the complete oxidation of ethene and propane
Source: (*van de Beld et al., 1995*)

The authors fitted Eq.(3.18) to the experimental data obtained from the Berty reactor (well-mixed and steady state operation) and best fit values for the kinetic parameters of these models listed in their work are used.

The authors also used a different experimental installation to obtain numerical values for the kinetic parameters whereby a dynamic method wherein the reactor was operated under transient conditions and behaved like a plug flow reactor. The dynamic method proved faster but was less accurate. For a detailed description, refer to van de Beld *et al.*,(1994). The rate expression for the dynamic method is similar to that of model I ($RHC = k_{1,\infty} e^{-Eact/RT}. P_{HC}$).

In this work, Model III (see Eq. 3.20) was employed for the prediction of the reaction rate because it is the most extensive of the models listed in Table (3.3). Its derivation is based on a reaction mechanism (van de Beld et al., 1994). It is equivalent to the kinetic model for complete VOC oxidation first proposed by Golodets (1983) (see Eq.(3.18)).

$$R_{HC} = \frac{k_{1,\infty} e^{-Eact/RT}.P_{HC}}{1 + K_{H2O}.P_{H2O} + k'_1.P_{HC}} \qquad (3.20)$$

where R_{HC} is the rate of reaction of the organic compound (mol kg^{-1} s^{-1}), P_{HC} and P_{H20} the partial pressures (Pa) of the organic compound and water respectively, K_{H20} the adsorption constant of water (Pa^{-1}), and $k_{1,\infty}$ the pre-exponential factor (mol $kg^{-1}s^{-1}$ Pa^{-1}).

The values of the parameters involved in the oxidation of ethene and propane are listed in Tables (3.5 and 3.6).

Catalyst Properties
Pd/ γ-Al_2O_3 cylinders
Diameter, 4.5mm; height 4.5mm
Particle density, 1327 kg m^{-3}
Approximate bed density, 796 kg m^{-3}
Active metal surface area, 350 m^2 kg^{-1}
BET surface area 192 m^2 g^{-1}
Pd content, 0.07 wt. %
Pd on outer surface only; penetration depth, <0.1mm

Table 3.4: Catalyst properties as utilised in the work of van de Beld *et al.*, (1995)

Parameter	Ethene				
	DM[a]	I	II	III	IV
E_{act}, kJ mol^{-1}	67.3	57.8	58.9	57.4	43.2
$k_{1,-}$ or $k_{r,-}$	1.2×10^{0}	1.8×10^{-1}	3.2×10^{-1}	2.3×10^{-1}	4.3×10^{2}
K_{H2O}, Pa^{-1}	-	-	9.4×10^{-4}	8.7×10^{-4}	-
k_1', Pa^{-1}	-	-	-	2.3×10^{-4}	-
N	-	-	-	-	0.71
M	-	-	-	-	-0.12
Error (%)	-	19.7	16.6	16.4	16.6

Table 3.5: Best fit values for parameters involved in the oxidation of ethene as derived from the various models listed in Table (3.3)

[a] Data obtained from experiments using a dynamic method. Reaction rate expression from model I. Source: *(van de Beld et al., 1995)*

Parameter	Propane				
	DM[a]	I	II	III	IV
E_{act}, kJ mol^{-1}	87.7	92.9	153.7	102.2	119.3
$K_{1,\infty}$ or $k_{r,\infty}$	7.2 x 10^{0}	1.4 x 10^{1}	9.9 x 10^{8}	3.2 x 10^{2}	4.8 x 10^{5}
K_{H20}, Pa^{-1}	-	-	5.3 x 10^{-1}	1.5 x 10^{-3}	-
K_1', Pa^{-1}	-	-	-	9.1 x 10^{-3}	-
N	-	-	-	-	0.61
M	-	-	-	-	-0.46
Error (%)	-	31.8	17.6	13.7	12.5

Table 3.6: Best fit values for parameters involved in the oxidation of propane as derived from the various models listed in Table (3.3)

[a] Data obtained from experiments using a dynamic method. Reaction rate expression from model I. Source: *(van de Beld et al., 1995)*

3.3 Mathematical Modelling of the M-AR

The monolith reactor has plenty of channels but for modelling purposes only one channel is modelled with the assumption that there is no interaction between the channels and that all conditions in the channels are equal. A 2D non-isothermal heterogeneous dynamic model has been developed and applied to describe both the adsorption dynamics and oxidative reaction kinetics of the process. Such an approach is well known to be capable of predicting axial concentration profiles of the relevant variables along the reactor length and of the radial profiles across the monolith channel and within the solid phase (Tomašić and Gomzi, 2004).

3.3.1 Governing Material and Energy Balances

In the development of the model, the governing model equations as presented by Hoebink and Marin (1998) and Tomašić and Gomzi, (2004) are employed and adapted to suit the requirements of this novel reactor. Transient and non-isothermal modes of operation are employed. The following assumptions are taken into account:

- Fully developed laminar flow inside the channel;
- The monolith channel is cylindrical with radius R_1 and symmetry around the axial axis;
- The monolith channel wall consists of porous material, with porosity ε_t and thickness equal to $R_2 - R_1$ (see Figs. (3.5 and 3.6));
- Perfect gas behaviour;
- The reactor is adiabatically operated;
- Adsorption occurs on the monolithic material that comprises the solid phase;
- Reaction occurs heterogeneously on the catalytic material within the solid phase;
- Thermal equilibrium between gas and solid phases (see Appendix B for justifications);
- Axial heat conductivity and axial diffusion in the core channel are neglected because of the usually large convective transport;
- The mass transfer in the monolith channel occurs by convection and diffusion in the axial direction and by molecular diffusion in the radial direction;

- Solid phase diffusion is described with an effective diffusivity and conduction with an effective heat conductivity;
- The gas flows in the axial direction and radial velocity profile is present. The axial velocity along radial distance obeys Newton's Law of Viscosity at maximum shear stress;
- Negligible radial convective velocity;
- Adsorption rate described by a linear driving force (LDF) approximation;
- Tóth isotherm considered for adsorption equilibrium;
- Mean specific heat capacities over the temperature range investigated;
- Dilute and isobaric operation: feed gas is a dilute mixture of a reactant and a non-adsorbable inert carrier gas. Changes in number of moles in the bulk gas upon adsorption and reaction can be neglected (see Appendix G);
- Negligible pressure drop along the monolith channel ;
- The solid phase is of constant voidage, bulk density and particle size ;

Physical properties of gas, such as density and molecular diffusion coefficients are estimated as temperature functions using correlations from the literature (see Appendix A).

Momentum transport equation

The momentum transport equation was derived on the basis of the Navier-Stokes equation (see Bird *et al.*, (1960)) and using the continuity equation $\frac{\partial v_z}{\partial z} = 0$. For fully developed laminar flow, the velocity profile considered is expressed as:

$$v_z = 2v\left[1 - \left(\frac{r}{R_1}\right)^2\right] \tag{3.21}$$

Where v (m s^{-1}), represents the average inlet velocity along the fully developed velocity profile across the core gas channel. Assuming incompressibility, the velocity is inversely proportional to R_1, which is the radius of the core gas channel. (Refer to Appendix C.1 for derivation).

Material balance

The mathematical model in this work distinguishes between two phases in the monolith adsorptive reactor i.e. the gas phase and solid phase. Figs. (3.5) and (3.6) illustrate this.

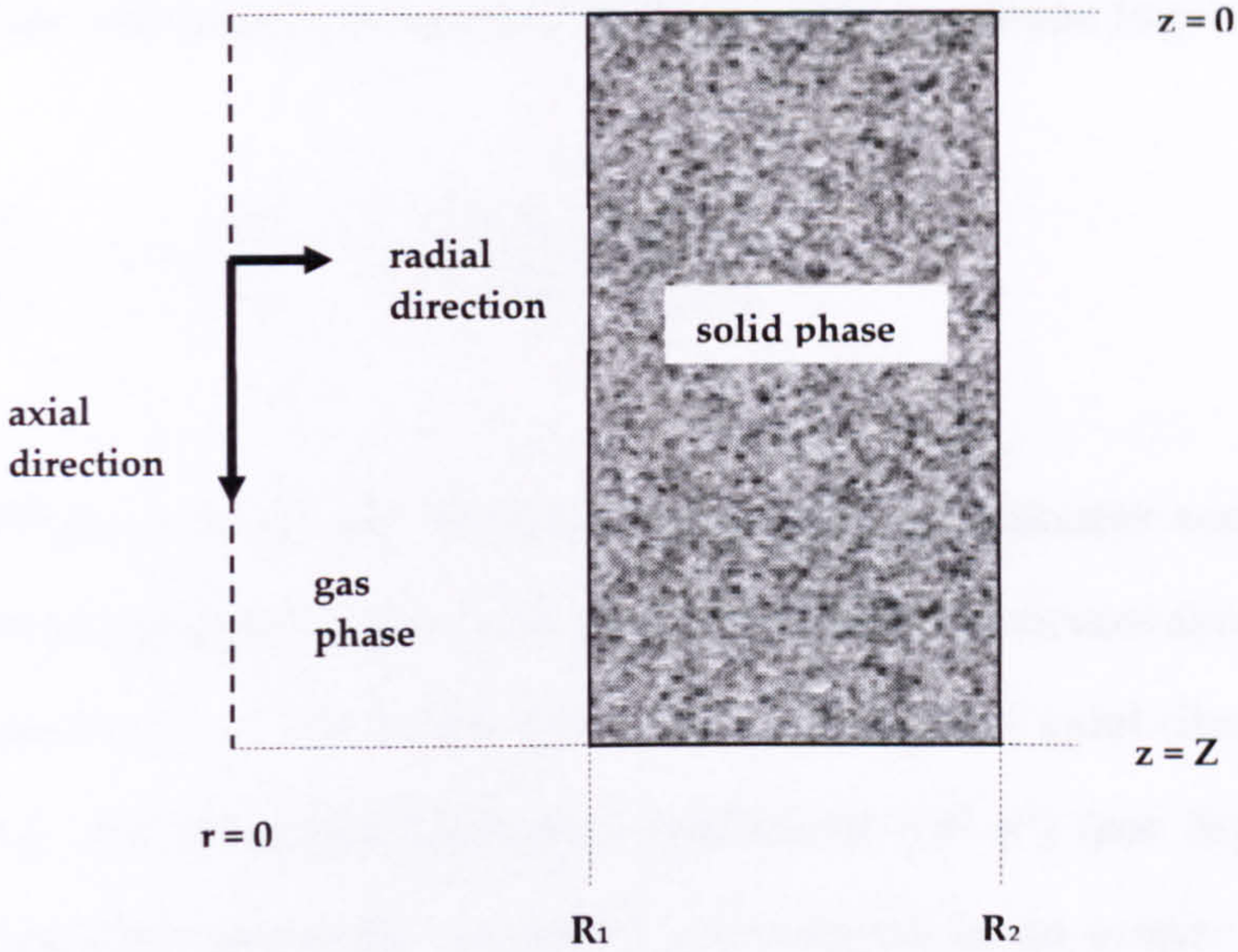

Fig 3.5: Schematic diagram of a section of the M-AR

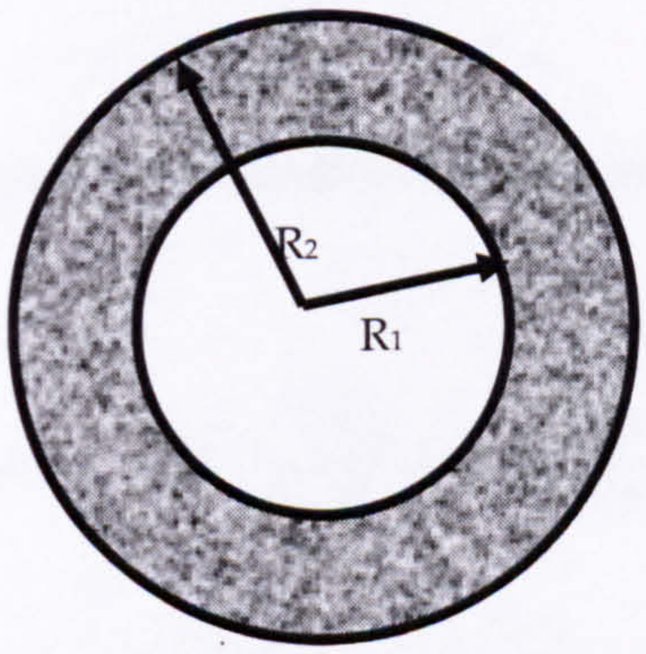

Fig 3.6: Schematic diagram of M-AR channel

Based on the above assumptions, the component material balance for the M-AR can be written as: (see Appendix C.2 for derivation)

The component material balance in the gas phase is given as:

$$\frac{\partial C_i}{\partial t} = -v_z \frac{\partial C_i}{\partial z} + D_m \left[\frac{1}{r} \frac{\partial}{\partial r} \left(r \frac{\partial C_i}{\partial r} \right) \right] \tag{3.22}$$

Where z and r are the axial and radial coordinates respectively, t is the time variable, C_i the bulk gas-phase molar concentration of component *i* (mol m^{-3}), ν_z the radial gas velocity along the axial direction (m s^{-1}), and D_m, the molecular diffusion coefficient (m^2 s^{-1}) (see Eq(3.10)). Eq. (3.22) describes the mass transport phenomena in an empty core gas channel where only the feed and reacted gas flows through the channel in both the axial and radial directions. Separation and /or reaction do not take place within this zone.

The component material balance in the solid phase is given as:

$$\varepsilon_t \frac{\partial Ci}{\partial t} + \rho r_{ads} = D_{ei} \frac{\partial^2 C_i}{\partial z^2} + D_{ei} \left[\frac{1}{r} \frac{\partial}{\partial r} \left(r \frac{\partial Ci}{\partial r} \right) \right] - \rho R_{HC} \tag{3.23}$$

Where C_i is the gas concentration in the solid phase (mol m^{-3}), r_{ads} the rate of adsorption (mol kg^{-1} s^{-1}) expressed in LDF form (see Eq.(3.4)), ρ is the bulk density of the catalyst and adsorbent (kg m^{-3}), R_{HC} the rate of reaction (mol kg^{-1} cat s^{-1}) (see Eq. (3.20)), D_e is the effective diffusion coefficient in the solid phase (m^2 s^{-1}) (see Eq. (3.7)). The total voidage of the reactor, ε_t is defined by:

$$\varepsilon_t = \varepsilon_b + (1 - \varepsilon_b)\varepsilon_p \tag{3.24}$$

Where ε_p denotes the intraparticle void fraction and ε_b denotes the bed particle void fraction.

Heat balance

For adiabatic operation with no heat transfer to the surroundings, the overall energy balance can be written as (see Appendix C.3 for derivation):

Heat balance in the gas phase:

$$\frac{\partial T}{\partial t}\rho_g C_{pg} = -\rho_g v_z C_{pg}\frac{\partial T}{\partial z} + \frac{\lambda_g}{r}\frac{\partial}{\partial r}\left(r\frac{\partial T}{\partial r}\right) \tag{3.25}$$

Heat balance in the solid phase:

$$\frac{\partial T}{\partial t}\rho_g C_{pg}\varepsilon_t + \frac{\partial T}{\partial t}\rho C_{ps} = \rho R_{HC}(-\Delta H_r) - \rho\Delta H_{ads} r_{ads} + \lambda\frac{\partial^2 T}{\partial z^2} + \frac{\lambda}{r}\frac{\partial}{\partial r}\left(r\frac{\partial T}{\partial r}\right) \tag{3.26}$$

Where ΔH_r is the heat of the reaction (J mol^{-1}), ΔH_{ads}, the heat of adsorption, (J mol^{-1}), c_{pg} the specific heat capacity of the gas (J mol^{-1} K^{-1}), c_{ps} the specific heat capacity of the solid (J kg^{-1} K^{-1}), ρ_g the gas density (mol m^{-3}), λ , the thermal conductivity (W m^{-1} K^{-1}), and *T*, the reactor temperature (K).

Assuming perfect gas behaviour, the component gas phase concentration is related to the total pressure P by:

$$\frac{P}{R\ T} = \sum_{i\ =\ 1}^{n} C_i \qquad (3.27)$$

Where P, is the total pressure (Pa), R is the universal gas constant (J mol^{-1} K^{-1}), T the operational temperature of the reactor (K) and n the total number of components. The component gas phase concentration is also related to the component mole fraction, y_i, as shown below:

$$C_i = y_i \sum_{i=1}^{n} C_i \qquad (3.28)$$

3.3.2 Initial and Boundary conditions

Initial conditions

For $t = 0$, $\forall z$ and $\forall r$:

$$y_i = 1\ ;\quad y_j = 0 \qquad j \neq 1 \qquad (3.29)$$

i.e. the gas phase is assumed to contain only the inert diluent gas nitrogen.

The solid phase is assumed to be at equilibrium with the gas which simply states that the rate of adsorption is initially zero everywhere in the bed, i.e.

$$\frac{\partial q_i}{\partial t}(z,r,0) = 0 \qquad (3.30)$$

The temperature of the reactor is initially set to equal the feed temperature, T_f:

$$T_{reactor} = T_f \tag{3.31}$$

Boundary conditions

Core channel

- At the reactor entrance, $z = 0$

$$C = C_i \; ; \; T = T_f \qquad 0 < r \leq R_1 \tag{3.32}$$

- At the channel centre, $r = 0$

$$\frac{\partial C_i}{\partial r} = 0 \quad , \quad \frac{\partial T}{\partial r} = 0 \qquad \forall z \tag{3.33}$$

- At the reactor exit, $z = L$

$$\frac{\partial C_i}{\partial z} = 0 \quad , \frac{\partial T}{\partial z} = 0 \qquad 0 \leq r \leq R_1 \tag{3.34}$$

- Velocity Profile

$$\upsilon_z = 0 \qquad R_1 < r \leq R_2 \tag{3.35}$$

Solid phase

- At $r = R_1$ (wall)

$$D_m \frac{\partial C_i}{\partial r} = D_e \frac{\partial C_i}{\partial r} \quad \text{and} \quad \lambda_g \frac{\partial T}{\partial r} = \lambda \frac{\partial T}{\partial r} \tag{3.36}$$

- At the top and bottom ends of the solid zone, $z = 0$ and $z = L$

$$\frac{\partial C_i}{\partial z} = 0 \quad \text{and} \quad \frac{\partial T}{\partial z} = 0 \qquad R_1 < r \leq R_2 \tag{3.37}$$

- At $r = R_2$

$$\frac{\partial C_i}{\partial r} = 0 \text{ and } \frac{\partial T}{\partial r} = 0 \qquad 0 < z < L \tag{3.38}$$

For the regeneration step operated in the same axial flow direction Eqs. (3.32 – 3.38) are again appropriate but in which the subscript *f* is replaced by subscript *r*, the latter denoting the feed conditions during the regeneration step i.e. from Eq. (3.32):

$$C = C_{i(r)}; \quad T = T_r \qquad 0 < r \leq R_1 \tag{3.39}$$

3.4 Model Simplifications

3.4.1 Monolith as an adsorber – M-ADS

A non-isothermal cyclic adsorber model was developed from the adsorptive reactor model. The governing equations, boundary conditions and initial conditions employed in this model are similar to that of the M-AR. It was also assumed that the reactor geometrical configurations were identical. Modifications made to the adsorptive reactor model resulting in the M-ADS model include:

- Neglecting reaction terms in the material and heat balances
- Deleting equations that involve reaction
- Changing parameter values to account for the solid adsorbent only (reaction terms are neglected or set to zero)

- Reducing the number of components to only the VOC and nitrogen
- In the regeneration step, desorption occurs without any reaction following and no oxygen is fed into the reactor. See Fig. (3.7).

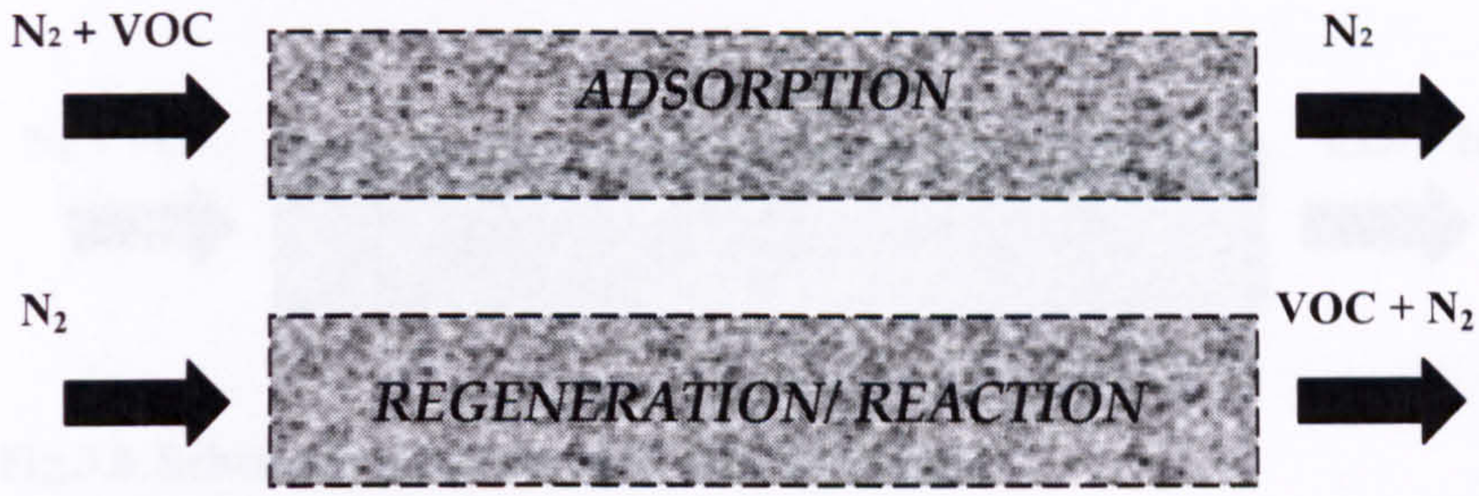

Fig.3.7: Schematic diagram of the two steps involved in M-ADS operation

3.4.2 Monolith as as a reactor – M-RXTN

A model of the monolith as a conventional catalytic reactor in which VOC oxidative reactions take place was also developed. As in the M-ADS, the governing equations, boundary conditions and initial conditions employed in this model were also similar to that of the M-AR. It was also assumed that the reactor geometrical configurations were identical. Modifications to the adsorptive reactor model resulting in the M-RXTN model include:

- Neglecting adsorption terms in the material and heat balances
- Changing parameter values to account for catalyst reaction only (adsorption parameters set to zero)
- The feed components into the reactor include the VOC, oxygen and nitrogen

- The operating conditions in this model are the same as that of the regeneration step in the M-AR.
- The reactor is operated as a single continuous step.

The monolith reactor is illustrated in Fig. (3.8).

Fig.3.8: Schematic diagram of M-RXTN operation

3.5 Mathematical modelling of the Packed Bed reactor

The concept of the novel M-AR from the packed bed reactor was outlined and discussed in Section 3.2.1.The limitations of using the packed bed reactor in terms of high pressure drop per unit length and plugging of the feed stream have been well documented in the literature. Nonetheless, 1D models of the packed bed reactor for adsorption only (PB-ADS) and reaction only (PB-RXTN) were developed to enable comparisons between the respective monolith reactors.

3.5.1 Governing Material and Energy Balances

Model Assumptions

A 1D non-isothermal and dynamic model was developed and model assumptions included:

- Perfect gas behaviour;
- Adiabatic operation;
- One dimensional bed (negligible radial temperature and concentration gradients);
- Dilute operation: feed gas is a dilute mixture of a reactant and non-adsorbable inert carrier gas. Changes in the number of moles in the bulk gas upon adsorption can be neglected (See Appendix G);
- Mean specific heat capacities over the temperature range investigated;
- Axially dispersed plug flow; axial dispersion is described by Fick's Law and dispersion coefficient of each component is constant;
- Linear driving force model considered for adsorption;
- Tóth isotherm considered for adsorption equilibrium;
- Thermal equilibrium between gas and solid phases;
- Adsorbent and catalyst are spherical in shape and are packed uniformly in the bed;
- Bed is of constant voidage, bulk density and particle size;
- No mass or heat transfer resistance at the surface or inside surface particles;
- Physical properties are constant over the range of operating conditions;

The component material balance is given as:

$$\varepsilon_t \frac{\partial C_i}{\partial t} + \rho_b \frac{\partial q_i}{\partial t} = -v\frac{\partial C_i}{\partial z} + D_z \frac{\partial^2 C_i}{\partial z^2} + \rho_b \nu_i R_{HC} \qquad (3.40)$$

Where v is the superficial gas velocity (m s^{-1}), ν_i is the stoichiometric coefficient of component *i* ($\nu_i < 0$ for reactants and $\nu_i > 0$ for products) and D_z, is the axial dispersion (m^2 s^{-1}).

Axial Dispersion

Axial dispersion in a packed bed involved Fickian type diffusion which can be expressed as:

$$\frac{\partial C_i}{\partial t} = D_A \frac{\partial^2 C_i}{\partial z^2} \tag{3.41}$$

where D_A is the effective axial dispersion coefficient $m^2 s^{-1}$. D_A accounts for all mechanisms responsible for the axial backmixing and intermixing effects which cause local fluctuations in flow velocities and molecular and turbulent (eddy) diffusion within the packed bed. It is usually expressed as a function of the molecular diffusion (D_m) and the superficial velocity (v). Experimental correlations usually involve the dimensionless Peclect number, Pe, where:

$$Pe = \frac{\nu d_p}{D_A} \tag{3.42}$$

The Peclet number is a function of the particle Reynolds number, Re_p ($= \frac{\rho_g \nu d_p}{\mu}$), and the Schmidt number Sc ($= \frac{\mu}{\rho_g D_m}$). Examples for such correlations can be found in Langer et al. (1978) for a variety of particle diameters and ratios of bed length to particle diameter. The axial

dispersion coefficient based on a bed cross sectional area which excludes the area occupied by particles, D_z can then be defined as:

$$D_z = \varepsilon D_A \tag{3.43}$$

Further details on the calculation of D_z are presented in Appendix A.

The heat balance is given as:

$$\varepsilon_t C_{pg}\rho_g \frac{\partial T}{\partial t} + \rho_b C_{ps} \frac{\partial T}{\partial t} = -vC_{pg}\rho_g \frac{\partial T}{\partial z} + \lambda \frac{\partial^2 T}{\partial z^2} - \rho_b \Delta H_{ads} \frac{\partial q_i}{\partial t} - \rho_b R_{HC} \Delta H_r \tag{3.44}$$

3.5.2 Initial and Boundary Conditions – P-BR

Initial Conditions

For $t = 0$, $\forall z$:

$$y_i = 1 ; \quad y_j = 0 \qquad\qquad j \neq 1 \tag{3.45}$$

i.e. the gas phase is assumed to contain only the inert diluent gas nitrogen.

$$T(z,0) = T_f \tag{3.46}$$

$$q_i(z,0) = 0 \tag{3.47}$$

Boundary conditions

At the reactor entrance, $z = 0$:

$$C = C_i^{feed} \tag{3.48}$$

At the reactor exit, z = L:

$$\frac{\partial C_i}{\partial z} = \frac{\partial T}{\partial z} = 0 \tag{3.49}$$

3.6 M-AR Process Performance

3.6.1 Performance Indices

Adsorptive reactors can be assessed in terms of separation performance, such as the purity and recovery of a key component, and in terms of reaction performance such as the overall yield of a component. The performance of the M-AR is affected by a number of highly interacting design and operating parameters but in order to assess its performance effectively, it is compared to a monolith reactor (M-RXTN) that is similar to it in terms of reactor design and regeneration operating parameters and conditions. The performance indices are described below:

a. Effectiveness of VOC disposal

VOC conversion is used as a measure of the effectiveness of VOC disposal. As the M-AR is operated cyclically, the conversion in this case is expressed as:

$$X = \frac{\left(\int_{r=0}^{R_1} C_{i=1,z=0,r} \upsilon_z dr - \int_{r=0}^{R_1} C_{i=1,z=L,r} \upsilon_z dr \right)}{\int_{r=0}^{R1} C_{i=1,z=0,r} \upsilon_z dr} \tag{3.50}$$

b. Energy input

The energy requirement for process operation is an important measure in evaluating the performance of reactor systems. Energy generation is usually given by ΔH_{rx} mole of VOC reacted and as such the energy released from the exothermic reaction in both reactors will not differ. A way to measure the energy requirement is through the feed stream energy input needed to sustain VOC conversion. The rate of energy input, E_{AR}, is defined as the cycle average rate of heat supply (J $m^{-2}s^{-1}$) which depicts feed pre-heating costs required to raise an inlet stream from ambient temperature (298K) to the reactor inlet temperatures T_f, T_{fa} and T_{fr}. It is defined as:

$$E_{AR} = \frac{c_{pg}P}{(t_a + t_r)R}\left\{\frac{\upsilon_{fa}t_a}{T_{fa}}(T_{fa} - 298) + \frac{\upsilon_r t_r}{T_r}(T_r - 298)\right\} \quad (3.51)$$

Where C_{pg} is the specific heat capacity of the gas (J mol^{-1} K^{-1}), P is the total pressure (Pa), R is the universal gas constant (= 8.314 J mol^{-1} K^{-1} or Pa m^3 mol^{-1} K^{-1}) and the subscripts f, a and r denote the feed / inlet, adsorption and regeneration step respectively. Eq. (3.51) was adapted from Yongsunthon (1999).

The energy input in the monolith reactor, M_{-RXTN} can be defined as:

$$E_{RXTN} = \frac{c_{pg}P}{RT_f}\upsilon_f t(T_f - 298) \quad (3.52)$$

In order to compare the energy consumed for both reactors, the time on the stream, t in Eq. (3.52) is defined to be equal to the time taken of one

cycle in an adsorptive reactor. It can then be compared to one another using Eq. (3.53):

$$\Delta E = E_{AR} - E_{RXTN} \tag{3.53}$$

Where ΔE is the difference of total energy input between an adsorptive reactor and a monolith reactor based on the same time taken which is equal to one cycle time of an adsorptive reactor and the same amount of VOC converted.

c. Temperature stability

VOC oxidation is highly exothermic and as such a runaway situation may be established due to changes in the reactor feed inlet temperatures T_f and T_r or due to changes in the VOC feed concentration. The M-AR is predicted to be able to decrease this parametric sensitivity due to heat integration of an endothermic desorption and exothermic reaction, and principally due to the controlled release of the VOC from the adsorbed phase into the reaction zone, which leads to runaway prevention. To demonstrate the performance of the M-AR to that of the monolith reactor, the change in feed VOC concentration is considered. Consideration is also given to changes in the inlet temperatures. The safety of the M-AR can be demonstrated by the decreased maximum temperature, T_{max} , propagating in the reactor bed under the same operating and process conditions.

3.7 Numerical Methods

Periodic adsorption / reaction can be described as a dynamic distributed parameter problem as the system property, x (*e.g.* concentration, temperature, pressure) varies with respect to spatial dimension(s) i.e. axial and radial positions in the reactor denoted as z and r respectively (see Fig.(3.5)) as well as time, t. We can, therefore, write: $x = x(z,r, r', t)$, $z \in [0,L]$, $r \in [0,R]$, $t \geq 0$ where L and R are the length and radius of the monolith reactor respectively. The model is a combination of lumped and distributed parameter systems to account for the differentiation of axial and radial dimensions which vary with time. Yongsunthon (1999) explains that under transient operation, the processes can be expressed by a set of partial differential equations (PDEs) describing the physical laws of conservation of material, energy and momentum, and algebraic equations (AEs) describing other (auxillary) relationships *e.g.* the adsorption isotherm. The overall system is represented by a set of partial differential algebraic equations (PDAEs).

The solution of a set of PDAEs is obtained through the discretisations of the spatial and temporal domains. The *method of lines* is employed when the two discretisations – (1) spatial domain (reducing PDAEs to DAEs) and (2) integration of DAEs over time as an initial value problem, are carried out in two separate steps. The second step is normally performed by an appropriate time integration algorithm *e.g. finite differences.* The finite difference method may involve simple first and second-order

approximations to the differential variables, or more sophisticated backward difference formulae (Jarvis and Pantelides, 1992). The finite difference method is solved using backward grid position with respect to the spatial domains: axial and radial. It is therefore known as the backward finite difference method, BFDM. In the *gPROMS* environment, BFDM method allows a user to specify the tolerance level by adjusting automatically the step size and integration order to maintain the desired integration error. This method transforms the PDEs to ODEs over a small interval of time and thus, convergence is assured for specific size of increments of interval length.

The spatial and temporal discretisations can also be performed simulatneously known as the *complete discretisation method.* The choice of discretisation methods (e.g. finite differences, orthogonal collocation or orthogonal collocation on finite elements) can be made independently for the spatial and temporal domains. The PDAEs are then transformed into nonlinear AEs and can be solved using standard numerical techniques such as Newton method.

The choice of numerical method for effective simulation and optimisation of periodic processes (adsorption, reaction, adsorption / reaction) is of great importance in order to ensure solution accuracy. The design demands (configurations / operating policies / cyclic steady state determination etc.) of periodic processes render the describing systems of model equations complex and depend on model assumptions. There are many numerical approaches and discretisation techniques in the

literature commonly employed to solve periodic process problems as detailed by Nilchan (1997) and Yongsunthon (1999).

The model equations described in this chapter were coded and solved in the gPROMS environment. Due to its ability to solve problems involving a strong convective component (Oh, 1995), the finite difference method (BFDM) is applied in this work. The discretisation involves a fixed number of points to the left and right of the integral approximation point (Oh, 1995). The spatial domain was discretised using BFDM applied at 50 grid points for axial and 15 grid points for radial. This approach was found to give a converged solution in which component balance errors (associated with numerical integration) were negligible. For more details on numerical method approaches see Oh (1995), Nilchan (1997) and Yongsunthon (1999).

3.7.1 Cyclic steady state operation

A common feature of all periodic adsorption processes is that they are intrinsically dynamic; never being allowed to reach steady state as no useful separation can be achieved at the latter. Nevertheless, all such processes are subjected to a fixed variation of the external conditions (e.g. feed) over a cycle, which is then repeated. After a sufficiently large number of cycles, each bed in the process normally reaches a *cyclic steady state* (CSS) in which the conditions in the bed at the end of each cycle are exactly the same as those at the beginning of the cycle. Although the number of cycles required to reach the CSS can be large, typically it is

relatively small in comparison to the total number of cycles between successive process start-ups and shut-downs. Thus most periodic processes (adsorption / combined adsorption and reaction) are practically at CSS for most of their useful operation. Consequently it is this CSS that determines their technical and economic performance.

In order to effectively compare the performance of the M-AR to a monolith reactor, data from the M-AR at cyclic steady state is required. The requirements for cyclic steady state are that the operating conditions at the beginning of the adsorption step be identical to those at the end of the precedent desorption step after the first cycle. The values at steady state are then used for comparison with the monolith reactor also at steady state. The dynamics of the M-AR process makes it rather complicated to judge when steady state is achieved as the number of cycles needed to attain steady state can potentially be computationally exhaustive. There are two approaches to achieving the solution of the process at cyclic steady state. The first approach is by dynamic simulation over a large number of cycles such that cyclic steady state convergence is achieved. This is the approach employed in this thesis. The second approach involves the complete discretisation of the partial differential and algebraic equation system in which both space and time are discretised simultaneously. This approach reduces the PDAEs to a system of algebraic equations which means that cyclic steady state can therefore be directly imposed by solving this algebraic system such that periodicity (or cyclic steady state) conditions are met. Periodicity constraints state that the bed conditions must be identical at the end and

the beginning of the cycle. This approach has been applied to periodic adsorption (Nilchan, 1997) and periodic adsorptive reaction (Cheng *et al.,* 1998). They also give comparisons between the complete discretisation and the dynamic approaches with the conclusion that irrespective of the fact that each cycle of operation can be solved relatively quickly, the large number of cycles in the dynamic approach led to a larger overall computational time than the one-off direct determination of cyclic steady state using complete discretisation.

In the monolith reactor, M-RXTN operation is non-cyclical and as such the two reactors are required to operate in similar modes. In order to achieve this, all process operating conditions and parameters need to be identical in the two reaction systems.

3.8 Conclusions

Models for the adsorptive reactor were developed based on the monolith reactor model developed by Hoebink and Marin (1998) and adapted to suit the particular process investigated in this work. The adsorptive reactor model parameters are given in Table (3.7) below. The next chapter presents the results from the dynamic simulation of the various models described in this chapter.

Parameters	Value	Remarks / Reference
Reactor geometry		
L, m	0.5	Williams (2001)
δ, m	3×10^{-4}	$(R_2 - R_1)$
R_1, m	1.2×10^{-3}	Williams(2001); Crittenden *et al.*, (1996); Hayes and Kolaczkowski (1994)
R_2, m	1.5×10^{-3}	Hayes *et al.*, (2001)
Solid zone properties		
ϱ_b, kg m^{-3}	728	$(\varrho_{b\,ads} + \varrho_{b\,cat}) / 2$
$\varrho_{adsorbent}$, kg m^{-3}	659	Zhu *et al.*, (2005)
$\varrho_{catalyst}$, kg m^{-3}	797	Van de Beld *et al.*, (1995)
ε_t	0.76	Marbán *et al.*, (2006)
r_p, m	1.5×10^{-4}	Zhu *et al.*(2004)
C_{ps}, J $kg^{-1}K^{-1}$	710	Estimated value
λ, W m^{-1} K^{-1}	10	Py *et al.*, (2005)
Adsorption parameters		See Table (3.2)
Reaction parameters		See Tables (3.5 and 3.6) Model III
Gas properties		
C_{pg}, J mol^{-1} K^{-1}	50	Ethene at T = 298K
C_{pg}, J mol^{-1} K^{-1}	75	Propane at T = 298K
Λ_g, W m^{-1} K^{-1}	0.01	Estimated value
Diffusion coefficients		See Appendix A

Table 3.7: Parameters used in the simulation of the M-AR model

CHAPTER 4 Results & Discussion: Monolith & Packed Bed Configurations

4.1 Introduction

The M-AR concept integrates adsorptive separation and reaction in a single unit. In this chapter, theoretical studies on the performance of the novel M-AR based on the 2D mathematical models described in Chapter 3 are presented. This enables the feasibility and therefore, potential of this novel process to be explored. Model equations are then solved within the *gPROMS* environment.

In order to understand and gain insight into the dynamics of the process it is necessary to formulate a strategy on how the process is run and the results interpreted. This strategy is outlined in Section 4.2 and includes justifications for equivalency between packed bed reactors and monoliths (for comparative purposes) and the need for dynamic models and steady state solutions. Following on from this, dynamic simulation results are split into three main sections - Single step operation, cyclic operation and temperature stability effects within the M-AR. A brief description of the different operational modes is given below:

- Single step operation: Single step operation results are presented in Section 4.3. The two individual steps of adsorption (M-ADS) and

reaction (M-RXTN) that occur in the M-AR are simulated initially with the aim of providing insight into the dynamics of the individual steps and thus the overall adsorptive-reactive process.

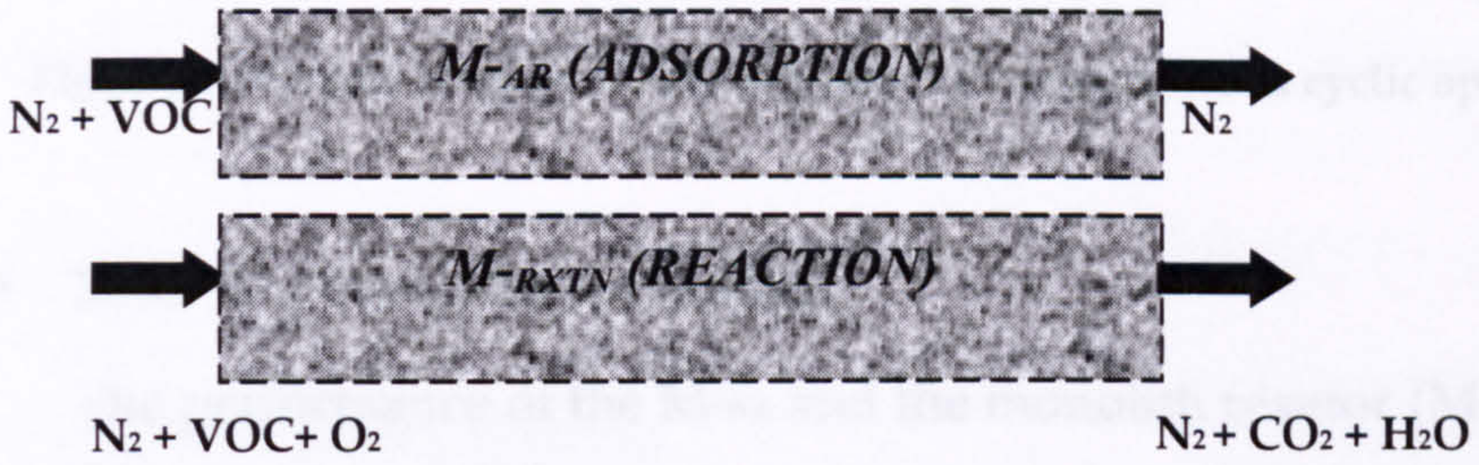

Fig.4.1: Schematic diagram of the two individual steps for single step operation

- Cyclic operation: The need for adsorbent regeneration renders the M-AR process cyclic in nature. The adsorption step with a periodic mode of operation is investigated with emphasis on the desorption step. The performance of the hybrid monolith, M-AR as an adsorptive reactor is also explored and its performance assessed with respect to the performance measures as described in Section 3.5. Cyclic simulation results are presented in Section 4.4.

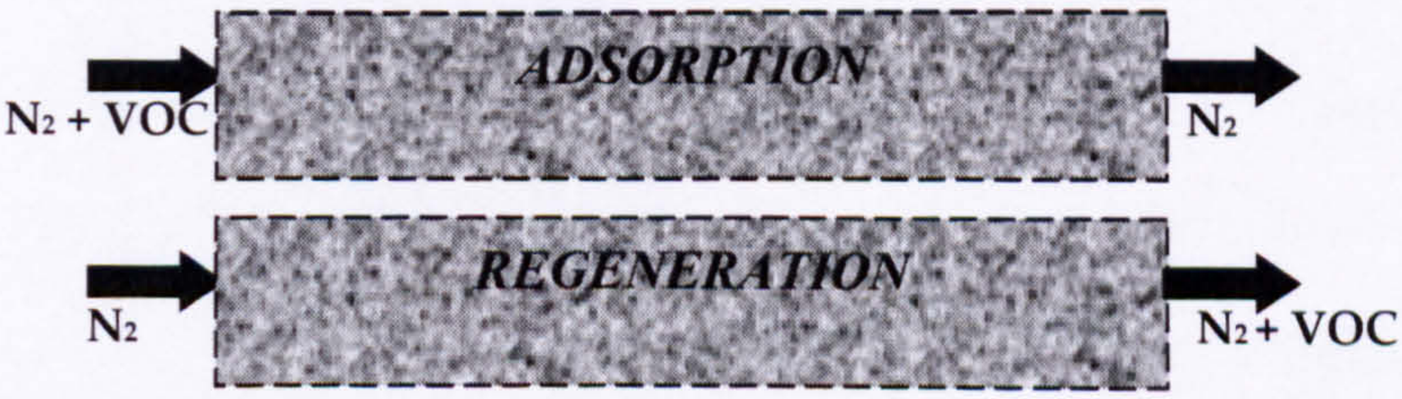

Fig.4.2: Schematic diagram of the two steps involved in M-ADS cyclic operation

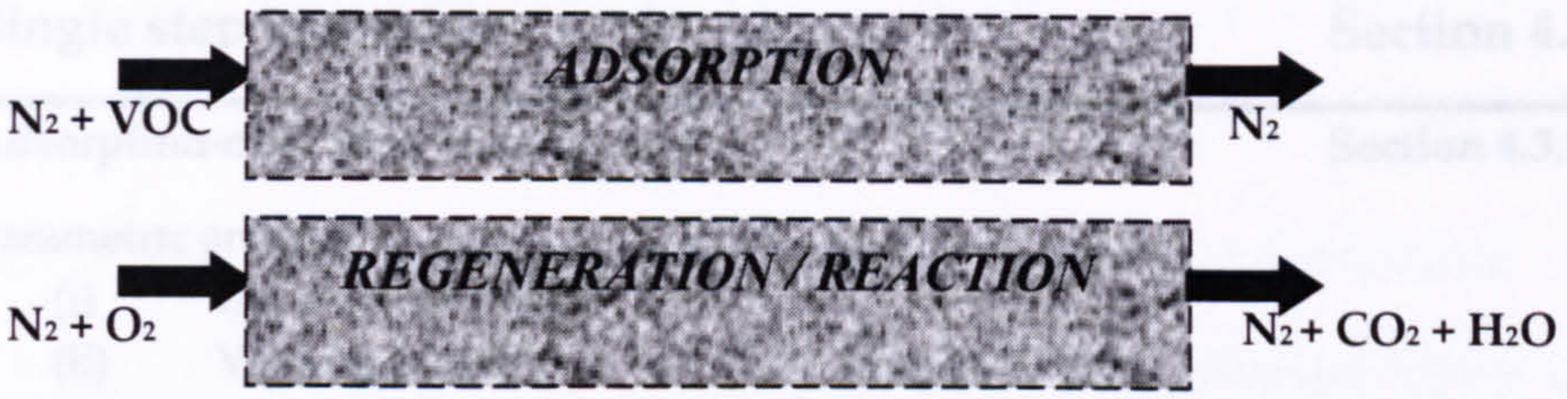

Fig.4.3: Schematic diagram of the two steps involved in M-AR cyclic operation

- M-AR and Temperature stability

  The performance of the M-AR and the monolith reactor (M-RXTN) are assessed in terms of thermal stability and the ability of both reactors, M-AR and M-RXTN to cope with changes in feed concentrations and temperatures. Finally, thermal stability results are detailed in Section 4.5.

Table (4.1) gives an outline on how results and data are presented within each of the sections detailed above.

Single step operation	**Section 4.3**
Adsorption-only Step (no reaction)	**Section 4.3.1**
Parametric analysis (i) Geometrical effects (ii) Velocity effects Packed bed reactor comparisons	
Reaction-only Step (no adsorption)	**Section 4.3.2**
Parametric analysis (i) Geometrical effects (ii) Velocity effects Packed bed reactor comparisons	
Summary of single-step operation	**Section 4.3.3**
Cyclic operation	**Section 4.4**
Cyclic adsorption (no reaction)	**Section 4.4.1**
M-AR operation (cyclic adsorption and reaction) (i) Heating time effects on M-AR performance (ii) Incomplete bed saturation along reactor length	**Section 4.4.2**
Parametric analysis (i) Effect of step times ▪ Adsorption step time ▪ Heating time (desorption step time) (ii) Temperature effects (iii) Velocity effects	
Summary of cyclic operation	**Section 4.4.3**
Temperature stability	**Section 4.5**
Equivalency between the M-AR and M-RXTN	
$T_{fa} = T_{fr}$ Operation (i) Concentration effects (ii) Temperature effects	**Section 4.5.1**
Temperature swing effect ($T_{fa} \neq T_{fr}$ Operation) (i) Concentration effects (t_a = 5s) (ii) Concentration effects (t_a = 50s) (iii) Temperature effects	**Section 4.5.2**
Summary of thermal stability investigations	**Section 4.5.3**
Further discussions	**Section 4.6**

Table 4.1: Results and data presentation

4.2 Simulation Strategy

4.2.1 Equivalency between packed bed reactors and monoliths

For laminar flow in the monolith reactor, the pressure drop can be estimated from the Hagen-Poisuille correlation. For tortuous interstitial flow in traditional packed bed reactors, the greater inter-phase momentum resistance (Dautzenberg and Mukherjee, 2001) leads to a large increase in pressure drop for equivalent flow rates. High pressure drop is often the major disadvantage of a conventional packed bed reactor relative to the monolith reactor. The pressure drop in the packed bed was calculated from the Ergun Equation. Comparisons in the performance of the packed bed reactor to that of the monolith reactor based on the models detailed in Chapter 3 are also performed. The monolith reactor is compared to a packed bed configuration under identical operating conditions. All comparisons between both reactor types are made under the constraints that both reactors treat equal amounts of feed and that both use the same amount of adsorbent. Section 3.2.1 described the M-AR concept (see Fig. (3.2)) and its adaptation from the conventional packed bed reactor, therefore this makes for interesting comparisons between the two reactor types.

The superficial velocity in the packed bed is calculated from the constraint that both systems treat the same amount of feed and is given by:

$$V_m = \frac{V_{pb}}{f^2 n_d \frac{\pi}{4}(D_{channel})^2} \tag{4.1}$$

Where V_m is the average fluid velocity in the monolith channel (cm s^{-1}), V_{pb} the superficial velocity in the packed bed (cm s^{-1}), f the ratios of diameters of the monolith and packed bed column, n_d the cell density (no. of cells cm^{-2}), and $D_{channel}$ the monolith channel diameter (m) (see Crittenden *et al.*, (1994)). For every velocity considered in the monolith reactor, the equivalent velocity in the packed bed was calculated from Eq. (4.1).

As previously outlined in Section 3.2.1, and with reference to Eqs.((3.1) – (3.3)), in this work the cell density considered was 40 cells cm^{-2}, with $\varepsilon_m = \varepsilon$ and $f = 1.5$. Based on this, equivalency between both reactor types is assured.

In Chapter 3, Table (3.7) lists the parameters employed for base case simulations. Table (4.2) lists the base case parameters for the monolith reactor (M-ADS / M-RXTN / M-AR), see also Figs. ((3.7) and (3.8)) and its equivalent packed bed reactor (PB-ADS / PB-RXTN / PB-AR).

Parameters	Value	Unit
Monolith core channel radius, R_1 / packed bed radius, R_{PB}	1.2	mm
Monolith total radius, R_2	1.5	mm
$L_{monolith}$ / L_{PB}	0.5 / 1.125	m
$V_{monolith}$ / V_{PB}	0.05	m s^{-1}

Table 4.2: Base case parameters for the monolith reactor and the packed bed reactor
Note: $D_{channel}$ is also equal to R_1

4.2.2 Dynamic Models and steady state solutions

The design and overall performance of the M-AR is assessed in terms of concentration profiles, conversion, energy input and thermal stability. Dynamic models of the individual steps of adsorption-only in the monolith reactor employed as an adsorber (M-ADS) and the monolith reactor operating continuously (M-RXTN) are first individually simulated to gain insight into the reactor performance. Steady state comparisons are then made to an equivalent packed bed reactor. From the insight gained from the performance of the individual steps, the M-AR is then investigated and its performance also assessed. Comparisons are also made to a similarly operating monolith reactor and equivalent packed bed reactor. Studying the effects of the various process parameters (geometrical, i.e. length and reactor radii, velocity) and operating conditions (e.g. feed temperatures) on the performance measures give a basic and crude indication to the best and worst case scenarios for the various reactor models.

In general, adsorption-only (M-ADS), reaction-only (M-RXTN) and adsorptive reactor (M-AR) performances are investigated for very low adsorbate concentrations (3000 ppm or 0.3 vol. %). For thermal stability considerations, ethene as the VOC gas is utilised and concentrations also explored between the lower explosive limits, LEL (2.7 vol. %) and upper explosive limits, UEL (36 vol. %) values. In order to effectively compare the thermal stability performance of the M-AR with the similarly operating M-RXTN, wherein both reactors are identical in terms of geometrical configurations, catalyst amount, feed inlet velocities and

operating conditions, the feed concentrations are required to be adjusted. The feed concentrations for the monolith reactor (M-RXTN) are adjusted accordingly to account for the fact that the M-AR is cyclically operated whereas the M-RXTN operates with a continuous feed of pre-mixed VOC and air. Thus the number of moles of ethene fed in during the adsorption step in the M-AR is first calculated, and on the basis of identical volumetric feed rates in both reactors, the number of moles of ethene required for feeding into the M-RXTN can thus be back calculated.

For cyclic operation, the results quoted are at cyclic steady state (see Section 3.7.1).

Parameters	Value	Unit
Feed inlet temperatures for adsorption (Ethene)	293 / 320 / 338	K
Feed inlet temperatures for desorption (Ethene)	460 / 475 / 490	K
Feed inlet temperatures for adsorption (Propane)	320 / 338/ 358	K
Feed inlet temperatures for desorption (Propane)	560 / 580 /600	K
Feed mole fraction, Ethene	0.003	-
Feed mole fraction , Propane	0.003	-
Feed mole fraction, O_2	0.21	-
Feed mole fraction, N_2 (adsorption)	0.997	-
Feed mole fraction, N_2 (desorption)	1* / 0.79	-

Table 4.3: Feed conditions (base case) * indicates single step adsorption

Tables (3.7, 4.2 and 4.3) illustrate base case parameters used for dynamic simulation. These parameters are utilised in all cases except where explicitly defined. In cases where adsorption-only occur there are no

reaction parameters and vice versa for cases where reaction-only takes place.

4.3 Single step operation

4.3.1 Adsorption-only Step (no reaction)

The adsorption step is modelled as a single step to gain an understanding of typical breakthrough profiles and times as well as loading capacities and the effectiveness of adsorption i.e. the purity of the inert gas N_2. The effects of geometrical parameters and velocity are assessed with reference to the breakthrough profiles. Furthermore, comparisons to the packed bed reactor (PB-ADS) are made in terms of breakthrough profiles and pressure drop characteristics.

In order to describe the concentration profiles of the adsorbate, in this work breakthrough and saturation have been defined as:

Breakthrough - the point where leakage of the adsorbate from the reactor bed occurs.

Saturation - the point where the concentration of the inlet adsorbate equilibrates with that of the adsorbate in the gas stream. At this point the adsorbent is saturated with adsorbate gas and no more potential adsorption can occur. The results described in this section are within this regime.

Figs. (4.4) and (4.5) show the exit concentration profiles of ethene and propane in the M-ADS reactor at base case conditions and inlet velocity 0.05 m s^{-1} for different feed temperatures of adsorption, T_{fa}.

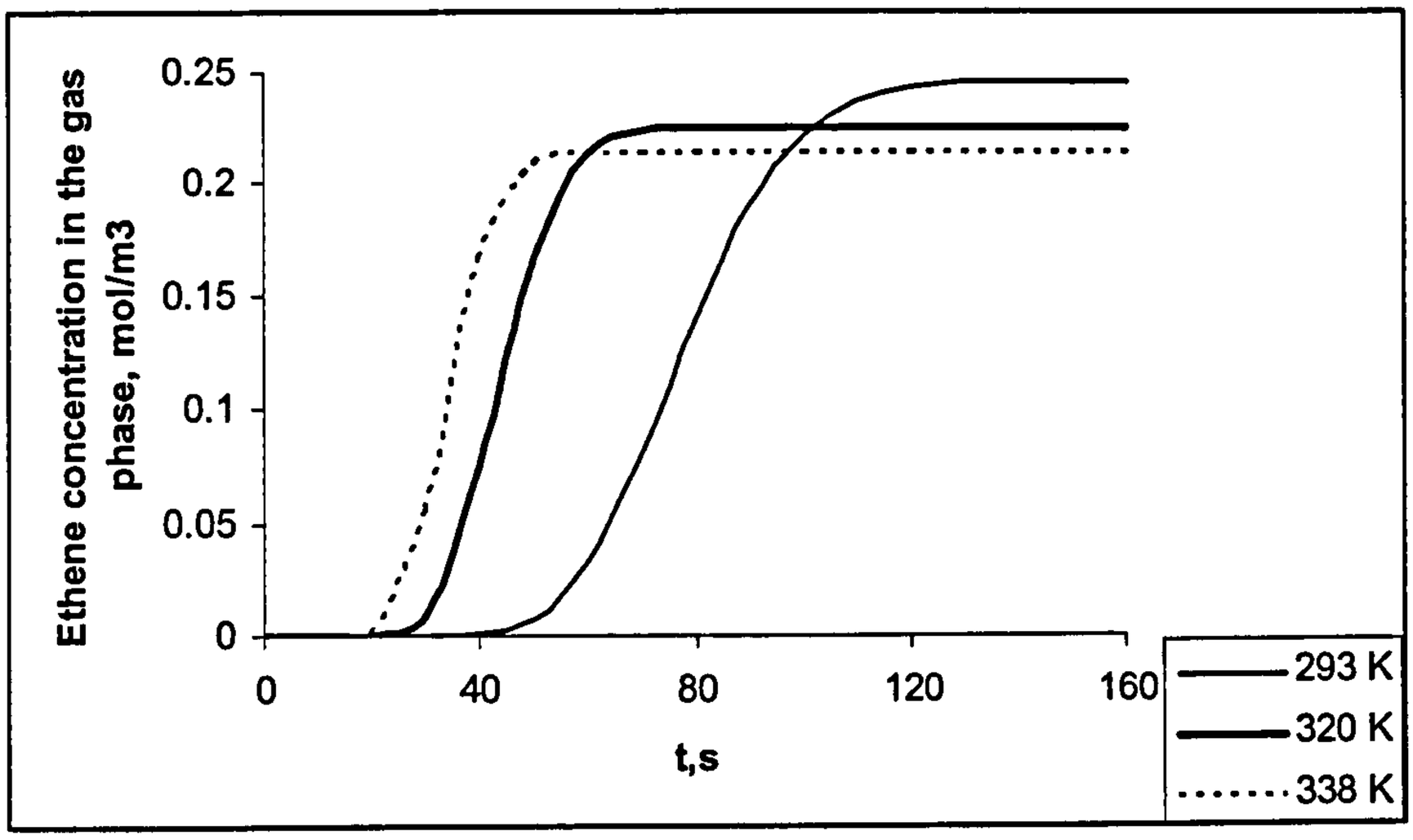

Fig 4.4: Ethene exit concentration profiles for different adsorption temperatures

With reference to Fig. (4.4), complete saturation of the adsorbent bed is achieved after 130 s, 70 s and 45 s for T_{fa} 293 K, 320 K and 338 K correspondingly. In the case of 293 K, true breakthrough of the adsorbate is seen after 40 s. As expected, the adsorbent capacity decreases rapidly with increasing temperature as predicted by the adsorption isotherm gradient and the van't Hoff equation. Therefore at 293 K, the adsorbent capacity is at its highest (hence the slow breakthrough) and parametric studies are performed at this temperature to investigate the effects on geometric and operational parameters on the adsorbate breakthrough profile.

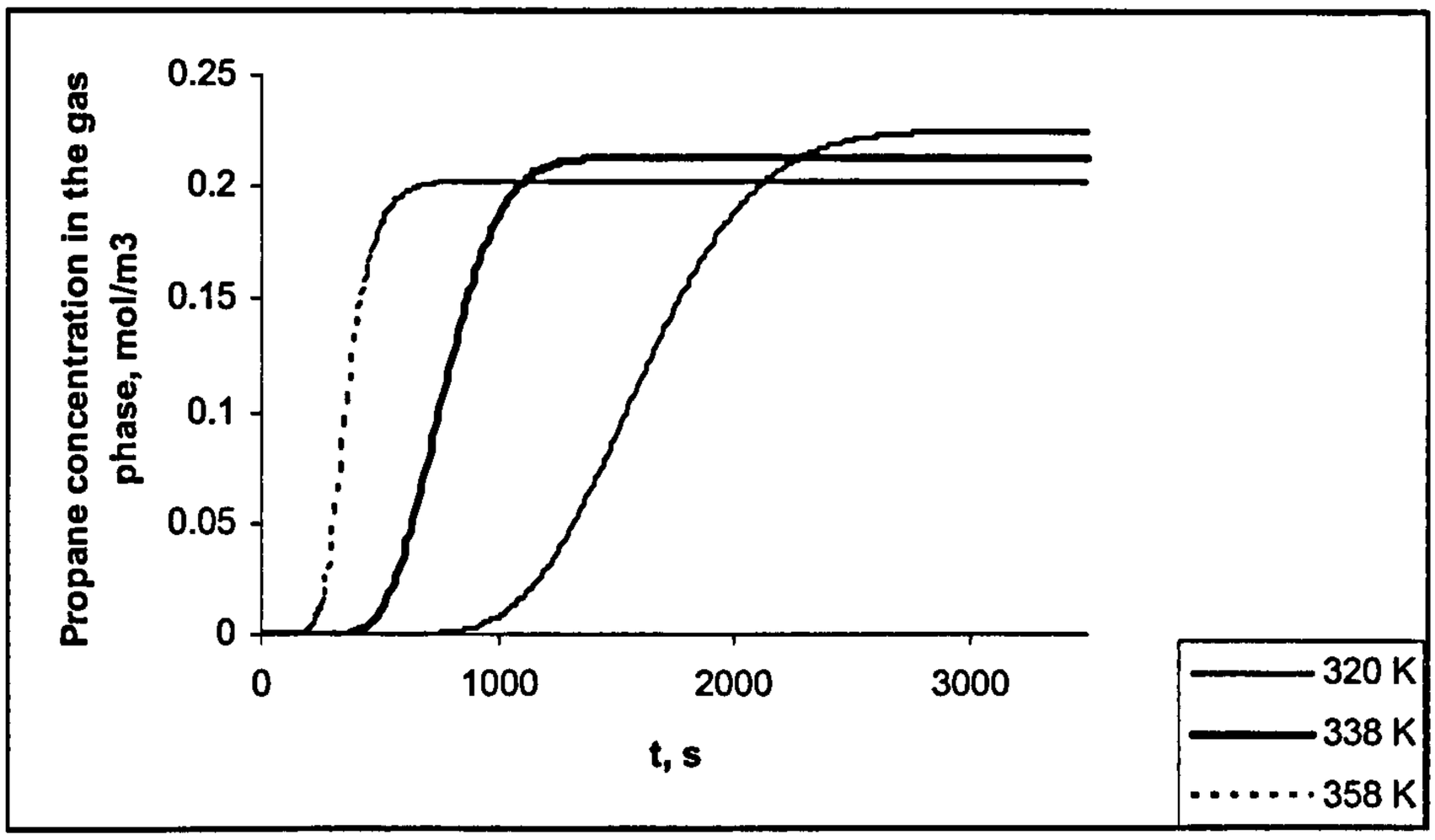

Fig 4.5: Propane exit concentration profiles for different adsorption temperatures

Fig. (4.5) follows the same trend as described in Fig. (4.4). Breakthrough and saturation times for propane are slower in comparison to ethene. At 320 K, breakthrough occurs after 800 s (c.f. ethene at 30 s). The adsorption kinetics and mass transfer properties of the two gases on activated carbon differ greatly as detailed in Table (3.2) and has a major effect on the adsorbent performance and breakthrough profiles.

Parametric Analysis

(i) Geometrical Effects

The effect of varying the core channel radius, R_1 and the length of the M-$_{ADS}$ reactor is investigated for the case of T_{fa} 293 K whilst keeping all other base parameters constant and the results illustrated in Figs. (4.6 and 4.7).

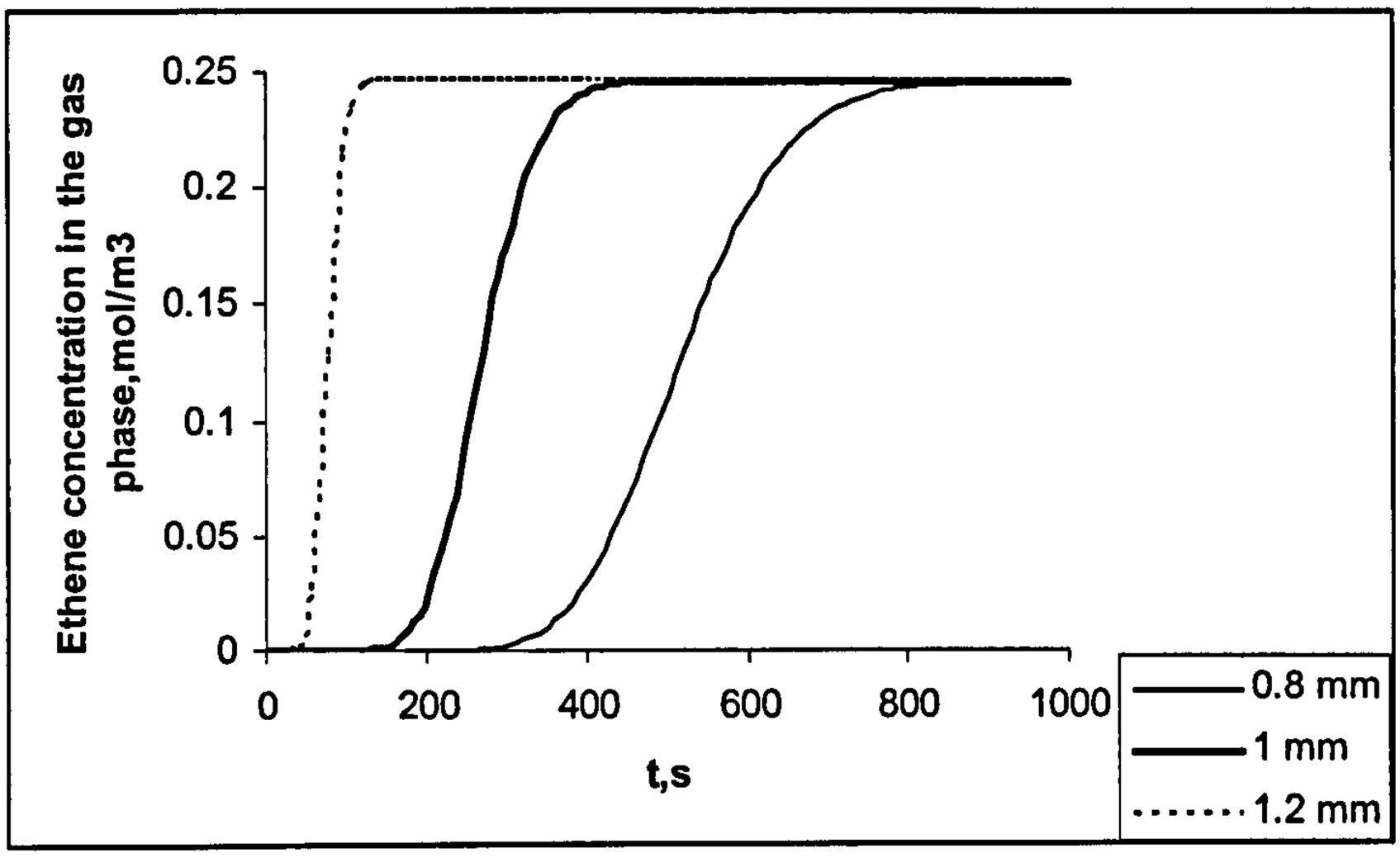

Fig 4.6: Ethene exit concentration profiles at different core channel radii

Fig. (4.6) illustrates the effect of varying R_1. The change in the core gas channel radius also affects the thickness of the solid adsorbent zone, δ. The overall monolith channel radius, R_2 is fixed at 1.5 mm and for values of the radii shown in Fig. (4.6), the corresponding δ is given as 0.7 mm, 0.5 mm and 0.3 mm respectively. The narrower core channel radius, results in a bigger δ. Despite the fact that the gas flows through and diffuses into the solid zone faster within a narrower channel for the case where R_1 is 0.8 mm, the increased solid zone thickness (0.7 mm) leads to slower adsorbate breakthrough and saturation time due to the longer distance and increased diffusion time. Likewise, for a wider core gas channel (and therefore smaller solid thickness, δ), the breakthrough time is faster due to the increased diffusion distance from the channel to the solid zone (where gas by-pass may potentially occur) and the short diffusion distance within the solid zone itself.

The effect of the length of the M-ADS on the breakthrough performance of the adsorbate is illustrated in Fig. (4.7). The adsorbate breakthrough effect is slower at longer reactor lengths again due to the longer distance and time required for diffusion. More importantly, a longer reactor length implies longer space time ($\tau = \frac{V}{v_0}$) with V the reactor volume (m^3) and v_0 the volumetric flowrate ($m^3\ s^{-1}$). At a length of 1m, τ is 20 s (c.f. 10 s at 0.5m).

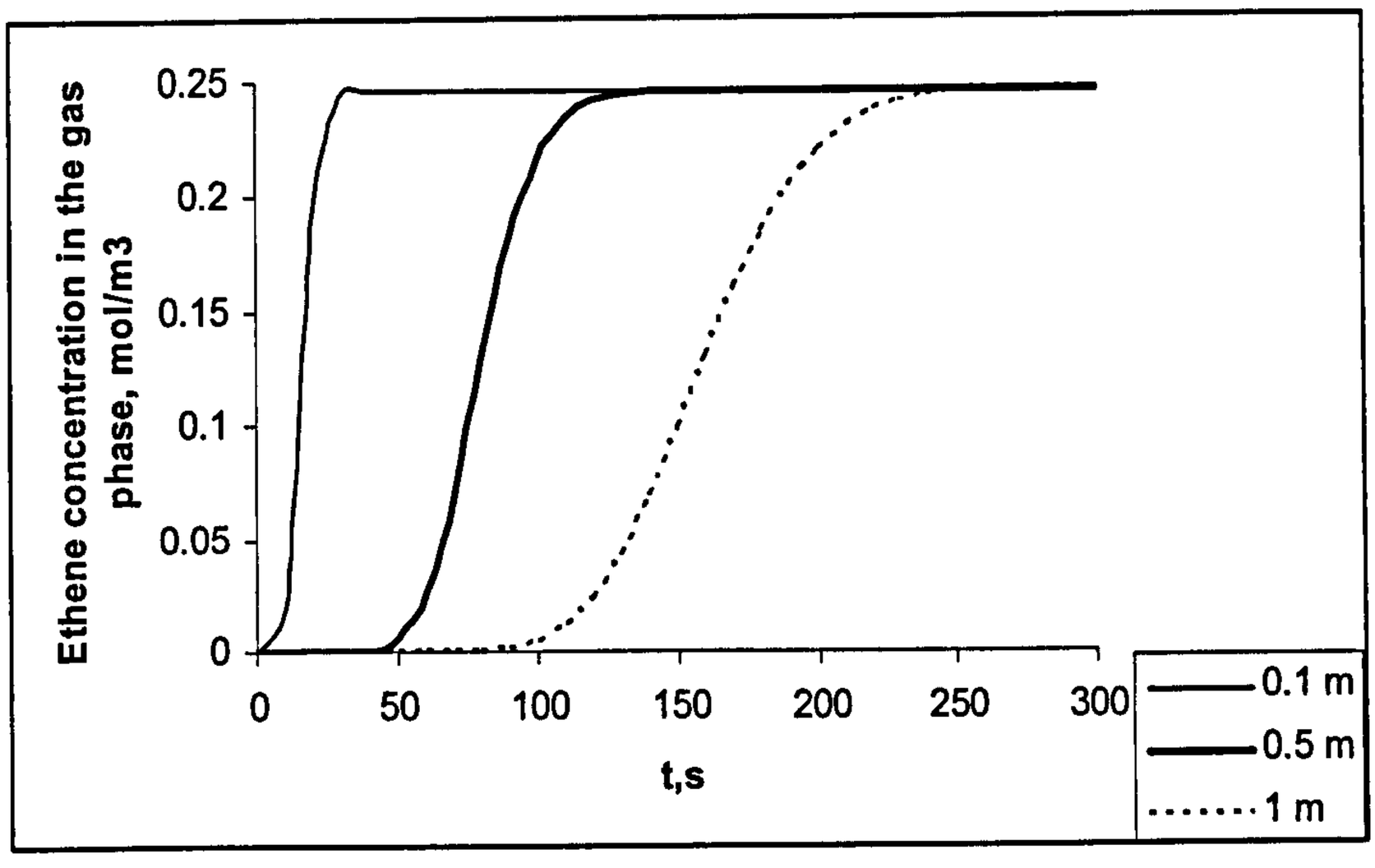

Fig 4.7: Ethene exit concentration profiles at different monolith lengths

(ii) Velocity Effects

The effect of the inlet velocity on the breakthrough performance of the monolith is shown in Fig. (4.8). Higher gas velocities lead to a decrease in the amount of gas from the core channel diffusing into the solid adsorbent zone. This means that there is only a small fraction of adsorbate available for adsorption and as such a lot of unadsorbed gas is

blown out of the reactor. In effect, the increase in the inlet velocity reduces the space time in the reactor and therefore, the potential gas-adsorbent contact time. Thus, adsorbate breakthrough is faster at higher gas velocities.

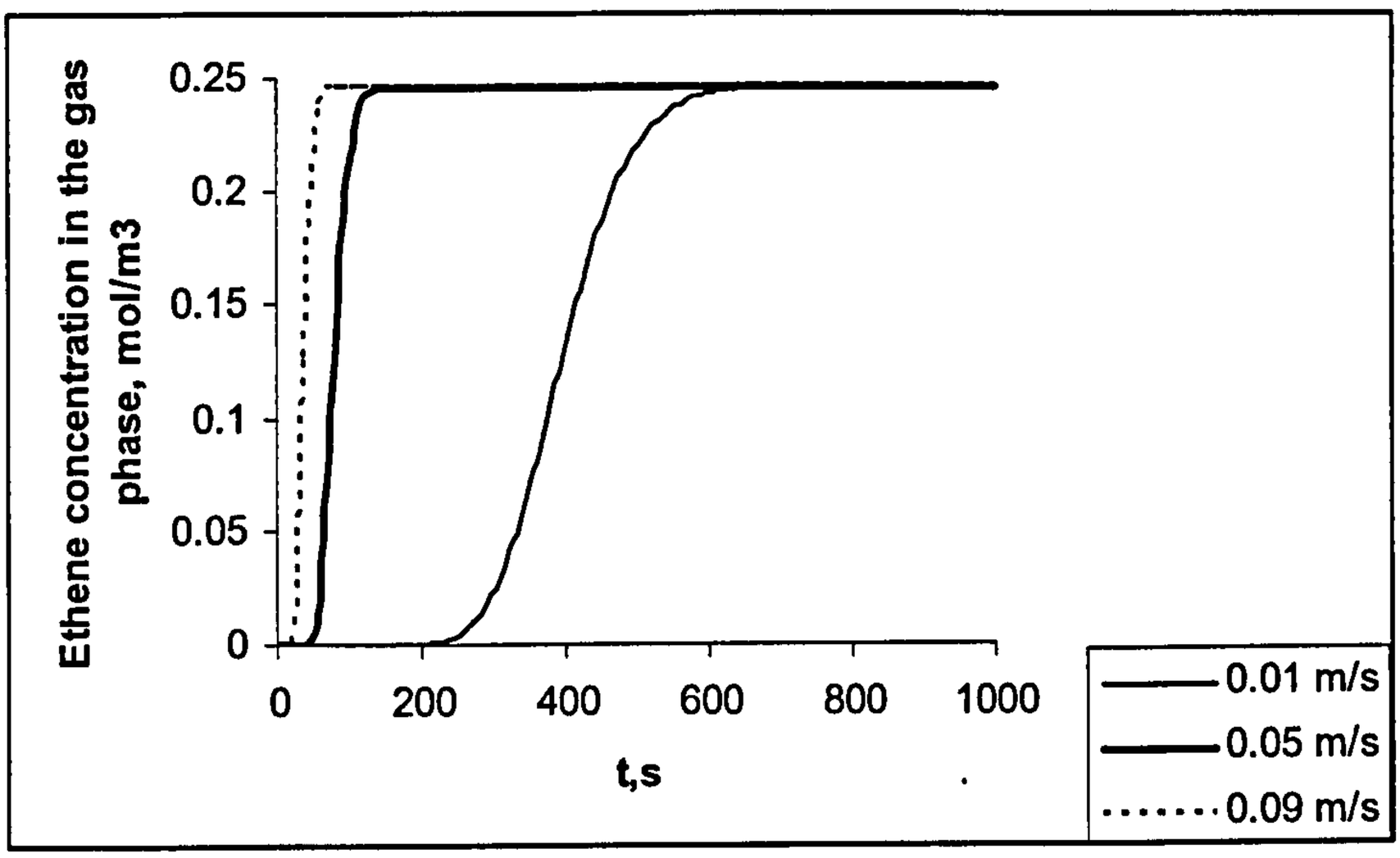

Fig 4.8: Ethene exit concentration profiles at different inlet velocities, T = 293 K

Packed bed reactor comparisons

The breakthrough profiles of the packed bed reactor acting as an adsorber, PB-ADS and that of the M-ADS at the three different temperatures (under base case conditions) for adsorption are presented in Figs. (4.9) – (4.11). The packed bed adsorber is of the same diameter (R_1) as that of the M-ADS and 2.25 times the length of the M-ADS. Comparisons are made between both reactor types based on the constraint that both systems

treat equal amounts of feed and the same quantities of adsorbent (see Table (4.2) and Section 3.2.1).

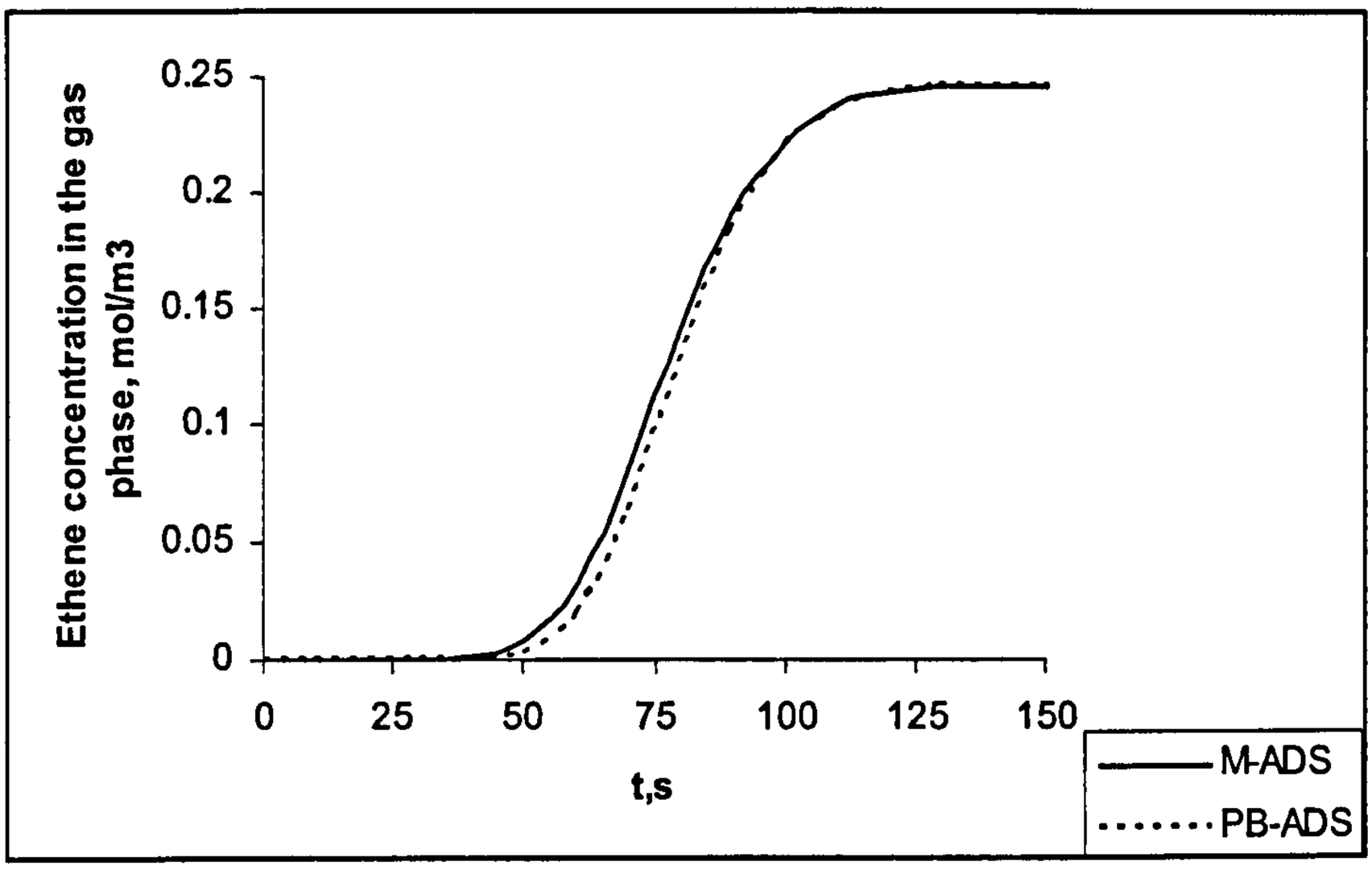

Fig 4.9: Ethene adsorption exit concentration profiles at T = 293K, u_m = 0.05 ms^{-1}

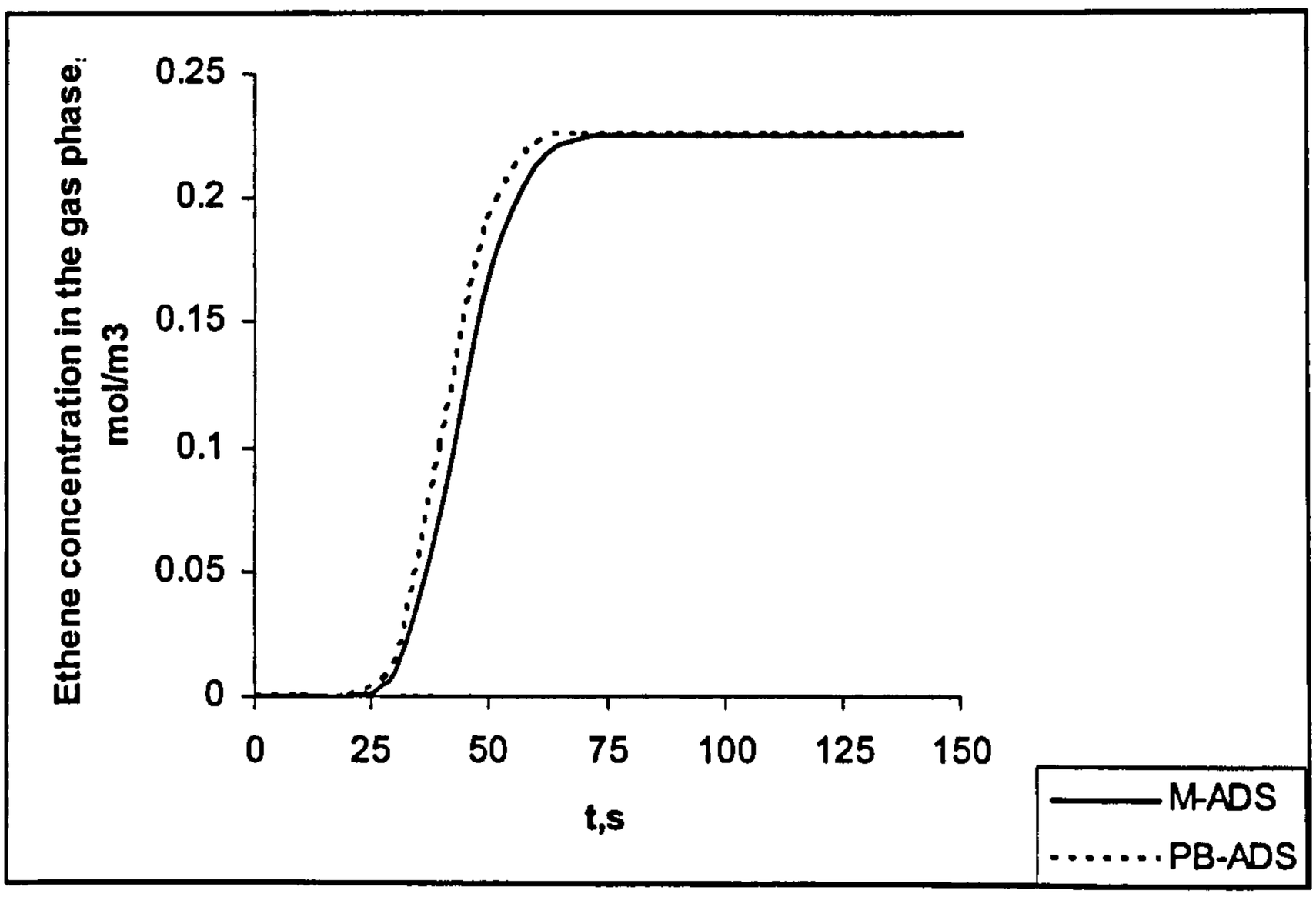

Fig 4.10: Ethene adsorption exit concentration profiles at T = 320K, u_m = 0.05 ms^{-1}

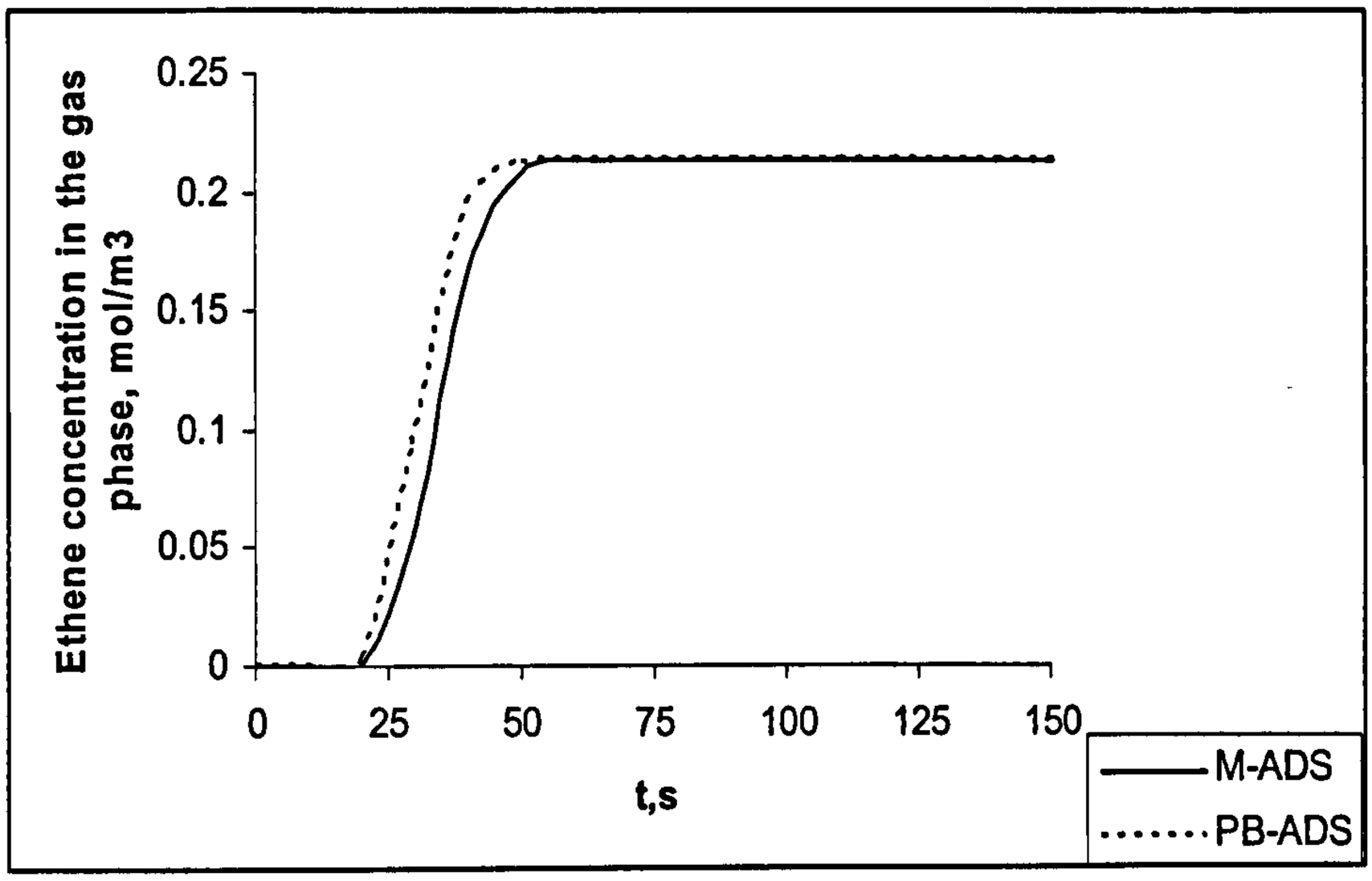

Fig 4.11: Ethene adsorption exit concentration profiles at T = 338K, u_m = 0.05 ms^{-1}

The PB-ADS adsorption performance conforms to the general trends outlined for the M-ADS in terms of the effect of increasing temperature on adsorption capacity wherein at higher temperatures the adsorption capacity decreases. At 293 K, both reactors are more or less identical in operation; however with an increase in temperature, the breakthrough effect is more pronounced in the PB-ADS where both breakthrough and saturation occur slightly faster than in the M-ADS.

Tables (4.4) – (4.6) give a summary of the associated pressure drop estimated for both the PB-ADS and M-ADS at different temperatures and gas inlet velocities. The viscosity of the bulk gas was calculated using the Sutherland formula details of which are given in Appendix D.

	M-ADS	PB-ADS	M-ADS	PB-ADS	M-ADS	PB-ADS
u (m/s)	0.01	0.01	0.05	0.05	0.09	0.09
N_{RE}	1.8	0.25	8.9	1.3	16	2.3
$\Delta P / L$ (Pa m^{-1})	0.93	1575	4.7	7875	8.4	14175

Table 4.4: Estimated pressure drop for both reactors at T = 293 K; $\mu = 1.68 \times 10^{-5}$ Pa.s

	M-ADS	PB-ADS	M-ADS	PB-ADS	M-ADS	PB-ADS
u (m/s)	0.01	0.01	0.05	0.05	0.09	0.09
N_{RE}	1.7	0.24	8.3	1.2	15	2.1
$\Delta P / L$ (Pa m^{-1})	1	1688	5	8438	9	15188

Table 4.5: Estimated pressure drop for both reactors at T = 320 K; $\mu = 1.8 \times 10^{-5}$ Pa.s

	M-ADS	PB-ADS	M-ADS	PB-ADS	M-ADS	PB-ADS
u (m/s)	0.01	0.01	0.05	0.05	0.09	0.09
N_{RE}	1.6	0.23	8	1.1	14.4	2
$\Delta P / L$ (Pa m^{-1})	1.04	1763	5.2	8813	9.4	15863

Table 4.6: Estimated pressure drop for both reactors at T = 338 K; $\mu = 1.88 \times 10^{-5}$ Pa.s

With reference to Tables (4.4) – (4.6), an increasing flow rate, leads to an increase in the estimated pressure drop especially for the packed bed system. There is also an increase in the pressure drop associated with an increase in temperature. This could be an effect of the change in physical properties of the bulk gas namely viscosity.

4.4.2 Reaction-only Step (no adsorption)

The reaction in the monolith reactor, M-RXTN, was also simulated for the case where the VOC (e.g. ethene) pre-mixed with air flows through the reactor in a continuous mode of operation. Product breakthrough profiles, reactant conversion and the rate of energy input are assessed. Parametric analysis on the effects of temperature, geometrical parameters and velocity are also performed with particular emphasis on the reactor temperature profile. As in the adsorption-only step, comparisons are also made to the packed bed reactor, PB-RXTN.

Fig. (4.12) shows plots of calculated conversion in the M-RXTN for the oxidation of ethene and propane derived from the different kinetic rate models listed in Table (3.3) as a function of the reactor temperature. From the graph it can be deduced that under the operating conditions applied, the conversions for the models I – III are comparable. As discussed in Section 3.2.2 the kinetic rate model used in this work is Model III.

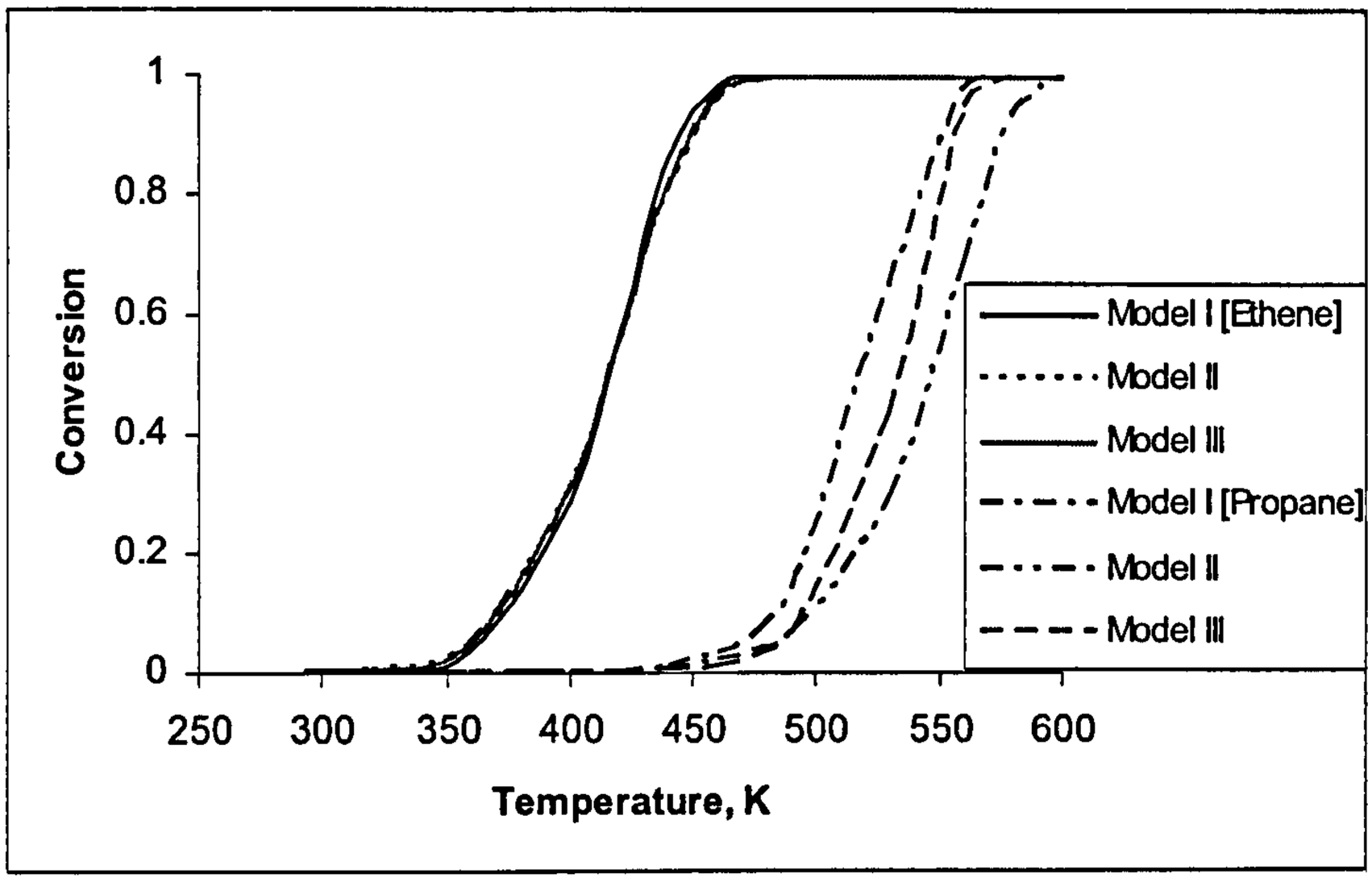

Fig. 4.12: Calculated conversions for the individual oxidations of ethene and propane as functions of operating temperature for the M-RXTN using the different kinetic models listed in Table (3.3); ($u = 0.1$ m s^{-1} , $C_{ethene\ in} = 3000$ ppm, $C_{propane\ in} = 3000$ ppm)

Figs. (4.13) and (4.14) show the concentration profiles of CO_2 and ethene along the length of the reactor at exit conditions. The products CO_2 and H_2O essentially have the same profiles due to their identical stoichiometric values. Therefore the concentration profile of the product, CO_2 only is shown.

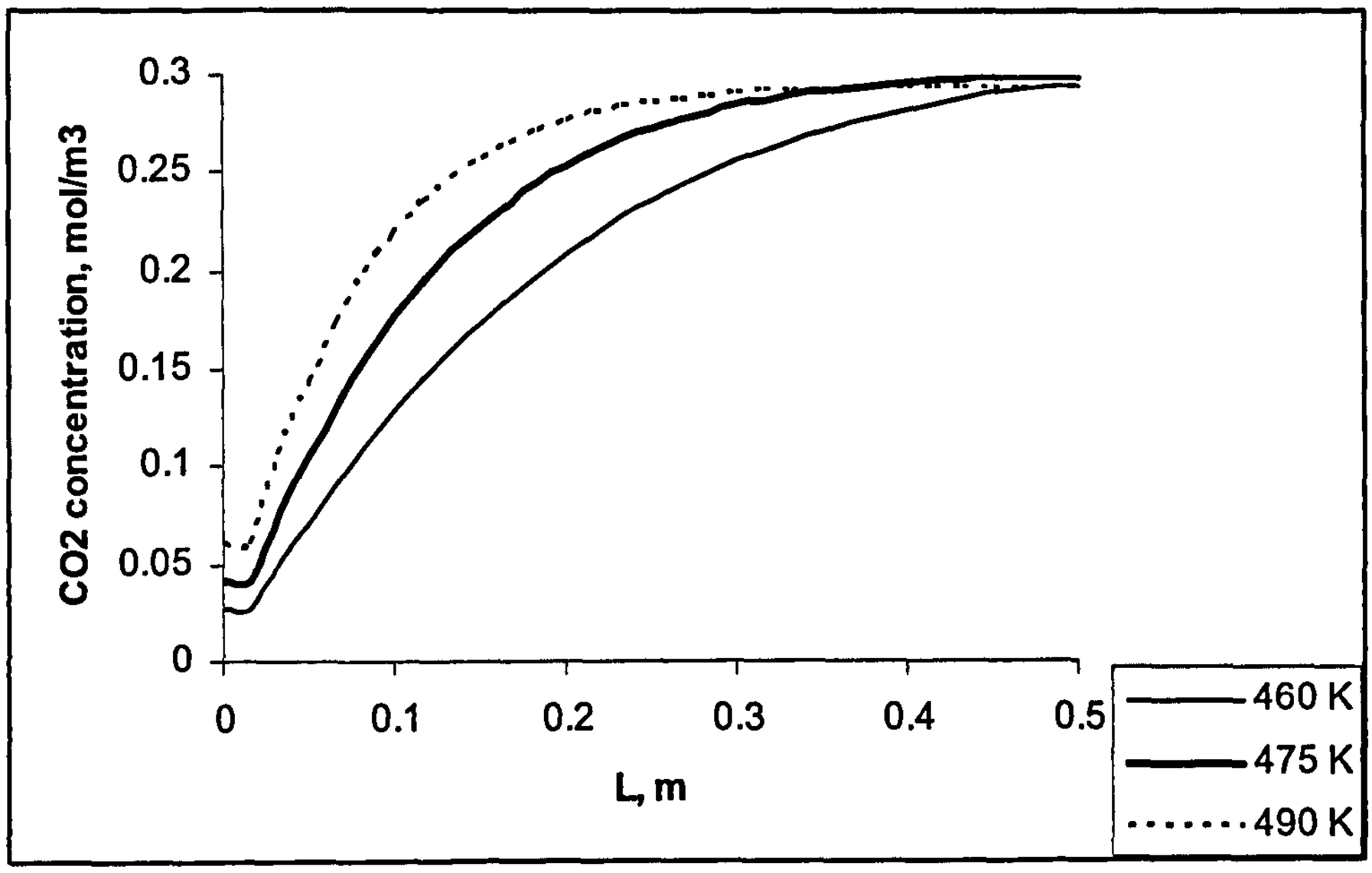

Fig. 4.13: CO_2 axial concentration profile at different T_{fr}

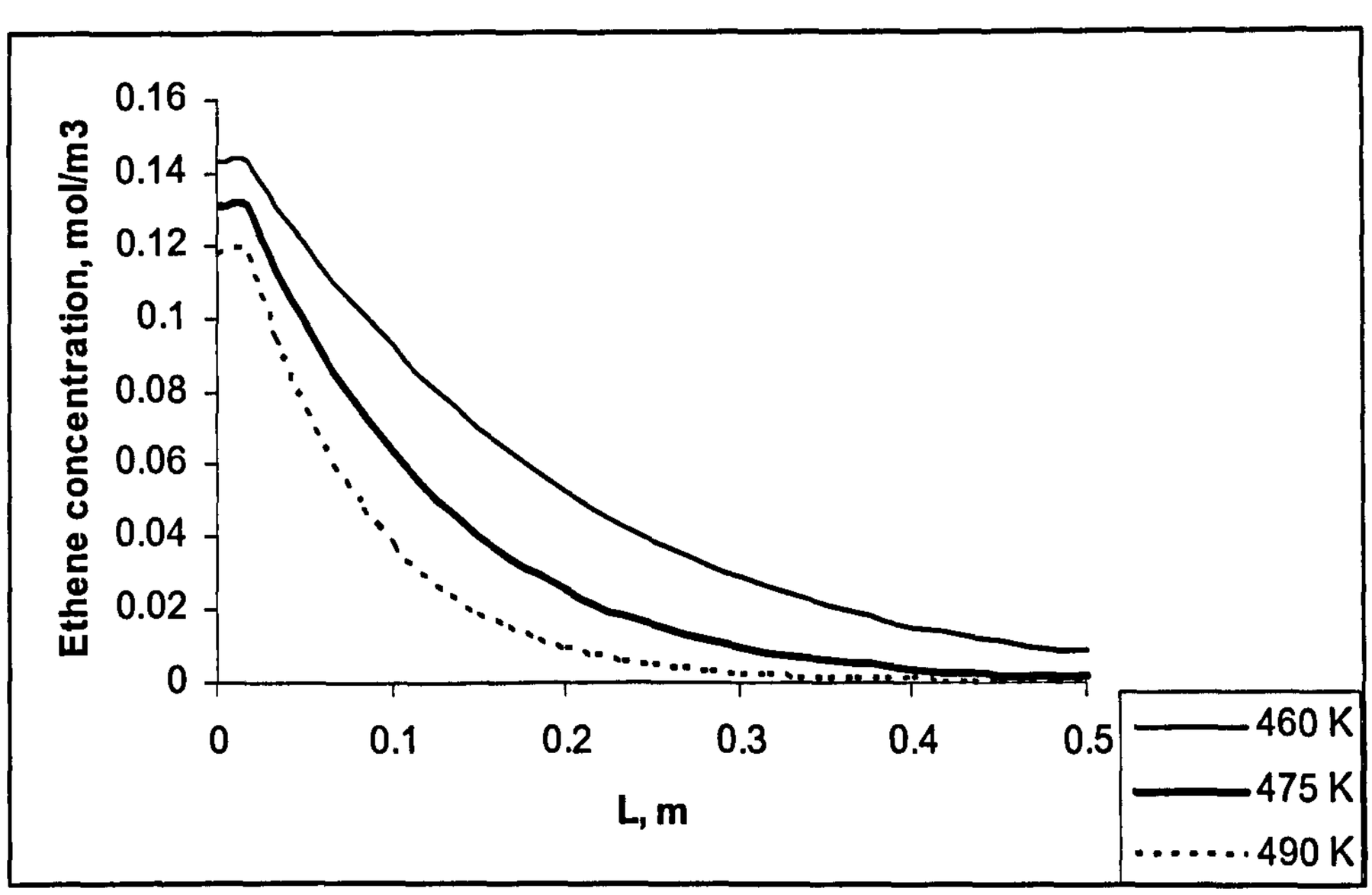

Fig. 4.14: Ethene axial concentration profile at different T_{fr}

The steady state temperature profile along the axial length of the reactor at the different reaction temperatures is illustrated in Fig. (4.15).

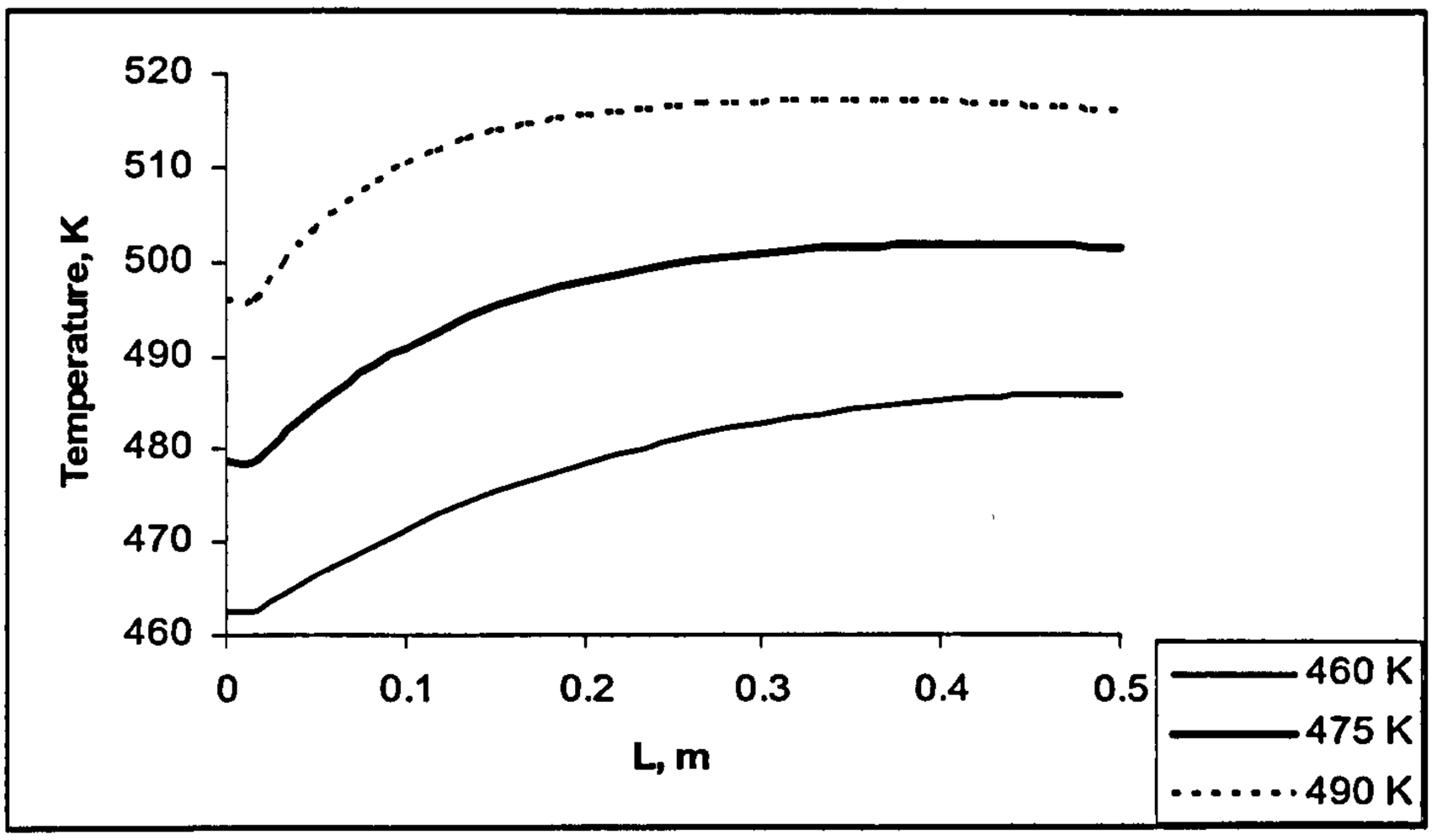

Fig. 4.15: Temperature profile of the reactor along axial distance at different T_{fr}

Parametric Analysis

(i) Geometrical Effects

Parametric analysis was performed at T_{fr} 460 K, and as in the adsorption-only step, the effects of changes to the core channel radius, R_1, (here R_2 is constant at 1.5 mm) the monolith total radius R_2 (here R_1 is constant at 1.2 mm) and the length of the reactor was investigated and their various effects on the conversion performance of the M-RXTN are as detailed in Table (4.7).

R_1 (mm)	X (%)	R_2 (mm)	X (%)	L (m)	X (%)
0.8	100	1.4	99.2	0.1	72
1	100	1.5	99.5	0.3	97
1.2	99.5	1.8	100	0.5	99.5

Table 4.7: M-RXTN and geometrical effects on conversion; 460 K - base conditions

The results presented in Table (4.7) are as expected; a smaller core gas channel radius, R_1 results in the gas reaching the solid zone quicker. An increase in the thickness of the solid zone also leads to the diffusion path of the adsorbate gas within the solid zone lengthened, which may result in longer gas-solid contact time and hence higher conversions. In all cases for increasing δ, longer breakthrough times were attained. This implies that the thickness of the solid zone, δ, plays an important part in overall process performance. Longer reactor lengths allow for a higher space time in the reactor and therefore increased gas-solid contact time available for reaction, hence the increase in conversion.

(ii) Velocity Effects

The effect of inlet velocity on the conversion performance of the M-RXTN is shown in Table (4.8). The gas inlet velocity is varied whilst keeping all other parameters and conditions constant. There is a decrease in conversion as is expected with a lower reactor space time due to the diminishing gas-solid contact time. Lower velocities lead to an increase in the reactor temperature as the higher space time leads to increased reaction time for the pre-mixed gases and therefore a lot more heat is released than at higher velocities for this case.

U_m (m s^{-1})	τ (s)	X (%)	Δ T (K)
0.01	10	100	+ 9.1
0.05	5	99.5	+ 8.5
0.1	1	94.7	+ 8.1

Table 4.8: The effect of inlet velocity on conversion in the M-RXTN; 460 K - base conditions

Packed bed reactor comparisons

Table (4.9) gives a summary of the performance of the M-RXTN as shown in the graphs detailed above relative to that of the PB-RXTN. With reference to Table (4.9) ΔT is defined as $T_{max} - T_{fr}$ where, T_{max} denotes the maximum temperature rise of the reactor at exit conditions. The conversion is denoted as X and the rate of energy input as E.

	M-RXTN			PB-RXTN		
T_{fr} (K)	460	475	490	460	475	490
Δ T (K)	+ 8.5	+ 8.5	+ 8.5	+ 83	+ 80	+ 76
X (%)	99.5	99.7	99.9	100	100	100
E (kJ m^{-2} s^{-1})	21.2	22.4	23.6	21.2	22.4	23.6
N_{RE}	5.7	5.6	5.4	0.54	0.54	0.52
$\Delta P / L$ (Pa m^{-1})	6.8	7	7.2	35921	36797	37819

Table 4.9: M-RXTN and PB-RXTN performance

The performance of the packed bed is comparable to that of the monolith reactor in terms of conversion especially at temperatures above 460 K. However, the temperature rise in the packed bed reactor is far greater than in the monolith.

4.3.3 Summary of single step operation

The above simulations for single step operation demonstrated expected trends. In general, geometrical, operating and design parameters determine the overall behaviour and dynamics of a process.

With regards to the single step for adsorption, it was concluded that shorter radial diffusion path lengths resulted in a shorter time to achieve results that were also similarly achieved with longer radial dimensions and at a much longer time.

Insight gained from the adsorption steps are the fact that operating at lower temperatures of adsorption yields a higher loading of adsorbed gas and also the breakthrough times at lower temperatures are slower than at higher temperatures of adsorption. At lower temperatures bed saturation was achieved much slowly than at higher temperatures.

For an equivalent packed bed reactor acting as an adsorber, the general trends were as for the monolith adsorbed but with slightly faster breakthrough and saturation times. The estimated pressure drop in the packed bed for all conditions was much higher than that of the equivalent monolith reactor.

Furthermore, though not specifically mentioned for each case in the adsorption step, the effectiveness of the process in achieving pure inert gas (N_2) was 100 % and the maximum temperature rise was typically

<0.1 K as expected for such low concentrations and the small magnitude of the heat of adsorption.

The insight that comes from the monolith reactor behaviour (M-RXTN) is in the form of the effects of increasing velocity. Lower velocities lead to an increase in reactor temperature and ultimately higher conversions. The associated temperature effects give an indication of the temperature stability of the reactor which is of main interest in this work. At such dilute feed concentrations (3000 ppm) used as a base case, the monolith reactor appears to be quite stable. The effects of changes in feed concentration and the reactor temperature on the stability of the reactor is explored in more detail in Section 4.5.

4.4 Cyclic operation

The need for the periodic regeneration of the adsorbent makes cyclic operation necessary. The cyclical nature of the M-AR also means that its assessment is not as straightforward as that of the monolith reactor investigated in Section 4.3.2.

4.4.1 Cyclic adsorption (no reaction)

Attention is given to the desorption step of the cyclic adsorption process with bed saturation assumed in the previous adsorption step. Fig. (4.16) illustrates the exit concentration profiles of ethene in the gas phase at the

different feed temperatures for adsorption, T_{fa}. The feed temperature for reaction (and also desorption), T_{fr} is kept constant at 460K. It should be noted that the feed temperature for reaction in the second step is essentially the same temperature utilised in the M-RXTN. Fig. (4.16) depicts complete bed saturation in the adsorption step for 1 cycle, where the total cycle time, C_{time} is 300 s, with the time for adsorption $t_a = t_d$ (the time for desorption) =150 s. As expected, the time taken to achieve both adsorbate and desorbate breakthrough decreases with increasing temperature. The time taken to achieve complete bed saturation and regeneration also decreases with increasing temperature.

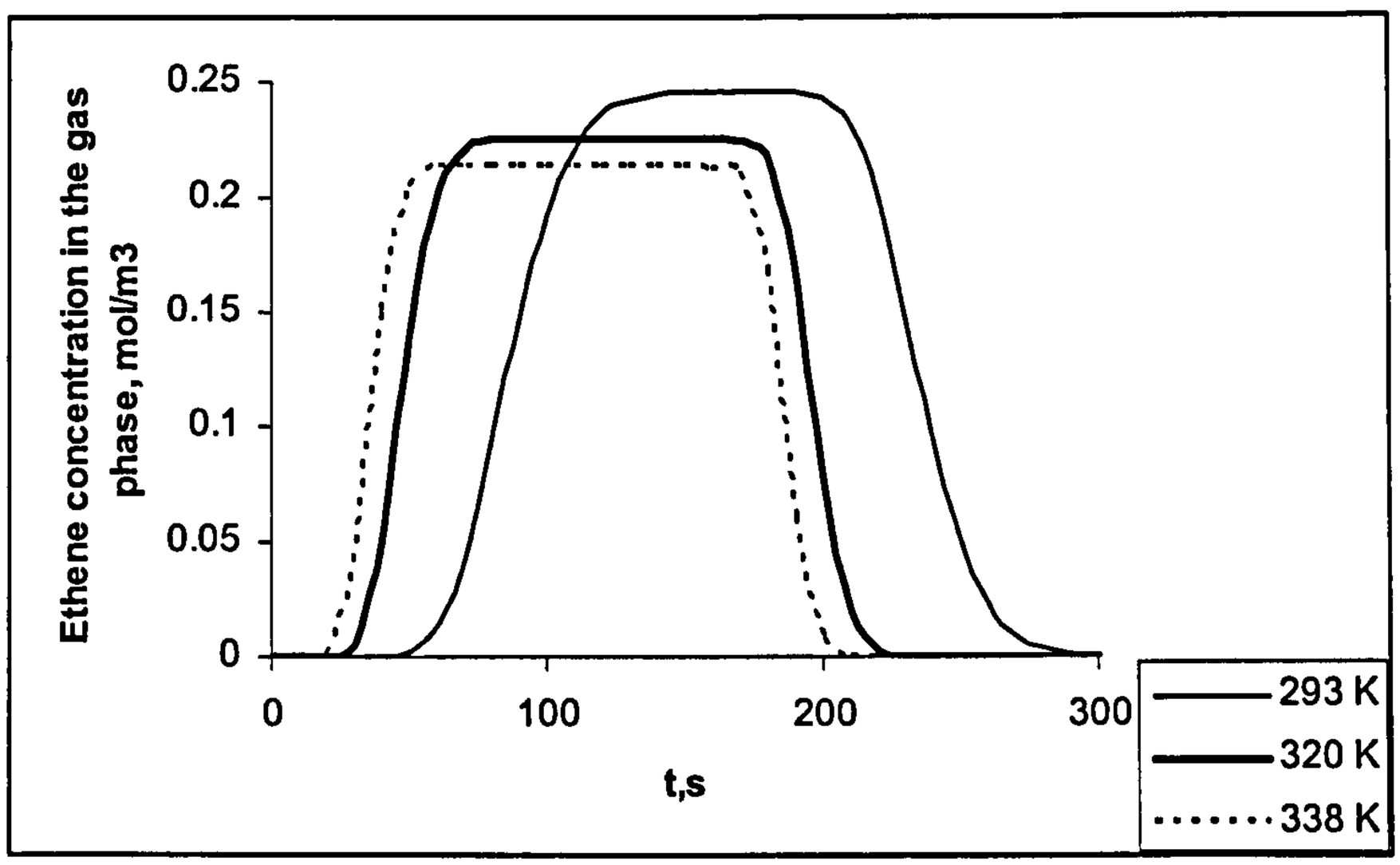

Fig. 4.16: Ethene exit concentration profiles at different adsorption temperatures

Parametric analysis in this section focuses on the desorption step and its profiles. In Fig. (4.17) the effect of desorption-step inlet velocity, u_d on the profile of the M-ADS is shown. This has an impact on the rate at which the gas is desorbed and therefore, the amount of gas available for

reaction. The adsorption-step inlet velocity, u_a, is kept constant at 0.05 m s^{-1} with T_{fa} 293 K and T_{fr} 460 K and step times t_a = 150 s and t_d = 750 s.

For the base case, where both $u_a = u_d$ = 0.05 m s^{-1}; the effect of increasing u_d (0.07 m s^{-1}) and decreasing u_d (0.01 m s^{-1}) from the base case is shown in Fig. (4.17). The graph illustrates that increasing the inlet desorption velocity shortens the desorbate breakthrough time from the bed. Faster desorption takes place with increased velocities at the higher desorption temperature of 460 K. Desorption is an endothermic process, and the increase in temperature from 293 K to 460 K facilitates this together with the change in concentration gradients (concentration swing) due to the increased concentration of the nitrogen inert gas.

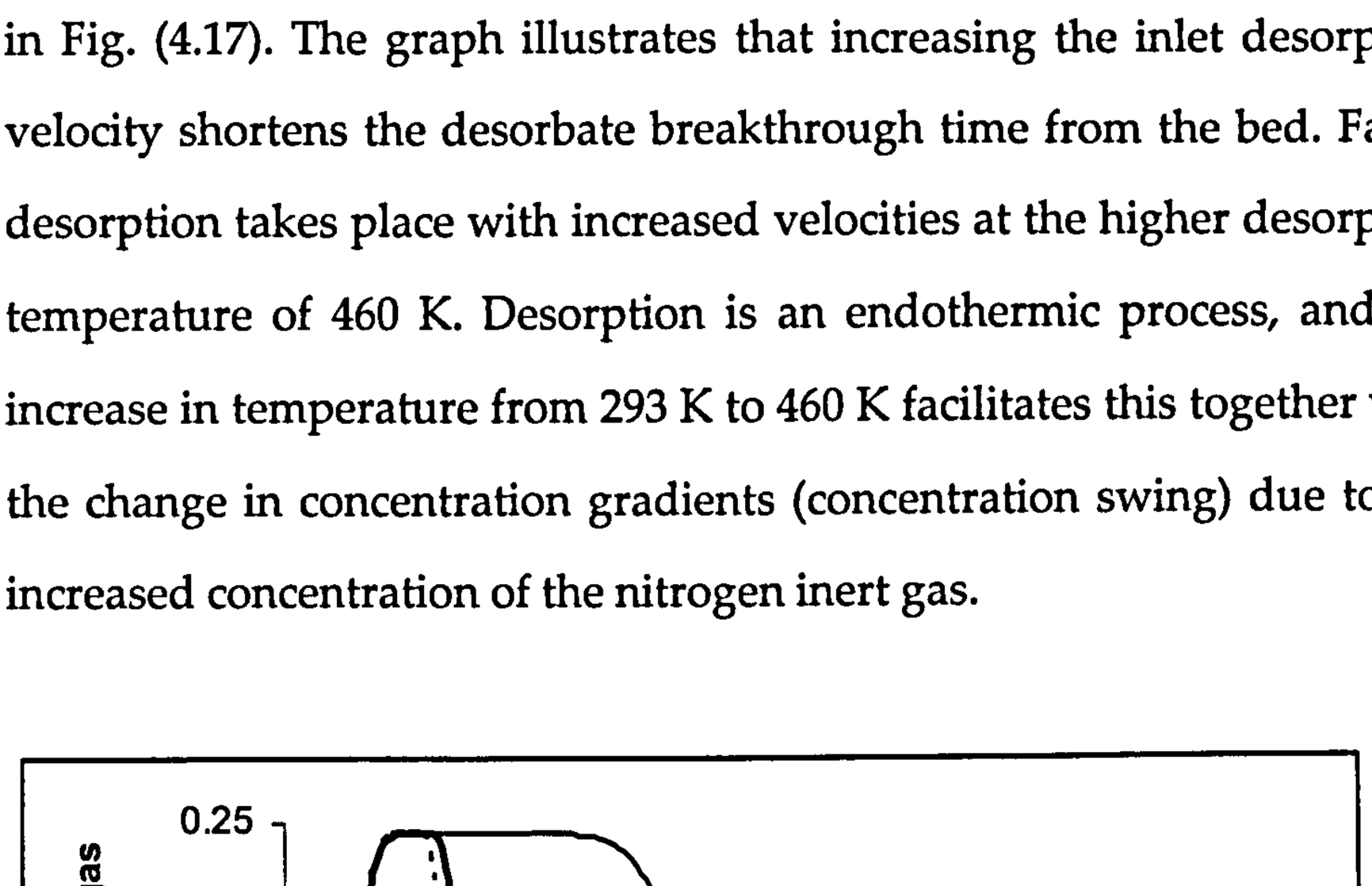

Fig. 4.17: Ethene exit concentration profiles at different desorption inlet velocities

For adiabatic operation, regeneration is assumed to be complete when the effluent temperature reaches the regeneration inlet temperature

(Yongsonthun, 1999). Therefore it is expected that utilising the same feed temperatures for adsorption and desorption will result in faster regeneration as the temperatures utilised are identical. For temperature swing, as in the cases presented above for 1 cycle, the duration of the desorption (or heating) step has an effect on the reactor performance as the reactor at 293 K does not heat up to 460 K. A longer heating time is perhaps needed to enable the reactor to heat up effectively. Yongsonthun, 1999, suggests that the duration of the heating step has an effect on the speed of convergence towards cyclic steady state (CSS) operation. With a long heating time the cyclic steady state is approached quickly, whereas for a short heating time, it is approached more slowly. For the case $T_{fa} = T_{fr} = 460$ K, operation under a fully saturated bed enables the steady state to be reached in effectively 1 cycle. This effect of temperature swing on heating and cycle times is further explored in the operation of the M-AR in Section 4.4.2.

4.4.2 M-AR operation (cyclic adsorption and reaction)

The performance of the hybrid monolith, M-AR is assessed in terms of conversion, energy input rate, and the maximum temperature rise. In the first instance, the M-AR operating with a very dilute feed concentration of ethene (ca. 3000 ppm) is investigated. Air is fed in during the desorption step with $T_{fa} = T_{fr} = 460$ K. The adsorption and desorption inlet velocities are identical at $u_a = u_d = 0.05$ m s^{-1}. Fig. (4.18) illustrates the resulting breakthrough profiles of ethene and product (CO_2 / H_2O).

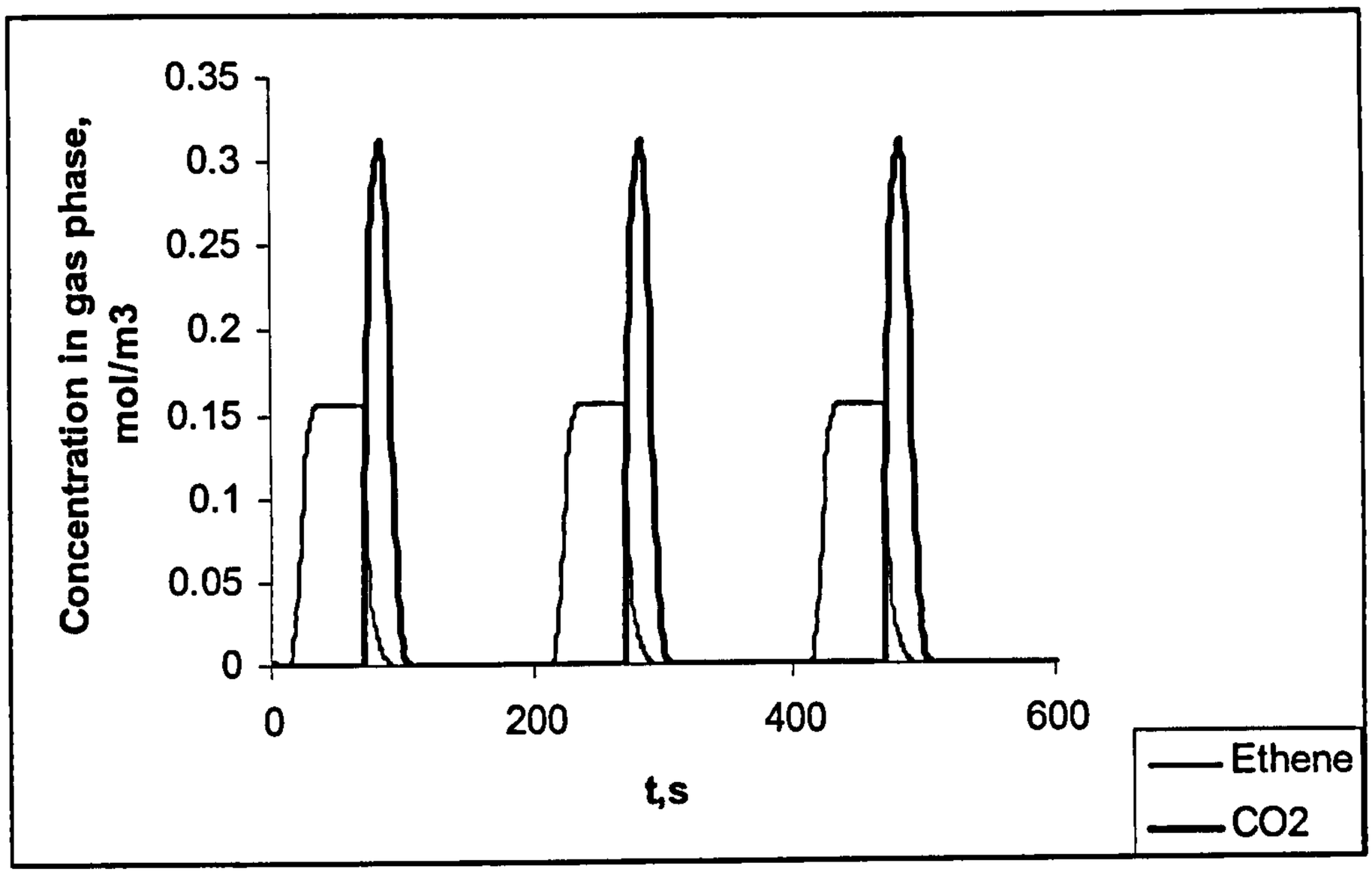

Fig. 4.18: Ethene and CO_2 exit concentration profiles; t_a = 70 s, t_d = 130 s, 3 cycles

The solid adsorbent in the adsorption step is fully saturated at the onset of desorption / reaction. The conversion obtained with this mode of operation was 27 % and the energy input rate was calculated to be 21.2 kJ m^2 s^{-1}.

Fig. (4.19) depicts the exit concentration profiles of ethene in the M-AR and illustrates the fact that ethene desorption occurs faster in the M-AR than in an equivalent operating M-ADS where only adsorption occurs. The combination of adsportion and reaction in a single unit provides efficiency in the integration of heat in the M-AR as the higher reaction temperature of 460 K provides the heat for endothermic desorption and the exothermic reaction that ensues provides further heat which further drives desorption. Concentration swing is also primarily responsible for desorption. Adsorbate in the gas phase is removed thereby reducing its

partial pressure and encouraging further desorption. This point is further illustrated in Fig. (4.20) which shows the steady state temperature profile of the reactor at exit conditions for both the M-AR and M-ADS reactors.

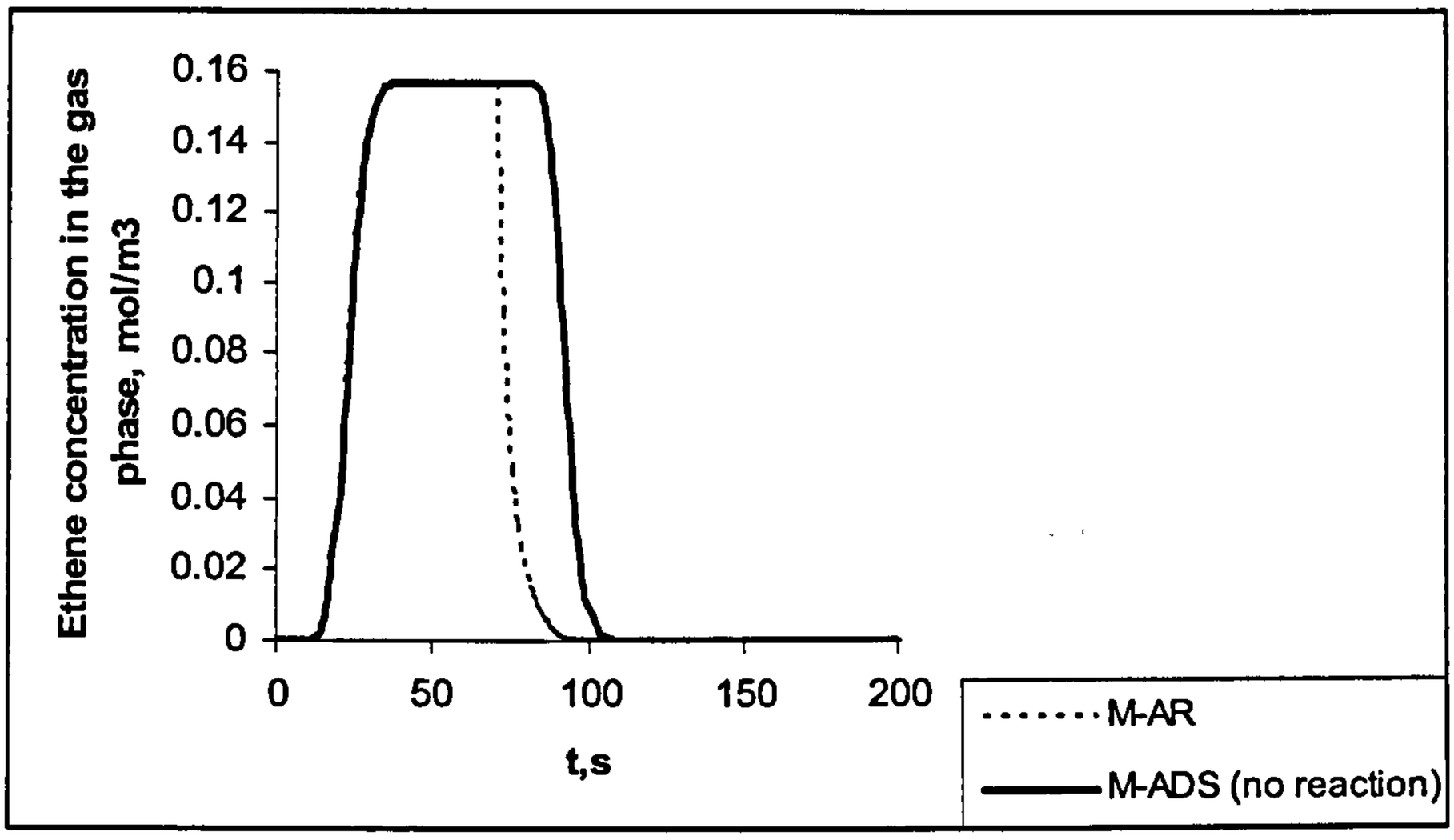

Fig. 4.19: Ethene exit concentration profile; t_a = 70 s, t_d = 130 s, 1 cycle

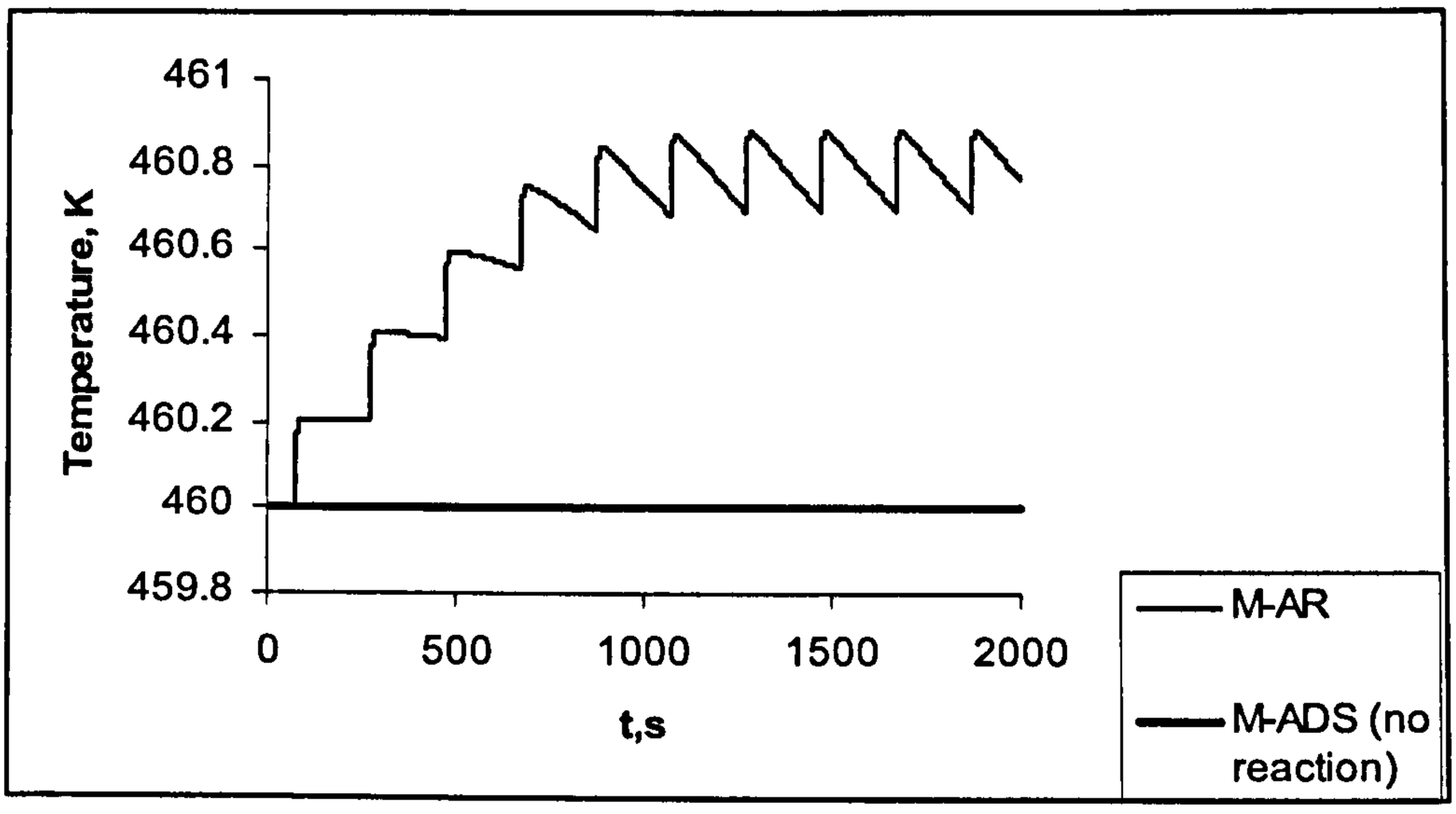

Fig. 4.20: Temperature profile of the reactor – exit conditions; t_a = 70 s, t_d = 130 s, 10 cycles

Step times of adsorption and reaction play an important role in terms of reactor stability, conversion, yield and purity of the inert gas. The step time ratio S_R, is defined as $\frac{t_a}{t_a + t_d}$ where t_a is the adsorption-step time and t_d the desorption heating and reaction-step time. Table (4.10) shows the effect of the step times on conversion and energy for process operation (i.e. $T_{fa} = T_{fr}$ 460 K, base conditions) as defined in Section 4.3.2. The base case results are highlighted in parentheses.

t_a (s)	t_d (s)	C_{time} (s)	S_R	X (%)	E (kJ m² s⁻¹)
150	100	250	0.6	12	21.2
(150)	(150)	(300)	(0.5)	(12)	(21.2)
150	200	350	0.43	12	21.2
150	250	400	0.38	12	21.2

Table 4.10: The effect of switching step times; $T_{fa} = T_{fr} = 460$ K

From Table (4.10) the results suggest that there is no change to either conversion or energy through the variation of the desorption-step time. This reflects the importance of the adsorption step as it determines the amount of adsorbate loaded in the reactor bed and therefore available for desorption and more importantly reaction. The very low value of conversion may arise from:

(i) The slow heat-up of the bed during desorption / reaction step and perhaps the need for lower temperatures to be utilised in the adsorption step.

(ii) The breakthrough of unreacted ethene during the adsorption step and similarly insufficient time for reaction for molecules adsorbed nearer the exit of the bed.

These issues are further explored in the sections below:

(i) Heating time effects on M-AR performance

The effect heating / desorption-step time on the performance of the M-AR operating at T_{fa} 293 K and T_{fr} 460 K is explored. Base case parameters where utilised with $u_a = u_d = 0.05$ m s^{-1}, and $t_a = 150$ s, $t_d = 150$ s. The adsorption-step time was kept constant at 150 s. Table (4.11) gives a summary of the effect this has on conversion and energy input. Fig. (4.21) shows the temperature profile of the reactor corresponding to the different heating times listed in Table (4.11).

t_a (s)	t_d (s)	C_{time} (s)	S_R	X (%)	E (kJ m^2 s^{-1})
(150)	(150)	(300)	0.5	2.0	10.1
150	350	500	0.3	6.7	14.5
150	550	700	0.21	9.4	16.4
150	750	900	0.17	11.8	17.5

Table 4.11: Effect of heating times on M-AR performance; T_{fa} = 293 K, T_{fr} = 460 K, 10 cycles

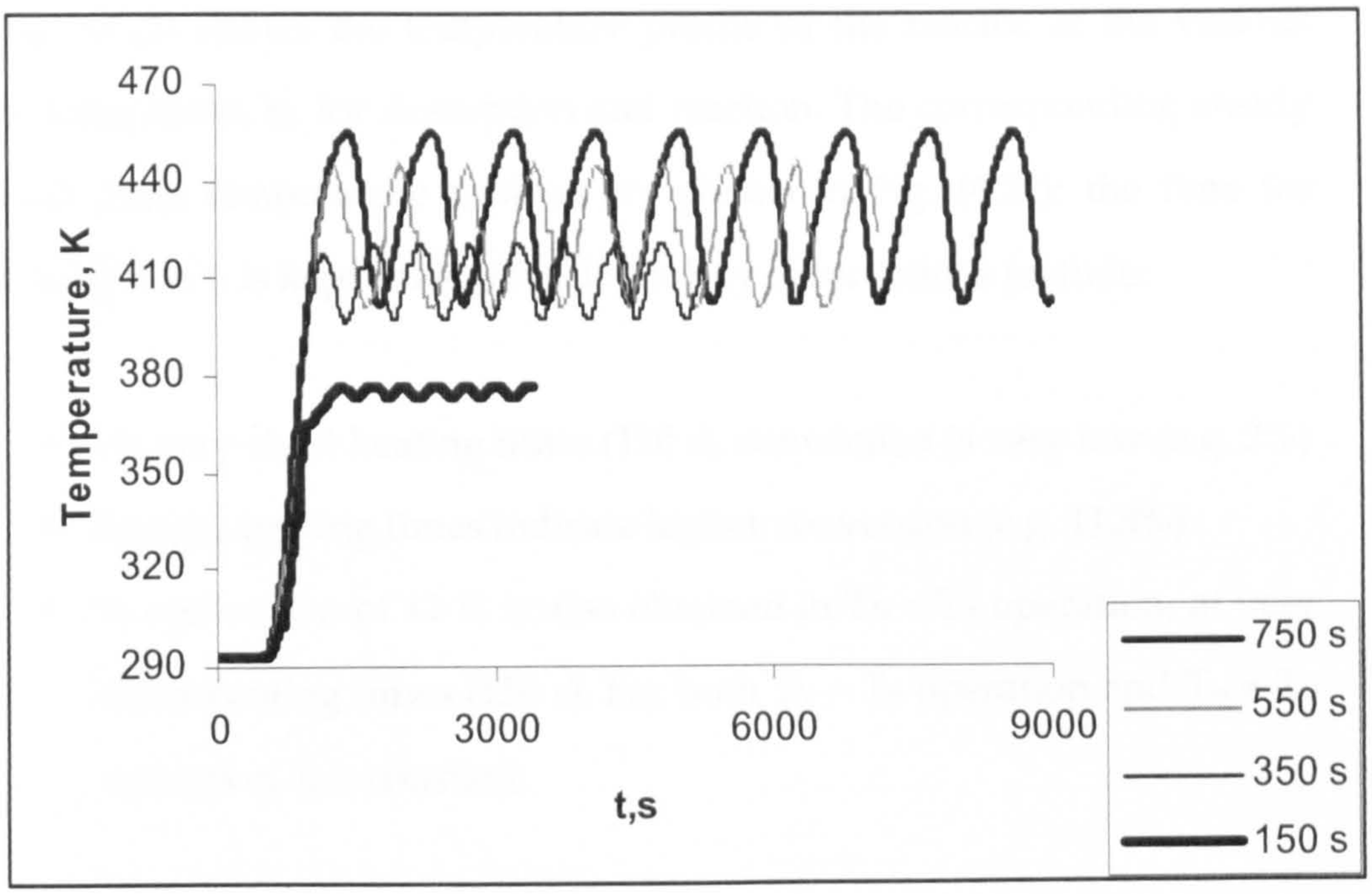

Fig. 4.21: Temperature profile of the reactor at different t_d; T_{fa} = 293 K, T_{fr} = 460 K

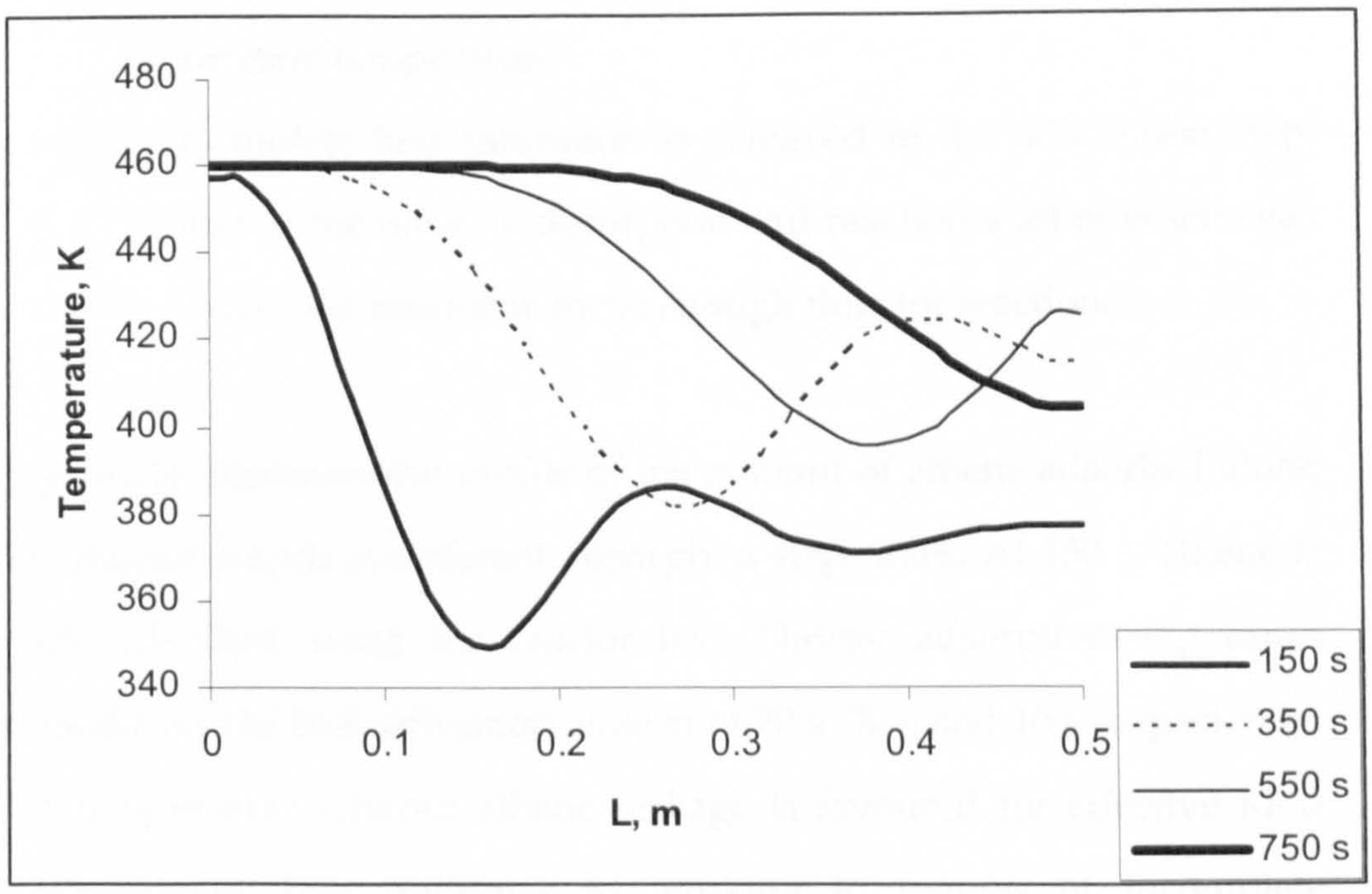

Fig. 4.22: Steady state axial temperature profiles at different t_d; Tfa = 293 K, T_{fr} = 460 K; 10 cycles

Fig. (4.21) shows the temperature profile of the reactor at the various heating times, t_d, for desorption and reaction. The corresponding steady state axial temperature profiles are shown in Fig. (4.22); the time for adsorption t_a is kept constant at 150 s. Key observations include:

- At very short heating times (150 s), conversion is very low (e.g. 2%)
- Longer heating times indicate higher conversion (e.g. 11.8%)
- A conversion of 12 % is also obtained in $T_{fa} = T_{fr}$ operation, at very short heating times (150 s). For both $T_{fa} = T_{fr}$ operation and $T_{fa} \neq T_{fr}$ operation, t_a is constant.

Poor conversion performance under $T_{fa} \neq T_{fr}$ operation may be attributed to:

(a) The length of time required to heat the cold reactor to the reaction temperature

(b) Complete bed saturation is achieved in the adsorption step, and at the onset of desorption and reaction a lot of ethene gas leaves the reactor without enough time for reaction.

Fig. (4.23) illustrates the profile of the amount of ethene adsorbed along the reactor length at different adsorption-step times. At 150 s, ethene is fully adsorbed along the reactor bed. Shorter adsorption-step times indicate partial bed utilisation as seen at 70 s, 30 s and 10 s respectively. Thus, operation without ethene leakage is favoured for effective M-AR performance. This translates to working in regions of incomplete

saturation along the reactor bed length which is further explored in the following sub - section (*ii*).

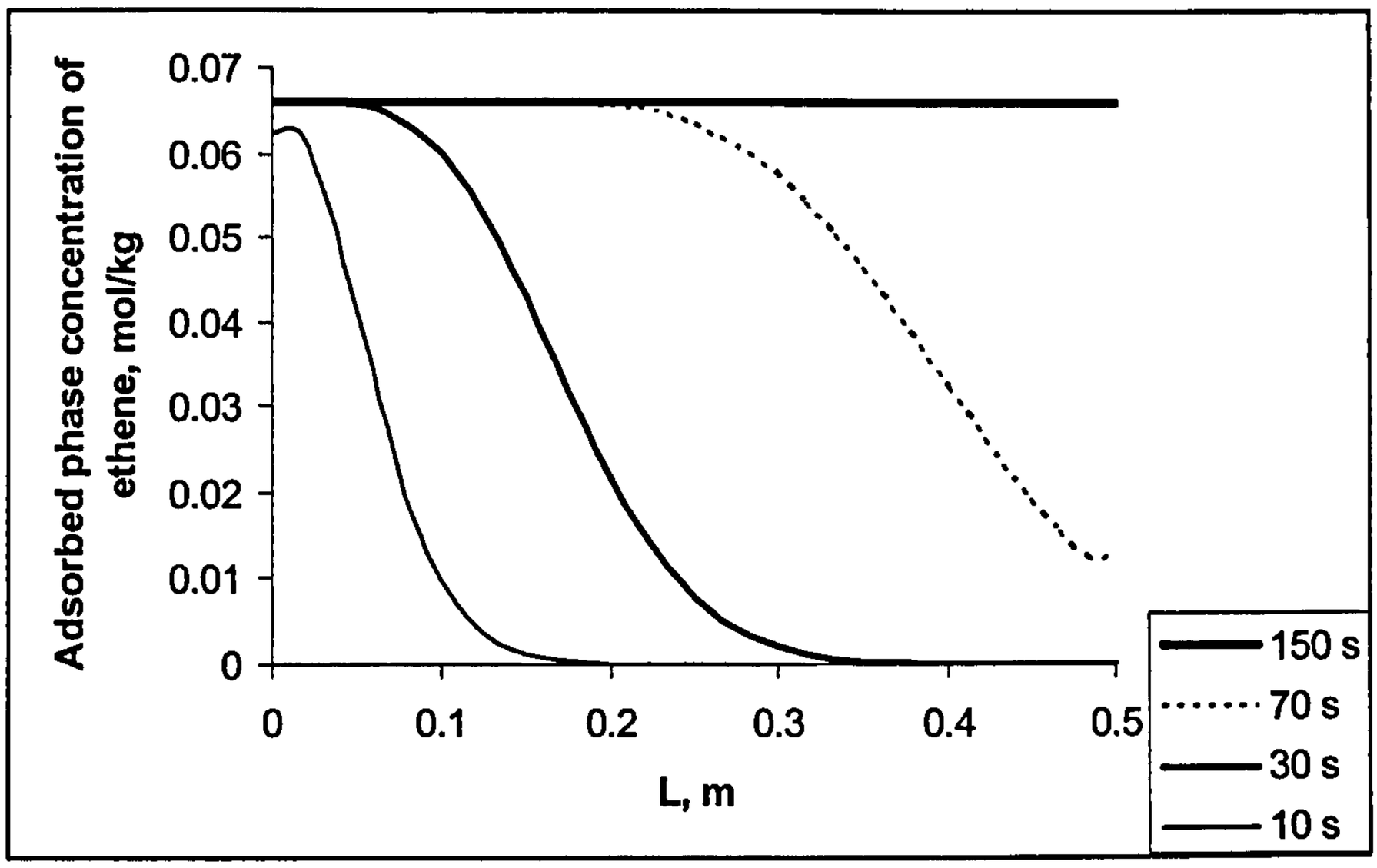

Fig. 4.23: Amount of ethene adsorbed at different t_s along reactor axial distance

It is also noted that the energy input rate is dependent on the step times for adsorption and desorption. The energy input rate increases with increasing t_d, although for identical feed temperature operation at 460 K, the value is still higher at 21.2 kJ m^2 s^{-1} (c.f. $T_{fa} \neq T_{fr}$ at 18.9 kJ m^2 s^{-1}).

One would also expect that the time for desorption and reaction is shortened for increasing T_{fa}. Though higher conversions may be attained, the trade off lies in the energy input requirements.

(ii) Incomplete bed saturation along the reactor length

For the case of $T_{fa} = T_{fr} = 460$ K, and utilising base parameters, the impact of incomplete bed saturation on the performance can then be assessed using shorter adsorption step times for a constant reactor length. The reaction (heating / desorption) time is kept constant at 150 s. Figs. (4.24) and (4.25) illustrate the effect of shorter adsorption step time on the ethene and CO_2 exit concentration profiles. The effects on conversion and energy are detailed in Table (4.12).

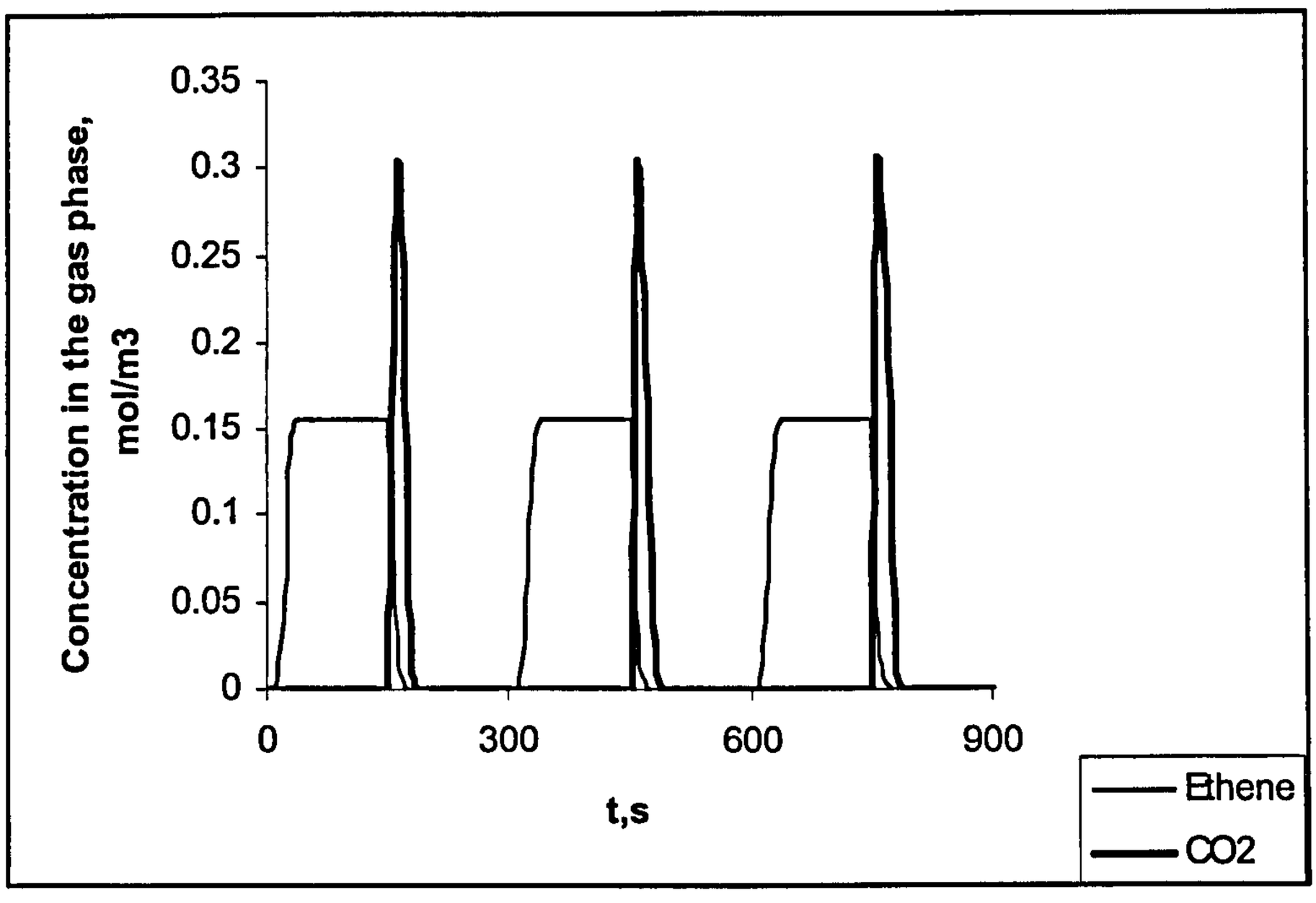

Fig. 4.24: Ethene and CO_2 exit concentration profiles; $T_{fa} = T_{fr} = 460$ K, $t_a = 150$ s, $t_d = 150$ s, 3 cycles

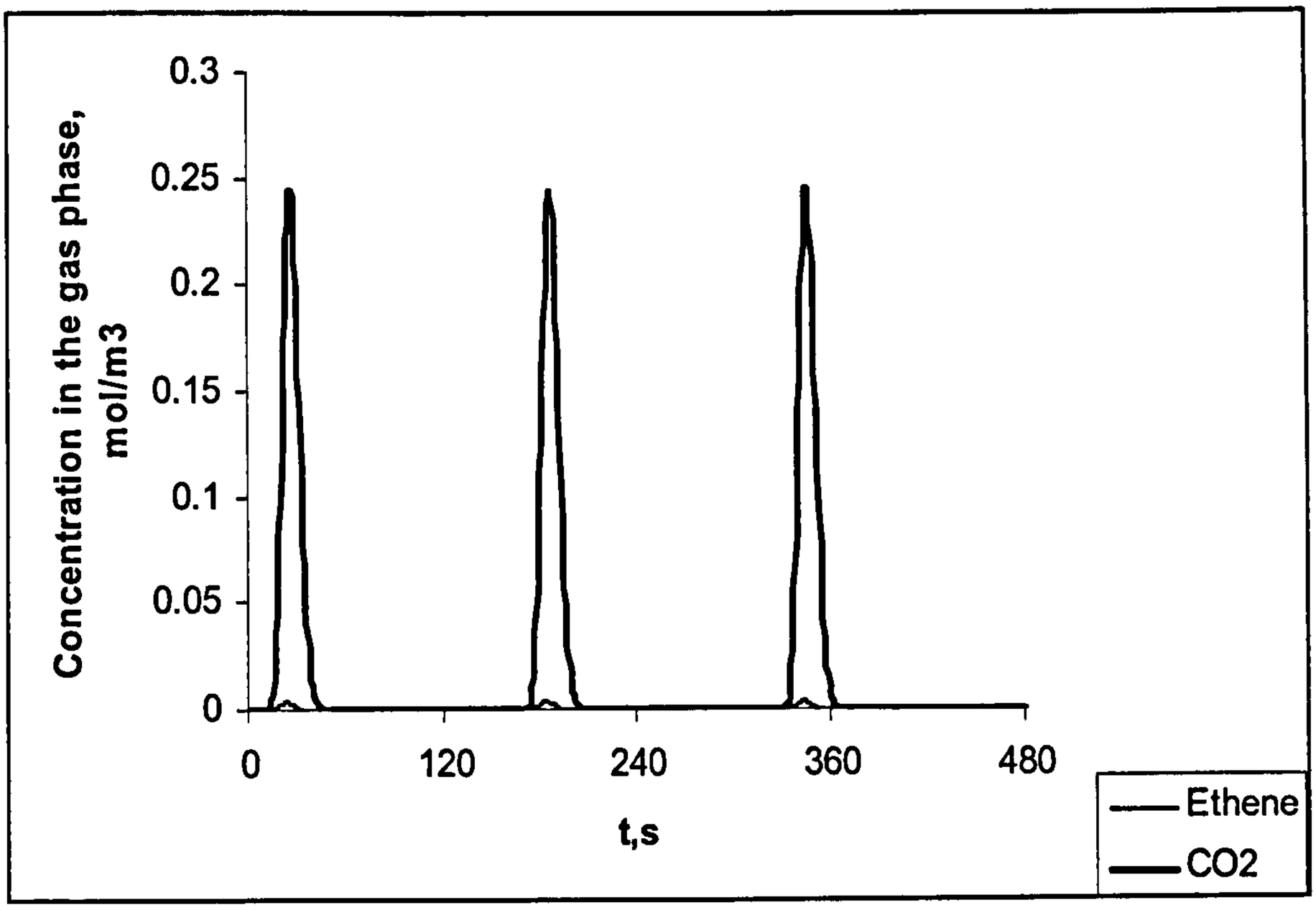

Fig. 4.25: Ethene and CO_2 exit concentration profiles; $T_{fa} = T_{fr} = 460$ K, $t_a = 10$ s, $t_d = 150$ s, 3 cycles

t_a (s)	t_d (s)	C_{time} (s)	S_R	X (%)	E (kJ m^2 s^{-1})	F_{PR} (mol cycle $^{-1}$)
150	150	300	0.50	12	21.2	1.07
70	150	220	0.32	27	21.2	1.07
30	150	180	0.17	62	21.2	1.07
10	150	160	0.06	97	21.2	0.9
5	150	155	0.03	99	21.2	0.5

Table 4.12: Effect of adsorption step times on M-AR performance; $T_{fa} = 460$ K, $T_{fr} = 460$ K, 10 cycles

In Table (4.12) F_{PR} is defined as the amount of ethene feed processed per cycle. It is clear from the results presented in the table that shorter adsorption-step times have advantages for conversion. At an adsorption step time of 150 s (complete saturation) the conversion is 12 % as reported earlier. At an adsorption step time of 10 s the conversion

amount increases to 97 % wherein we have a reduced amount of feed processed per cycle. The residence time for ethene to react is greater when ethene is adsorbed nearer the entrance of the reactor. Less ethene is wasted and blown away at the reactor exit, but is used up efficiently for reaction.

In the next section, the performance of the M-AR under this mode of operation is investigated in terms of the parametric effects of temperature, step times, and inlet velocity on conversion and energy.

Parametric Analysis

(i) Effect of step times

- ***Adsorption step time***

The case study of T_{fa} = 293 K and T_{fr} = 460 K is once again explored for incomplete bed saturation (the previous section explored same temperature operation for desorption and adsorption at 460 K) utilising base case conditions and $u_a = u_d$ = 0.05 m s^{-1}. The reaction heating time in this case is kept constant at 150 s. The effect of adsorption step times on the performance of the M-AR is shown in Table (4.13).

t_a (s)	t_d (s)	C_{time} (s)	S_R	X (%)	E (kJ m^2 s^{-1})	F_{PR} (mol cycle $^{-1}$)
150	150	300	0.50	2	10.1	0.4
70	150	220	0.32	9	14.1	0.9
30	150	180	0.17	35	17.5	1.5
10	150	160	0.06	85	19.8	1.2
5	150	155	0.03	95	20.5	0.7

Table 4.13: Effect of adsorption step times on M-AR performance; T_{fa} = 293 K, T_{fr} = 460 K, 20 cycles

From Table (4.13), it is observed that the performance of the M-AR increases in terms of conversion when shorter adsorption step times are utilised as discussed in the previous section. The energy input rate (see Eq. (3.51)) is again dependent on t_a and T_{fa} and increases with shorter adsorption-step times. Fig. (4.26) depicts the steady state axial temperature profiles at the various adsorption-step times. The heating time for desorption remains constant at 150 s. The shorter t_a, results in increased conversion values and together with the desorption / heating time increases the reactor temperature as is shown in the graph. This also ties in with the increase in energy requirements due to the higher temperature. It is also interesting to note that the energy input rate decreases under temperature swing operation than in the case of same temperature operation. As an example, from Table (4.13), at an adsorption step time of 5 s, the energy input rate was calculated as 20.5 kJ m^2 s^{-1} (c.f. 21.2 kJ m^2 s^{-1} from Table (4.12)).

With regards to the amount of ethene feed processed per cycle, F_{PR}, one would expect a decrease in this amount which corresponds to the shorter step-time for adsorption. From Table (4.13), it is observed that this value fluctuates and is smaller at 150 s and 70 s respectively. The reduction in F_{PR} may again arise from the fact that at these times ethene leakage occurs and much of the gas is blown away or wasted along the reactor length resulting in a reduced amount of ethene available for reaction.

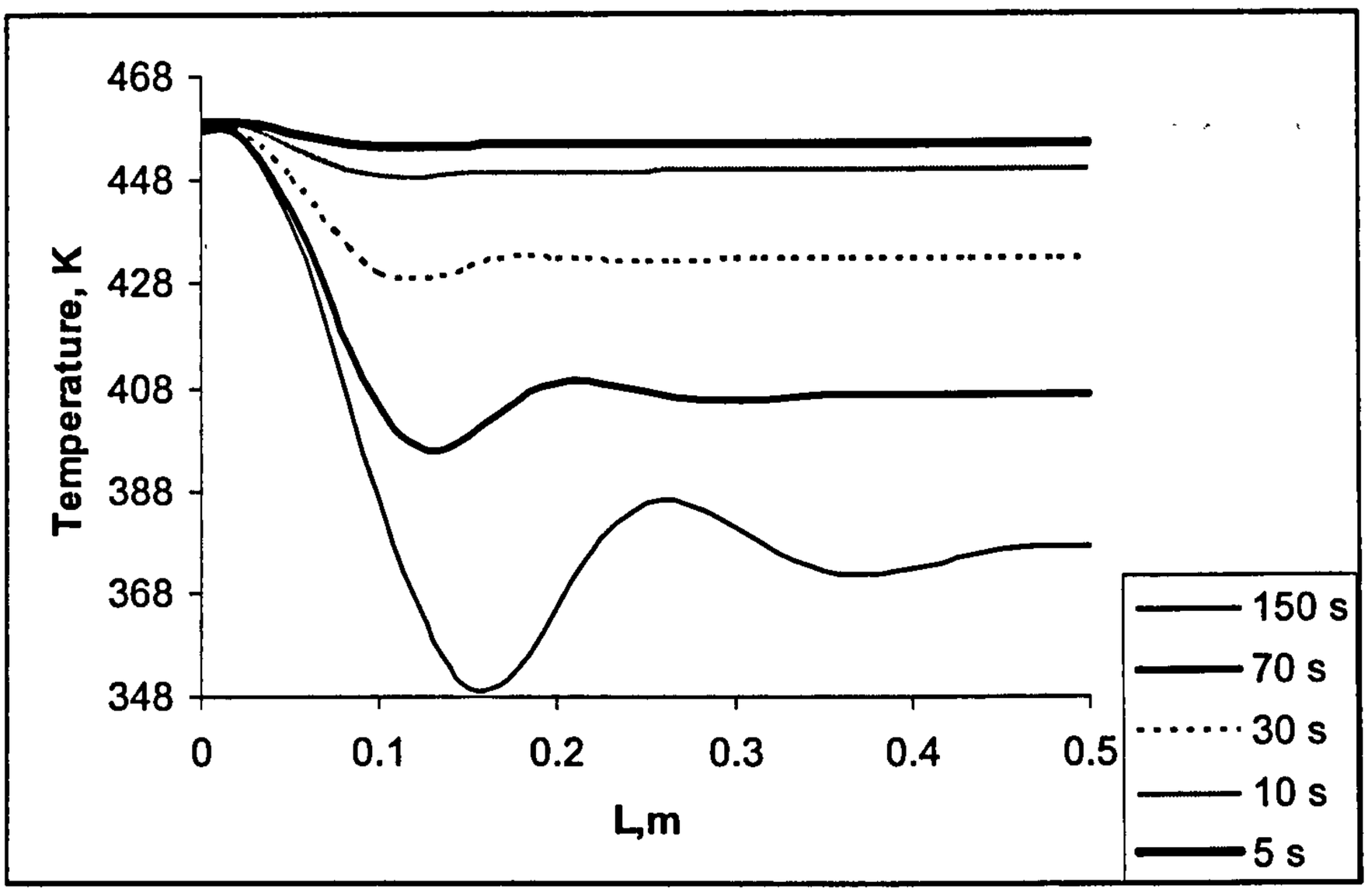

Fig 4.26: Steady state axial temperature profiles, T_{fa} = 293 K and T_{fr} = 460 K, 20 cycles.

- ***Heating Time (desorption step time)***

For the same case study as detailed above and utilising base case conditions and $u_a = u_d = 0.05$ m s^{-1} the effect of desorption heating

time on the performance of the M-AR is shown in Table (4.14). The adsorption step time is kept constant at 5 s.

t_a (s)	t_d (s)	C_{time} (s)	S_R	X (%)	E (kJ m² s⁻¹)	F_{PR} (mol cycle ⁻¹)	CSS
5	250	255	0.02	96	20.7	0.68	10
5	150	155	0.03	95	20.5	0.70	20
5	100	105	0.05	94	20.1	0.67	20
5	50	55	0.09	89	19.2	0.64	30
5	20	25	0.2	71	16.7	0.51	75

Table 4.14: Effect of heating times on M-AR performance; T_{fa} = 293 K, T_{fr} = 460 K, 20 cycles

As discussed earlier, the length of the heating / reaction step time has an effect on the conversion performance of the reactor as there is more time not only for the reactor to heat up to the required reaction temperature for reaction but also the gas-solid contact time is increased due to longer reactor residence time. The energy input rate, as expected increases with longer heating time on stream. The number of cycles required to reach steady state is denoted in Table (4.14) by CSS (cyclic steady state). Section 4.4.1 discussed briefly, the effect of heating time on the approach to cyclic steady state; with longer heating times (10 cycles), steady state is approached more quickly than with shorter heating times (75 cycles). The value of F_{PR} also varies with heating time. The adsorption step time is fixed at 5 s and the trend observed is a decrease in the amount of ethene feed processed with shorter heating times. The F_{PR} is therefore dependent

on the complex interactions of the adsorption and desorption step times.

(ii) Temperature Effects

For the case of the M-AR operating at an adsorption step time of 5 s and reaction / heating step time of 150 s (base case conditions), the effect of both feed adsorption temperature, T_{fa} and feed reaction temperature, T_{fr} on the reactor performance is detailed in Tables (4.15) – (4.17). The temperatures investigated are in the range: 293 K - 338 K for adsorption and 460 – 490 K for reaction.

- **T_{fa} 293 K**

T_{fr} (K)	X (%)	E (kJ m² s⁻¹)	F_{PR} (mol cycle ⁻¹)
460	95	20.5	0.70
475	98.8	21.7	0.71
490	100	22.7	0.71

Table 4.15: M-AR performance; T_{fa} = 293 K, T_{fr} = 460 K, 20 cycles

- **T_{fa} 320 K**

T_{fr} (K)	X (%)	E (kJ m² s⁻¹)	F_{PR} (mol cycle ⁻¹)
460	96	20.6	0.63
475	99.1	21.8	0.65
490	100	22.9	0.65

Table 4.16: M-AR performance; T_{fa} = 320 K, T_{fr} = 460 K, 20 cycles

- **T_{fa} 338K**

T_{fr} (K)	X (%)	E (kJ m² s⁻¹)	F_{PR} (mol cycle ⁻¹)
460	97	20.7	0.60
475	99.3	21.9	0.62
490	100	23	0.62

Table 4.17: M-AR performance; T_{fa} = 338 K, T_{fr} = 460 K, 20 cycles

The energy input rate increases with increasing temperature (T_{fr}) for all cases investigated as expected. Furthermore, F_{PR} remains fairly constant with increasing T_{fr}, but decreases with an increase in T_{fa}. This accounts for the fact that there is less adsorbate loading with the increase in temperature, and thus a smaller amount of ethene available for reaction per cycle. The constant value of F_{PR} with increasing T_{fr} illustrates the importance of the adsorption step on the process performance, not just with adsorption step times but also the temperatures utilised for adsorption.

Fig. (4.27) illustrates the temperature profile of the reactor at exit conditions for both the M-AR and M-ADS operating at T_{fa} = 293 K and T_{fr} = 460 K (base conditions). The extra heat released from such a dilute system and exothermic reaction is shown as the M-AR temperature profile is slightly higher than that of the adsorption-only M-ADS.

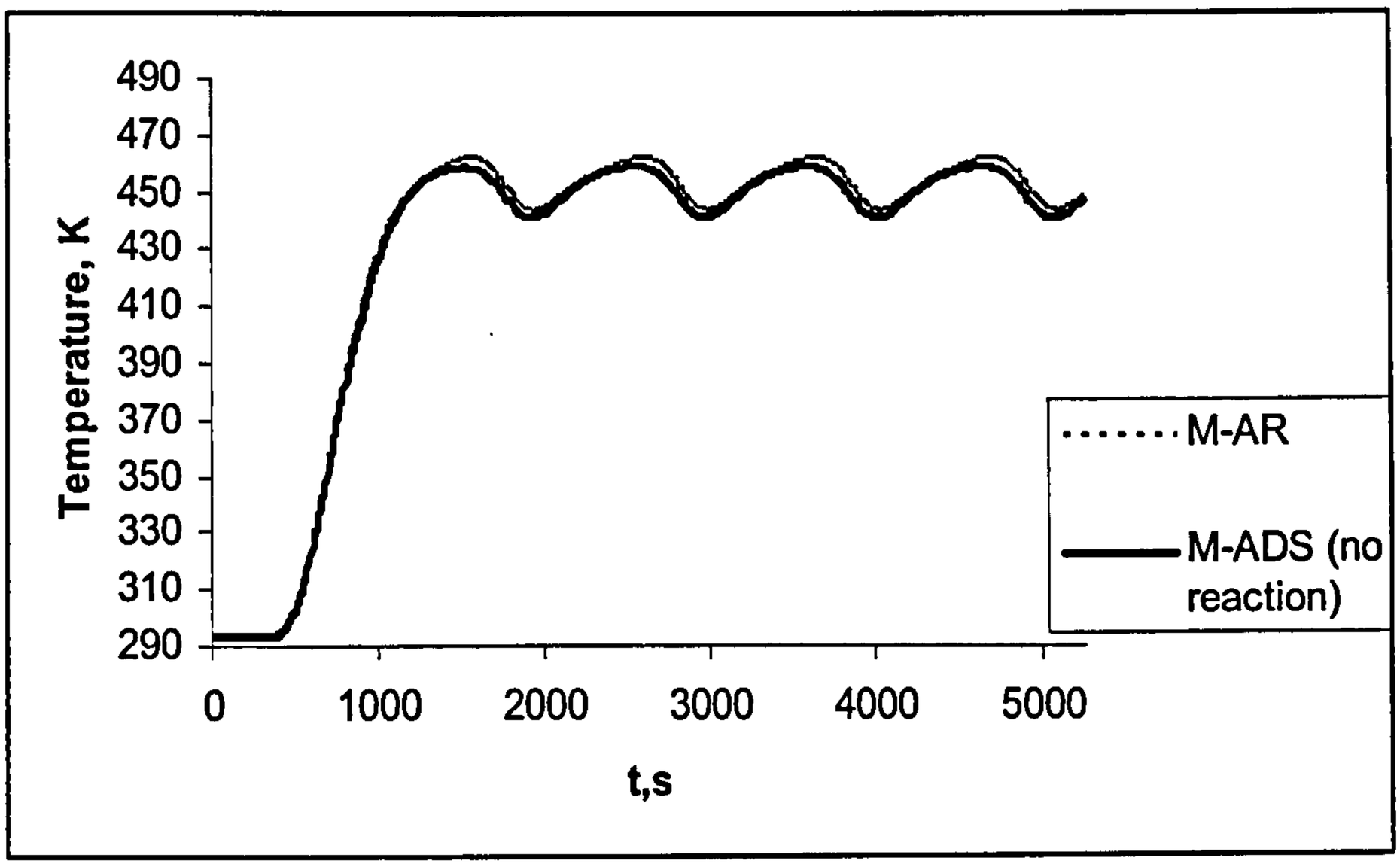

Fig. 4.27: Temperature profile of the reactor – exit conditions; t_a = 50 s, t_d = 1000 s, T_{fa} = 293K, T_{fr} = 460 K, 5 cycles

(iii) Velocity Effects

For the case of T_{fa} = 293 K and T_{fr} = 460 K, the effect of varying the desorption inlet velocity, u_d on the performance of the M-AR is performed with fixed step times of adsorption and desorption of 5 s and 150 s respectively. The adsorption inlet velocity, u_a is also kept constant at 0.05 m s^{-1}, while u_d is varied.

t_a (s)	t_d (s)	u_d (m s^{-1})	X (%)	E (kJ m^2 s^{-1})	F_{PR} (mol cycle $^{-1}$)
5	150	0.03	98.4	12.3	0.70
5	150	0.05	95	20.5	0.68
5	150	0.07	90	28.6	0.64

Table 4.18: M-AR performance; T_{fa} = 293 K, T_{fr} = 460 K, 10 cycles; u_a = 0.05 ms^{-1}

Table (4.19) illustrates the effect of decreasing the adsorption inlet velocity from 0.05 m s^{-1} as shown in Table (4.18) to 0.01 m s^{-1}. This velocity is kept constant and the desorption inlet velocity is again varied.

t_a (s)	t_d (s)	u_d (m s^{-1})	X (%)	E (kJ m^2 s^{-1})	F_{PR} (mol cycle $^{-1}$)
5	150	0.01	100	4.02	0.14
5	150	0.03	99.9	12.3	0.14
5	150	0.05	99.2	20.5	0.14
5	150	0.07	97.3	28.6	0.14

Table 4.19: M-AR performance; T_{fa} = 293 K, T_{fr} = 460 K, 10 cycles; u_a = 0.01 ms^{-1}

Tables (4.18) and (4.19) depict the importance of the inlet velocity on M-AR process performance. Lower inlet velocities lead to better conversion with emphasis on the adsorption inlet velocity which plays an important part in the crucial step of adsorption. It is also observed that F_{PR} is dependent on the inlet velocities.

4.4.3 Summary of cyclic operation

An important insight gained here is the role the step times of adsorption and desorption play on the overall performance of the M-AR. In the adsorption step, working in regions of incomplete bed saturation is favourable (i.e. shorter adsorption-step times) as one is sure that the adsorbed molecules all react nearer the front end of the reactor bed. In terms of desorption, this is fully dependent on the amount of gas available for desorption (from the adsorption step) and the operating

conditions i.e. feed temperatures for desorption and the inert regeneration gas.

In terms of switching ratios, the lower the value of S_R, the higher the conversion attained. The reaction step is then fully dependent on the adsorption step and the amount of gas adsorbed and thus available for reaction. Likewise, the adsorption-step time controls the degree of bed saturation, which in turn has an effect on the residence time for reaction during the desorption step.

The performance of the M-AR is a complex balance of achieving the right operating conditions in terms of the conversion and energy input. In cases where the bed is fully saturated, clearly an increase in adsorption feed temperature increases the energy input but not necessarily the conversion amount. Under partial saturation conditions, the dynamics of the process changes with respect to both conversion and energy and these are again dependent on the variables of inlet velocity and feed temperatures for both adsorption and desorption. For example working with a low temperature of adsorption of say 293 K and reaction temperature 460 K, the shorter adsorption-step times give higher conversion values, and the rate of energy input decreases under temperature swing operation than in the case of identical feed temperature operation.

The amount of ethene feed processed per cycle was found to also be dependent on the interaction between the step times for adsorption and

desorption, the inlet velocities and the mode of operation i.e. $T_{fa} = T_{fr}$ operation or temperature swing operation.

Fig. (4.28) shows the interaction between the energy input rate and conversion for the cases investigated.

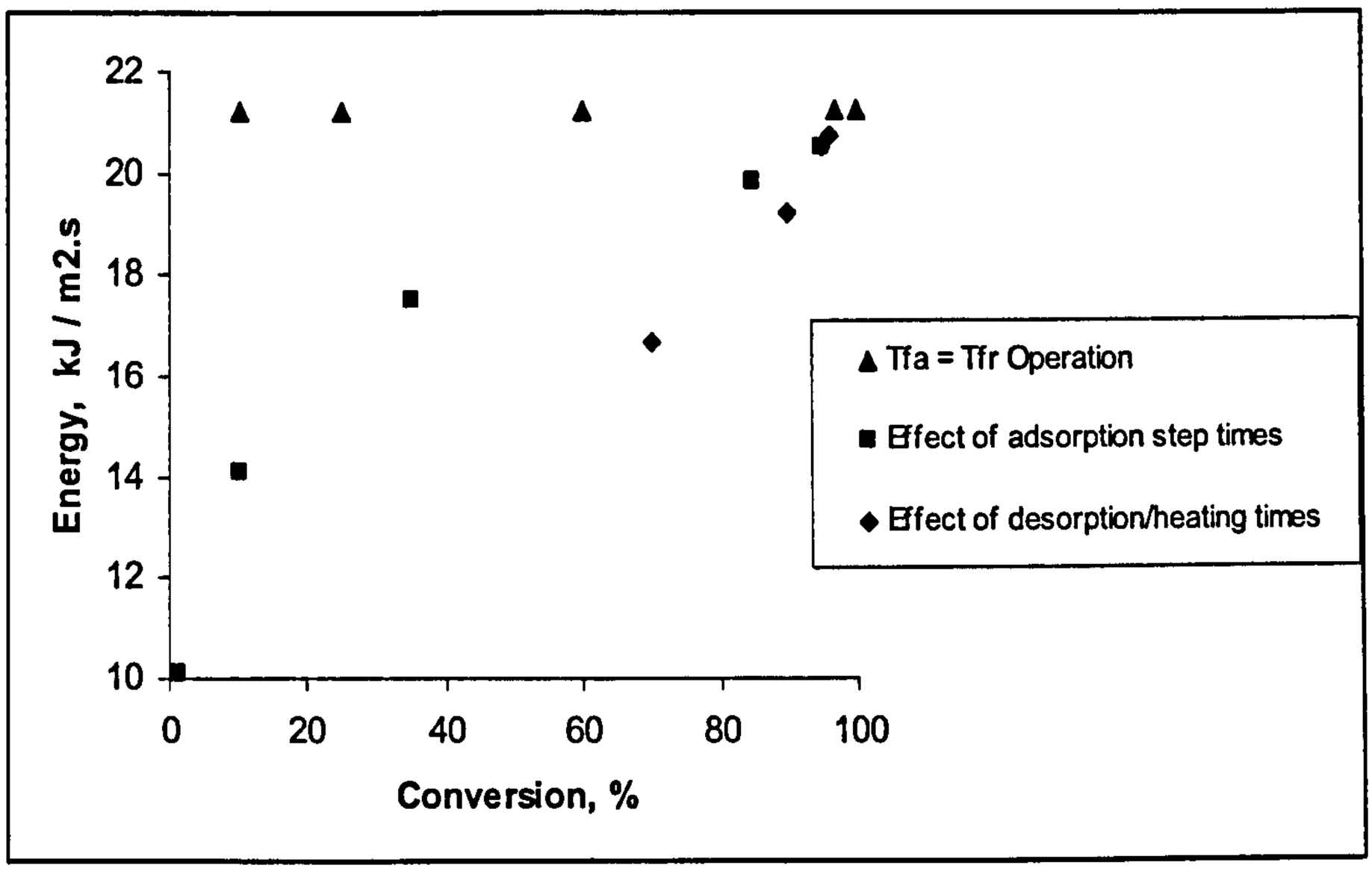

Fig. 4.28: Energy and conversion

These results depict the general performance of the M-AR in terms of conversion and energy requirement under the range of operating conditions and geometrical configurations specified. Emphasis was not given to the stability of the reactor as a very dilute feed concentration was used and the reactor was thermally stable. Section 4.5 explores the reactor stability issue for regions of incomplete saturation (no VOC breakthrough during the adsorption step) and for cases where the

concentration is increased both under and within the limits of explosivity for ethene as detailed previously.

4.5 Temperature stability

The performance of the novel hybrid monolith, M-AR and the monolith reactor, M-RXTN in which reaction-only takes place is assessed in terms of thermal stability. The stability of the reactor for an exothermic reaction is dependent on the feed concentrations and the feed inlet temperatures. Minor changes to the feed concentration have been known to cause situations of thermal runaway especially in packed bed reactors. The emphasis here is to comparatively assess the ability of both the M-AR and M-RXTN to cope with changes in inlet feed concentrations and temperatures. For the M-AR, regions of incomplete bed saturation are investigated.

The M-AR is predicted to be able to decrease the parametric sensitivity of an exothermic runaway due to the heat integration of an endothermic desorption and exothermic reaction and, principally due to the controlled release of reactant (VOC) from the adsorbed phase into the reaction zone.

Equivalency between the M-AR and M-RXTN

Thermal stability considerations were mentioned briefly in Section 4.2.2. The M-AR, M-RXTN and PB-AR performances in general, are conducted within regions of very low adsorbate concentration (3000 ppm or 0.3 vol. %). For thermal stability considerations, ethene as the VOC gas is utilised and feed inlet concentrations explored between the lower explosive limits, LEL (2.7 vol %) and upper explosive limits, UEL (36 vol. %) values.

The two reactors, M-AR and M-RXTN are identical in geometrical configuration, catalyst loading, feed inlet velocities and general operating conditions (with the exception of feed inlet temperature and feed inlet concentrations). These exceptions account for the fact that the M-AR is operated cyclically and the M-RXTN is operated as a single step continuous-fed reactor pre-mixed with VOC and air. The feed inlet concentrations in the M-RXTN were adjusted to account for the fact that adsorption at a temperature, T_{fa} takes place first in the M-AR, under regions of incomplete saturation. Therefore, the ethene feed inlet concentrations in the M-RXTN were much lower than in the M-AR. In the M-AR, air (O_2 – 21%; N_2 – 79%) is fed in during the desorption step at reaction temperature, T_{fr} i.e. 460 K. The feed reaction temperature in the monolith reactor, T_r is equal to the reaction temperature, T_{fr} in the second step of M-AR operation.

Thus the number of moles of ethene fed in during the adsorption step (which is also dependent on the step time for adsorption, t_a) at temperature of adsorption T_{fa} in the M-AR is first calculated and on the basis of identical volumetric feed rates in both reactors, the number of moles of ethene required for feeding into the M-RXTN can therefore be back-calculated. This gives the required feed inlet concentration in the M-RXTN. For a fair comparison, assessment is made for the same time period in both reactors at steady state.

4.5.1 $T_{fa} = T_{fr}$ Operation

(i) Concentration effects

For the case study $T_{fa} = T_{fr} = 460$ K operating with identical adsorption and desorption inlet velocities of 0.01 m s^{-1} with $t_a = 50$s and $t_d = 150$ s, the effect of changes in feed concentration are investigated. The operating conditions are chosen from the favourable results of conversion and energy observed from the various parametric studies previously performed on the M-AR (see Table (4.19)) whereby operating at lower inlet velocities improved conversion and energy profiles are attained. The inlet feed reaction temperature in the monolith reactor T_r, is equal to the reaction temperature, T_{fr} in the second step of M-AR operation. The performance of the PB-AR (cyclical packed bed adsorptive reactor) is also assessed in terms of reactor thermal stability. Table (4.2) gives the base case parameters for the M-AR and equivalent PB-AR. For both periodic reactors cyclic steady state values are reported unless stated otherwise.

M-AR / PB-AR (Vol. %)	M-RXTN (Vol. %)
1	0.33
3	1
5	1.7
10	3.3
20	6.7

Table 4.20: Feed concentrations for the M-AR, PB-AR and similarly operated M-RXTN; $T_{fa} = T_{fr} = = 460$ K

Table (4.20) lists the feed concentrations explored for ethene in the M-AR within the operating conditions specified and the corresponding feed concentrations for the monolith reactor. Reactor performance is assessed in terms of conversion, energy and thermal stability for each feed concentration.

The calculation of the M-RXTN feed concentration from the M-AR is detailed below:

$$C_i = \frac{y_i P}{RT} \tag{4.2}$$

where C_i is the concentration of the gas, mol m^{-3}, y_i the gas phase mole fraction, P the pressure, Pa, R the universal gas constant J mol^{-1} K^{-1} and T the inlet temperature, K.

$$n_i = C_{i\,[M\text{-}AR]}\, \nu \tag{4.3}$$

where n_i is the molar flow rate of the gaseous species, mol s^{-1} and ν the volumetric flow rate, $m^3 s^{-1}$.

The number of moles of ethene adsorbed, N_{ads} in the M-AR is also calculated and on the basis of identical volumetric flow rates the required feed concentration into the M-RXTN can be calculated (i.e. back calculated) from Eq. (4.5).

$$N_{ads} = C_{i\,[M\text{-}AR]}\, v\, t_a \qquad (4.4)$$

$$C_{i\,[M\text{-}AR]}\, v\, t_a / (t_a + t_d) = C_{i\,[M\text{-}RXTN]}\, v \qquad (4.5)$$

Appendix E gives the detailed calculations of equivalency between the concentrations in the M-AR and M-RXTN.

Table (4.21) shows the effect of changes in feed concentration on the performance of the three reactors, M-AR, PB-AR and the M-RXTN for concentrations of ethene at 1 vol. % (c.f. M-RXTN 0.33 vol. %) and 3 vol. % (c.f. M-RXTN 1 vol. %). As is the case for T_{fa} - T_{fr} operation, the energy input rate is the same for all reactors. The high conversion in the M-AR reflects operation within a bed not fully saturated and at such low velocities allowing for greater gas-solid contact time. The temperature difference at steady state exit conditions, ΔT, rises with increasing feed concentration. The rate of reaction increases as a result of changes in feed concentration, and thus extra heat is given off, reflected by the increase in temperature. With operation at 1 vol. % of ethene, the hybrid M-AR shows the least rise in temperature of +7 K, compared to that of the monolith reactor at +10 K and the packed bed at +69 K. Despite the fact that the packed bed is operating as an adsorptive reactor, the

temperature excursion is still quite high and this justifies the use of structured reactors over the conventional fixed beds.

	M-AR	M-RXTN	PB-AR	M-AR	M-RXTN	PB-AR
Feed$_{C2H4}$ (Vol. %)	1	0.33	1	3	1	3
Δ T (K)	+7	+10	+69	+22	+31	+124 *
X (%)	99.9	100	99.9	99.9	100	99.9
E (kJ m^{-2} s^{-1})	4.2	4.2	4.2	4.2	4.2	4.2
F$_{PR}$ (mol s^{-1})	0.02	0.02	0.02	0.05	0.06	0.05 *

Table 4.21: Performance of the M-AR, PB-AR and similarly operated M-RXTN; $T_{fa} = T_{fr} = 460$ K
Note: * indicates reactor instability

At 3 vol. % of ethene feed, both the monolith and M-AR attain steady state (~50 cycles for the M-AR). In the packed bed, it takes a lot longer to reach steady state as compared to the monolith reactors (both M-AR and M-RTXN); see Figs.(4.30) and (4.31). However, as shown in Table (4.21) the PB-AR does not attain steady state at this point (3 vol. %) and runaway is established.

The steady state axial temperature profiles for all three reactor types are shown in Figs. (4.29) – (4.33). Axial temperature profiles for the M-AR are shown at cyclic steady state (CSS) unless stated otherwise. The corresponding axial temperature profile within the M-RXTN is also depicted at steady state. The total amount of time spent on stream for both reactors is also the same.

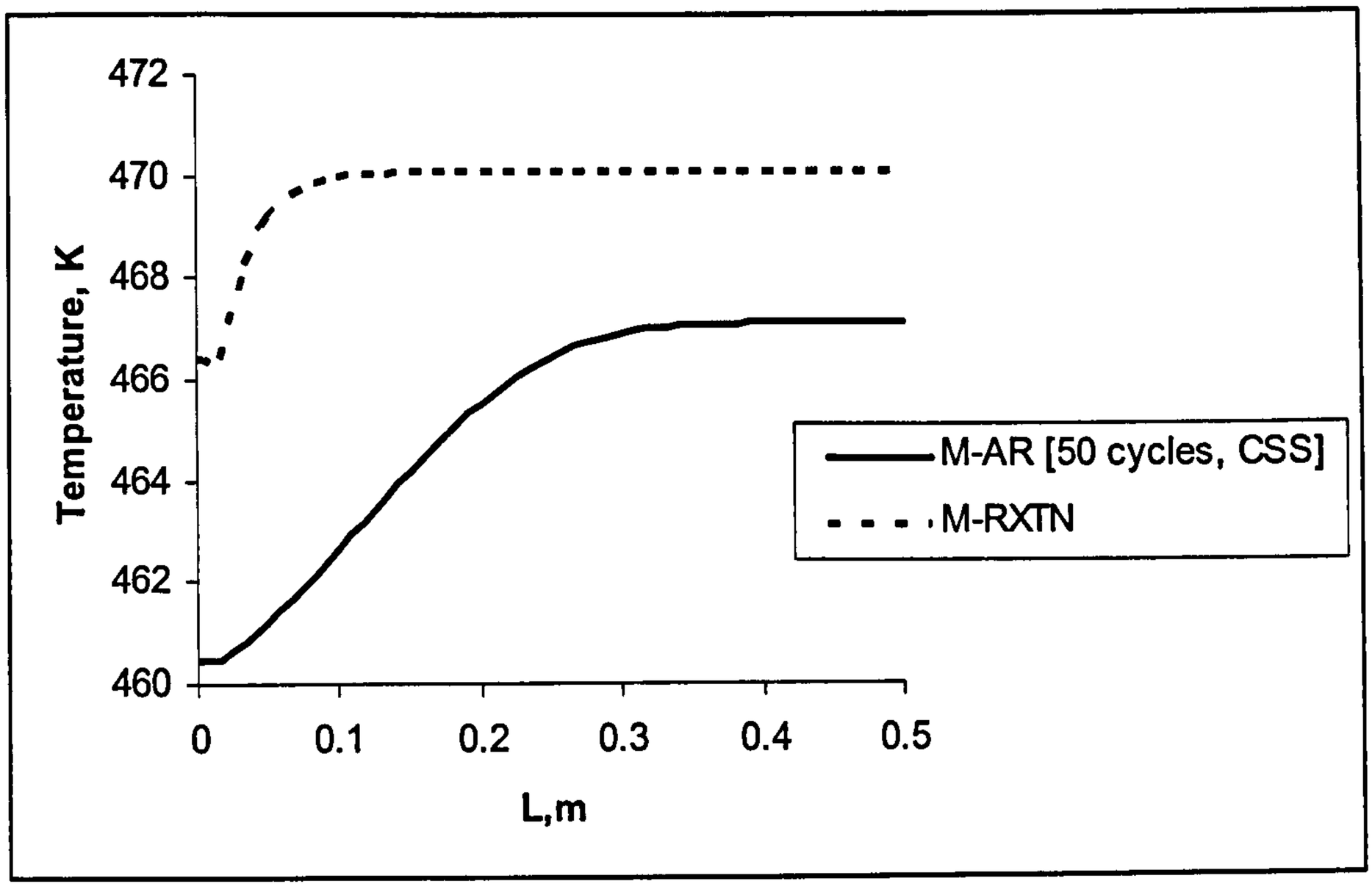

Fig. 4.29 (a): Steady state temperature profiles along axial distance for the M-$_{AR}$ (1 vol. %) and equivalent M-$_{RXTN}$ (0.33 vol. %)

Fig. 4.29 (b): Temperature profiles along axial distance for the PB-$_{AR}$ (1 vol. %)

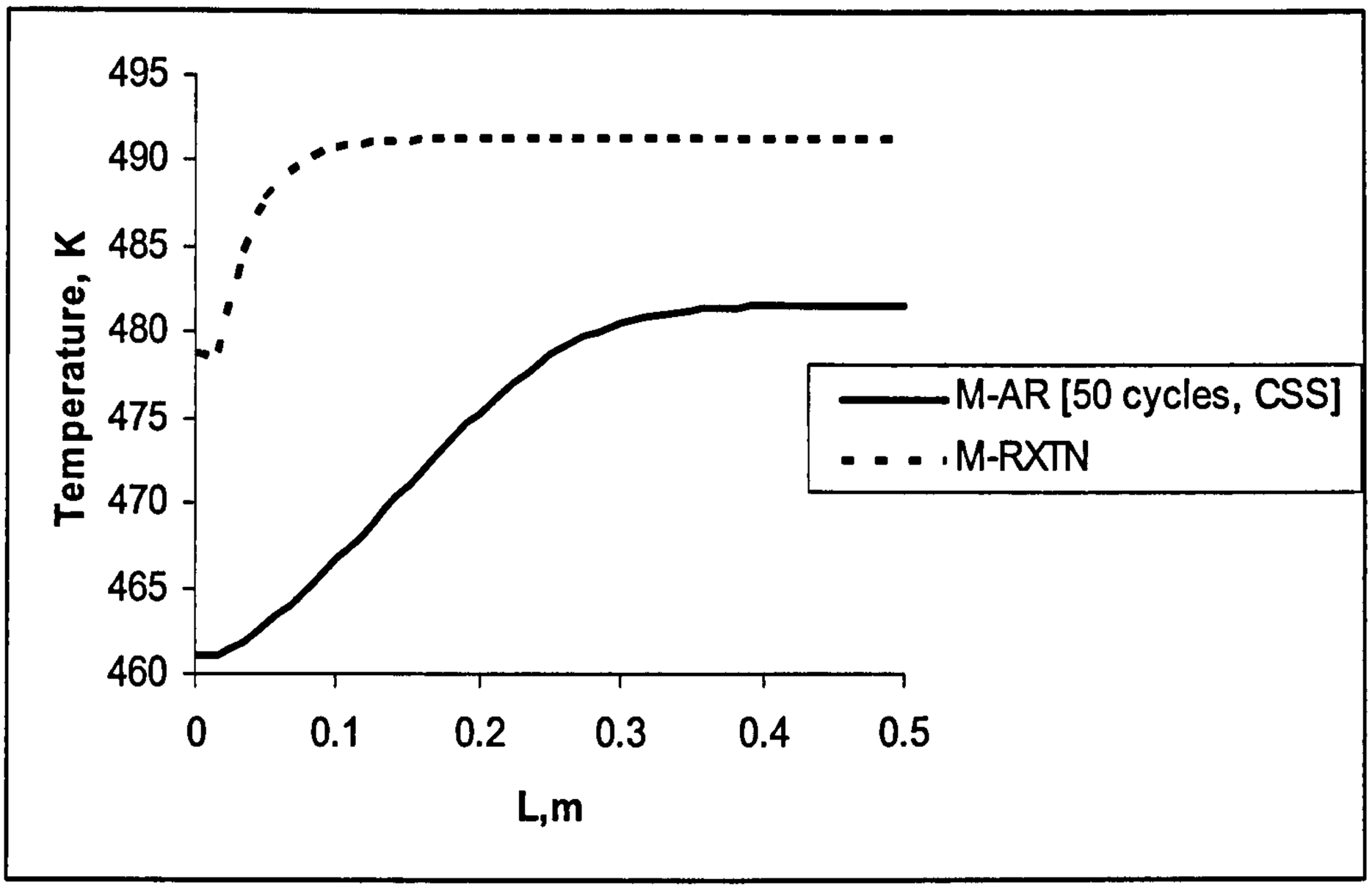

Fig. 4.30 (a): Steady state temperature profiles along axial distance for the M-$_{AR}$ (3 vol. %) and equivalent M-$_{RXTN}$ (1 vol. %)

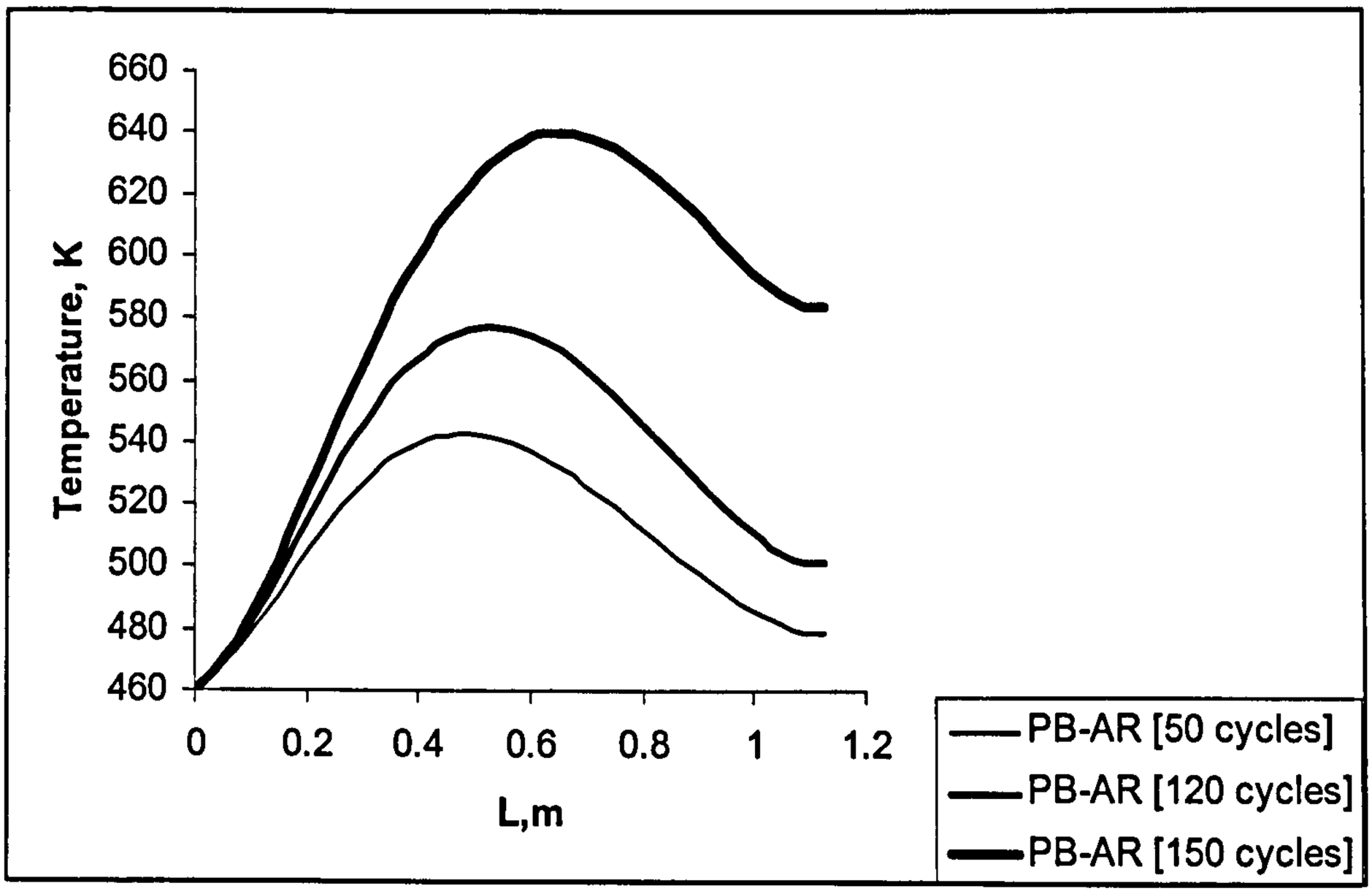

Fig. 4.30 (b): Temperature profiles along axial distance for the PB-$_{AR}$ (3 vol. %)

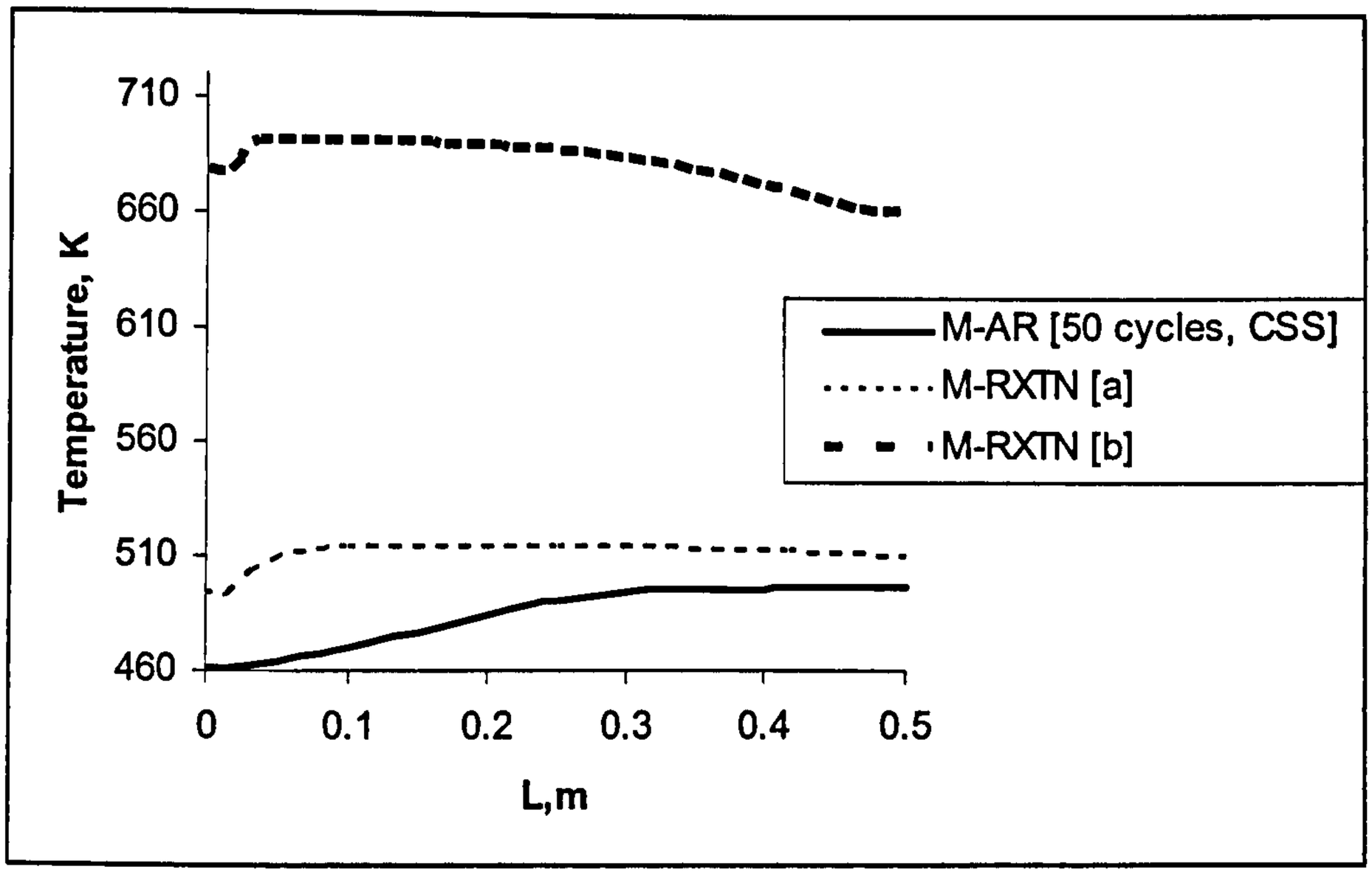

Fig. 4.31(a): Steady state temperature profiles along axial distance for the M-$_{AR}$ (5 vol. %) and equivalent M-$_{RXTN}$ (1.7 vol. %) [a] and M-$_{RXTN}$ (5 vol. %) [b]

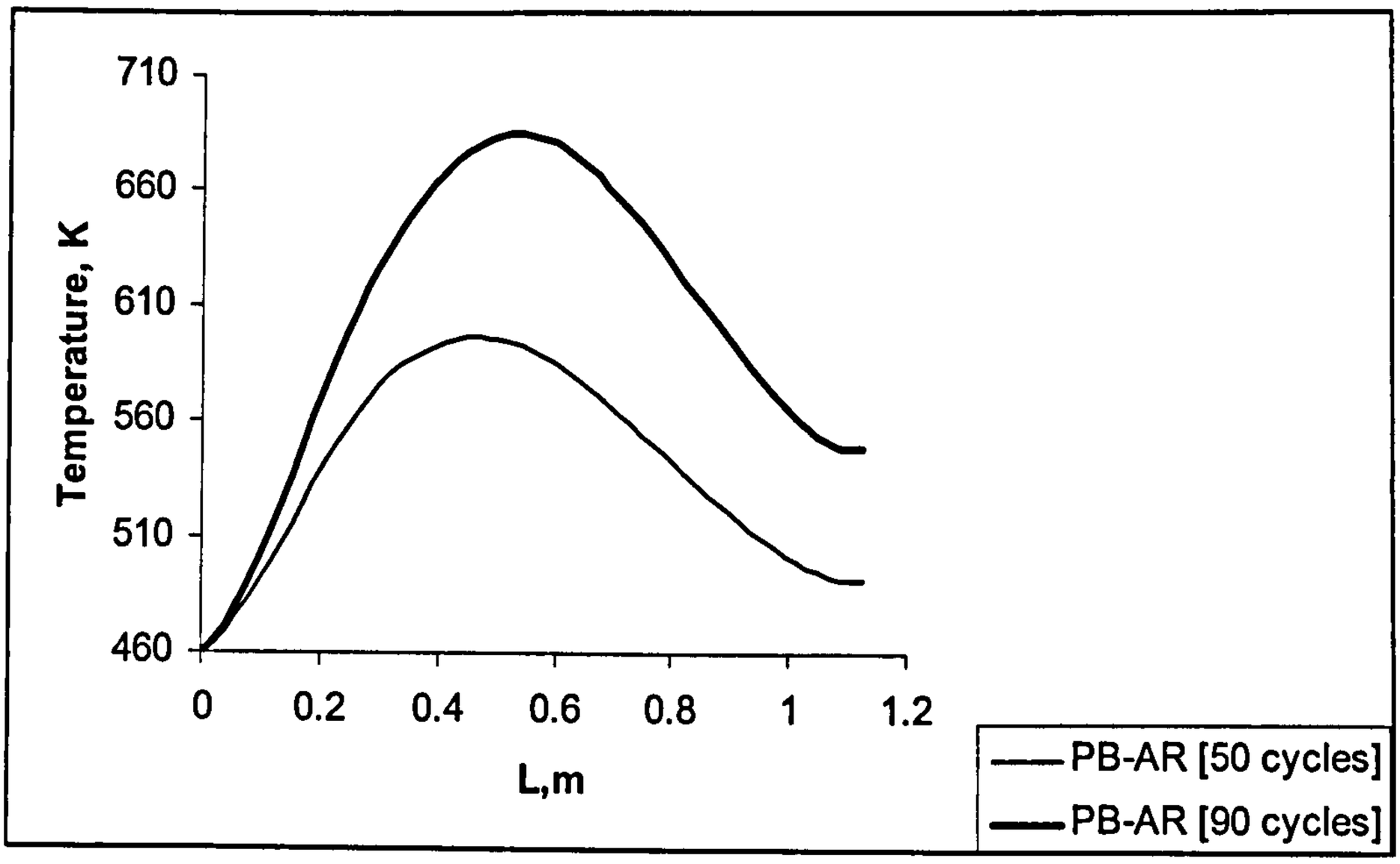

Fig. 4.31 (b): Temperature profiles along axial distance for the PB-$_{AR}$ (5 vol. %)

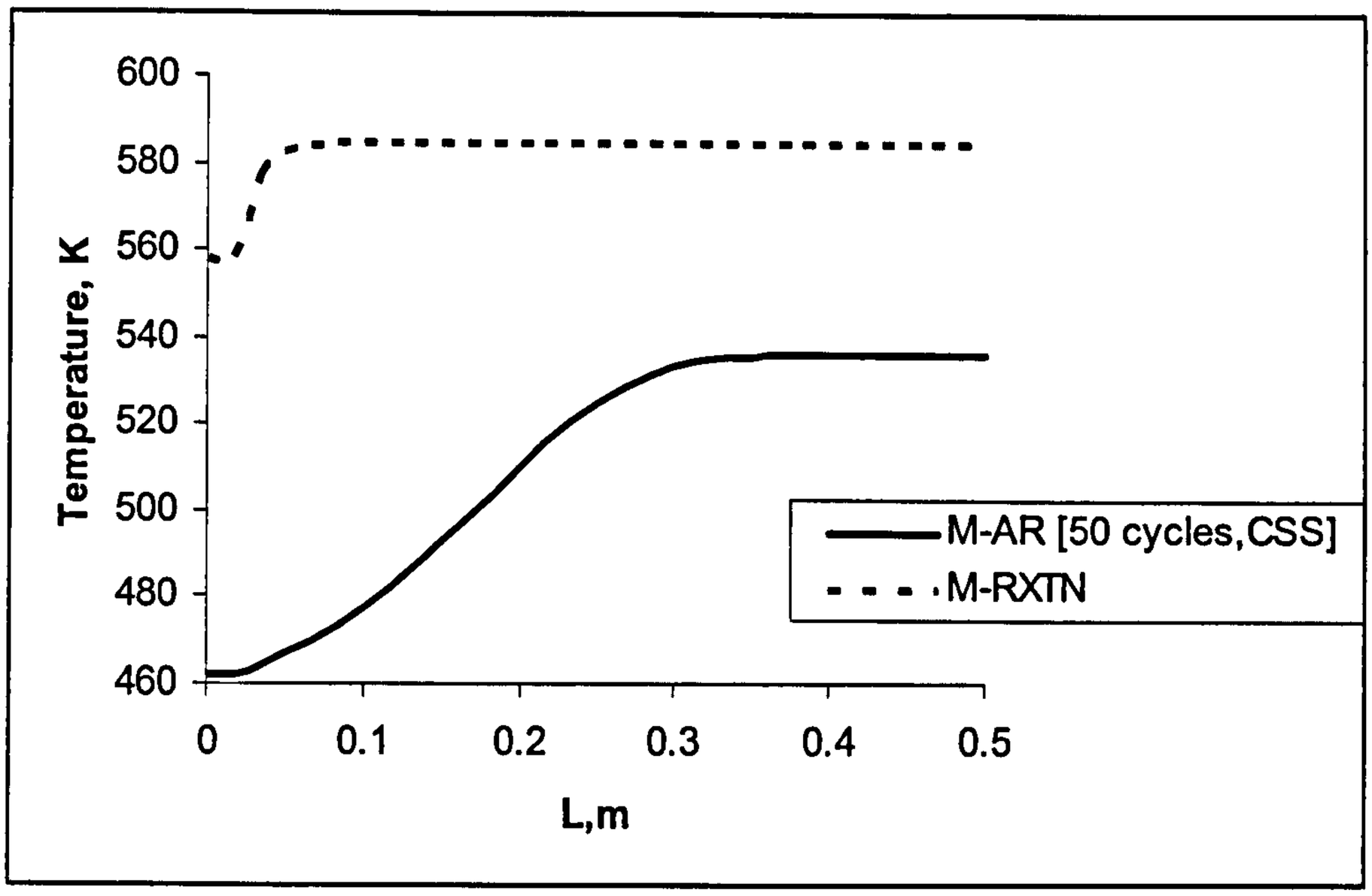

Fig. 4.32 (a): Steady state temperature profiles along axial distance for the M-$_{AR}$ (10 vol. %) and equivalent M-$_{RXTN}$ (3.3 vol. %)

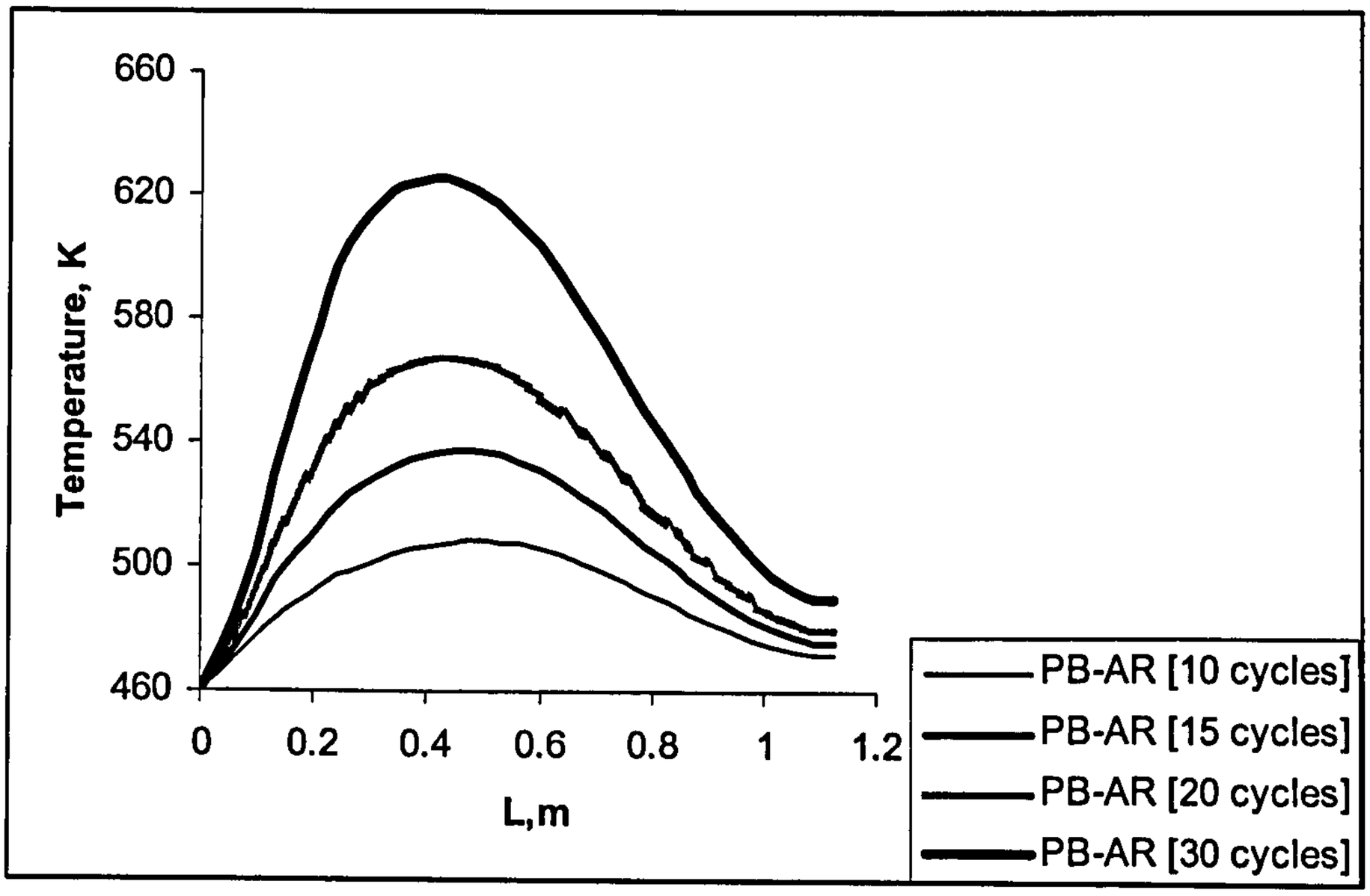

Fig. 4.32 (b): Temperature profiles along axial distance for the PB-$_{AR}$ (10 vol. %)

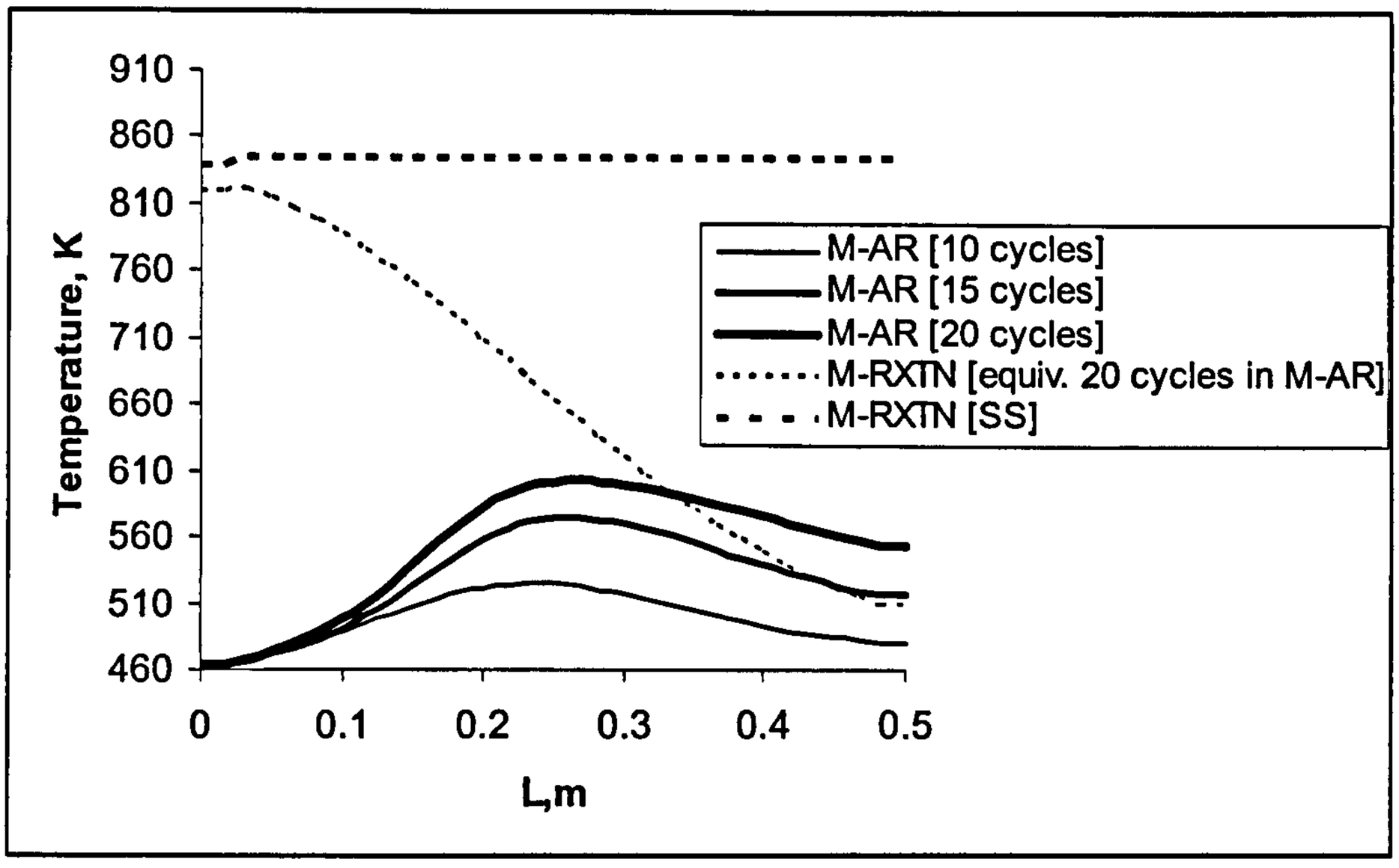

Fig. 4.33 (a): Temperature profiles along axial distance for the M-$_{AR}$ (20 vol. %) and equivalent M-$_{RXTN}$ (6.7 vol. %)

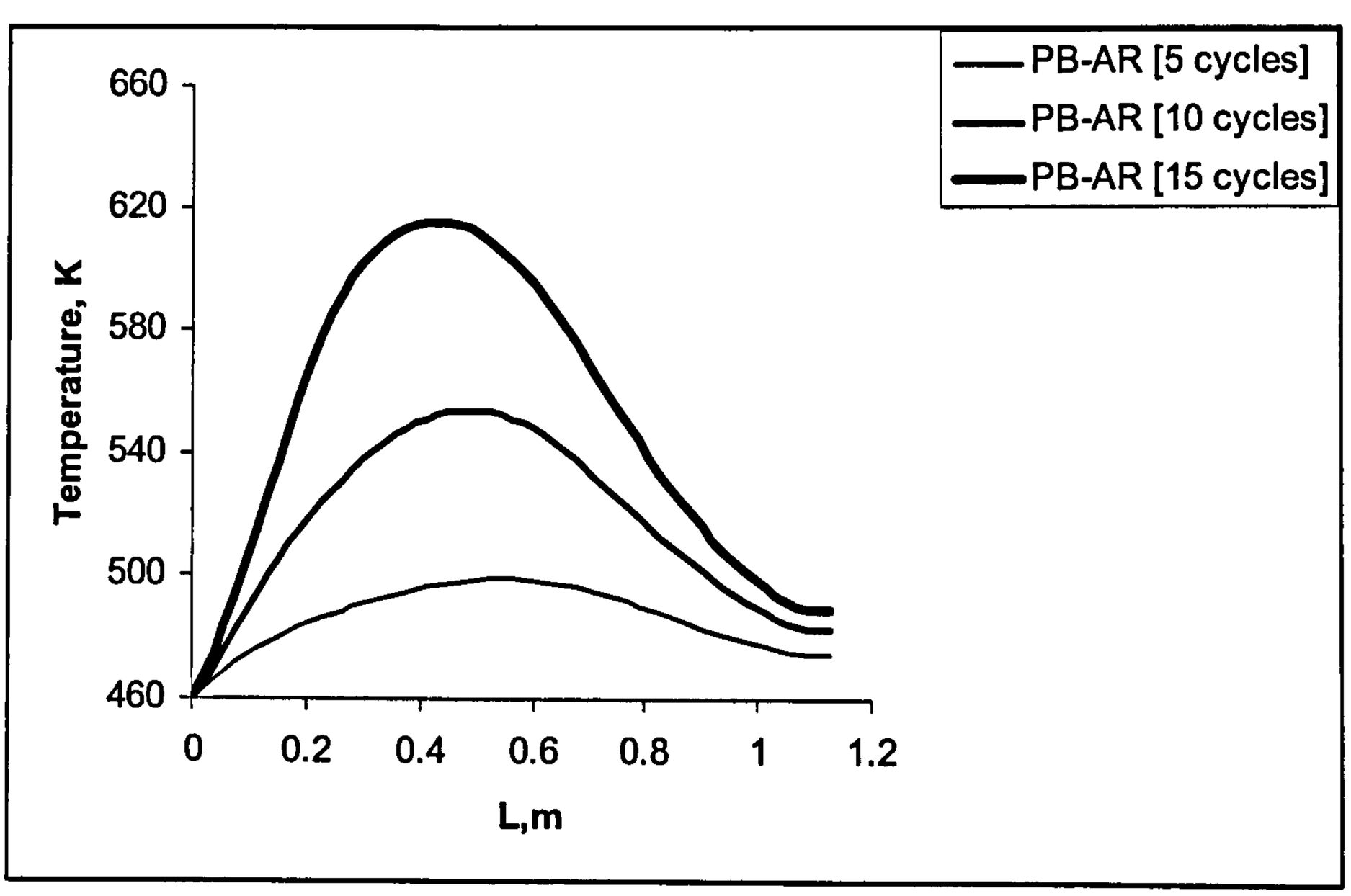

Fig. 4.33(b): Temperature profiles along axial distance for the PB-$_{AR}$ (20 vol. %)

The graphs listed in Figs. (4.29) – (4.33) above illustrate the axial temperature profiles of the reactors. Key findings on the reactor

performance under ethene feed concentrations in the range of 1 vol. % to 10 vol. % (c.f. M-RXTN 0.33 vol. % to 6.7 vol. %) are summarised below:

- The steady state temperature profile in the M-RXTN is higher than that of the M-AR also at cyclic steady state. For example in Fig (4.31 (a)), the steady state temperature in the M-AR at an ethene feed concentration of 5 vol. % is 497 K. The steady state temperature for an equivalent M-RXTN with feed concentration 1.7 vol. % is 513K. This gives a temperature difference of + 16 K. Utilising the same feed concentration for the M-AR in the M-RXTN i.e. 5 vol. %, resulted in thermal runaway as depicted by Fig (4.31(a)[b]) with temperatures reaching as high as 690 K, and steady state not yet attained.

- The energy input rate (4.2 kJ m^2 s^{-1}) for all reactors (M-AR, PB-AR and M-RXTN) is the same. 100 % conversion is attained in the M-RXTN for all concentrations. Both the M-AR and PB-AR achieve 99.9 % conversion for the range of feed concentrations investigated.

- In the packed bed reactor, a longer time is required to achieve steady state. At 1 vol. % it takes 500 cycles to reach cyclic steady state. With increasing feed concentrations, runaway was established with reactor thermal stability occurring only during shorter cycles. For example, at 3 vol. % of ethene instability occurs after about 150 cycles with a temperature of 638 K; after 90 cycles

for 5 vol. % of ethene with temperature 690 K and after 30 cycles for 10 vol. % with temperature 630 K.

- The axial temperature profile in the PB-AR is higher than that of both the M-AR and M-RXTN. For example for 3 vol. % of ethene, the M-AR reaches steady state at about 50 cycles with a temperature of 482 K. The temperature in the PB-AR at 50 cycles is 530 K and peaks at 638 K for 150 cycles.

At 20 vol. % of ethene (c.f. M-RXTN 6.7 vol. %), see also Figs. (4.33 (a) and (b)), runaway is established in the M-AR which becomes unstable after 20 cycles. As expected, thermal runaway also occurs in the PB-AR which becomes unstable after 15 cycles. The maximum temperature in the M-RXTN at a time equivalent to the 20 cycles of M-AR operation was 818K. At steady state the temperature in the M-RXTN rose to 850 K.

(ii) Temperature effects

For the case study $T_{fa} = T_{fr}$, operating with identical adsorption and desorption inlet velocities of 0.01 m s^{-1} and with t_a = 50s and t_d = 150 s, the effect of feed inlet temperature was also investigated for a feed concentration of 1 vol. % ethene. The feed temperatures at 475 K and 490 K were investigated with $T_{fa} = T_{fr}$.

	M-AR	M-RXTN	PB-AR	M-AR	M-RXTN	PB-AR
$T_{fa} = T_{fr}$	475 K	475 K	475 K	490 K	490 K	490 K
$Feed_{C2H4}$ (Vol. %)	1	0.5	1	1	0.5	1
ΔT (K) Exit temp	+ 7	+ 10	+ 66*	+ 7	+ 10	+ 66 *
X (%)	99.9	100	96.3*	99.9	100	96.7*
E (kJ m^{-2} s^{-1})	4.5	4.5	4.5	4.7	4.7	4.7
F_{PR} (mol s^{-1})	0.015	0.02	0.013*	0.014	0.02	0.013*

Table 4.22: Performance of the M-AR , PB-AR and similarly operated M-RXTN; $T_{fa} = T_{fr}$
Note: * indicates reactor instability

With reference to Table (4.22), the M-AR and M-RXTN at increasing feed temperatures appears more stable than the PB-AR where for both 475 K and 490 K, runaway occurs. The M-AR temperature rise was again lower than that of the M-RXTN.

4.5.2 Temperature swing effect ($T_{fa} \neq T_{fr}$ Operation)

The previous section dealt with identical feed temperature operation for adsorption and reaction. In reality, the novel concept of this reactor requires operation at low temperatures of adsorption (where adsorbate loading is largest) and desorption at higher temperatures via temperature and concentration swing. Furthermore energy requirement benefits are seen under this mode of operation than for identical temperature operation (as shown in the parametric studies).

(i) Concentration effects (adsorption step- time = 5 s)

The effect of feed inlet concentrations for feed temperature operation at T_{fa} = 293 K and T_{fr} = 460 K is taken as a case study. In this case, the reaction temperature, T_r for the M-RXTN is also set to T_{fr}. The reactor is operated under incomplete bed saturation, with $u_a = u_d = 0.01$ m s^{-1} and t_a = 5 s, t_d = 150 s.

Table (4.23) lists the feed concentrations explored for ethene within the operating conditions specified and the corresponding feed concentrations for the monolith reactor. Thus the number of moles of ethene fed in during the adsorption step (which is also dependent on the step time for adsorption, t_a) at temperature T_{fa} in the M-AR is first calculated and on the basis of identical volumetric feed rates in both reactors, the number of moles of ethene required for feeding into the M-RXTN can therefore be back-calculated. This gives the required feed inlet concentration in the M-RXTN. See Appendix E for more details.

M-AR (Vol. %)	M-RXTN (Vol. %)
1	0.05
5	0.26
10	0.52
20	1.05
30	1.31
40	2.09

Table 4.23: Feed concentrations for the M-AR and similarly operated M-RXTN; T_{fa} = 293 K, T_{fr} = 460 K

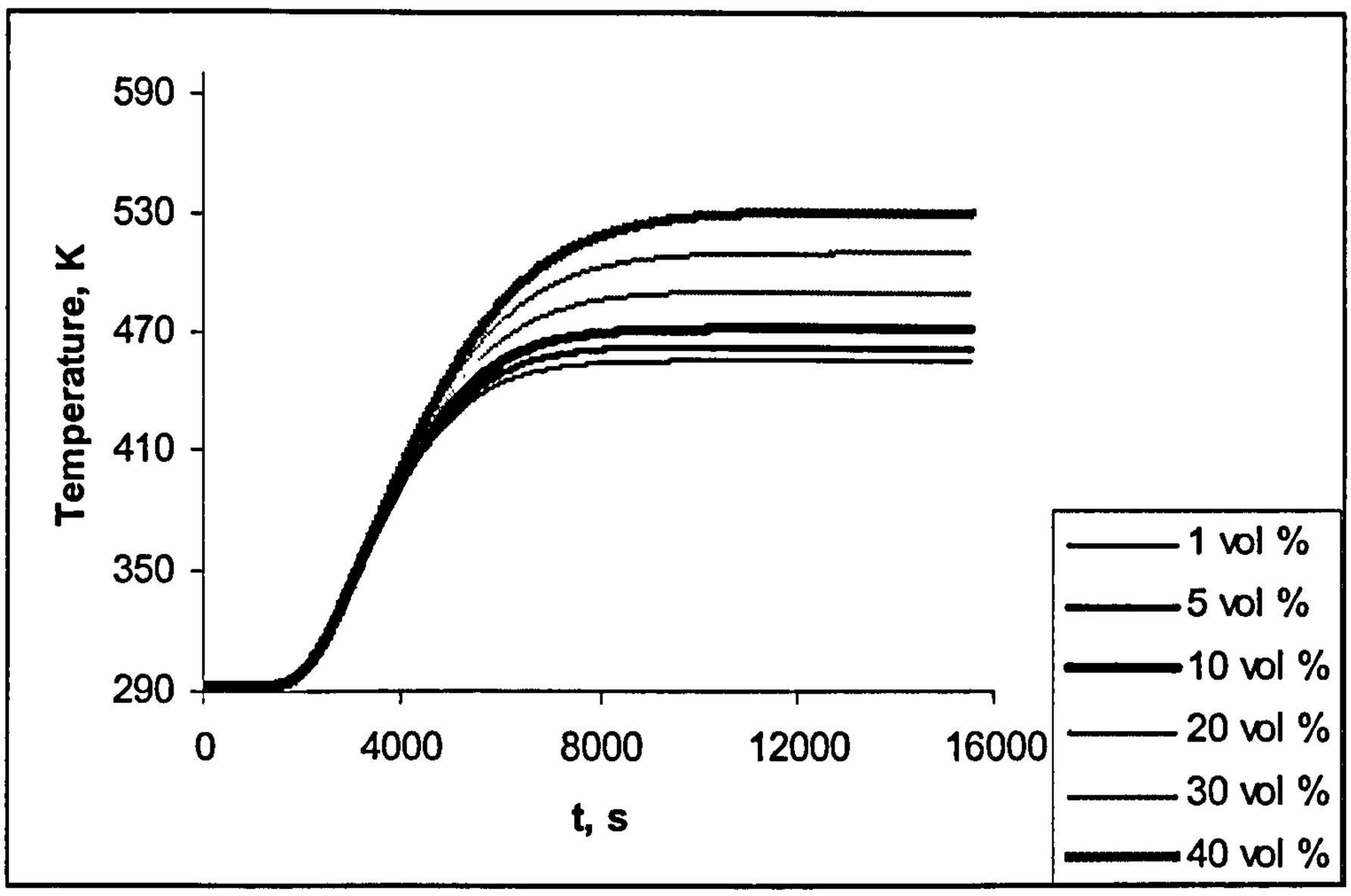

Fig. 4.34: Steady state temperature profiles of the M-$_{AR}$ at different ethene concentrations

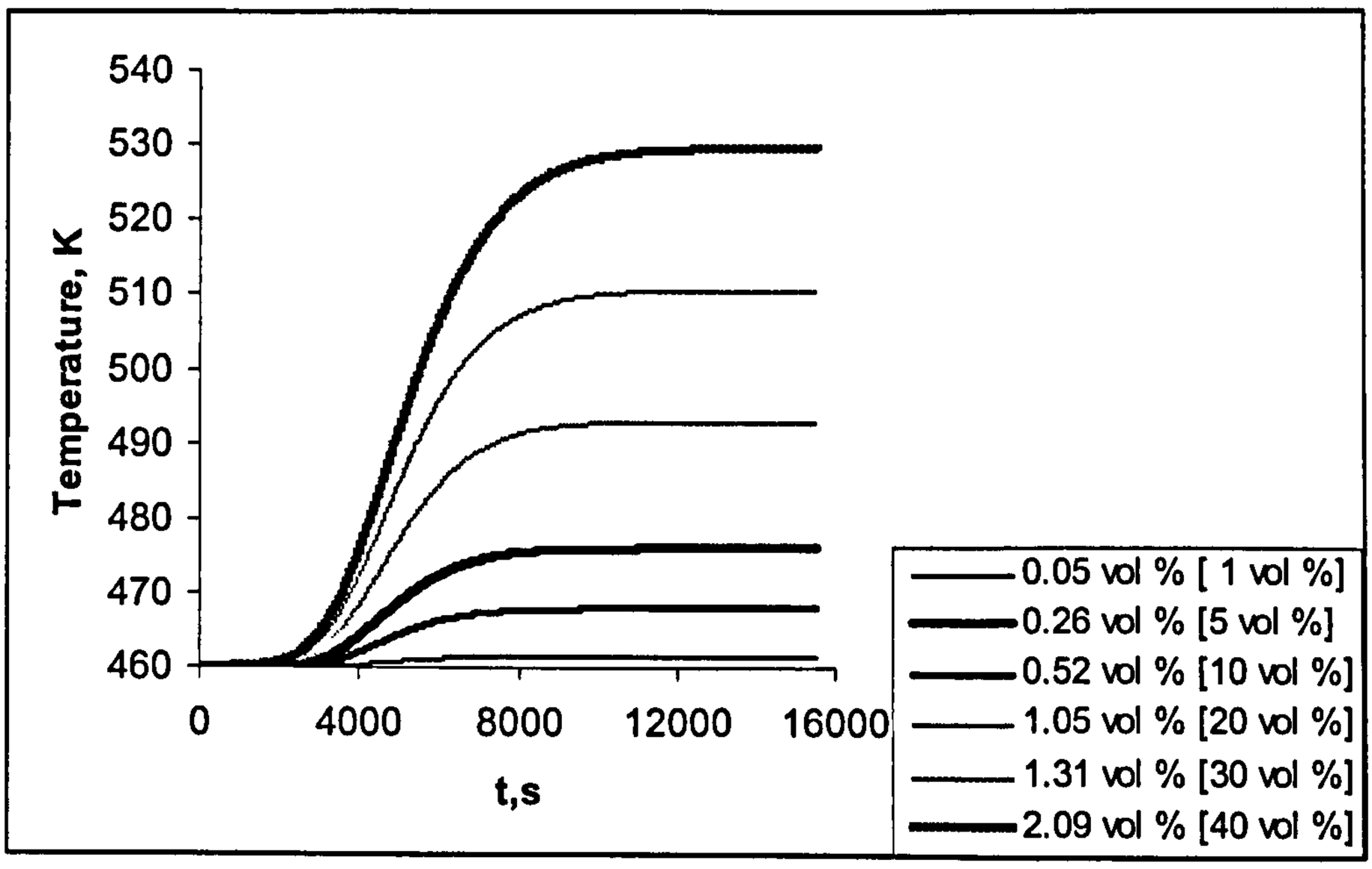

Fig. 4.35: Steady state temperature profiles of the M-$_{RXTN}$ at different ethene concentrations

Figs (4.34) and (4.35) depict the steady state temperature profiles for both the M-AR and equivalent M-RXTN. As expected, the temperature of the reactor increases with an increase in ethene concentration. The temperature swing effect enables the M-AR to operate with concentrations as high as 40 vol. % (c.f. in $T_{fa} = T_{fr}$ operation where reactor instability occurs at 20 vol. %).

Feed$_{C2H4}$ (Vol. %)	**1**	**5**	**10**
X (%)	99.5	99.5	99.9
E (kJ m^{-2} s^{-1})	4.02	4.02	4.02
F_{PR} (mol s^{-1})	0.003	0.015	0.03

Table 4.24: Performance of the M-AR; T_{fa} = 293 K, T_{fr} = 460 K, 100 cycles

The performance of the M-AR at the different feed concentrations is shown in Table (4.24) above. The M-AR in general is thermally stable even at 40 vol. % of ethene. This is illustrated in Figs. (4.36 and 4.37)

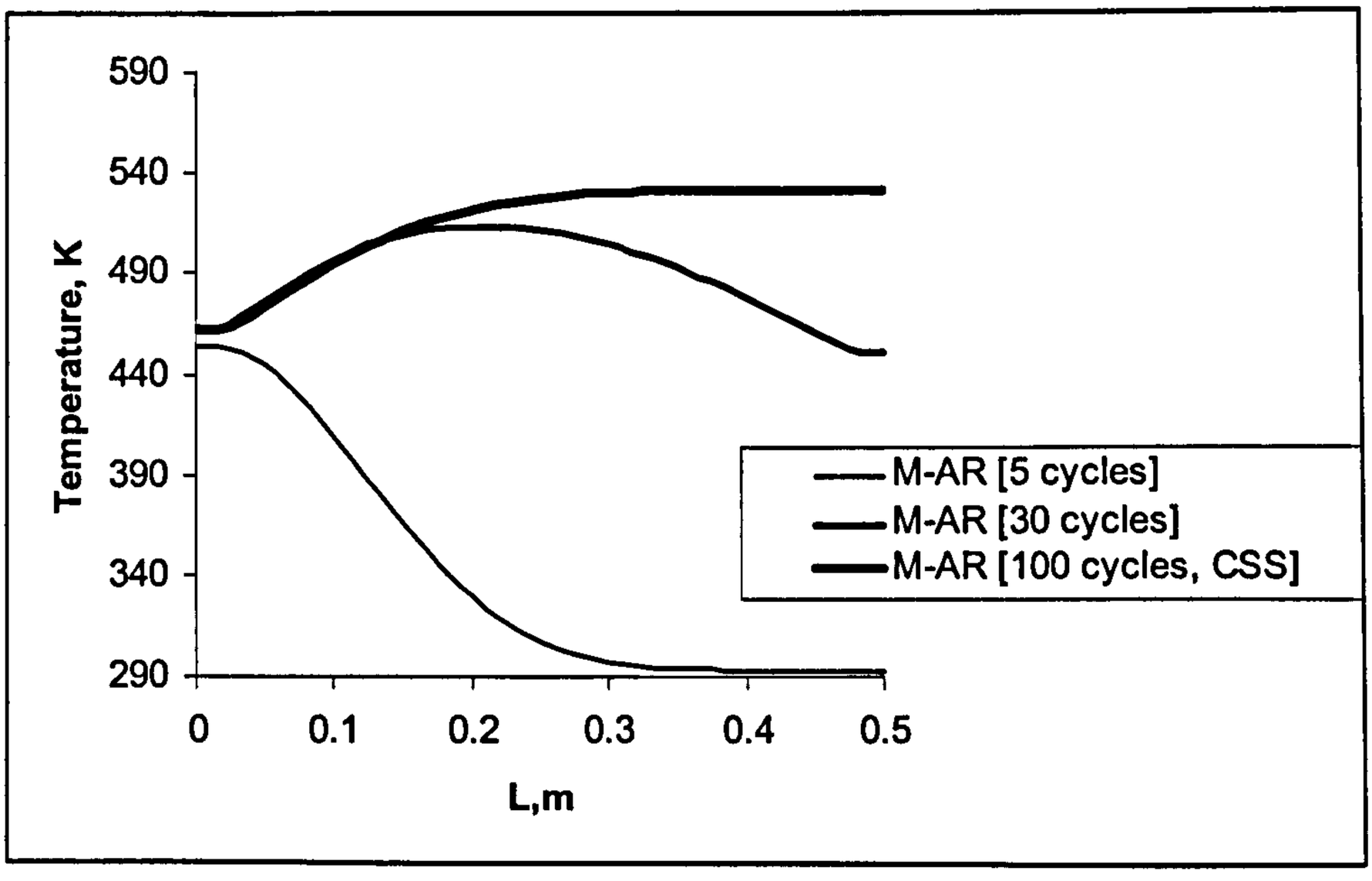

Fig. 4.36: Axial temperature profiles of the M-$_{AR}$ at 40 vol. % ethene

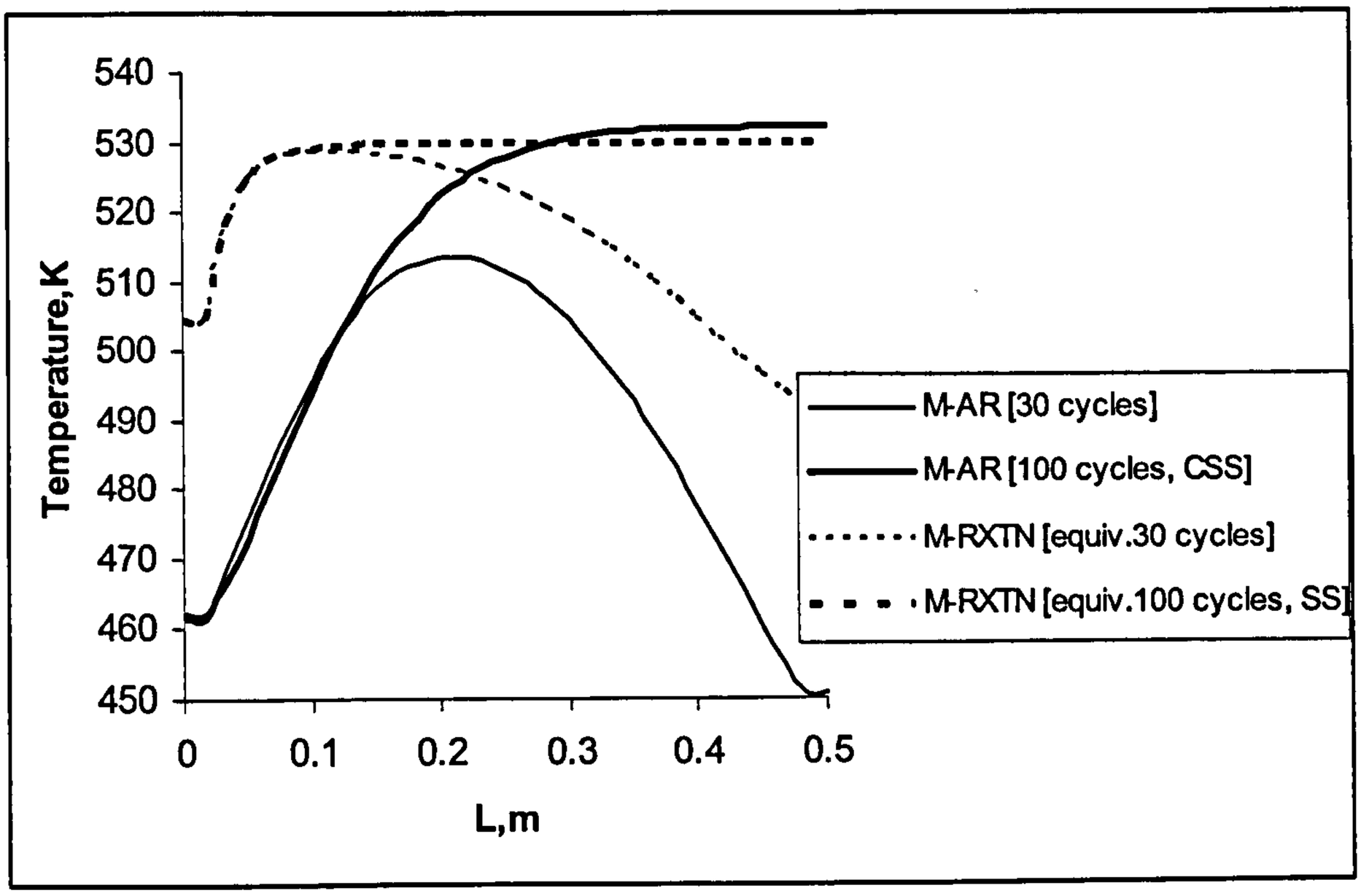

Fig. 4.37: Axial temperature profiles of the M-$_{AR}$ and M-$_{RXTN}$ at 40 vol. % ethene (c.f. M-$_{RXTN}$ 2.09 vol. %)

Operating at t_a = 5 s leads to stable operation for the M-AR. The lower feed concentration in the M-RXTN also leads to stable operation but with temperatures in the M-RXTN still higher than in the M-AR. 100 % conversion is achieved in the M-RXTN, with conversion in the M-AR at 99.9%. The effect of a longer adsorption step time on reactor thermal stability is also investigated for t_a = 50 s and detailed below:

(ii) Concentration effects (adsorption step- time = 50 s)

The effect of feed inlet concentrations for feed temperature operation at T_{fa} = 293 K and T_{fr} = 460 K is taken as a case study. In this case, the reaction temperature, T_r for the M-RXTN is also set to T_{fr}. The reactor is operated with $u_a = u_d = 0.01$ m s^{-1} and t_a = 50 s, t_d = 150 s.

Table (4.25) lists the feed concentrations explored for ethene within the operating conditions specified and the corresponding feed concentrations for the monolith reactor. Thus the number of moles of ethene fed in during the adsorption step (which is also dependent on the step time for adsorption, t_a) at temperature T_{fa} in the M-AR is first calculated and on the basis of identical volumetric feed rates in both reactors, the number of moles of ethene required for feeding into the M-RXTN can therefore be back-calculated. This gives the required feed inlet concentration in the M-RXTN. See Appendix E for more details.

M-AR (Vol. %)	M-RXTN (Vol. %)
5	2.6
20	10.5
40	21

Table 4.25: Feed concentrations for the M-AR and similarly operated M-RXTN; T_{fa} = 293 K, T_{fr} = 460 K

The effect of utilising longer adsorption step times on reactor stability is illustrated in Figs. (4.38) – (4.40). Three ethene feed concentrations, 5 vol. %, 20 vol. % and 40 vol. % in the M-AR are studied. The M-AR becomes unstable with increasing feed concentration; at 5 vol. % cyclic steady state is attained but this in not achieved at 20 vol.% and 40 vol. % where instability (thermal runaway) occurs. In the M-RXTN, the increase in step time increases the concentration of ethene fed into the reactor and as such thermal runaway occurs at 10.5 vol % (i.e. 20 vol. % in the M-AR) and 21 vol % (i.e. 40 vol. % in the M-AR). Therefore, longer step times,

fully utilising the adsorption bed results in unstable reactor operation with changes in the feed concentration.

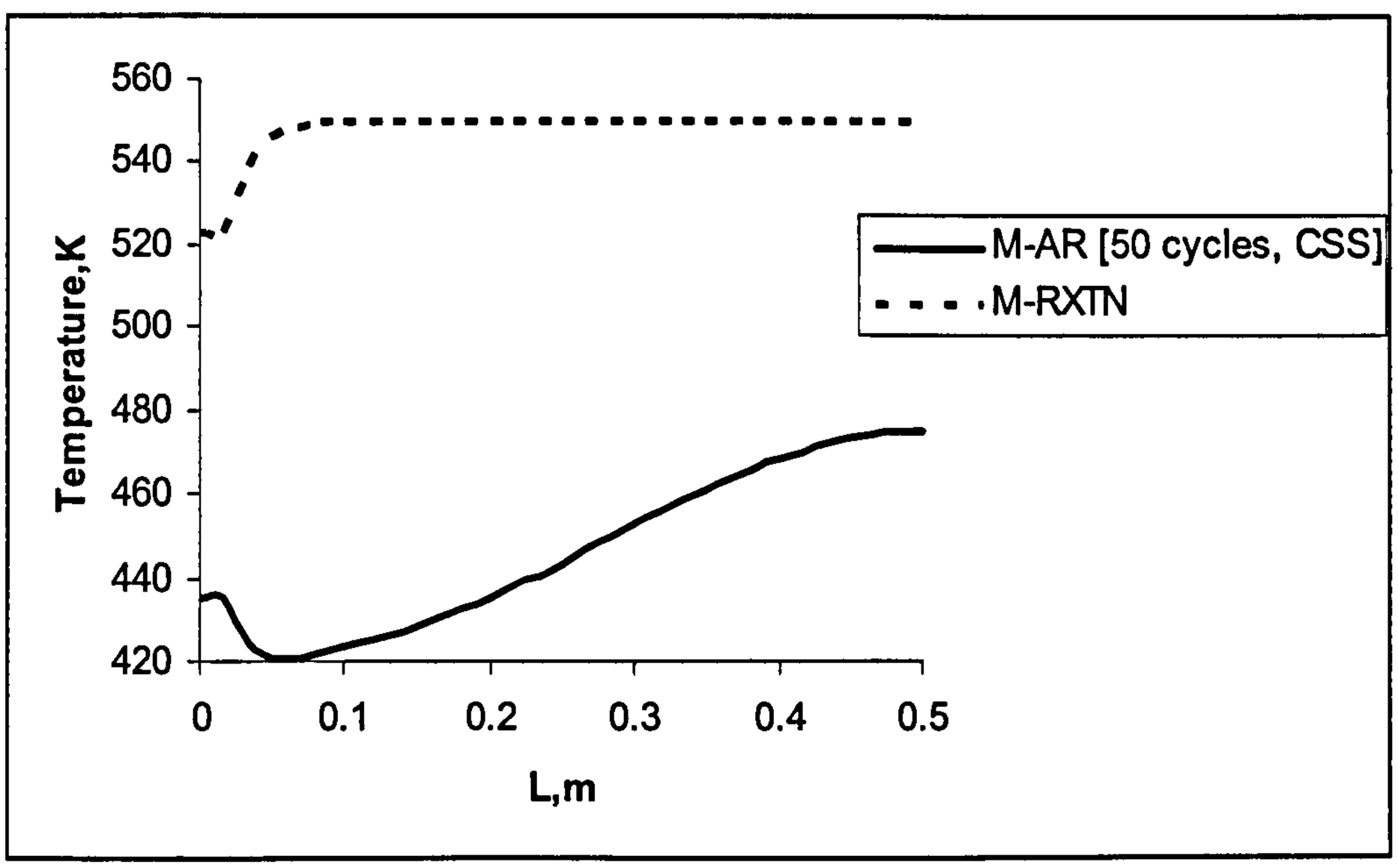

Fig. 4.38: Steady state axial temperature profiles of the $M\text{-}_{AR}$ and $M\text{-}_{RXTN}$ at 5 vol. % ethene (c.f. $M\text{-}_{RXTN}$ 2.6 vol. %)

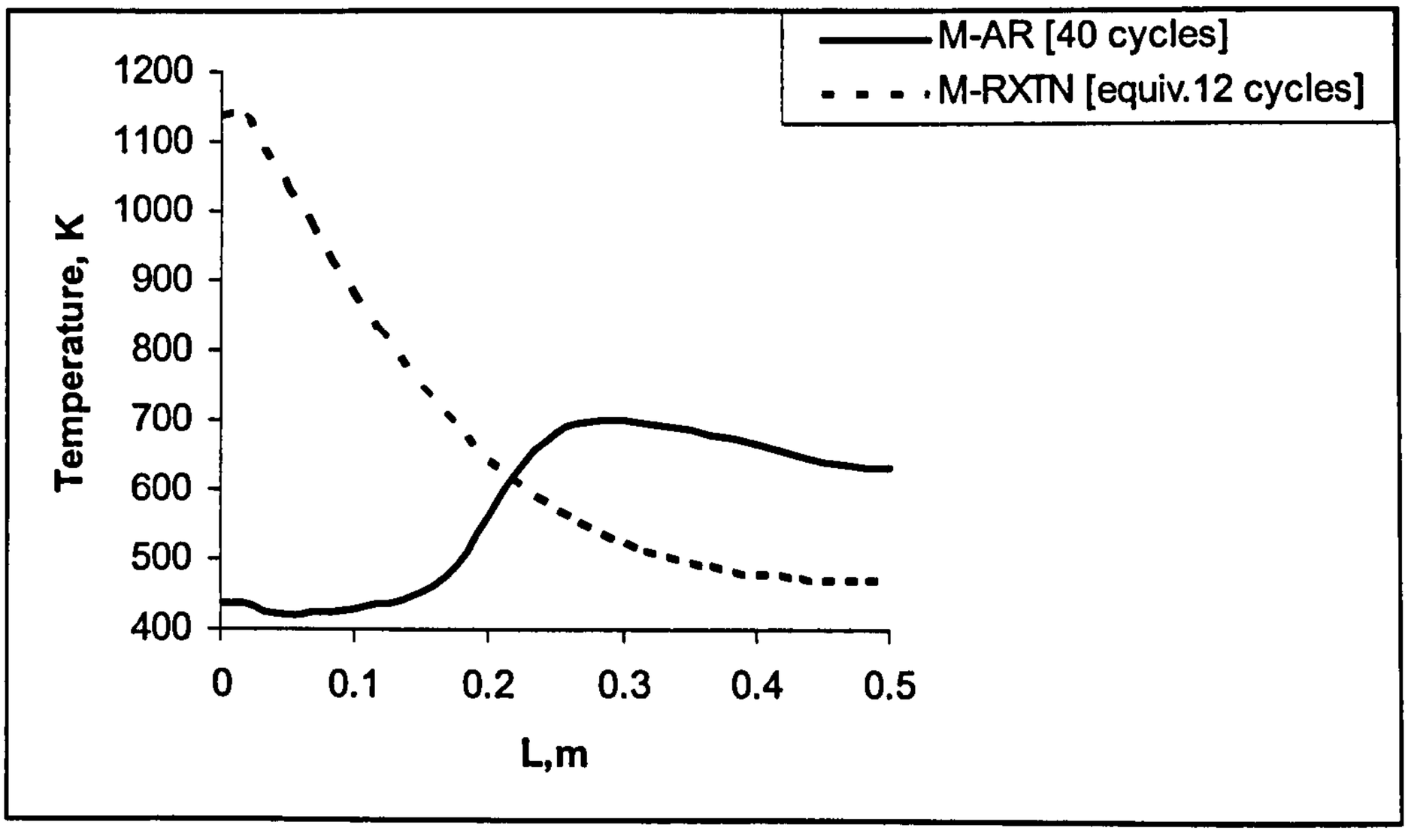

Fig. 4.39: Axial temperature profiles of the $M\text{-}_{AR}$ and $M\text{-}_{RXTN}$ at 20 vol. % ethene (c.f. $M\text{-}_{RXTN}$ 10.5 vol. %)

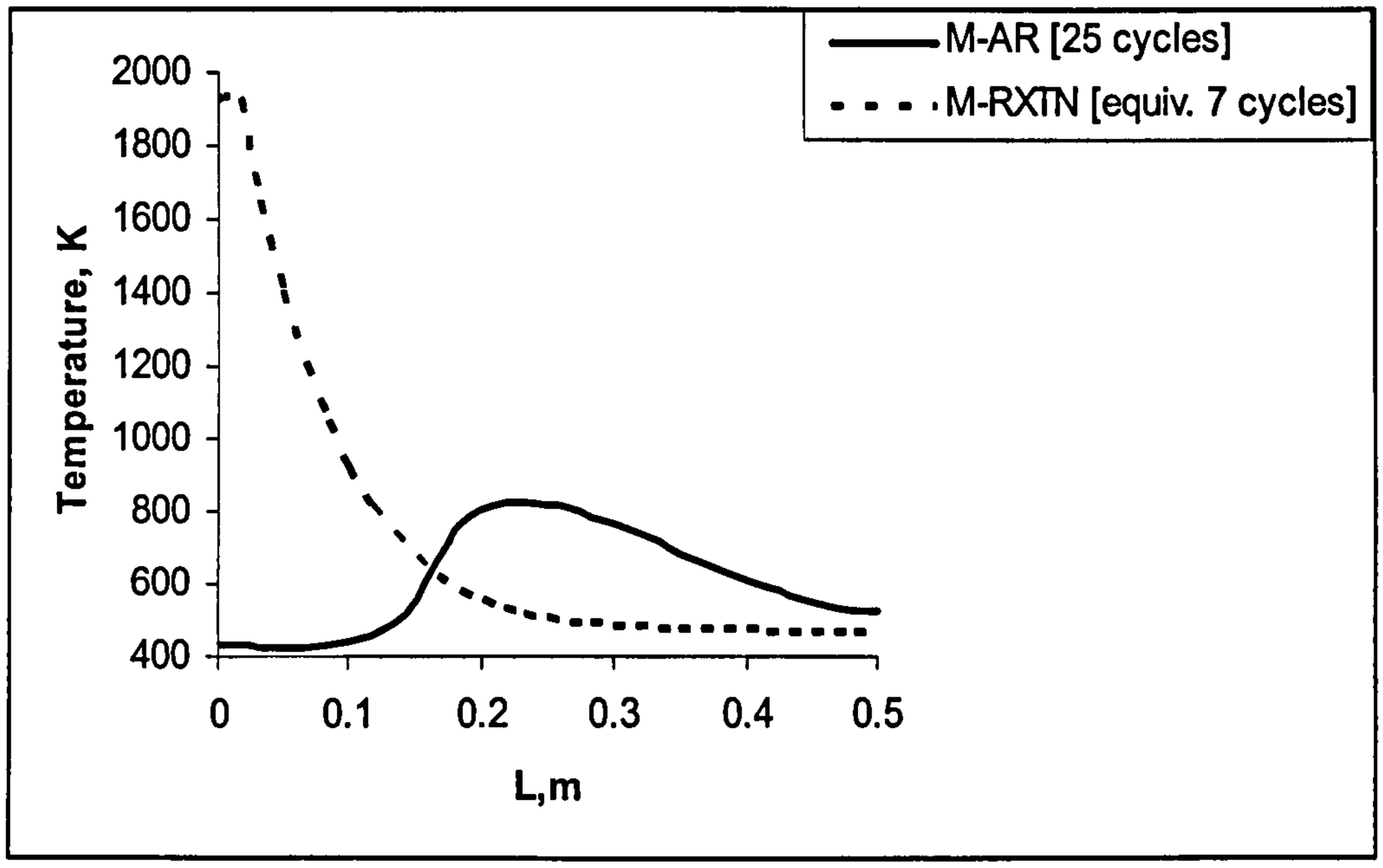

Fig. 4.40: Axial temperature profiles of the M-$_{AR}$ and M-$_{RXTN}$ at 40 vol. % ethene (c.f. M-$_{RXTN}$ 21 vol. %)

(iii) Temperature effects

Temperature operation at T_{fa} = 338 K and T_{fr} = 460 K for different ethene feed concentrations in the M-$_{AR}$ is also assessed and the results shown in Figs. (4.41) and (4.42). The reactor is operated with inlet velocities $u_a = u_d$ = 0.01 m s^{-1} and t_a = 50 s, t_d = 150 s. In all cases the conversion achieved exceeds 99.8 %.

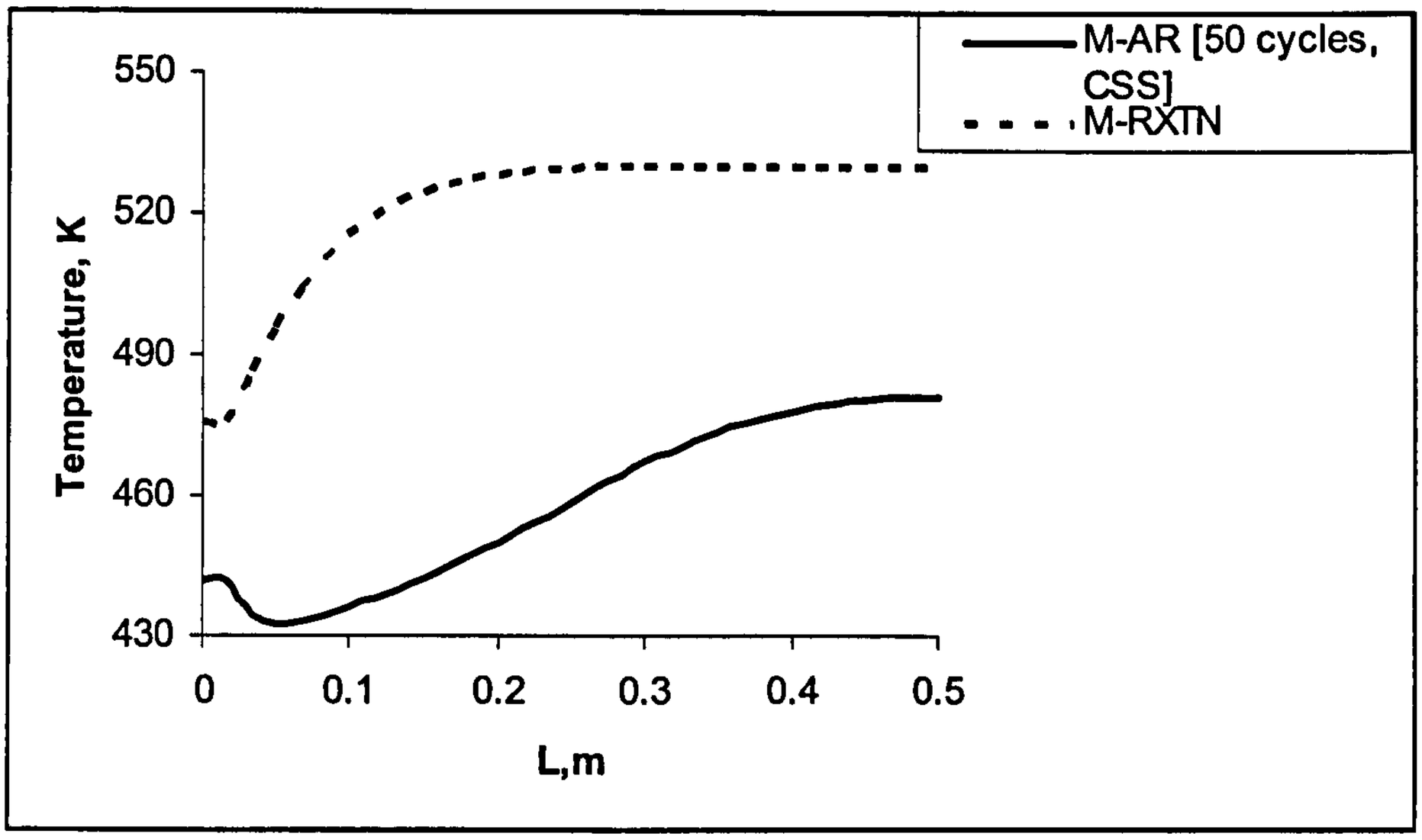

Fig. 4.41: Steady state axial temperature profiles of the M-$_{AR}$ and M-$_{RXTN}$ at 20 vol. % ethene (c.f. M-$_{RXTN}$ 8.9 vol. %)

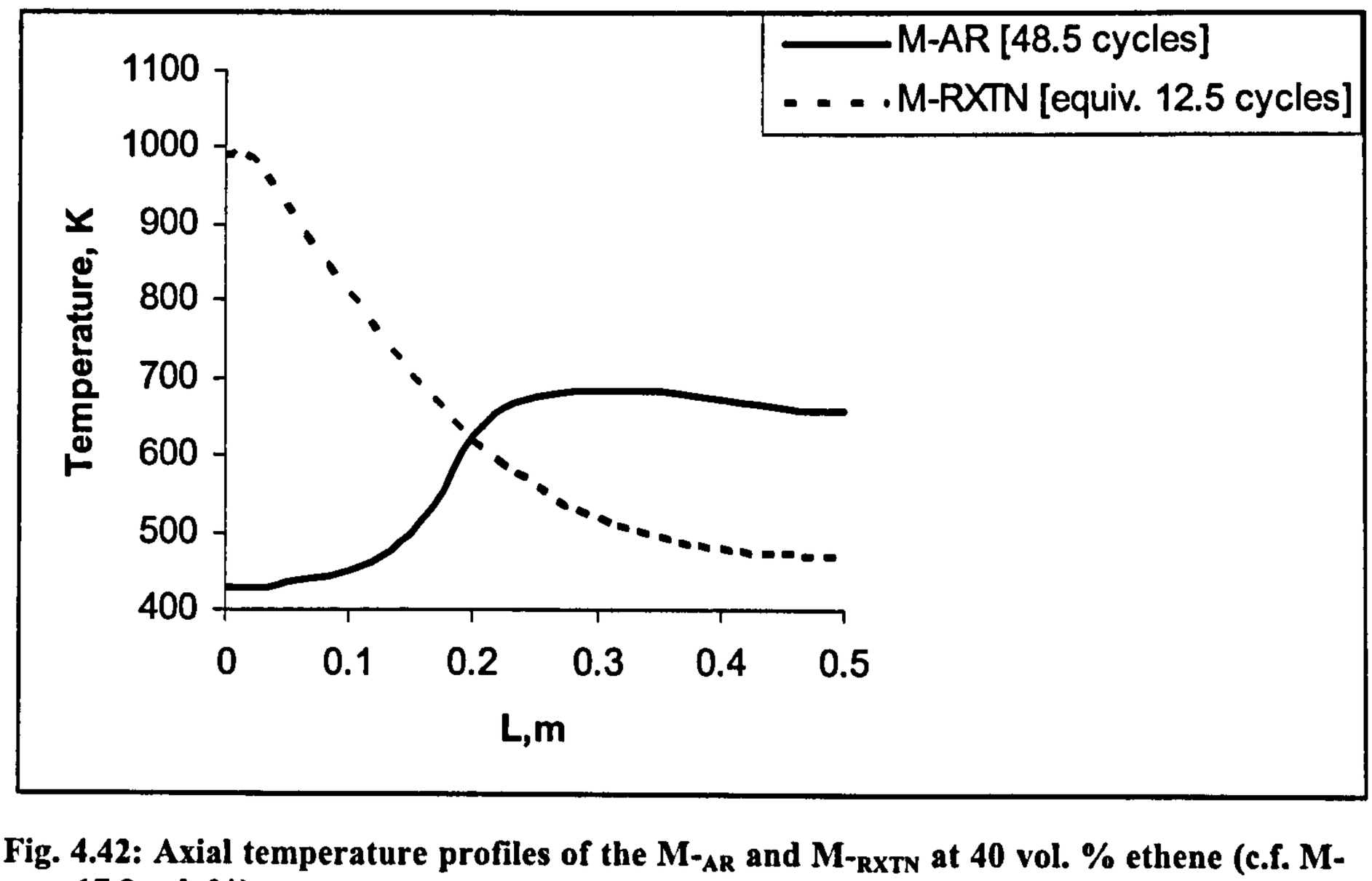

Fig. 4.42: Axial temperature profiles of the M-$_{AR}$ and M-$_{RXTN}$ at 40 vol. % ethene (c.f. M-$_{RXTN}$ 17.8 vol. %)

4.5.3 Summary of Thermal Stability Investigations

The hybrid monolith reactor, M-AR is thermally more stable than the monolith reactor M-RXTN. For the range of operating conditions studied, reactor runaway and explosion occurs in the monolith at ethene concentrations above 5 vol. % while in the M-AR this occurs at ethene concentrations above 20 vol. % for identical feed temperature operation, and above 40 vol. % for temperature swing operation. The LEL and UEL for ethene were found to be 2.7 vol % and 36 vol%. For practical purposes reactor operation under these conditions would never occur but in order to illustrate the thermal stability point concentrations (especially for the M-AR) within these limits are utilised. For a Pd/ Al_2O_3 catalyst, sintering occurs at ~ 800 K. A major consequence of runaway is reactor explosion which is very dangerous from a safety point of view.

Note that the concentrations in the M-RXTN were adjusted to account for the fact that adsorption takes place first in the M-AR, operating under regions of incomplete saturation. Therefore, concentrations in the M-RXTN were much lower than in the M-AR and at these very low concentrations, the M-AR temperature was lower than that of the M-RXTN for all cases studied i.e. $T_{fa} = T_{fr}$ operation, and $T_{fa} \neq T_{fr}$ operation.

For M-AR operation, reactor stability was greater with a temperature swing effect than at same temperature operation. Nevertheless, for all concentrations in the M-AR, the reactor was thermally more stable due to the staged and controlled release of reactants as opposed to the

explosive mix of reactants being continuously fed. The key point here is that the heat / energy used for desorption is not wasted but is used to preheat the bed for the reaction step in the cycle, providing the heat to drive the endothermic reaction as is reflected in the energy input rates. Under same temperature operation, the reactor is already hot and any further heat drives desorption but the extra heat from the exothermic reaction cause the temperature excursion.

4.6. Further Discussions

The simulation of adsorption and reaction within the monolith reactor has provided insight into the propagation of mass and thermal waves. Key process parameters included feed inlet temperatures, inlet velocities, reactor geometrical configurations (length and radial thickness). These parameters had an effect on the performance of the individual steps in terms of key performance indices which included inert gas purity, energy input and conversion.

Due to the need for adsorbent regeneration, the M-AR was operated under a periodic mode and this mode of operation provided further challenges due to the complex interaction between the adsorption and reaction step. The performance of the M-AR is affected by a number of design and operating parameters as illustrated through the parametric studies performed. Step times for adsorption and desorption, feed temperatures, inlet velocities, and reactor geometry (length and radial

thickness) play an integral part in the overall performance of the M-AR. In the operation of the M-AR, the performance of the regeneration step was dependent on the crucial first step of adsorption and as such both steps are interconnected. The efficiency and effectiveness of desorption depended on how much adsorbate was adsorbed in the first place. Desorption occurred by means of thermal and concentration swing and the length and duration of this step was a factor in terms of heating times or the number of cycles needed to achieve steady state.

Operating under conditions of incomplete bed saturation was deemed more favourable as the performance of the reactor under these conditions far exceeded reactor performance under conditions of complete saturation. One explanation for this is the fact that under complete saturation, there is not enough time for reaction for molecules adsorbed nearer the exit of the bed. Working under incomplete saturation implied that shorter bed lengths (near the reactor entrance) were utilised and as such better reactor performance attained.

Working with a temperature swing rather than with the same feed temperature for both the adsorption and desorption steps gave better reactor performance in terms of energy requirements, and more importantly reactor thermal stability. Under temperature swing operation, the same conversion could be achieved as with same temperature operation, and at lower energy input requirements and reactor stability.

The operating conditions and process parameters were chosen from the favourable results of conversion and energy observed from the various parametric studies previously performed on the M-AR (see Table (4.19)).This was achieved using very low velocities and operating at very short adsorption step times.

The next chapter presents an optimisation strategy for the M-AR in order to determine the optimal values of important design and operating parameters as identified by the parametric studies performed. Scaling rules are also derived for M-AR operation and their application demonstrated.

CHAPTER 5 Process Optimisation and Scaling Rules

5.1 Introduction

In the previous chapter, parametric studies were performed on the hybrid monolith reactor, M-AR. These provided theoretical insights into adsorptive reactor operation, with reactor performance dependent on a number of design and operating parameters. As mentioned previously, step times for adsorption and desorption, feed temperatures, inlet velocities and reactor geometry play an important part in process performance. Optimum values of these important design and operating parameters would therefore be useful in attaining optimum process performance. In this chapter, an optimisation strategy for the M-AR is outlined and presented in Section 5.2.

Section 5.3 discusses the utilisation of scaling rules as a mathematical tool for transforming a process that already has a basic satisfactory performance to another system that meets new and / or additional system specifications (and / or constraints) without the need for further simulation. The M-AR can therefore be scaled to the demands of industrial production while basic process performance such as conversion, is maintained. A new optimal solution can also be reached driven of course by new sets of constraints such as a new production rate or new bounds for inlet velocities. This new optimal solution which depends on the nature of the new set of constraints may be different to

the operating policy obtained from scaling rules. Thus, scaling rules can provide an initial guess for the new optimisation problem.

In this chapter, scaling rules are derived for the M-AR operation and their application demonstrated through the scaling of production rate and maintaining process performance when step times are changed. Results from the parametric studies performed in Chapter 4 indicated that step times for adsorption and reaction had an impact on the conversion and energy performance of the reactor and illustrate the importance of adjusting step times in overall reactor design for e.g. altering step durations for the effective scheduling of multi-bed systems.

5.2 Optimisation Strategy

5.2.1 Introduction

As shown in Chapter 4, the performance of the M-AR is affected by a number of design and operating parameters. The goal, therefore of process optimisation is to select the values of a set of decision variables that yield the best value of a given performance criterion whilst satisfying all other constraints (Nilchan, 1997). Traditionally this has been achieved by repeated dynamic simulations, each corresponding to a different combination of decision variable values. However, since periodic adsorptive reactor processes are intrinsically complex and involve many interacting decision variables and constraints, obtaining an optimal solution by repeated simulations is often inconvenient and

time consuming. The applications of formal optimisation techniques have therefore been developed to help solve this problem.

From the M-AR model presented in Chapter 3, optimisation is performed by gOPT (Process Systems Enterprise Ltd.), an optimisation tool based on the successive reduced quadratic programming method (Macchietto and Chen, 1989) and converts the optimisation problem to a non linear programming (NLP) problem. The solution tolerance for the optimisation is 0.001. In other words, convergence is deemed to occur when a linear combination of the gradients of the Lagrangian function and violation of the constraints drops below this tolerance.

5.2.2 Problem Formulation

The optimisation approach seeks to determine the optimal values of important design and operating parameters as identified by the parametric studies presented in Chapter 4. Optimisation is performed for reactor operation under conditions of partial bed saturation with optimisation of both single-step operation (in the first instance) and cyclic operation carried out. Single-step optimisation is performed initially to give insight into optimum process performance within a less complex mode of operation. It is the goal of the process optimisation to determine the optimum values of the design and operating parameters that will enhance reactor performance.

The set of optimisation decision variables may include the following model parameters:

- The reactor length, L;
- Core channel radius, R_1;
- Total reactor radius, R_2;
- Inlet velocities for adsorption and desorption, u_a and u_d;
- Step times for adsorption and desorption/reaction, t_a and t_r;
- Feed temperatures, T_{fa} and T_{fr};

The general form of the mathematical non-linear programming problem considered in this work takes the general form:

Minimise **Performance objective** (5.1)

subject to

Decision variables

$$\Omega^{min} \leq \Omega \leq \Omega^{max} \quad (5.2)$$

Performance indices

$$\prod \geq \text{set point} \quad (5.3)$$

In the first instance, a single performance objective is optimised. The performance objective is typically a performance measure for the reactor and process at hand. The optimisation objective was to minimise the rate of energy input required whilst maintaining a high conversion performance (≥ 95 %). With reference to the optimisation formulation given in Eq. (5.2), the upper and lower bounds for the decision variables are listed in Table (5.1). These bounds were chosen to depict real-life applications as collated from published data with the bounds of

temperature constrained to the ranges suitable for both adsorption and temperature (see Zhu *et al.*, 2005, Van de Beld *et al.*, 1995).

Variable	Lower - bound	Upper – bound	Units
L	0.05	1	m
R_1	0.0008	0.01	m
R_2	0.0010	0.01	m
u_a	0.01	1	m s^{-1}
u_d	0.01	1	m s^{-1}
t_a	0	150	s
t_d	150	2000	s
T_{fa}	293	500	K
T_{fr}	460	500	K

Table 5.1: Bounds for decision variables in the optimisation of the M-AR

5.2.3 Optimisation Results and Discussion

Optimisation is performed in all cases (single-step and cyclic operation) for reactor operation under conditions of partial bed saturation as illustrated in Fig. (5.1). At an adsorption step time t_a, of 150 s the bed is fully saturated whilst at shorter step times i.e. 70 s, 30 s the bed is only partially saturated with adsorbent.

- **Single-step operation**

Optimisation is performed for the case where $T_r = T_{fr} = 460$ K with $t_a = 70$ s and $t_a = 10$ s.

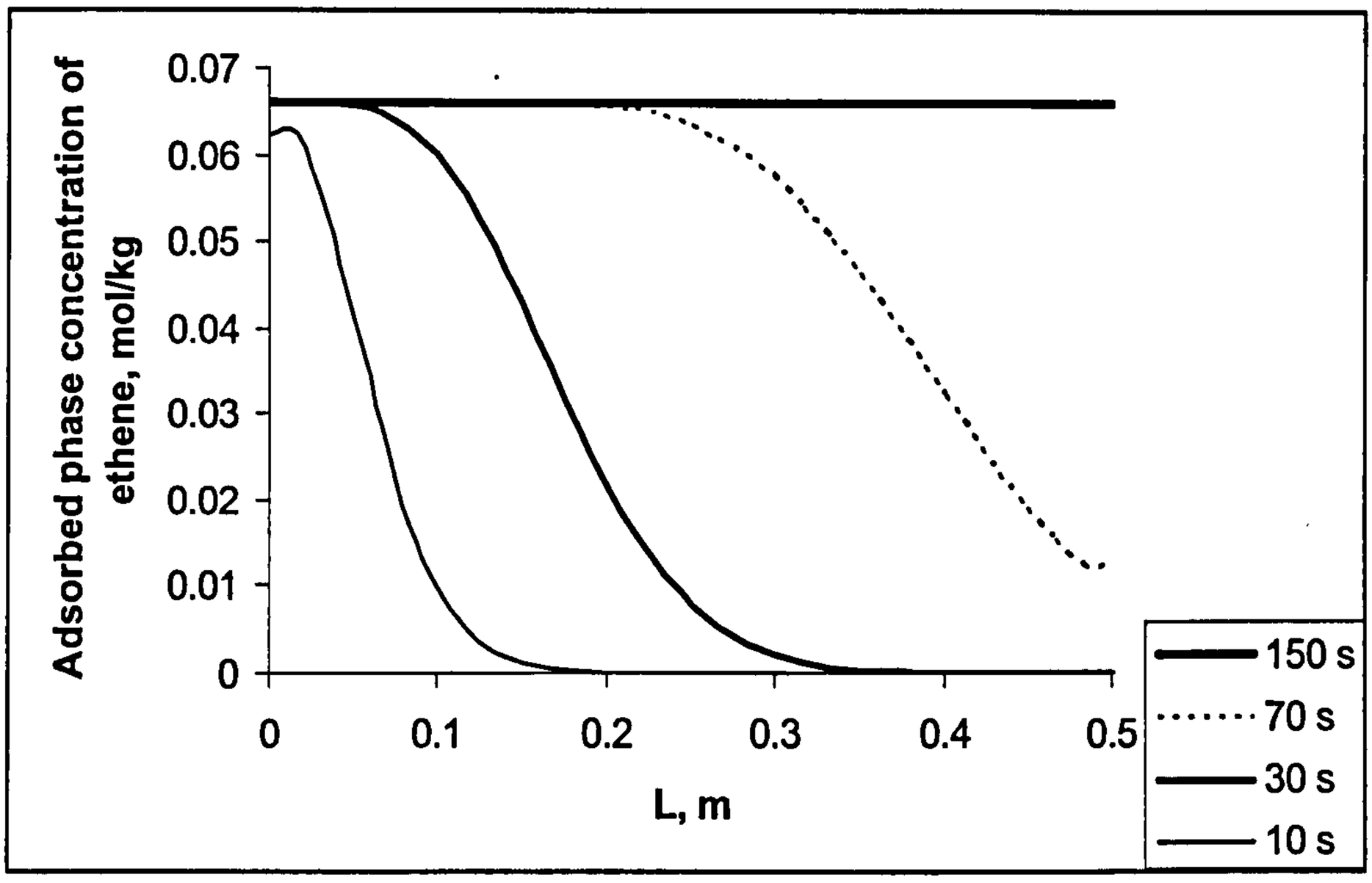

Fig. 5.1: Adsorbed amount of ethene at different t_a along reactor bed length

a. t_a = 70 s

The optimal operating policy of the M-AR is given below in Table (5.2). Base case parameter results are also shown as well as the numerical verification of the optimisation via dynamic simulation.

For the above optimisation, the total CPU time was 24 s, 2 NLP iterations and 2 line search steps were required.

Operating Policy	Optimal Values	Base case	Units
L	0.05	0.5	m
R_1	0.0008	0.0012	m
R_2	0.0010	0.0015	m
u_a	0.01	0.05	m s^{-1}
u_d	0.01	0.05	m s^{-1}
Performance Indices			
E	4.8 (4.8)	21.2	kJ m^{-2} s^{-1}
X	100 (99.7)	25	%

Table 5.2: Optimisation results, verification and base case comparisons for M-AR operation – (t_a = 70s)
Note: Numerical verification shown in brackets

b. t_a = 10 s

The optimal operating policy of the M-AR is given below in Table (5.3). Base case parameter results are also shown as well as the numerical verification of the optimisation via dynamic simulation.

Operating Policy	Optimal Values	Base case	Units
L	0.05	0.5	m
R_1	0.0008	0.0012	m
R_2	0.0010	0.0015	m
u_a	0.01	0.05	m s^{-1}
u_d	0.01	0.05	m s^{-1}
Performance Indices			
E	4.8 (4.8)	21.2	kJ m^{-2} s^{-1}
X	100 (99.9)	98	%

Table 5.3: Optimisation results, verification and base case comparisons for M-AR operation - (t_s = 10 s)
Note: Numerical verification shown in brackets

For the above optimisation, the total CPU time was 7 s, 2 NLP iterations and 2 line search steps were required.

- **Cyclic operation**

Optimisation is also performed for the case where $T_r = T_{fr}$ = 460 K under conditions of t_s = 70 s and t_s = 10 s (see Fig. (5.1)).

a. t_s = 70 s

The optimal operating policy of the M-AR is given below in Table (5.4). Base case parameter results are also shown as well as the numerical verification of the optimisation via dynamic simulation.

Operating Policy	Optimal Values	Base case	Units
L	0.05	0.5	m
R_1	0.0008	0.0012	m
R_2	0.0010	0.0015	m
u_a	0.01	0.05	m s^{-1}
u_d	0.01	0.05	m s^{-1}
t_a	150	70	s
t_d	375	150	s
Performance Indices			
E	4.2 (4.2)	21.2	kJ m^{-2} s^{-1}
X	100 (99.8)	30	%

Table 5.4: Optimisation results, verification and base case comparisons for M-AR operation - (t_a = 70 s)
Note: Numerical verification shown in brackets

For the above optimisation, the total CPU time was 34 s, 2 NLP iterations and 2 line search steps were required.

b. t_a = 10 s

The optimal operating policy of the M-AR is given below in Table (5.5). Base case parameter results are also shown as well as the numerical verification of the optimisation via dynamic simulation.

Operating Policy	Optimal Values	Base case	Units
L	0.05	0.5	m
R_1	0.0008	0.0012	m
R_2	0.0010	0.0015	m
u_a	0.01	0.05	m s^{-1}
u_d	0.01	0.05	m s^{-1}
t_a	150	10	s
t_d	170	150	s
Performance Indices			
E	4.2 (4.2)	21.2	kJ m^{-2} s^{-1}
X	100(99.9)	99	%

Table 5.5: Optimisation results, verification and base case comparisons for M-AR operation - (t_a = 10 s)

Note: Numerical verification shown in brackets

For the above optimisation, the total CPU time was 22 s, 2 NLP iterations and 2 line search steps were required.

The bounds for the decision variables in the optimisation of the M-AR were chosen to reflect typical adsorptive-reactor applications. It was observed that optimisation performance was limited by these bounds. Since the objective is to minimise the rate of energy input whilst maintaining a high conversion the optimisation search within this constraint naturally tends towards the lower bounds of the inlet velocity for all cases in order to achieve this i.e. longer space time for both adsorption and regeneration steps. The optimisation process was also performed under conditions of partial bed saturation. In cyclic operation, results tended towards the upper bounds regarding the step

times of adsorption. Optimisation results indicate that inlet velocity and step times play an important role in reactor performance.

5.3 Scaling Rules

5.3.1 Overview

In deriving the scaling rules for the M-AR operation, the system variables are first normalised. These are then substituted into the underlying model equations to form normalised equations containing terms with dimensionless variables and dimensional groups. The normalised variable profiles are then preserved by fixing the dimensional groups of the new (scaled) system as identical to those of the base system. Thus, a set of system constraints involving variables that can be scaled, such as step durations and feed velocities can be derived. When scaling is performed according to these rules, dimensionless performance indices (e.g. conversion) are unchanged, while the dimensional ones are modified (e.g. productivity, energy input rate) as they are functions of the scalable variables. This gives scope in improving upon dimensional performance variable and thus scope for process intensification. The derivation of scaling rules for the M-AR is detailed in Section 5.3.2.

5.3.2 Model Normalisation

The dimensionless temporal, axial and radial co-ordinates are defined as:

$$\Omega = \frac{t}{t_0}, \qquad Z^* = \frac{z}{z_0}, \qquad R^* = \frac{r}{r_0} \tag{5.4}$$

where subscript 0 denotes a reference parameter.

Dimensionless dependent variables are defined as:

$$C_i^* = \frac{c_i}{c_0}, \qquad T^* = \frac{T}{T_0}, \qquad V^* = \frac{v}{v_0} \tag{5.5}$$

Dimensionless variables for the rates of reaction and adsorption are also introduced and defined as:

$$\tilde{r} = \frac{r_r}{r_\infty}, \quad Q_i = \frac{q_i}{q_0} \tag{5.6}$$

where subscript 0 and ∞ denotes a reference parameter.

<u>General material and energy balances</u>

Substitution of the above dimensionless variables into the material balances (Eqs. (3.22), (3.23)), the energy balance (Eqs. (3.25), (3.26)), the reaction rate (Model I, seeTable (3.3)) and the adsorption rate (Eq. (3.4))

is detailed below where ∏ denotes a dimensionless group resulting from the normalisation (see below also for definitions).

Material balance

Normalised core channel:

$$\frac{\partial(y_i/T^*)}{\partial\Omega} = -\Pi_m^{(a)}\frac{\partial(y_i/T^*)V^*}{\partial Z^*} + \Pi_m^{(b)}\frac{\partial^2(y_i/T^*)}{\partial R^{*2}} + \Pi_m^{(b)}\frac{1}{R^*}\frac{\partial(y_i/T^*)}{\partial R^*} \tag{5.7}$$

Normalised solid zone:

$$\Pi_m^{(c)}\frac{\partial(y_i/T^*)}{\partial\Omega} + \frac{\partial Q_i}{\partial\Omega} = \Pi_m^{(d)}\frac{\partial^2(y_i/T^*)}{\partial Z^{*2}} + \Pi_m^{(e)}\frac{1}{R^*}\frac{\partial(y_i/T^*)}{\partial R^*} + \Pi_m^{(e)}\frac{\partial^2(y_i/T^*)}{\partial R^{*2}} + \Pi_m^{(f)}\tilde{r} \tag{5.8}$$

Energy balance

Normalised core channel:

$$\frac{1}{T^*}\frac{\partial T^*}{\partial\Omega} = -\Pi_e^{(a)}\frac{V^*}{T^*}\frac{\partial T^*}{\partial Z^*} + \Pi_e^{(b)}\frac{\partial^2 T^*}{\partial R^{*2}} + \Pi_e^{(b)}\frac{1}{R^*}\frac{\partial T^*}{\partial R^*} \tag{5.9}$$

Normalised solid zone:

$$\left(\frac{\Pi_e^{(c)}}{T^*} + 1\right)\frac{\partial T^*}{\partial\Omega} = -\Pi_e^{(d)}\tilde{r} - \Pi_e^{(e)}\frac{\partial Q_i}{\partial\Omega} + \Pi_e^{(f)}\frac{\partial^2 T^*}{\partial Z^{*2}} + \Pi_e^{(g)}\frac{\partial^2 T^*}{\partial R^{*2}} + \Pi_e^{(g)}\frac{1}{R^*}\frac{\partial T^*}{\partial R^*} \tag{5.10}$$

Reaction rate

$$\tilde{r} = \prod_r y_i\, e^{-1/T^*} \tag{5.11}$$

Rate of adsorption

$$\frac{\partial Q_i}{\partial \Omega} = \prod_a \left(Q_i^* - Q_i\right) \tag{5.12}$$

where $Q_i^* = \dfrac{m_i P y_i}{q_0}$

Boundary conditions

The boundary conditions for the feeding step (Eqs. (3.32 – 3.35)) are also normalised.

Gas phase

$$\text{At } Z^* = 0 \quad C_i^* = C_i^{*f} \quad T^* = T^{*f} \tag{5.13}$$

Channel centre $R^* = 0$

$$\prod_b^{(a)} \frac{\partial C_i^*}{\partial R^*} = 0, \qquad \prod_b^{(b)} \frac{\partial T^*}{\partial R^*} = 0 \tag{5.14}$$

Reactor exit

$$\text{At } Z^* = 1$$

$$\prod_b^{(c)} \frac{\partial C_i^*}{\partial Z^*} = 0, \qquad \prod_b^{(d)} \frac{\partial T^*}{\partial Z^*} = 0 \tag{5.15}$$

Solid phase

$$R^* = \theta \quad (\text{i.e. } r = R_1)$$

$$\prod_b^{(e)} \frac{\partial C_i^*}{\partial R^*} = \frac{\partial C_i^*}{\partial R^*} \qquad \prod_b^{(f)} \frac{\partial T^*}{\partial R^*} = \frac{\partial T^*}{\partial R^*} \tag{5.16}$$

Ends of solid zone

$$Z^* = 0\,, \quad Z^* = 1$$

$$\Pi_{bs}^{(c)} \frac{\partial C_i^*}{\partial Z^*} = 0, \qquad \Pi_{bs}^{(d)} \frac{\partial T^*}{\partial Z^*} = 0 \tag{5.17}$$

$$R^* = 1$$

$$\Pi_{bs}^{(a)} \frac{\partial C_i^*}{\partial R^*} = 0, \qquad \Pi_{bs}^{(b)} \frac{\partial T^*}{\partial R^*} = 0 \tag{5.18}$$

Velocity profile

$$V^* = V_f^* \tag{5.19}$$

The subscript *f* denotes the inlet conditions during the feeding step. For the regeneration step, these analogous equations are written with the inlet conditions denoted by the subscript *r*.

Dimensionless groups

The dimensionless groups that appear in the normalised equations above are now listed in Table (5.6).

Material balance	*Energy balance*
$\Pi_m^{(a)}=\frac{v_0 t_0}{z_0}$ $\Pi_m^{(b)}=\frac{D_m t_0}{r_0^2}$	$\Pi_e^{(a)}=\frac{v_0 t_0}{z_0}$ $\Pi_e^{(b)}=\frac{\lambda_s T_0 t_0 R}{P C_{pg} r_0^2}$
$\Pi_m^{(c)}=\frac{\varepsilon P}{R T_0 \rho_b q_0}$ $\Pi_m^{(d)}=\frac{D_e P t_0}{R T_0 z_0^2 \rho_b q_0}$	$\Pi_e^{(c)}=\frac{\varepsilon P C_{pg}}{R \rho_b C_{ps} T_0}$ $\Pi_e^{(d)}=\frac{\Delta H_r r_\infty t_0}{C_{ps} T_0}$
$\Pi_m^{(e)}=\frac{D_e P t_0}{R T_0 r_0^2 \rho_b q_0}$ $\Pi_m^{(f)}=\frac{v_i r_\infty t_0}{q_0}$	$\Pi_e^{(e)}=\frac{q_0 \Delta H_{ai}}{C_{ps} T_0}$
	$\Pi_e^{(f)}=\frac{\lambda t_0}{\rho_b C_{ps} z_0^2}$ $\Pi_e^{(g)}=\frac{\lambda t_0}{\rho_b C_{ps} r_0^2}$
Adsorption	***Rate***
$\Pi_a=k_i t_0$	$\Pi_r=\frac{P k_{1,\infty} e^{-E_{act}/RT_0}}{r_\infty t_0}$
Boundary conditions	
$\Pi_b^{(a)}=\Pi_{bs}^{(a)}=\frac{c_0}{r_0}$ $\Pi_b^{(b)}=\Pi_{bs}^{(b)}=\frac{T_0}{r_0}$	$\Pi_b^{(c)}=\Pi_{bs}^{(c)}=\frac{c_0}{z_0}$
	$\Pi_b^{(d)}=\Pi_{bs}^{(d)}=\frac{T_0}{z_0}$
$\Pi_b^{(e)}=\frac{D_e}{D_m}$ $\Pi_b^{(f)}=\frac{\lambda_s}{\lambda_g}$	

Table 5.6: Dimensionless groups

Reference variables

The reference spatial and radial coordinate is set to be equal to the bed length and radii respectively i.e. $z_o = L$ so that $Z^* \in (0,1)$ and $r_o = R$ so that $R^* \in (0,1)$. A distinction is made between the normalised temporal domain of the feeding step (Ω_f) and that of the regeneration step (Ω_r).

The reference step time, t_o, is equated to t_f for the feeding step and t_r for the regeneration step, such that

Feeding : $\Omega = \Omega_f \in (0,1); \quad t_o = t_f$

Regeneration : $\Omega = \Omega_r \in (0,1); \quad t_o = t_r$

$$S(Z^*, R^*, \Omega_f = 0) = S(Z^*, R^*, \Omega_r = 1) \quad \forall\ Z^*, R^* \in (0,1) \tag{5.20}$$

Where S denotes all state variables in the system. Normalisation in this way enables the step durations t_f and t_r to be scaled separately and independently of total cycle time.

Other reference variables are equated to the feed conditions, i.e.

Feeding : $c_o = c_{if}, \quad v_o = v_f$

$T_o = T_f$

Regeneration : $c_o = c_{ir}, \quad v_o = v_r$

$T_o = T_r$ (5.21)

5.3.3 Performance Criteria

The performance criteria as defined in Section 3.5.1 can be written in terms of dimensionless variable.

Definitions

Energy Input rate, E

$$E = \frac{c_{pg}}{t_f + t_r}\left\{\left(\frac{v_f Pt_f}{R}\right)\frac{V_f^*(T_f^* - T_a^*)}{T_f^*} + \left(\frac{v_r Pt_r}{R}\right)\frac{V_r^*(T_r^* - T_a^*)}{T_r^*}\right\} \tag{5.22}$$

where $T_a^* = \frac{T_a}{T_0}$, T_a is the ambient temperature.

Conversion, X

$$X = 1 - \frac{\left(\frac{v_r T_f}{T_r v_f}\right)\int_0^1 \frac{y_i(1)V^*(1)}{T^*(1)}\partial\Omega_r}{\int_0^1 \frac{y_i(1)V^*(1)}{T^*(1)}\partial\Omega_f} \tag{5.23}$$

Productivity, P_R

$$P_R = \frac{\left(\frac{Pt_f v_f}{RT_f}\right)\frac{y_i V^*}{T^*}X}{\rho\pi r^2 L} \tag{5.24}$$

The above performance criteria depicted in Eqs. (5.22 – 5.24) can be categorised as, dimensionless i.e. X, and dimensional, i.e. E, P_R

5.3.4 Operator Ratios

Let us assume the existence of a base system with satisfactory (basic) performance which is to be transformed into a new (scaled) system. The two systems can be compared through the use of the operator ration, R (Rota *et al.*, 1990), which is defined as:

$$\zeta(\alpha) = \frac{\alpha_{new}}{\alpha_{base}} \tag{5.25}$$

Where α is any parameter related to the process for example, feed velocities, feed temperatures, step durations), and the subscripts *new* and *base* refer to the new and base configurations respectively. This implies that the operator ratios are equal to unity for corresponding parameters that are identical in the base and new system. Therefore, for an identical M-AR, with the same adsorbent and catalyst properties, $\zeta(\varepsilon) = \zeta(\varrho_b) = \zeta(c_{ps}) = \zeta(\Delta H_{ai}) = 1$. Similarly, with the same reaction scheme and fluid heat capacity, $\zeta(\upsilon_i) = \zeta(\Delta H_r) = \zeta(c_{pg}) = 1$.

The normalised variable profiles must be preserved in the transformation, to ensure the dimensionless performance of the base system is maintained. This can only be achieved if all the dimensionless groups in Eqs. ((5.7) – (5.19)) are identical in the base and the new system for both operating steps. For notational convenience the general reference variables (subscripted 0) are used in the following mathematical treatise. Thus from:-

Material balance:

$$\zeta(\Pi_m^{(a)}) = \frac{\zeta(v_0)\zeta(t_0)}{\zeta(z_0)} = 1 \tag{5.26}$$

$$\zeta(\Pi_m^{(b)}) = \frac{\zeta(t_0)}{\zeta(r_0^2)} = 1 \tag{5.27}$$

$$\zeta(\Pi_m^{(c)}) = \frac{\zeta(P)}{\zeta(T_0)\zeta(q_0)} = 1 \tag{5.28}$$

$$\zeta(\Pi_m^{(d)}) = \frac{\zeta(P)\zeta(t_0)}{\zeta(T_0\ \ )\zeta(q_0)\zeta(z_0^2)} = 1 \tag{5.29}$$

$$\zeta(\Pi_m^{(e)}) = \frac{\zeta(P)\zeta(t_0)}{\zeta(T_0)\zeta(q_0)\zeta(r_0^2)} = 1 \tag{5.30}$$

$$\zeta(\Pi_m^{(f)}) = \frac{\zeta(r_\infty)\zeta(t_0)}{\zeta(q_0)} = 1 \tag{5.31}$$

Energy Balance:

$$\zeta(\Pi_e^{(a)}) = \frac{\zeta(v_0)\zeta(t_0)}{\zeta(z_0)} = 1 \tag{5.32}$$

$$\zeta(\Pi_e^{(b)}) = \frac{\zeta(T_0)\zeta(t_0)}{\zeta(P)\zeta(r_0^2)} = 1 \tag{5.33}$$

$$\zeta(\Pi_e^{(c)}) = \frac{\zeta(P)}{\zeta(T_0)} = 1 \tag{5.34}$$

$$\zeta(\Pi_e^{(d)}) = \frac{\zeta(r_\infty)\zeta(t_0)}{\zeta(T_0)} = 1 \tag{5.35}$$

$$\zeta(\Pi_e^{(e)}) = \frac{\zeta(q_0)}{\zeta(T_0)} = 1 \tag{5.36}$$

$$\zeta(\Pi_e^{(f)}) = \frac{\zeta(t_0)}{\zeta(z_0^2)} = 1 \tag{5.37}$$

$$\zeta(\Pi_e^{(g)}) = \frac{\zeta(t_0)}{\zeta(r_0^2)} = 1 \tag{5.38}$$

Adsorption

$$\zeta(\prod_a) = \zeta(k_i)\zeta(t_0) = 1 \tag{5.39}$$

Rate

$$\zeta(\prod_r) = \frac{\zeta(P)\zeta(1/T_0)}{\zeta(r_\infty)\zeta(t_0)} = 1 \tag{5.40}$$

Boundary conditions

$$\zeta(\prod_b^{(a)}) = \frac{\zeta(c_0)}{\zeta(r_0)} = 1 \tag{5.41}$$

$$\zeta(\prod_b^{(b)}) = \frac{\zeta(T_0)}{\zeta(r_0)} = 1 \tag{5.42}$$

$$\zeta(\prod_b^{(c)}) = \frac{\zeta(c_0)}{\zeta(z_0)} = 1 \tag{5.43}$$

$$\zeta(\prod_b^{(d)}) = \frac{\zeta(T_0)}{\zeta(z_0)} = 1 \tag{5.44}$$

Since the normalised variables profiles are now identical in the transformation process, the normalised feed conditions must also be identical, i.e.

$$\zeta(y_{if}) = \zeta(y_{ir}) = \zeta(V^*_f) = \zeta(V^*_r) = \zeta(T^*_f) = \zeta(T^*_r) = 1 \tag{5.45}$$

Any integrals involving normalised variables evaluated at any points in the bed must be identical. It follows that the operator ratios of all dimensionless performance criteria i.e. $\zeta(X)$ are equal to unity. In other words, by preserving the normalised variable profiles, the dimensionless

(basic) performance indices are maintained during the transformation process. For dimensional indices this is not the case as they also contain dimensional reference variables i.e.

$$\zeta(X) = \frac{\left\{1 - \frac{\left(\frac{v_r T_f}{T_r v_f}\right)\int_0^1 \frac{y_i(1)V^*(1)}{T^*(1)}\partial\Omega_r}{\int_0^1 \frac{y_i(1)V^*(1)}{T^*(1)}\partial\Omega_f}\right\}_{new}}{\left\{1 - \frac{\left(\frac{v_r T_f}{T_r v_f}\right)\int_0^1 \frac{y_i(1)V^*(1)}{T^*(1)}\partial\Omega_r}{\int_0^1 \frac{y_i(1)V^*(1)}{T^*(1)}\partial\Omega_f}\right\}_{base}} = 1 \tag{5.46}$$

$$\zeta(P_R) = \frac{\left\{\frac{\left(\frac{Pt_f v_f}{RT_f}\right)\frac{y_i V^*}{T^*}X}{\rho\pi r^2 L}\right\}_{new}}{\left\{\frac{\left(\frac{Pt_f v_f}{RT_f}\right)\frac{y_i V^*}{T^*}X}{\rho\pi r^2 L}\right\}_{base}} \tag{5.47}$$

$$\zeta(E) = \frac{\frac{c_{pg}}{t_f + t_r}\left\{\left(\frac{v_f Pt_f}{R}\right)\frac{V_f^*(T_f^* - T_a^*)}{T_f^*} + \left(\frac{v_r Pt_r}{R}\right)\frac{V_r^*(T_r^* - T_a^*)}{T_r^*}\right\}_{new}}{\frac{c_{pg}}{t_f + t_r}\left\{\left(\frac{v_f Pt_f}{R}\right)\frac{V_f^*(T_f^* - T_a^*)}{T_f^*} + \left(\frac{v_r Pt_r}{R}\right)\frac{V_r^*(T_r^* - T_a^*)}{T_r^*}\right\}_{base}} \tag{5.48}$$

Depending on the specific scaling of the reference variables, the operator ratio for P_R and E can deviate from 1.

Scaling Rules

Eqs ((5.26) – (5.48)) are now constraints or rules for the transformation process, and are functions of common reference variables. These can be further simplified in the following manner:

From Eqs. ((5.34) $\frac{\zeta(P)}{\zeta(T_0)} = 1$ (5.49)

and substituting this into Eq. (5.28) yields:

$\zeta(q_0)=1$ (5.50)

Furthermore, we note that Eqs. ((5.26) and (5.32)) are identical as illustrated:

$$\zeta(\prod_m^{(a)}) = \frac{\zeta(v_0)\zeta(t_0)}{\zeta(z_0)} = 1 \;=\; \zeta(\prod_e^{(a)}) = \frac{\zeta(v_0)\zeta(t_0)}{\zeta(z_0)} = 1 \qquad (5.51)$$

Eqs. ((5.26) – (5.48)) reduce to the following scaling rules for the feeding and regeneration steps.

Feeding step

Rule f1: $\frac{\zeta(v_f)\zeta(t_f)}{\zeta(L)} = 1$

Rule f2: $\zeta(k_\infty)\zeta(t_f) = 1$

Rule f3: $\zeta(k_i)\zeta(t_f) = 1$

Regeneration step

Rule r1: $\frac{\zeta(v_r)\zeta(t_r)}{\zeta(L)} = 1$

Rule r2: $\zeta(k_\infty)\zeta(t_r) = 1$

Rule r3: $\zeta(k_i)\zeta(t_r) = 1$

Rule f1 (Rule r1) represents the inter-relationship between the inlet velocity, step duration and reactor length for the transformation process. **Rule f2 (Rule r2)** and **Rule f3 (Rule r3)** represent the effects of step duration on the rate of reaction and adsorption rate respectively.

5.4 Utilisation of Scaling Rules

Applications of the above derived scaling rules for the M-AR are detailed in the following sections:

5.4.1 Scaling of Production rate and scaling of energy input rate

Scaling production rate by a factor of F_{pr} implies that:

$$(P_R)_{new} = F_{pr}\,(P_R)_{base} \tag{5.52}$$

Note that the conversion remains unchanged (dimensionless performance index).The only variables that can be scaled from Eq. (5.47) are v_f and t_f, thus the scaling options are:

I. Scaling v_f (v_r) with t_f (t_r) unchanged

$(v_f)_{new} = F_{pr}\,(v_f)_{base}$ i.e.

$$(P_R)_{new} = \frac{\left(\frac{[F_{pr}v_f]Pt_f}{RT_f}\right)\frac{y_i V^*}{T^*}X}{\rho\pi r^2 L} \qquad (5.53)$$

In terms of the operator ratio, this also implies that $\zeta\,(v_f) = \zeta\,(v_r) = F_{pr}$. **Rule f1** and **Rule r1**, requires that

$$\frac{\zeta(v_f)\zeta(t_f)}{\zeta(L)} = \frac{\zeta(v_r)\zeta(t_r)}{\zeta(L)} = 1 \qquad (5.54)$$

$\zeta\,(t_f) = \zeta\,(t_r)=1$, this implies $\zeta(L) = F_{pr}$. For example doubling the production rate, involves doubling both the inlet velocities and the bed length in order to maintain dimensionless performance. The other dimensional criterion, the energy input rate, is also a direct function of v_f (and v_r) and so will also double. The numerical validation of the scaled designs was carried out by dynamic simulation. Numerical validation is presented in Table (5.7).

II. Scaling both v_f (v_r) and t_f (t_r) concurrently

Following the same steps discussed in scaling (I), with t_f and t_r also considered, then:

$$(v_f t_f)_{new} = F_{pr}(v_f t_f)_{base} \qquad (5.55)$$

$$(P_R)_{new} = \frac{\left(\frac{[F_{pr} v_f t_f]P}{RT_f}\right)\frac{y_i V^*}{T^*} X}{\rho \pi r^2 L} \tag{5.56}$$

$$\text{Thus, } \zeta(v_f)\zeta(t_f) = \zeta(v_r)\zeta(t_r) = F_{pr} \tag{5.57}$$

Given Eq. (5.57), an example is given below:

<u>An example with $\zeta(t_f) = \zeta(t_r) \neq 1$</u>

$\zeta(v_f)\zeta(t_f)$ and $\zeta(v_r)\zeta(t_r)$ can only be equal to F_{pr} if $\zeta(v_f) = \zeta(v_r) = F_{pr}$. If $\zeta(t_f) = \zeta(t_r) = f_{pr}$ then according to **Rule f1** and **Rule r1**:

$$\zeta(L) = \zeta(v_f)\,\zeta(t_f) = \zeta(v_r)\,\zeta(t_r) = F_{pr}\, f_{pr} \tag{5.58}$$

Rule f2, Rule f3, Rule r2, Rule r3 state that:

$$\zeta(k_\infty) = \frac{1}{f_{pr}} \qquad \zeta(k_i) = \frac{1}{f_{pr}} \tag{5.59}$$

Assume $f_{pr} = 0.75$; then $\zeta(k_i) = \zeta(k_\infty) > 1$, which means that by decreasing the step duration times, the reaction and adsorption rates of the new system are required to be $1/f_{pr}$ faster than those of the base system (i.e. 1.3 times faster). If $f_{pr} = 1.5$ on the other hand, increasing step times means that we only need to use a catalyst and adsorbent that is 0.6 times as efficient in the new system without sacrificing the dimensionless

criteria. Numerical verifications are given in Table (5.7) where $F_{pr} = 2$ for the following cases:

II a. fpr = 0.75 ; $\zeta(k_i) = \zeta(k_\infty) > 1$;

II b. fpr = 1.5; $\zeta(k_i) = \zeta(k_\infty) < 1$;

II c. fpr = 1.5; $\zeta(k_i) = \zeta(k_\infty) = 1$;

5.4.2 Maintaining process performance when step times are changed

In this section, the effect of the change in step times on process performance of the cyclic operation is assessed. Corresponding transformations of inlet velocities and bed length, in order to maintain both dimensionless and dimensional performance indices are determined. In terms of the operator ratios, scaling the step durations by a factor f_{st} gives:

$$\zeta(t_f) = \zeta(t_r) = f_{st}; \tag{5.60}$$

Maintaining the dimensional performance criteria is equivalent to having $\zeta(P_R) = \zeta(E) = 1$. The argument presented in the previous example (see scaling option **II**) applies with $F_{pr} = 1$. Therefore,

$$\zeta(v_f)\zeta(t_f) = \zeta(v_r)\zeta(t_r) = 1 \tag{5.61}$$

and $\zeta(t_f) = \zeta(t_r)$, which makes:-

$$\zeta(v_f) = \zeta(v_r) = 1 \tag{5.62}$$

From **Rule f1** and **Rule r1**

$$\zeta(L) = \zeta(v_f)\,\zeta(t_f) = \zeta(v_r)\,\zeta(t_r) = f_{st} \tag{5.63}$$

From **Rule f2, Rule f3, Rule r2, Rule r3:**

$$\zeta(k_i) = \zeta(k_\infty) = 1/\,f_{st} \tag{5.64}$$

Therefore, the scaling of cycle time is directly proportional to scaling the reactor length and inversely proportional to the reaction and adsorption rate constants. Table (5.7), section **III,** illustrates this example for $f_{st} = 5$.

It is noted that whenever the step times increase, the requirements on the reaction and adsorption rates are reduced by the same proportion. The inverse proportionality arises from **Rule f2, Rule f3, Rule r2, and Rule r3.** Thus, gas-solid mass transfer resistances can potentially be solved by increasing the step times with the required adjustments made to the inlet velocities and /or bed length **Rule f1 and Rule r1.**

	Base Case	I	IIa	IIb	IIc	III
$\zeta(v_f)$	1	2	2	2	2	1
$\zeta(v_r)$	1	2	2	2	2	1
$\zeta(t_f)$	1	1	0.75	1.5	1.5	5
$\zeta(t_r)$	1	1	0.75	1.5	1.5	5
$\zeta(L)$	1	2	1.5	3	3	5
$\zeta(k_\infty)$	1	1	1.3	0.6	1	0.2
$\zeta(k_i)$	1	1	1.3	0.6	1	0.2
Performance Indices						
X	98.8	98.8	98.8	98.8	98.8	98.8
P	0.045	0.09	0.09	0.09	0.09	0.045
E ($\times 10^4$)	4.2	8.5	8.5	8.5	8.5	4.2

Table 5.7: Scaling and corresponding numerical verification on performance indices Base case as specified in Table (3.7) with $u_a = u_d = 0.01$ m s^{-1}, $T_{fa} = T_{fr} = 460$ K

5.5 Conclusions

Results for the optimisation of the M-AR have been presented in this section, based on the mathematical model presented in Chapter 3. A non-linear approach was employed (i.e. gOPT) to identify key operating parameters to enhance reactor performance. Optimisation results indicated that inlet velocity and step times play an integral part in reactor performance.

The derivation of scaling rules for the M-AR was also presented. These rules are based on the concept that if the normalised variable profiles are preserved during the transformation i.e. scaling, then the basic performance of the process remains unchanged.

Scaling rules were derived for both the feed and regeneration steps and applied to two examples:

(i) Scaling production rate by a factor F_{pr} and thus scaling energy input rate;

(ii) Scaling the step times by a factor f_{st} where both dimensionless and dimensional performance indices are maintained if the bed length, L was scaled by f_{st} and the reaction and adsorption rate coefficients by $1/f_{st}$.

From (ii), adjusting step times also plays an important role in overall reactor design for e.g. altering step durations for the effective scheduling of multi-bed systems. In cyclic operation, the number of beds required for continuous product delivery depends on the number of steps and the duration of these steps thereby creating another measure of complexity in terms of step scheduling.

CHAPTER 6 Conclusions and Recommendations for Future Work

6.1 Conclusions

The novelty of this research was in exploring the possibilities of using the monolith reactor as an adsorptive reactor for exothermic reaction schemes, with VOC abatement as an example in the first instance. The overall aim of this thesis was to perform theoretical studies on the feasibility of non-isothermal adsorptive reactor operations via mathematical modelling, thereby providing a framework for future investigations and studies. The monolith reactor is currently used for catalytic combustion of VOCs and also for adsorption of low concentration VOCs, but the combination of both oxidation and adsorption of the VOC within the monolith structure has yet to be explored. Thus in this thesis the nature of work was to investigate theoretically, the feasibility, dynamics and potential of this novel configuration.

Prior to the theoretical studies, theoretical background information on the basic concepts of adsorption and adsorptive-reactor processes was presented. An overview of studies, past and present within this field and in particular, monolith reactors were also presented. As discussed in Chapter 2, past studies on adsorptive reactors have focused mainly on reversible endothermic reaction schemes and as such in this work issues

such as thermal runaway and efficient heat and energy integration are addressed.

The adsorptive reactor process considered a monolith-type adsorptive reactor (M-AR) over a Pd/γ-Al_2O_3 catalyst and activated carbon adsorbent for ethene oxidation. The process was operated in two steps – adsorption and desorption / reaction. Ethene and the inert carrier gas, N_2 were fed into the reactor in the adsorption step. The nitrogen gas in the effluent stream could then be recovered and reused further as a carrier gas. In the second step, ethene was desorbed by means of temperature swing (an increase in temperature) and concentration swing (inert regeneration gas, N_2 and reactant, O_2 gas). In the adsorptive reactor process, the amount of heat released during the regeneration step is from the integration of endothermic desorption of ethene (+ 29.5 kJ $mol^{-1}_{C2H4desorbed}$) and exothermic combustion of ethene (-1322 kJ $mol^{-1}_{C2H4gas}$). The source of heat initially required to heat up the bed may come from pre-heating the feed gas for reaction prior to entering the reactor or heating the monolith itself electrically. The key point in this step is the fact that the energy used for adsorbent regeneration and release of the desired reactant is not wasted. The largest part of that energy remains as sensible heat in the reactor bed and is used to further preheat the bed for the subsequent reaction step and provide further heat to drive desorption. The nitrogen in the effluent stream may be recovered and used as a carrier gas. The reaction products - the more concentrated CO_2 stream available for treatment can be employed for many different uses in industry e.g. as a reactant in many chemical reactions, for inert blanketing, use in

carbonated beverages, as dry ice and for refrigeration equipment. The H_2O stream can be sent directly to the atmosphere.

A mathematical model for the adsorptive reactor model was developed. Models utilizing the monolith reactor for purposes of adsorption only (M-ADS) and reaction only (M-RXTN) were also developed. In addition, one-dimensional models of the packed bed reactor for adsorption only (PB-ADS) and reaction only (PB-RXTN) were developed to enable comparisons between the respective monolith reactors. The numerical approach adopted in this work was dynamic simulation over a large number of cycles (such that cyclic steady state convergence is achieved).

In order to understand and gain insight into the dynamics of the process, studies were initially performed on the two individual steps of adsorption and desorption / reaction. The simulation of the adsorption and reaction steps within the monolith reactor provided insight into the propagation of mass and thermal waves. Key process parameters included feed inlet temperatures, inlet velocities, reactor geometrical configurations (length and radial thickness). These parameters had an effect on the performance of the individual steps in terms of key performance indices which included inert gas purity, energy input and conversion. Relative to the equivalent packed bed reactor configurations, the monolith reactor proved feasible. In the adsorption step for example, the general trends were as for the monolith adsorbed but with slightly faster breakthrough and saturation times. The estimated pressure drop

in the packed bed for all conditions was much higher than that of the equivalent monolith reactor.

Due to the need for adsorbent regeneration, the M-AR was operated under a periodic mode and this mode of operation provided further challenges due to the complex interactions between the adsorption and reaction steps. The performance of the M-AR is affected by a number of design and operating parameters as demonstrated through the parametric studies performed in Chapter 4. Step times for adsorption and desorption, feed temperatures, inlet velocities, and reactor geometry (length and radial thickness) also play an integral part in the overall performance of the M-AR. Varying the length of the step times had an effect on the amount adsorbed and on ethene conversion. The efficiency and effectiveness of desorption depended on how much adsorbate was adsorbed in the first place. The length and duration of the desorption step was a factor in terms of heating times and the number of cycles required to achieving steady state. In the regeneration step, typically two stationary travelling fronts are formed – the thermal front propagation velocity, W_{therm}, (m s^{-1}) (dependent on the heat capacities of the gas and solid phases) and the reaction front propagation velocity, W_R, (m s^{-1}). W_{therm} and W_R are independent of each other and the effective temperature rise in the reactor depends on the ratio of W_{therm} and W_R. In the M-AR, the reaction front is faster than the thermal front i.e. $W_R > W_{therm}$. This case occurs at high inlet oxygen concentrations or small initial adsorbent loading i.e. combustion is limited by the amount of

ethene available. Thus the heat generated by reaction exceeds the heat consumption for desorption and heating up the cold gas stream.

Operating under conditions of incomplete bed saturation was deemed more favourable as the performance of the reactor under these conditions outperformed reactor performance under conditions of complete saturation. One explanation for this is the fact that under complete saturation, breakthrough of unreacted ethene is possible. Working under incomplete saturation implied that shorter bed lengths (nearer the reactor entrance) were utilised and as such better reactor performance attained.

Working with a temperature swing (rather than with the same feed temperature for both adsorption and desorption steps) gave better reactor performance in terms of energy requirements and more importantly reactor thermal stability. Under temperature swing operation, the same conversion could be achieved as with identical temperature operation, and at lower energy input requirements and reactor stability. In temperature swing, reactor operation occurs at low temperatures of adsorption, and desorption at higher temperatures via temperature and concentration swing. There is thus efficient heat integration in this case than under same temperature operation.

The most outstanding feature of the M-AR was its ability to prevent thermal runaway. The stability of the reactor for an exothermic reaction is dependent on the feed concentrations and the feed inlet temperatures where minor changes to the feed concentrations especially have been

known to cause situations of thermal runaway especially in packed bed reactors. This performance of the M-AR was compared to that of an equivalent monolith reactor (M-RXTN) in which reaction only takes place. In general, reactor performances were conducted within regions of very low adsorbate concentrations (3000 ppm). For thermal stability considerations, feed inlet concentrations were explored between the lower explosive limits, LEL (2.7 vol %) and the upper explosive limits, UEL (36 vol. %). In all cases studied (see Section 4.5), the hybrid monolith was found to be thermally more stable than the monolith reactor (M-RXTN). It was further observed that reactor stability within the M-AR was greater with a temperature swing effect than with same temperature operation. Nevertheless, for all combinations in the M-AR, the reactor was thermally more stable due to the controlled release of the reactant from the adsorbed phase into the reaction zone, and also the heat integration of an endothermic desorption and exothermic reaction.

The performance of the monolith reactor was also compared to that of the packed bed reactor. As reviewed in Section 2.6, the M-AR provides an alternative to the fixed bed catalytic reactor and thus the conventional fixed bed adsorptive reactor. With regards to thermal stability, the packed bed reactor was found to be thermally unstable within the concentration range studied. The M-RXTN and M-AR were observed to be more stable. The two reactors, M-AR and M-RXTN are identical in geometrical configuration, catalyst loading, feed inlet velocities and general operating conditions (with the exception of feed inlet temperature and feed inlet concentrations). These exceptions account for

the fact that the M-AR is operated cyclically and the M-RXTN is operated as a single step continuous-fed reactor pre-mixed with VOC and air. The feed inlet concentrations in the M-RXTN were adjusted to account for the fact that adsorption at a temperature, T_{fa} takes place first in the M-AR, under regions of incomplete saturation. Therefore, the ethene feed inlet concentrations in the M-RXTN were much lower than in the M-AR. In the M-AR, air (O_2 – 21%; N_2 – 79%) is fed in during the desorption step at reaction temperature, T_{fr} i.e. 460 K. The feed reaction temperature in the monolith reactor, T_r is equal to the reaction temperature, T_{fr} in the second step of M-AR operation.

A non-linear approach was employed to identify key operating parameters in order to enhance reactor performance. Optimisation results indicated that inlet velocity and step times play an integral part in reactor performance. Scaling rules were also derived which enabled the M-AR process to be scaled to one which met new and / or additional system specifications. For example, the production rate of a given M-AR operation could be increased by a factor F_{pr} by scaling the inlet velocities and reactor length by the same factor. Thus, basic performance such as conversion could be maintained.

The work done in this thesis indicate that there is much scope in the use of the monolith reactor as an adsorptive reactor, not only in terms of the obvious advantages over conventional adsorptive reactors but also in terms of thermal stability which is of great importance in such exothermic schemes. The key characteristics of this novel reactor in

terms of its utilization as an adsorptive reactor for VOC abatement is highlighted below:

Advantages:

- Low pressure drop
- Can be used for reaction-only, adsorption-only as well as combined in-situ adsorption and reaction processes
- Relatively high thermal stability
- Low energy input requirements
- High conversions (> 98 %) achieved for both dilute and non-dilute feed concentrations of ethene

Disadvantages:

- Adsorption performance decreases at higher gas velocities due to an increase in feed gas bypass and reduced reactor residence time
- Dependent on axial and radial mixing in the core gas channel
- Dependent on step times of both adsorption and desorption
- Desorption heating time has an effect on reaching cyclic steady state

A comparative summary of both the M-AR and monolith reactor, (M-RXTN) is given in Table (6.1)

M-AR	M-RXTN
Cyclical operation	Continuous operation
Can achieve conversions > 98 %	Generally achieve 100 % conversion
Lower energy input rate for $T_{fa} \neq T_{fr}$ operation	Higher energy input rate
Relatively thermally stable. Higher stability occurs in $T_{fa} \neq T_{fr}$ operation	Thermally unstable

Table 6.1: M-AR vs. M-RXTN Performance

The performance of the M-AR can also be compared to that of hydrocarbon trap utilised in automotive car exhaust systems. This approach of the so called hydrocarbon traps (adsorbent-reaction system) is similar in context to the operation of the M-AR whereby the harmful hydrocarbons are captured and stored in the first instance and released upon sufficient heat or increase in temperature when the catalyst becomes active and oxidation occurs. The use of monolithic catalysts in car exhaust emission control was one of the most important industrial applications for monoliths. The vast majority of the harmful gases are emitted into the atmosphere when the engine is still cold. The catalyst in an automotive converter is inactive until it is warmed up to a certain temperature. The time taken for an exhaust emission-control catalyst to reach its operating temperature for hydrocarbon oxidation is a major barrier to achieving ultra-low emissions from vehicles. During this period carbonaceous material is deposited on the active sites of the catalyst, decreasing its activity. Deactivation of this sort is reversible. The deposit is quickly burned off after the temperature reaches the level that the catalyst becomes active in combustion processes. Hydrocarbon traps that adsorb possible emissions before light-off and desorb them

after light-off are used to decrease emissions in cold or idle operation. The traps delay the exposure of the catalyst to these potentially inhibiting species until it has reached a temperature at which it can effectively combust hydrocarbons. A comparative summary of both the M-AR and Hydrocarbon trap is given in Table (6.2).

M-AR	HC-Trap
2 steps of operation - adsorption at low temperatures followed by desorption and reaction at higher temperature	2 steps of operation – adsorption at low temperatures followed by desorption and reaction at higher temperature
Typically use different adsorbent (activated carbon) and catalyst system e.g. Pd, Pt	Typically use the same catalyst that functions as an adsorbent in low temperatures and as a catalyst after light-off e.g. zeolites H-ZSM-5 or H-Beta
Can achieve conversions > 98 %	Generally can achieve high levels of hydrocarbon conversion throughout the start-up phase. Engine out emissions reduced
Low concentration VOCs available for combustion (dilute)	Typically longer chained HCs especially in older car engines available for combustion
Dependent on step times of both adsorption and desorption. Duration of heating time in seconds and has an effect on reaching cyclic steady state	Dependent on the duration of the warm up period. Duration of warm up periods is in order of minutes, though for metallic catalysts this is significantly reduced
Flexibility in operational modes	Only $T_{fa} \neq T_{fr}$ mode of operation
Catalysts have to be compatible with adsorbent system.	Flexibility in use of catalysts that are active at lower temperatures with the potential of lowering light-off

Table 6.2: M-AR vs. Hydrocarbon traps

6.2 Recommendations for Future Work

Having established in this thesis that the concept of adsorptive reactor technology works with the use of the exothermic VOC abatement process as a case study; this concept could be further extended to other exothermic reaction schemes. For example, the catalytic combustion of methane. The use of VOC oxidation is for the abatement of hydrocarbon emissions whilst fuel combustion generates heat and electric power. The fundamental difference between the two processes lie in their operating temperatures, which is generally between 373 – 800 K for catalytic oxidation and between 600 – 1700 K for catalytic fuel combustion. The other main difference is in the concentration of combustible compounds which for VOC oxidation is present in trace amounts. Adsorptive reactor technology in particular may be favourable for reversible reactions of the general type $\nu_A A + \nu_B B + \ldots \Leftrightarrow \nu_C C + \nu_D D + \ldots$; with $\sum_j \nu_j < \sum_i \nu_i$; $j \in$ [products] and $i \in$ [reactants]. In this case, reaction enhancement may occur in a high pressure feeding step due to both the removal of product and the fact that high pressure favours the forward reaction (Kodde, 2001; Yongsunthon, 1999). Examples of reversible exothermic reactions include ammonia production via the Haber process, an important industrial process for fertiliser production and the water gas shift reaction which plays an important role in many current technologies such as menthol synthesis and steam reforming.

M-AR operation with $T_{fa} = T_{fr}$ operation may further be enhanced by use of reverse flow purge stripping for regeneration. At high temperatures

for adsorption, temperature swing operation may not be effective and as such the regeneration of the adsorbent can be improved by reverse flow purge stripping. Gelbin *et al.* (1983) advocated that reverse-flow desorption would be better choice as a higher separation efficiency can be achieved at shorter cycle times. Other steps include pressure swing and purge gas (multiple beds) and catalyst / adsorbent zoning.

With regards to scaling rules, new applications that could be utilised include choosing design parameters in order to overcome inefficiencies due to solid-gas mass transfer resistance in the catalyst / adsorbent, and altering the step durations for the effective scheduling of multiple beds.

There is scope for the choice and configuration of the monolith structure. Activated carbon monoliths are considered for use in this work. Different methods or forms are available for the monolith geometrical structure in terms of using activated carbon monoliths that exhibit adsorptive properties, with a layer of catalytically active material coated on them, impregnating the monolith structure itself with catalysts or placing a catalytically active metal rod in the core gas channel. The monolith configuration and how the catalysts are arranged or integrated is in itself a challenge as the feasibility and performance of the process is dependent on this.

The work presented in this thesis has provided some theoretical understanding and insight into the non-isothermal adsorptive reactors

for exothermic process schemes. Experimental validation of these theories will be just as challenging.

Recommendations for an experimental programme are two-fold:

- In the first instance, the use of a Berty reactor would enable adsorption and reaction studies and measurements to be carried out. The mixed-flow set-up provides a relatively easy means for data analysis. The reactor is suitable for high temperature and pressure operations, and appropriate for multiphase processes. The equilibria and kinetics of VOC adsorption on activated carbon adsorbent at different temperatures and the characterisation of the various adsorbent materials available should be investigated experimentally in order to obtain accurate adsorption data for use in theoretical studies. This would also allow for the characterisation of bits of monolith adsorbent impregnated with catalyst. Reaction rate expressions and data can therefore also be determined.

- Building an experimental rig for the monolith M-AR configuration, and performing detailed adsorbent and catalyst characterisation work for the purposes previously outlined above.

References

- Alpay, E. (1992). Rapid pressure swing adsorption processes. *Ph.D thesis, University of Cambridge.*
- Alpay, E., D. Chatsiriwech, S.Kershenbaum, C.P.Hull, and N.K. Kirkby (1994). Combined Reaction and Separation in Pressure Swing Processes. *Chem. Eng.Sci.* **49,** 5845 – 5864.
- Alpay,E., and D.M. Scott (1992). The linear driving force model for short-cycle adsorption and desorption in a spherical particle. *Chem.Eng.Sci.* **47,** 499-502.
- Alpay, E., N.Haq, L.S.Kershenbaum, and N.F.Kirkby (1996). Adsorption parameters for strongly adsorbed hydrocarbon vapours on some commercial sorbents. *Gas. Sep.Pur.***10,** 25-33
- Ament, F., D.A. Singer (1996). Zeolite / catalyst wall-flow monolith adsorber. *Journal of Cleaner Production* **4,** 79-80.
- Andrews, R., M. Jagotoyen, and E.A. Grulke (1998). Butane adsorption on activated carbon fibre composites: modelling and simulation. In: Science and technology of carbon, Strastbourg, France I, pp 141-142.
- Belfort, G. (1989). Membranes and bioreactors – a technical challenge in biotechnology. *Biotechn.Bioeng.* **33,** 1047-1066.
- Bilous, O and N.R. Amundson (1956). *AIChE J.* **2,** 117.
- Bird, R.B., W.E. Stewart and E.N. Lightfoot (1960). Transport phenomena. *John Wiley & Sons , New York.*
- Boehman, A.L. (1998). Radiation heat transfer in catalytic monoliths. *AIChE J.* **44,** 2745-2755.
- Blocki, S.W. (1993). Hydrophobic zeolite adsorption: a proven advancement in solvent separation technology. *Environmental Progress* **12,** 226-237.
- Bjorklund, M.C. and R.W. Carr (1995). The simulated counter current moving bed chromatographic reactor: a catalytic and separative reactor. *Cat. Today* **25,** 159-168 .

- Burchell, T.D., C.E. Weaver, B.R. Chilcoat, F.Derbyshire, M.Jagtoyen (2001). Activated carbon fibre composite material and method of making. *US Patent 6258300 B1.*
- Carta, G.(1993). Linear driving force approximation for cyclic mass transfer in spherical particles. *Chem. Eng. Sci.* **48**, 622-625.
- Carter, J.W. (1975). On the regeneration of fixed bed adsorbers. *AIChE J.***21**, 380.
- Carvill, B.T., J.R. Hufton, M. Anand and S.Sircar (1996). Sorption – enhanced reaction process. *AIChE J.* **42**, 2765 – 2772.
- Chatsiriwech, D., E. Alpay, L.S. Kershenbaum, C.P. Hull and N.F. Kirkby (1994). Enhancement of catalytic reaction by pressure swing adsorption. *Cat. Today* **20**, 351-366.
- Chen, J., Y.Wang and C. Zheng (1997). Synthesis of nano-particles of $CaCO_3$ in a novel reactor. 2nd International Conference Process Intensification in Practice in: Semel, J.(Ed), BHR Group Conf. Series, Publ, No 28, Mechanical Engineering Publications Limited, London. pp 157 – 164.
- Cheng, Y., E.Alpay, and L. Kershenbaum (1998). Simulation and optimisation of a rapid pressure swing reactor. *Comp.Chem.Eng.* **22**, S45-S52.
- Chihara, K. and M. Suzuki (1983). Simulation of non-isothermal pressure swing adsorption. *J.Chem. Eng. of Japan* **16**, 53.
- Choong, T.S.Y., and D.M.Scott (1998). Linear drving force model for cyclic adsorption and desorption: The effect of fluid-film mass transfer. *Chem.Eng.Sci.* **53**,847-851.
- Cottrell, F.G. (1938). Purifying gases and appartus therefore. *US Patent, June.*
- Crittenden, B.D., J. Guan, W.N. Ng and W.J. Thomas (1994). Dynamics of pressurisation and depressurisation during pressure swing adsorption. *Chem. Eng. Sci.* **49**, 2657-2669.
- Cybulski, A. and J.A. Moulijn (1998). The present and future of structured catalysts – an overview, structured catalysts and reactors, Ch 1, edited by Cybulski, A., Moulijn, J.A., *Marcel Dekker, Inc.*
- Dandekar, H.W., G.A. Funk, S.H.Hobbs, M. Kojima, R.D. Gillespie, H.A. Zinnen and C.P. McGonegal. Process for continuous reaction and deparation using reactive chromatography. US Patent 5744683 to UOP (1998).

- Davis, M.M and M.D. LeVan (1987). Theory for complete adiabatic adsorption cycles. *AIChE J.* **33**, 470.
- Davis, M.M and M.D. LeVan (1989). Experiments on optimization of thermal swing adsorption. *Ind.Eng.Chem.Res.* **28**, 778-785.
- Derbyshire, F., M. Jagtoyen, R. Andrews, A.Rao, Martin-Gullon and E.A. Grulke (2001). In: L.R.Radovic, Editor, *Chemistry and physics of carbon* **vol.21**, Marcel Dekker, New York pp 1-66.
- Ding, Y. and E.Alpay (2000). Equilibria and kinetics of CO_2 adsorption on hydrotalcite adsorbent. *Chem. Eng. Sci.* **55**, 3461-3474.
- Do, D.D. and R.G. Rice (1986). Validity of the parabolic profile assumption in adsorption studies. *AIChE J.* **32**, 149-154.
- Doong, S.J. and R.T.Yang (1987). Bidisperse pore diffusion model for zeolite pressure swing adsorption. *AIChE J.* **33**, 1045-1049.
- Eigenberger, G., G. Kolios, J.Frauhammer (2000). Authothermal fixed-bed reactor concepts. *Chem. Eng. Sci.* **55**, 5945-5967.
- Farooq, S., M.M.Hassan, and D.M.Ruthven (1988). Heat effects in pressure swing adsorption Systems. *Chem.Eng.Sci.* **43**, 1017-1031.
- Ferreira, R.Q., C.A. Costa, and S.Masetti (1999). Reverse-flow reactor for a selective oxidation process. *Chem. Eng. Sci.* **54**, 4615- 4627.
- Finlayson, D. and A.J. Sharp (1932). Separating gaseous mixtures. *British Patent 365092 to Britisch Celanese Ltd.*
- Foster, K.L., R.G. Fuerman, J.Economy, S.M. Larson and M.J. Rood (1992). Adsorption characteristics of trace volatile organic compounds in gas streams onto activated carbon fibres. *Chem Mater* **4**, 1068-1073.
- Fuertes, A.B., G.Marban and D.M.Nevskaia (2003). Adsorption of volatile organic compounds by means of activated carbon fibre-based monoliths. *Carbon* **41**, 87-96.
- Funk, G.A., J.R. Lansbarkis, and A.K.Chandhok(1995). Process for concurrent esterification and separation using a simulated moving bed. *US Patent 5405992 to UOP.*
- Gadkaree, K.P.(1998). Carbon honeycomb structures for adsorption applications. *Carbon* **36**, 981-989.

- Garcia-Bordeje, E. , F.Kapteijn and J.A.Moulijn (2002). Preparation and characterisation of carbon-coated monoliths for catalyst supports. *Carbon* **40**, 1079-1088.
- Gildert, G.R., K. Rock, and T.McGuirk (1998). Advances in process technology through catalytic distillation. *Proceedings of the International Symposium on Large Chemical Plants* **10**, 103-113.
- Glueckauf and Coates (1947). Theory of chromatography (Part IV). *J.Chem.Soc.*, pp1315.
- Golodets, G.I. (1983). Heterogeneous catalytic reactions involving molecular oxygen, studies in surface science and catalysis, Elsevier, Amsterdam, Vol.15.
- Gore, F.E. (1967). Performance of chromatographic reactors in cyclic operation. *Ind. Eng. Proc. Design Dev.* **6**, 10-16.
- gPROMS Introductory User's Guide, 1998, Process Systems Enterprise Ltd.
- Groppi, G. and E. Tronconi (2001). Simulation of structured catalytic reactors with enhanced thermal conductivity for selective oxidation reactions. *Cat. Today* **69**, 63-73.
- Hayes, R.E. and S.T. Kolaczkowski (1994). Mass and heat transfer effects in catalytic monolith reactors. *Chem.Eng.Sci.* **49**, 3587-3599.
- Hayes, R.E., S.T. Kolaczkowski, P.K.C. Li and S.Awdry (2001). The palladium catalysed oxidation of methane: reaction kinetics and the effects of diffusion barriers. *Chem.Eng.Sci.***56**, 4815-4835.
- Heiszwolf, J.J, A.K. Heibel, M.T. Kreutzer, F.Kapteijn and J.A. Moulijn (2000). Hydrodynamics of Two-Phase Flow in Monolith Reactors.
  Website: http://www.dct.tudelft.nl/monoliet/Intro/introduction.html. Last visited August 2007.
- Hoebink, J.H.B.J. and G.B. Marin (1998). Modeling of monolith reactors for automotive exhaust gas treatment, structured catalysts and reactors, Ch. 8, edited by Cybulski, A., and J.A. Moulijn, *Marcel Dekker, Inc.*
- Hsieh, H.P. (1996). Inorganic membranes for separation and reaction. *Elsevier Science B.V., Amsterdam*
- Huang, C.C, T.L. Hwu and Y.S. Hsia (1993). Recovery of acetone vapour by a thermal swing adsorber with activated carbon. *J. Chem. Eng. Japan* **26**, 21-27.

- Hufton, J.R., S. Mayorga, and S.Sircar (1999). Sorption-enhanced reaction processes for hydrogen production. *AIChE J.* **45** , 248-256.
- Hufton, J.R., W.E. Waldron and S.Sircar (2001). Production of hydrogen by cyclic sorption enhanced reaction process. *AIChE J.* **47**, 1477-1479.
- Hwang, K.S., D.K.Choi, S.Y. Gong and S.Y. Cho (1997). Adsorption and thermal regeneration of methyl chloride vapour on activated carbon. *Chem. Eng. Sci.* **52**, 1111-1123.
- Ito, T., H. Kanesaka and T. Ikeda (1996). Zeolite based adsorbents for hydrocarbons. *Zeolites* **16**, 220.
- James, D.H. and C.S.G. Phillips (1974). *J.Chem.Soc.* **10**, 61.
- Jaroniec, M., R.K. Gilpin, K.Kaneko and J.Choma (1991). *Langmuir* **7**, 2719.
- Jeong, Y.O. and D.Luss (2003). Pollutant destruction in a reverse flow chromatographic reactor. *Chem.Eng.Sci.* **58**, 1095-1102.
- Kadlec, R.H. and G.C.Vaporciyan (1993). Periodic chemical processing system. *US Patent 5254368 to the University of Michigan.*
- Kahle, H. (1941). Apparatus for drying gases. German Patent 871886 to Gesellschaft für Linde's Eismaschienen AG.
- Kapoor, A. and R.T.Yang (1991). Contribution of concentration-dependent surface diffusion to rate of adsorption. *Chem.Eng.Sci.* **46**, 1995-2002.
- Kauzmann, W.(1966). Kinetic Theory of Gases. *New York: Benjamin.*
- Kelkar, V.V. and K.M. Ng (1999). Systematic development of extractive reaction process. *Chem.Eng.Tech.* **22**, 877-880.
- Kershenbaum. L.S., E.Alpay, and D.Chadwick (1999). Strategies for enhanced conversion and yields in catalysed reversible reactions. Presented originally at the "Colloquium on chemical reactor engineering" CCRE-16, Hungary
- Khan, F.I., and A.K. Ghoshal (2000). Removal of volatile organic compounds from polluted air. *J.Loss Prev.Proc.Ind.* **13**, 527-545.
- Kikkinides, E.S., R.T. Yang and S.H. Cho (1993). Concentration and recovery of CO_2 from flue gas by pressure swing adsorption. *Ind.Eng.Chem.Res.***32**, 2714-2720.
- Kirkby, N.F. and J.E.P. Morgan (1994). A Theoretical investigation of pressure swing reaction. *Chem.Eng.Res.Des.* **72**, 541-550.

- Kodde, A.J. (2001). Operation of irreversible series reactions in pressure swing reactors. *Ph.D thesis, University of Amsterdam.*
- Kohl, A.L.(1987). Absorption and Stripping. In Rousseau, R.W., ed., Handbook of Separations Process Technology, chapter 6, pp. 340-404. John Wiley & Sons, New York.
- Khinast, J., Y.O. Jeong and D. Luss (1999). Dependence of cooled reverse flow reactor dynamics on reactor model. *AIChE J.* **43**, 2034-2047.
- Kolaczkowski, S.T. (1999). Modelling catalytic combustion in monolith reactors – Challenges faced. *Cat. Today* **47**, 209-218.
- Krishna,R.(2002). Reactive separations: More ways to skin a cat. *Chem.Eng.Sci.* **57**, 1491-1504.
- Kumar, R. (1994). Pressure swing adsorption process – performance optimum and selection. *Ind.Eng.Chem.Res.* **33**, 1600 – 1605.
- Kumar, R. and G.R. Dissinger (1986). Nonequilibrium, nonisothermal desorption of single adsorbate by purge. *Ind.Eng.Chem.Proc.Des.Dev.***25**, 456.
- Law, T.S.C., C.Chao, G.Y.W. Chan, and A.K.Y. Law (2003). Confined catalytic oxidation of volatile organic compounds by transition metal containing zeolites and ionizer. *Atmos. Envt* **37**, 5433-5437.
- Langmuir, I. (1918). *J. Amer. Chem.Soc.* **40**, 1361.
- LeVan, M.D. and D.T. Croft (1995). Determination of periodic states of pressure swing adsorption cycles. *Gas.Sep.Purif.* **9**, 13-16.
- Liow, J.L. and C.N. Kenney (1990). Backfill cycle of the pressure swing adsorption process. *AIChE J.* **36**, 53-65.
- Loureiro, J., C.Costa and A.Rodrigues (1990). Dynamics of adsorptive reactors I – instantaneous non linear adsorption and finite zero order irreversible reaction. *Can.J.Chem.Eng.* **68**, 127-138.
- Loureiro, J.and A.Rodrigues (1989). In *Adsorption: Science and Technology*, pp 223, Kluwer Academic Publishers, New York.
- Lu, Z.P., J.M. Loureiro, M.D. LeVan and A.E. Rodrigues (1993). Pressure swing adsorption processes - intraparticle diffusion convection models. *Ind. Eng. Chem. Res.* **32**, 2740 – 2751.

- Lu, Z.P. and A.E. Rodrigues (1994). Pressure swing adsorption reactors: simulation of a three-step one-bed process. *AIChE J.* **40**, 1118-1137.
- Magee, E.M. (1963). The course of reaction in a chromatographic reactor. *Ind.Eng.Chem.Fund.* **2**, 32-36.
- Martin, P.D. and S.W. Swanton. Improved efficiency of adsorption processes. *Applied Thermal Engineering* **7**, 869-877.
- Matros, Y.S. (1989). Catalytic processes under unsteady-state conditions. *Studies of surface science and catalysis* (**Vol 43**). Amsterdam: Elsevier.
- Matros, Y.S., A.S. Noskov and A. Chumachenko (1993). Progress in reverse-process application to catalytic incineration problems. *Chem.Eng.Proc.* **32**, 89-98.
- Matros, Y.S. and G.A. Bunimovich (1995). Control of volatile organic compounds by the catalytic reverse process. *Ind.Eng.Chem.Res.* **34**, 1630-1640.
- Matros, Y.S. and G.A. Bunimovich (1996). Reverse flow operations in fixed bed catalytic reactors. *Cat.Rev.Sci.Eng.* **38**, 1-68.
- Matros Y.S., G.A. Bunimovich, V.O. Strots and E.A. Mirosh (1999). Reversed flow converter for emission control after automotive engines. *Chem.Eng.Sci.* **54**, 2889-2898.
- Marban, G., A.B. Fuertes and D.M. Nevskaia (2000). Dry formation of low density Nomex™ rejects-based activated carbon fibre composites. *Carbon* **38**, 2167-2170.
- Mazzarino, I. and A.A. Barresi (1993). Catalytic combustion of voc mixtures in a monolithic reactor. *Cat. Today* **17**, 335-348.
- Minotti, M., M.F.Doherty, and M.F. Malone (1998). Design for simultaneous reaction and liquid-liquid extraction. *Ind.Eng.Chem.Res.* **37**,4748-4755.
- de Montgareuil, P.G. and D.Domine. Process for separating a binary gaseous mixture by adsorption. US Patent 3155468 to Air Liquide (1964).
- Nilchan, S. and C.C. Pantelides (1998). On the optimisation of periodic adsorption processes. *Adsorption Journal of the International Adsorption Society* **4**, 113-147.
- Olivares, J. (2002). D.G. de Investigacion de la Consejeria de Educacion y Cultura de la CAMCentro de Enlace de Madrid, 30-32 Planta baja, Madrid 28014.
- Pacheco, M.A. and G.T. Rochelle (1998). Rate-based modelling of reactive absorption of CO_2 and H_2S into aqueous methyldiethanolamine. *Ind.Eng.Chem. Res.* **37**, 4107 – 4117.

- Pahori, P.K. and N.N.Sharma (1991). Recovery of morpholine via reactive extraction. *Ind.Eng.Chem.Res.* **30**, 2015-2017.
- Pandya. M. and E. Alpay (2000). Reverse flow adsorptive reactor operation for the oxidation of volatile organic compounds. *MSc thesis, Imperial College, London.*
- Prezeres, D.M.F. and J.M.S. Carbral (1994). Enzymatic membrane bioreactors and their applications. *Enzyme and Microbal Technology* **16**, 738-750.
- Rege, S.U., J. Padin and R.T. Yang (1998). Olefin/paraffin separations by adsorption: π-complexation vs. kinetic separation. *AIChE J.* **44**, 799-809.
- Rhee, H.K., E.D. Heerdt and N.R. Amundson (1972). An analysis of an adiabatic adsorption column Part III adiabatic adsorption of two solutes. *Chem.Eng.J.* **3**, 122.
- Ritter, J.A. and R.T. Yang (1991). Pressure swing adsorption – experimental and theoretical study on air purification and vapour recovery. *Ind. Eng. Chem. Res.* **30**, 1023 – 1032.
- Ritter, J.A. and Y.J. Liu (1998). Tapered pressure swing adsorption columns for simultaneous air purification and solvent vapour recovery. *Ind. Eng. Chem. Res.* **37**, 2783 – 2791.
- Rodriguez, A.E., P.Li, and G.Xiu (2002). Sorption-enhanced reaction process with reactive regeneration. *Chem.Eng.Sci.* **57**, 3893-3908.
- Roginskii, S.Z., M.I. Yanovskii and G.A. Gaziev (1961). *Dokl. Akad. Nauk.* USSR, 140, 1125.
- Rouse, A.J. (2004). Fast cycle low pressure drop systems for the separation of CO_2. *PhD Thesis, University College London.*
- Ruthven, D.M. (1984). Principles of adsorption and adsorption processes. *John Wiley & Sons, New York.*
- Ruthven, D.M., and C.B. Ching (1989). Countercurrent and simulated countercurrent adsorption separation processes. *Chem.Eng.Sci.* **44**, 1011-1038.
- Ruthven, D.M., S. Farooq and K.S. Knaebel (1994). Pressure swing adsorption. *VCH*
- Ruthven, D.M. (1997). In Encyclopedia of separation technology, Vol.1, John Wiley, New York, 1997, pp 94-129.
- Salinger, A.G. and G. Eigenberger (1996). The direct calculation of periodic states of the reverse flow reactor – I . Methodology and propane combustion results. *Chem.Eng.Sci.* **51**, 4903-4913.

- Salomons, S., R.E. Hayes, M.Poirier, H. Sapoundjiev (2003). Flow reversal reactor for the catalytic combustion of lean methane mixtures. *Cat. Today* **83**, 59-69.
- Salomons, S., R.E. Hayes, M.Poirier, H. Sapoundjiev (2004). Modelling a reverse flow reactor for the catalytic combustion of fugitive methane emissions. Comp.Chem.Eng.
- Sarafik, D.J. and R.B.Eldridge (1998). Olefin/paraffin separations by reactive absorption: A review. *Ind. Eng. Chem. Res.* **37**, 2571-2581.
- Schork, J.M. and J.R. Fair (1988). Periodic states for thermal swing adsorption of gas mixtures. *Ind. Eng. Chem. Res.* **27**, 457.
- Seader. J.D. and E.J. Henley (1998). Separation process principles. *John Wiley & Sons, New York.*
- Sheikh, J., L.Kershenbaum, and E.Alpay (1998). Analytical Basis for Separation Enhanced Reaction in Continuous Flow Processes. *Chem.Eng.Sci.*, **53**, 2933-2939.
- Sheikh, J. (1999). Rapid pressure swing reaction processes. *Ph.D thesis, Imperial College London.*
- Sheng, P. and C.A.V. Costa (1997). Modified linear driving force approximations for cyclic adsorption-desorption processes. *Chem.Eng.Sci.* **52**, 1493-1499.
- Siirola, J.J. (1995). An industrial perspective on process synthesis. *AIChE. Symp.Ser.* **91**, 222-233.
- Singh, K. and J. Jones (1997). Numerical simulation of air separation by piston-driven pressure swing adsorption. *Chem. Eng. Sci.* **52**, 3133-3145.
- Sircar, S., R. Kumar and K.J. Anselmo (1983). Effects of column nonisothermality or nonadiabaticity on adsorption breakthrough curves. *Ind.Eng.Chem.Proc.Des.Dev.* **22**, 10-15.
- Sircar, S., T.C.Golden and M.B.Rao (1996). Activated carbon for gas separation and storage. *Carbon* **34**, 1-12.
- Sirkar, K.K., P.V. Shanbhag and A.S.Kovvali (1999). Membrane in a reactor: a functional perspective. *Ind.Eng.Chem.Res.* **38**, 3715-3737.
- Skarstrom, C.W. (1960).Method and apparatus for fractionating gaseous mixtures by adsorption. *US Patent 2,944,627 to Exxon Research and Engineering.*
- Smith, O.J. and A.W. Westerberg (1990). Mixed-integer programming for pressure swing adsorption cycle scheduling. *Chem.Eng. Sci.* **45**, 2833-2842.

- Stankiewiez, A. (2003). Reactive separations for process intensification: An industrial perspective. *Chem.Eng.Process.* **42,** 137 -144
- Spivey, J.J. (1987). *Ind.Eng.Chem.* **26,** 2165-2180.
- Takeuchi, Y., N. Hayato, S.A. Miyata and A. Harada (1995). Adsorption of 1-butanol and p-xylene vapour and their mixtures with high silica zeolites. *Sep.Tech.* **5,** 23.
- Taylor, R. and R. Krishna (2000). Modelling reactive distillation. *Chem.Eng.Sci.*, **55,** 5183-5228.
- Tierney, M.J. (2003)*. Measurement of the bulk adsorption properties of powders.
- Tomasic, V. Gomzi, Z (2004). Experimental and theoretical study of NO decomposition in a catalytic monolith reactor. *Chem.Eng.Process.***43,** 765-774.
- Treybal, R.E. (1980). Mass Transfer Operations. *McGraw-Hill, Inc.*
- Tsai, W.T., C.Y. Chang and H.C.Lee (1996). Adsorption of N,N-Dimethylformamide vapour on activated carbon and hydrophobic zeolite. *Proceedings of AWMA.*
- Tsotsis, T.T., A.M. Champagnie, S.P. Vasileiadis, Z.D. Zraka and R.G. Minet (1992). Packed bed catalytic membrane reactor. *Chem.Eng.Sci.* **47,** 2903.
- Turnock, P.H. and R.H.Kadlec (1971). Separation of nitrogen and methane via periodic adsorption. *AIChE J.*, **17,** 335 – 342.
- Van de Beld, L., M.C. van der Ven and K.R.Westerterp(1995). A kinetic study of the complete oxidation of ethene, propane and their mixtures on a Pd/Al_2O_3 catalyst. *Chem. Eng.Process.* **34,** 469-478.
- Van den Beld, B., R.A. Borman, O.R. Derkx, A.A. van Woezik and K.R. Westerterp (1994). Removal of volatile organic compounds from polluted air in a reverse flow reactor: an experimental study. *Ind.Eng.Chem.Res.* **33,** 2946-2956.
- Van den Beld, B. and K.R. Westerterp(1996). Air purification in a reverse flow reactor: Model simulation vs experiments. *AIChE J.* **42,** 1139.
- Van Welsenaere, R.J. and G.F. Froment (1970). *Chem.Eng.Sci.* **25,** 1503.
- Vaporciyan,G.G. and R.H.Kadlec (1987). Equilibrium-limited periodic separating reactors. *AIChE J.*, **33,** 1334-1343.
- Vaporciyan,G.G. and R.H.Kadlec (1989). Periodic separating reactors: experiments and theory. *AIChE J.*, **35,** 831-844.

- Vermuelen, T., M.D. LeVan, N.K. Hiester and G.Klien (1984). Adsorption and ion exchange. *Perry's Chemical Engineers' Handbook (6th Ed.)* pp.16.
- Vilaplana-Ortego, E., J. Alcaniz-Monge, D. Cazorla-Amoros and A. Linares-Solano (2002). Activated carbon fibre monoliths. *Fuel Process. Tech.*, **77-78**, 445-451.
- Wangruangsatit, T. and E. Alpay (2002). In-situ recovery and oxidation of volatile organic compounds. *MSc thesis, Imperial College, London.*
- Waldron, W.E., J.R. Hufton, S.Sircar (2001). Production of hydrogen by cyclic sorption enhanced reaction process. *AIChE J.*, **47**, 1477-1479.
- Werner, K. (1994). Heat transfer with reaction in monoliths. *Chem.Eng. Process.* **33**, 227-236.
- Williams, J. (2001). Monolith structures, materials, properties and uses. *Cat. Today* **69**, 3-9.
- Wilson, K.A., T.D. Burchell, R.R. Judkins (1998). Carbon fibre composite molecular sieve electrically regenerable air filter media. *US Patent 5827355.*
- Wu, J.C.S., T.E. Gerdes, J.L. Pszczolowski, R. Bhave and P.K.T. Lui (1990). Dehydrogenation of ethylbenzene to styrene using commercial ceramic membranes as reactors. *Sep.Sci.Tech.* **25**, 1489.
- Yang, R.T. (1987). Gas separation by adsorption processes. *Butterworths, Boston.*
- Yang, R.T. and E.S. Kikkinides (1995). New sorbents for olefin/paraffing separations by adsorption via π-complexation. *AIChE J.* **41**, 509-517.
- Yates, M., J.Blanco, P.Avila, M.P. Martin (2000). Honeycomb monoliths of activated carbons for effluent gas purification. *Microporous and Mesoporous Materials* **37**, 201-208.
- Yongsunthon, I. and E. Alpay (1998). Design and optimisation of temperature cycled adsorptive reactors. *Comp.Chem.Eng.* **22**, S733 – S736.
- Yongsunthon, I. and E. Alpay (1999). Design of periodic adsorptive reactors for the optimal integration of reaction, separation and heat exchange. *Chem.Eng.Sci.* **54**, 2647-2657.
- Yongsunthon, I. (1999). Design of periodic adsorptive reactors for the optimal integration of reaction, separation and heat-exchange. *PhD thesis, Imperial College, London.*

- Zagoruiko, A.N., O.V. Kostenko and A.S. Noskov (1996). Development of the adsorption-catalytic reverse-process for incineration of volatile organic compounds in diluted waste gases. *Chem.Eng.Sci.* **51**, 2989-2994.
- Zhu, W., F. Kapteijn, J.A. Moulijn, M.C. den Exter, and J.C. Jansen (2000). Shape selectivity in adsorption on the All-Silica DD3R. *Langmuir* **16**, 3322-3329.
- Zhu, W., F. Kapteijn, J.C. Groen, J.A. Moulijn (2004). Adsorption of butane isomers and SF_6 on Kureha activated carbon. 1. Equilibrium. Langmuir **20**, 5277-5284.
- Zhu, W., F. Kapteijn, J.C. Groen, M.J.G. Linders, J.A. Moulijn (2004). Adsorption of butane isomers and SF_6 on Kureha activated carbon. 2. Kinetics. Langmuir **20**, 1704-1710.
- Zhu, W., F. Kapteijn, J.C. Groen, A. van Miltenburg, J.A. Moulijn (2005). Comparison of adsorption behaviour of light alkanes and alkenes on Kureha activated carbon. *Carbon* **43**, 1416-1423

Appendix A

ADSORBATE-PARTICLE MASS DIFFUSIONS

A.1 Intraparticle Diffusion

Kureha activated carbon covers a pore size range from 2 nm to 100 μm (Zhu *et al.*, 2005). Therefore, in this work both molecular and knudsen diffusion are considered as important in terms of the resistance to mass transfer.

The intraparticle diffusion depends on the relative magnitude of the solid pore diameter to the mean free path of gas molecules. The mean free path, γ, is given as:

$$\gamma = \frac{1}{\pi\sqrt{2\sigma^2}}\frac{RT}{PN_{av}} \qquad (A.1)$$

Where N_{av} is the Avogadro constant (= 6.02×10^{23} molecules mol^{-1}) and σ the Lennard-Jones collision diameter (m). The mass transfer resistance is said to be molecular diffusion dominated if $d_{pore} / \gamma > 20$, and Knudsen diffusion dominated if $d_{pore} / \gamma < 0.2$. For intermediate values of the ratio, a parallel mechanism of Knudsen and molecular diffusion dominates.

For ethene oxidation in the M-AR, at 293 K and 2bar and for the activated carbon pore diameter ($d_{pore} = 1 \times 10^{-7}$m), $d_{pore} / \gamma \approx 4$. For propane

oxidation in the M-AR, $d_{pore} / \gamma \approx 6$. Therefore both molecular and knudsen diffusion are of importance.

For a binary gas in a porous solid at constant pressure, the approximation of equimolar counter diffusion is used (see Yang, 1987). D_m and D_k are used to determine the diffusion in a single cylindrical pore i.e. the pore diffusivity, D_p:

$$\frac{1}{D_p} = \frac{1}{D_m} + \frac{1}{D_k} \tag{A.2}$$

where D_m and D_k denote the molecular and Knudsen diffusion coefficients ($m^2 s^{-1}$) respectively.

The molecular diffusion coefficient can be calculated from the Chapman-Enskog kinetic theory:

$$D_m = 1.8583 \times 10^{-7} \frac{\sqrt{T^3 (\frac{1}{M_A} + \frac{1}{M_B})}}{P \sigma_{AB}^2 \Omega_{AB}} \tag{A.3}$$

Where M_A and M_B are the molecular weights of species A and B respectively, σ_{AB} is the Lennard-Jones collision diameter for A and B, Ω_{AB} is the corresponding dimensionless collision integral, T is the temperature of the reactor (K), and P the total pressure (atm). σ_{AB} and Ω_{AB} are approximated using the method outlined in Bird *et al.* (1960).

$$D_k = 48.5 d_{pore} \sqrt{\frac{T}{M_A}} \qquad (A.4)$$

It is often convenient for design and modelling, however to use the effective intraparticle diffusion coefficient D_e ($m^2\ s^{-1}$), which accounts for the various mechanisms of the intraparticle transport described above and the complex pore structure within the particle. This is given by:

$$D_e = \frac{\varepsilon_p D_p}{\tau_p} \qquad (A.5)$$

Where ε_p denotes the intraparticle void fraction (~ 0.6) and τ_p the particle tortuosity factor (≈ 3 for cylindrical pores).

Table (A.1) gives a summary of the parameters used to calculate the various diffusion coefficients. Table (A.2) lists the values of Ω_{AB} for ethene and propane oxidation respectively.

Parameters	Values	Unit
M_A (ETHENE)	28.05	g mol^{-1}
M_A (PROPANE)	44.09	g mol^{-1}
M_B (NITROGEN)	28.02	g mol^{-1}
σ_A (ETHENE)	4.23Å	m
σ_A (PROPANE)	5.06Å	m
σ_{AB} (ETHENE)	3.96Å	m
σ_{AB} (PROPANE)	4.37Å	m
P	2	atm
d_{pore}	1×10^{-7}	m
r_p	17×10^{-5}	m
ε_p	0.6	-
τ_p	3	-
N_{AV}	6.02×10^{23}	molecules mol^{-1}

Table A.1: Summary of parameters used to calculate diffusion coefficients

Ethene		Propane	
T (K)	Ω_{AB}	T (K)	Ω_{AB}
293	1.05	320	1.06
320	1.03	338	1.04
338	1.01	358	1.02
360	0.99	400	0.98
400	0.96	450	0.95
460	0.92	560	0.90
475	0.92	580	0.89
490	0.91	600	0.87

Table A.2: Feed temperatures (adsorption and reaction) and their corresponding collision integrals

A.2 Axial dispersion coefficient

The axial dispersion coefficient, D_z is used in the packed bed reactor systems modelled in this work. For a randomly packed bed of porous particles at low Reynolds number, the axial dispersion arises due to the tortuous fluid particle transfer process and is principally affected by molecular diffusion; D_m and the interstitial bed velocity distribution (see Edwards and Richardson, 1968, Gunn and England, 1971).

The axial dispersion coefficient used in this work is a simplified form of the Langer *et al.* correlation (relevant when particle sizes are < 3mm):

$$D_z = \frac{\varepsilon_b D_m}{\tau_z} + \frac{(v d_p)^2}{Pe_\infty (v d_p + \beta_r \varepsilon_b \frac{D_m}{\tau_z})} \qquad (A.6)$$

Where ε_b is the bed particle voidage, τ_z the axial bed turtuosity factor, v the interstitial inert gas velocity (m s^{-1}), d_p, the mean particle diameter (m), D_m the molecular diffusion for binary systems (see A.1), Pe_∞ is the limiting value of the dimensionless Peclet number and β_r is the radial dispersion factor.

To account for the effect of radial dispersion in the intermediate region where the effect of D_m and D_z are of importance, the Wicke correlation for axial bed turtuosity factor, τ_z is used (see Langer *et al.* 1978):

$$\tau_z = 0.45 + 0.55\varepsilon_b \qquad (A.7)$$

For $d_p < 0.0025m$, the assumption is made for the limiting value of Pe_∞ as:

$$Pe_\infty = 670\, d_p \qquad (A.8)$$

A typical value of $\beta_r \approx 0.5$ can be assumed.

Table A.3 gives a summary of the parameters used to determine D_z at any given value.

Parameters	Values	Unit
ε_b	0.40	-
τ_z	0.67	-
d_p	3×10^{-5}	m
Pe_∞	0.23	-
β_r	0.50	-

Table A.3: Summary of parameters used to calculate D_z

Appendix B

SOLID – GAS HEAT TRANSFER

Justification for the Instantaneous Thermal Equilibrium Assumption

In all cases considered in this work, the M-AR operations were isobaric. Any changes (regardless of the magnitude) in the temperature due to reaction and / or adsorption were accounted for in the energy balance. The non-isothermicity, however, mainly arose from the temperature swing effect. For the solid-gas heat transfer analysis of such a system, it is appropriate to consider an activated carbon particle surrounded by bulk (inert diluent) gas. In specific, suppose both the gas and solid were initially at temperature T_{p0}, for a step change in gas temperature from T_{p0} to T_g (where $T_g > T_{p0}$), the heat gained by the particle can be described by a simple first order rate law as

$$H_{gp}\frac{dT_p}{dt} = T_g - T_p \qquad \text{(B.1)}$$

Where T_p is the particle temperature at time t (Eq.(B.1) neglects any heat transfer resistance within the particle), and

$$H_{gp} = \frac{\rho_b c_{ps} r_p}{3h_f} = \frac{\rho_b c_{ps} r_p^2}{3k_p Bi_h} \qquad \text{(B.2)}$$

Where ϱ_b denotes the particle density (mol m^{-3}), c_{ps} the solid heat capacity (J mol^{-1} K^{-1}), r_p the particle radius (m), h_f the heat transfer coefficient (W m^{-2} K^{-1}), k_p, the particle thermal conductivity (W m^{-1} K^{-1}) and Bi_h the Biot number. Rearranging Eq. (B.1) and integrating yields:

$$\ln\left(\frac{T_g - T_p}{T_g - T_{p0}}\right) = \ln(\theta_{gp}) = -\frac{t}{H_{gp}} \tag{B.3}$$

The temperature response half-time, t_h, is then given for $\theta_{gp} = ½$, i.e.

$$t_h = H_{gp} \ln(2) \tag{B.4}$$

Table B.1 gives a summary of parameters used to calculate H_{gp} for a typical activated carbon type particle.

Parameters	Values	Unit
ϱ_b	659	kg m^{-3}
r_p	15×10^{-5}	m
C_{ps}	710	J kg^{-1} K^{-1}
k_p	1	W m^{-1} K^{-1}

Table B.1: Summary of parameters for the calculation of H_{gp}

A typical correlation for the Biot number for heat transfer in a fixed bed (Yang, 1987) is given as a function of Prandtl number (Pr) and Reynolds number (Re_p):

$$Bi_h = \frac{0.36}{2\varepsilon_b}\frac{k_g}{k_p} Re_p^{0.64} Pr^{1/3} \qquad (B.5)$$

For nitrogen inert, Pr ~1; the ratio of nitrogen to activated carbon thermal conductivity, $\frac{k_g}{k_p} < 0.1$; Eq.(B.5) results in:

$$Bi_h = 0.045 Re_p^{0.64} \qquad (B.6)$$

For a typical M-AR operation, $Re_p \sim 217 \rightarrow Bi_h \sim 0.2$ (Note that $Bi_h < 1$ is also an indication of external film controlling heat transfer (Ruthven, 1984).

With the above physical properties, $H_{gp} < 0.05$, it follows then that $t_h <$ 0.025 s. This is negligibly very small compared to a typical M-AR step duration of tens or hundreds of seconds. Thus, instantaneous thermal equilibrium is a reasonable assumption.

Appendix C

MOMENTUM, MASS AND ENERGY BALANCES FOR MONOLITH ADSORPTIVE REACTOR

C.1 Velocity Profile

Newton's Law of Viscosity:

$$\tau_{rz} = -\mu_{gas} \frac{\partial v(r)_z}{\partial r} \tag{C.1}$$

At maximum shear stress, Eq. (C.1) becomes:

$$\frac{\partial v(r)_z}{\partial r} = -\left(\frac{P_0 - P_L}{2\mu_{gas} L}\right) R_1 \tag{C.2}$$

P_0 and P_L denote inlet and outlet pressures (Pa), μ_{gas} is the gas viscosity in (Pa.s), L is the respective reactor length and R_1 the core gas channel radius.

Integrating Eq. (C.2) at $r = R$ and $v(r)_z = 0$ we obtain:

$$v(r)_z = \left(\frac{P_0 - P_L}{4\mu_{gas}L}\right)R_1{}^2\left[1-\left(\frac{r}{R_1}\right)^2\right] \qquad (C.3)$$

Maximum velocity occurs at r = 0, hence Eq. (C.3) becomes:

$$v(r)_{z,max} = \left(\frac{P_0 - P_L}{4\mu_{gas}L}\right)R_1{}^2 \qquad (C.4)$$

where $v(r)_{z,max} = 2\,v(r)_{z,ave}$ i.e. double the average velocity, $v(r)_{z,ave}$

substituting $v(r)_{z,max} = 2\,v(r)_{z,ave}$ into Eq. (C.3) we obtain:

$$v(r)_z = 2v\left[1-\left(\frac{r}{R_1}\right)^2\right] \qquad (C.5)$$

C.2 Mass Balance Derivation for Monolith Adsorptive Reactor

The molar flux of species *i*, W_i (mol m^{-2} s^{-1}) has two components, the radial component W_{ir} and the axial component, W_{iz}. The molar flow rate is defined as:

$$F_{iz} = W_{iz}\,A_{Cz} \qquad (C.6)$$

where A_{cz} is the cross sectional area of the reactor.

The molar fluxes consist of a diffusional component, $\left(-D_i \frac{\partial C_i}{\partial z}\right)$, and a convective flow component, ($v_z C_i$)

$$W_{iz} = -D_i \frac{\partial C_i}{\partial z} + \upsilon_z C_i \tag{C.7}$$

where v_z is the velocity of the gas along the axial direction (m s^{-1}) and D_i is the diffusivity component of *i* (m^{-2} s^{-1}).

$$W_{ir} = -D_i \frac{\partial C_i}{\partial r} + \upsilon_r C_i \tag{C.8}$$

where v_r is the velocity of the gas in the radial direction (m s^{-1}). A mole balance on a cylindrical system volume of length Δz and radius Δr gives:

Mole Balance

$$(\text{Moles IN at r}) = W_{ir} \bullet \begin{pmatrix}\text{cross sectional area}\\ \text{normal to radial flux}\end{pmatrix} = W_{ir} \bullet 2\pi r \Delta z$$

$$(\text{Moles IN at z}) = W_{iz} \bullet \begin{pmatrix}\text{cross sectional area}\\ \text{normal to axial flux}\end{pmatrix} = W_{iz} \bullet 2\pi r \Delta r$$

$$\begin{pmatrix}\text{Moles IN}\\ \text{at r}\end{pmatrix} - \begin{pmatrix}\text{Moles OUT}\\ \text{at } (r+\Delta r)\end{pmatrix} + \begin{pmatrix}\text{Moles IN}\\ \text{at z}\end{pmatrix} - \begin{pmatrix}\text{Moles OUT}\\ \text{at } (z+\Delta z)\end{pmatrix} + \text{Generation} = \text{Acc.}$$

Note: Acc. denotes accumulation.

$$W_{ir} 2\pi r \Delta z\,|_r - W_{ir} 2\pi r \Delta z\,|_{r+\Delta r} + W_{iz} 2\pi r \Delta r\,|_z - W_{iz} 2\pi r \Delta r\,|_{z+\Delta z} + r_i 2\pi r \Delta r \Delta z = \frac{\partial C_i (2\pi r \Delta r \Delta z)}{\partial t} \tag{C.9}$$

Dividing by $2\pi r \Delta r \Delta z$ and taking the limit as Δr and $\Delta z \rightarrow 0$

$$-\frac{1}{r}\frac{\partial (r W_{ir})}{\partial r} - \frac{\partial W_{iz}}{\partial z} + r_i = \frac{\partial C_i}{\partial t} \tag{C.10}$$

Substituting for W_{iz} and W_{ir} from Eqs.(C.7 and C.8) we obtain:

$$-\frac{1}{r}\frac{\partial}{\partial r}\left[\left(-D_i\frac{\partial C_i}{\partial r}r\right)+\upsilon_r C_i\right]-\frac{\partial}{\partial z}\left[-D_i\frac{\partial C_i}{\partial z}+\upsilon_z C_i\right]+r_i=\frac{\partial C_i}{\partial t} \qquad (C.11)$$

Assuming $\nu_r = 0$ and distinguishing between the two distinct phases in the adsorptive reactor, from Eq. (C.11) we obtain:

Material balance for the gas phase (r= 0):

$$\frac{\partial C_i}{\partial t}=-\upsilon_z\frac{\partial C_i}{\partial z}+D_m\left[\frac{1}{r}\frac{\partial}{\partial r}\left(r\frac{\partial C_i}{\partial r}\right)\right] \qquad (C.12)$$

where D_m is the Chapman-Enskog molecular diffusion of component *i* (m^{-2} s^{-1}). The axial diffusion in the gas phase is neglected due to the usually large convective transport.

Material balance for the solid phase:

Gas flux is governed by diffusion, there are no radial or axial convective gas flows. Reaction occurs in this phase and the process is depicted by the kinetic rate expression and the rate of adsorption. D_e is the effective diffusion component in the solid phase (m^{-2} s^{-1}) and ε_m the solid phase porosity.

$$\varepsilon_m\frac{\partial Ci}{\partial t}=D_e\frac{\partial^2 C_i}{\partial z^2}+D_e\left[\frac{1}{r}\frac{\partial}{\partial r}\left(r\frac{\partial Ci}{\partial r}\right)\right]-\rho R_{HC}-\rho r_{ads} \qquad (C.13)$$

C.3 Energy Balance Derivation for Monolith Adsorptive Reactor

Neglecting work terms, we have:

$$\overbrace{Q^{Y}}^{\text{Conduction}} + \left(\overbrace{\sum_{i}^{n} F_{i0}H_{i0} - \sum_{i} F_{i}H_{i}}^{\text{Convection}} \right) = \frac{\partial E_{sys}}{\partial t} \qquad \text{(C.14)}$$

The total energy of the system, E_{sys} is given as:

$$E_{sys} = \Sigma N_i H_i = \Sigma C_i H_i * \text{Volume} = \Sigma (C_i + \rho) H_i * 2\pi r \Delta r \Delta z \qquad \text{(C.15)}$$

We define energy flux, e, (J m^{-2} s^{-1}) as e = conduction + convection

$$e = Q + \Sigma W_i H_i \qquad \text{(C.16)}$$

where Q, (kg m^{-2} s^{-1}) is given by Fourier's law and for axial conduction Fourier's law is given by:

$$Q_z = -\lambda \frac{\partial T}{\partial z} \qquad \text{(C.17)}$$

where λ is the thermal conductivity (J m^{-1} s^{-1} K^{-1}). The energy flow is the product of the flux and cross sectional area and is given in Eq.(C.19) where A_c is the cross sectional area.

$$\text{Energy flow} = e * A_c \qquad \text{(C.18)}$$

Energy balance:

Using the flux, e, to carry out an energy balance on our system volume $2\pi r\Delta r\Delta z$ we have:

(Energy Flow IN at r) = $e_r A_{cr} = e_r\, 2\pi r\Delta z$

(Energy Flow IN at z) = $e_z A_{cz} = e_z 2\pi r\Delta r$

$$\begin{pmatrix}\text{Energy Flow IN}\\ \text{at } r\end{pmatrix}-\begin{pmatrix}\text{Energy Flow OUT}\\ \text{at } (r+\Delta r)\end{pmatrix}+\begin{pmatrix}\text{Energy Flow IN}\\ \text{at } z\end{pmatrix}-\begin{pmatrix}\text{Energy Flow OUT}\\ \text{at } (z+\Delta z)\end{pmatrix}$$
$$=\begin{pmatrix}\text{Accumulation of Energy}\\ \text{in Volume } 2\pi r\Delta r\Delta z\end{pmatrix}$$

$$(e_r 2\pi r\Delta z)\,|_r-(e_r 2\pi r\Delta z)\,|_{r+\Delta r}+(e_z 2\pi r\Delta r)\,|_z-(e_z 2\pi r\Delta r)\,|_{z+\Delta z}=\frac{\partial\Sigma H_i C_i(2\pi r\Delta r\Delta z)}{\partial t}+\frac{\partial\Sigma H_i\rho(2\pi r\Delta r\Delta z)}{\partial t} \tag{C.19}$$

Dividing by $2\pi r\Delta r\Delta z$ and taking limits as $\Delta r \to 0$, and $\Delta z \to 0$,

$$-\frac{1}{r}\frac{\partial(re_r)}{\partial r}-\frac{\partial e_z}{\partial z}=\frac{\partial\Sigma H_i C_i}{\partial t}+\frac{\partial\Sigma H_i\rho}{\partial t} \tag{C.20}$$

$$\begin{aligned}e_r &= Q_r+\Sigma W_{ir}H_i\\ e_z &= Q_z+\Sigma W_{iz}H_i\end{aligned} \tag{C.21}$$

$$\frac{\partial\Sigma H_i C_i}{\partial t}+\frac{\partial\Sigma H_i\rho}{\partial t}=\Sigma C_i\frac{\partial H_i}{\partial t}+\Sigma H_i\frac{\partial C_i}{\partial t}+\Sigma\rho\frac{\partial H_i}{\partial t}=\Sigma C_i C_{Pi}\frac{\partial T}{\partial t}+\Sigma H_i\frac{\partial C_i}{\partial t} \tag{C.22}$$

Substituting for e :

$$-\frac{1}{r}\frac{\partial r[Q_r+\Sigma W_{ir}H_i]}{\partial r}-\frac{\partial[Q_z+\Sigma W_{iz}H_i]}{\partial z}=\Sigma C_i C_{Pi}\frac{\partial T}{\partial t}+\Sigma H_i\frac{\partial C_i}{\partial t}+\Sigma\rho C_{Pi}\frac{\partial T}{\partial t} \tag{C.23}$$

we expand the convective energy flux $\sum W_i H_i$ to give

$$\frac{\partial(\Sigma W_{iz} H_i)}{\partial z} = \Sigma H_i \frac{\partial W_{iz}}{\partial z} + \Sigma W_{iz} \frac{\partial H_{iz}}{\partial z} \tag{C.24}$$

and from the material balance - Eqs. (C.10 and C.13) we obtain:

$$-\frac{1}{r}\frac{\partial}{\partial r}(rQ_r) - \frac{\partial Q_z}{\partial r} - \Sigma H_i\left[\frac{1}{r}\frac{\partial(rW_{ir})}{\partial z} + \frac{\partial W_{iz}}{\partial z} + \frac{\partial C_i}{\partial t} + \rho r_{ads}\right] - \Sigma W_{ir}\frac{\partial H_i}{\partial r} - \Sigma W_{iz}\frac{\partial H_i}{\partial z} = \Sigma C_i C_{Pi}\frac{\partial T}{\partial t} + \Sigma \rho C_{Pi}\frac{\partial T}{\partial t} \tag{C.25}$$

The bracketed term denotes the rates of reaction and adsorption and we have:

$$-\frac{1}{r}\frac{\partial}{\partial r}(rQ_r) - \frac{\partial Q_z}{\partial r} + \Sigma H_i r_i - \Sigma H_i r_{ads}\rho - \Sigma W_{ir}\frac{\partial H_i}{\partial r} - \Sigma W_{iz}\frac{\partial H_i}{\partial z} = \Sigma C_i \frac{\partial H_i}{\partial t} + \Sigma \rho \frac{\partial H_i}{\partial t} \tag{C.26}$$

Note that:

$$Q_r = -\lambda\frac{\partial T}{\partial r},\quad Q_z = -\lambda\frac{\partial T}{\partial z},\quad \frac{\partial H_i}{\partial z} = C_{Pi}\frac{\partial T}{\partial z},\quad \frac{\partial H_i}{\partial r} = C_{Pi}\frac{\partial T}{\partial r} \tag{C.27}$$

and

$$\Sigma r_i H_i = -\Sigma \upsilon_i H_i(-r_A) = \Delta H_R r_A \tag{C.28}$$

$$\Sigma r_{ads} H_i = -\Sigma \Delta H_{ads,i}(r_{ads}) = \Delta H_{ads} r_{ads} \tag{C.29}$$

$$\rho_g = \frac{P}{RT} = C \tag{C.30}$$

Assumptions: $v_r = 0$; The convective flux in the axial direction, $v_z C_i$ is greater than the diffusive flux $\left(-D_i\frac{\partial C_i}{\partial r}\right)$, thus flux in the axial direction

$$W_{iz} = \upsilon_z C_i \tag{C.31}$$

Distinguishing between the two distinct phases in the adsorptive reactor:

Energy balance gas phase:

$$\frac{\partial T}{\partial t}\rho_g C_{pg} = -\rho_g \nu_z C_{pg}\frac{\partial T}{\partial z} + \frac{\lambda_g}{r}\frac{\partial}{\partial r}\left(r\frac{\partial T}{\partial r}\right) \qquad \text{(C.32)}$$

Solid phase:

$$\frac{\partial T}{\partial t}\rho_g C_{pg}\varepsilon_m + \frac{\partial T}{\partial t}\rho C_{ps} = \rho R_{HC}(-\Delta H_r) - \rho\Delta H_{ads} r_{ads} + \lambda\frac{\partial^2 T}{\partial z^2} + \frac{\lambda}{r}\frac{\partial}{\partial r}\left(r\frac{\partial T}{\partial r}\right)$$

(C.33)

Appendix D

SUTHERLAND'S FORMULA

The Sutherland's formula can be used to derive the dynamic viscosity of an ideal gas as a function of the temperature:

$$\eta = \eta_0 \frac{T_0 + C}{T + C}\left(\frac{T}{T_0}\right)^{\frac{3}{2}} \qquad \text{(D.1)}$$

where:

η = viscosity in (Pa.s) at input temperature T

η_0 = reference viscosity in (Pa s) at reference temperature T_0

T = input temperature (K)

T_0 = reference temperature (K)

C = Sutherland's constant for gaseous material in question

Gas	C(K)	T_0 (K)	η_0 (10^{-6} Pa.s)
Air	120	291.15	18.27
Nitrogen	111	300.55	17.81
Oxygen	127	292.25	20.18

Table D.1: Sutherland's constant and temperature for some gases

The formula is valid for temperatures between 0 < T < 555 K with an error due to pressure less than 10 % below 3.45 MPa (*Source: www.wikepedia.org*)

Appendix E

EQUIVALENCY BETWEEN M_{-AR} AND M_{-RXTN}

SAMPLE CALCULATION

Base case T_{fa} = 460 K and T_{fd} = 460 K

$u_a = u_d$ = 0.01 ms^{-1}

Area = 7.069E-06 m^2

LEL 2.7%

y_f calculations

UEL 36%

M_{-AR}

y (ethene)	%	P	R	T	C	Vol rate	n (mol s^{-1})	t_a	No.moles
0.003	0.3	2E5	8.314	460	0.15	7.1E-08	1.1E-08	50	5.3E-07
0.01	1	2E5	8.314	460	0.5229	7.1E-08	3.7E-08	50	1.8E-06
0.03	3	2E5	8.314	460	1.568	7.1E-08	1.1E-07	50	5.5E-06
0.05	5	2E5	8.314	460	2.6145	7.1E-08	1.8E-07	50	9.2E-06
0.1	10	2E5	8.314	460	5.229	7.1E-08	3.7E-07	50	1.8E-05
0.2	20	2E5	8.314	460	10.458	7.1E-08	7.4E-07	50	3.7E-05

t_d	n (mol s^{-1})
150	3.5E-09
150	1.2E-08
150	3.7E-08
150	6.2E-08
150	1.2E-07
150	2.5E-07

M_{-RXTN}							**M_{-RXTN}**		**M_{-AR}**
n (mol s^{-1})	Vol rate	C	R	T	P	y	Vol.%	y	Vol.%
3.5E-09	7.1E-08	0.05	8.314	460	2E5	0.00096	0.10%	0.003	0.3%
1.2E-08	7.1E-08	0.1743	8.314	460	2E5	0.00333	0.33%	0.01	1%
3.7E-08	7.1E-08	0.52267	8.314	460	2E5	0.00999	0.99%	0.03	3%
6.2E-08	7.1E-08	0.8715	8.314	460	2E5	0.01666	1.67%	0.05	5%
1.2E-07	7.1E-08	1.743	8.314	460	2E5	0.03333	3.33%	0.1	10%
2.5E-07	7.1E-08	3.486	8.314	460	2E5	0.06666	6.67%	0.2	20%

Appendix F

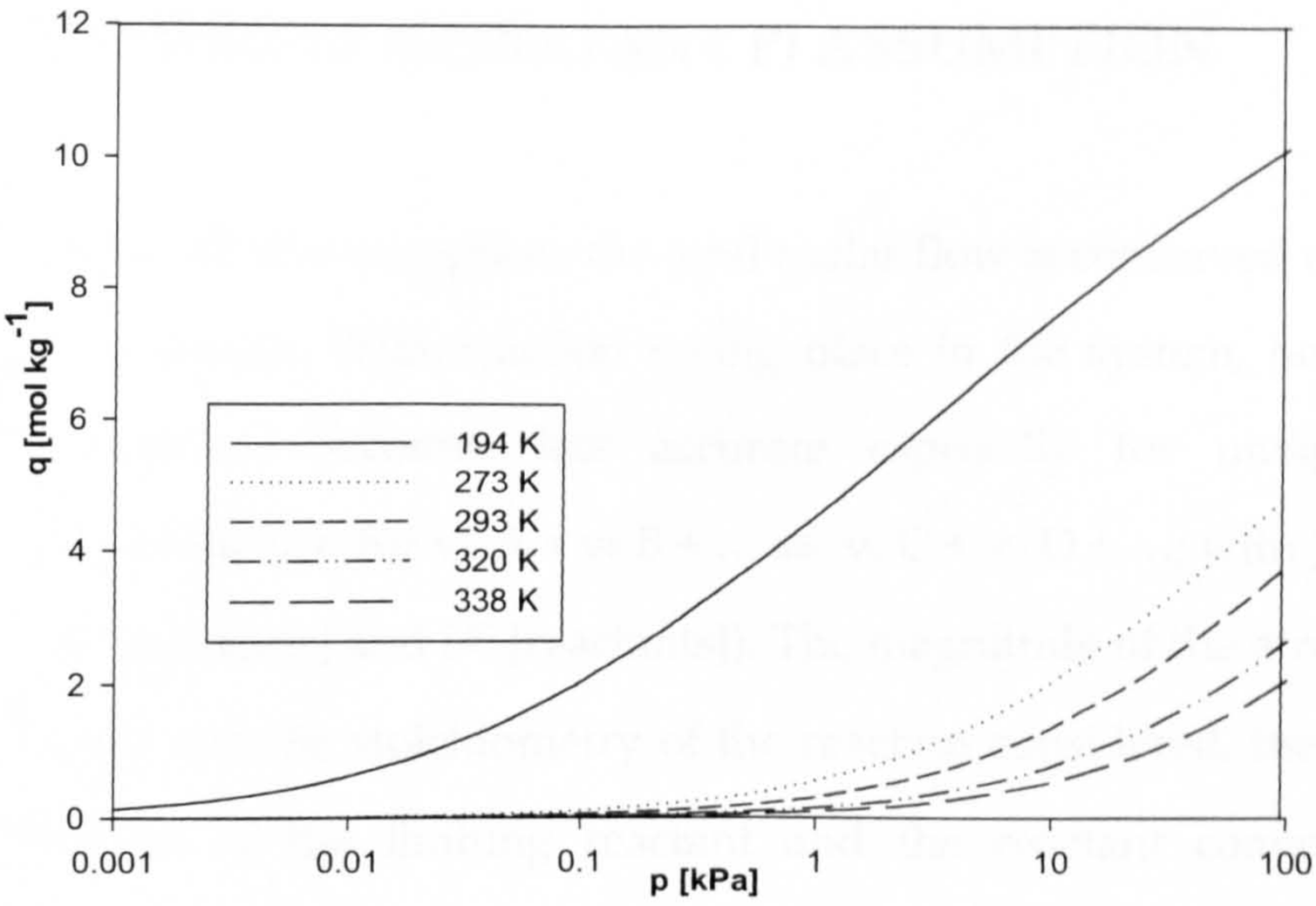

Fig. F.1: Ethene Isotherms on Kureha carbon

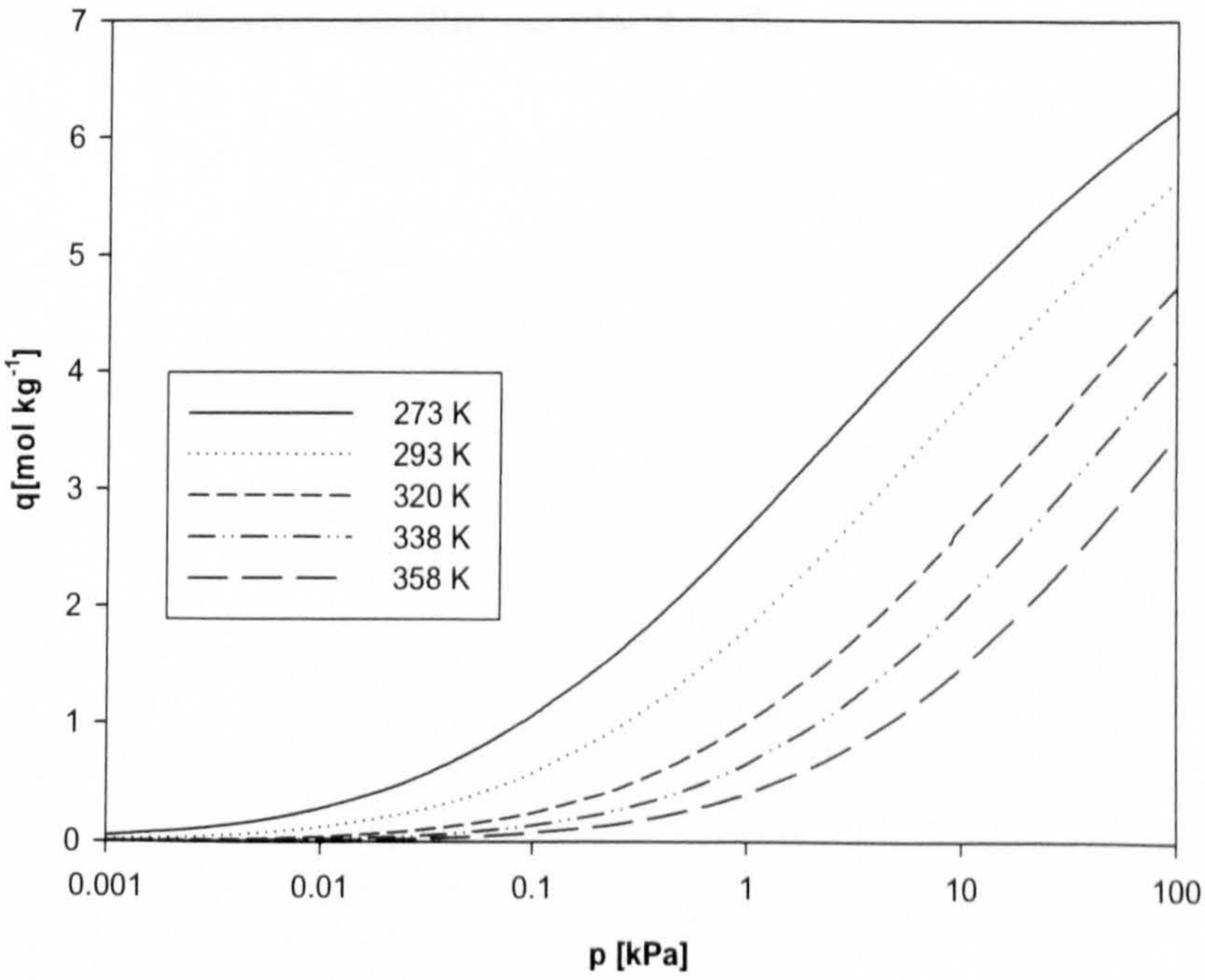

Fig. F.2: Propane Isotherms on Kureha carbon

Appendix G

THE DILUTE (CONSTANT P) ASSUMPTION

Under dilute assumption; the total molar flow is conserved over a cycle of operation. With reaction taking place in the system, however this assumption becomes less accurate especially for unequal molar conversion (i.e. for $\nu_A A + \nu_B B + \ldots \Leftrightarrow \nu_C C + \nu_D D + \ldots$; with $\sum_j \nu_j \neq \sum_i \nu_i$; $j \in$ [products] and $i \in$ [reactants]). The magnitude of the error depends on the specific stoichiometry of the reaction considered, the inlet mole fraction of the limiting reactant and the reactant conversion. The maximum error for a given reaction scheme and inlet mole fraction of A would occur when the reaction goes to completion. For the system under consideration with an inlet mole fraction of ethene of 0.3 vol %, the maximum error that occurs is < 1%.